Characterising the Senescence-like Phenotype Induced by the Typhoid Toxin of *Salmonella* Typhi

Mohamed ElGhazaly

This thesis is submitted in partial fulfillment
of the requirements for the degree of
Doctor of Philosophy

Department of Biomedical Science
The University of Sheffield

June 2021

Declaration

I, Mohamed ElGhazaly, confirm that the thesis is my own work. I am aware of the University's Guidance on the Use of Unfair Means (www.sheffield.ac.uk/ssid/unfair-means). This work has not been previously presented for an award at this, or any other, university. Part of my PhD work has been published prior to submission of this thesis in the following research papers:

- Ibler, A.E.M., **ElGhazaly, M.**, Naylor, K.L., Bulgakova N.A., El-Khamisy S., Humphreys D. Typhoid toxin exhausts the RPA response to DNA replication stress driving senescence and *Salmonella* infection. Nat Commun 10, 4040 (2019). https://doi.org/10.1038/s41467-019-12064-1

- Humphreys D, **ElGhazaly M**, Frisan T. Senescence and Host-Pathogen Interactions. Cells. 2020 Jul 21;9(7):1747. doi: 10.3390/cells9071747. PMID: 32708331; PMCID: PMC7409240.

My published figures are marked by an asterisk at the end of the figure legend and indicated in a footnote with a link to the relevant paper.

<div align="right">

Mohamed ElGhazaly

June 2021

</div>

Acknowledgements

I would like to sincerely thank my brilliant supervisor, **Dr Daniel Humphreys**, who has certainly become my mentor, champion and after 4 years, a friend. Daniel has always had his door open (pre-covid), and Google Meet on (post-covid), for spontaneous discussions. I would not be the scientist I am today without his guidance, encouragement, and support for research freedom. I simply could not have wished for a better supervisor. My thanks are extended to **Dr Mark Collins** who shared my excitement and was extremely supportive and patient with all of my mass spectrometry experiments and discussions. I would also like to acknowledge Sheffield' Mass Spectrometry Facility, particularly **Dr Adelina Acosta** who always provided moral and technical support every time I visited. I am also very grateful for the continuous advice of my amazing advisors **Dr Kai Erdmann** and **Dr Jason King**, which were incredibly useful to propel my project forward. In addition, I would also like to express my deep thanks to **Dr Angela Ibler** who has taught me invaluable skills during my PhD, and have provided me with constructive advice. Our discussion on the whiteboard in the office was the greatest fun I had, and resulted in great imaginative thinking in our projects. Thanks to **Dr Kate Naylor**, who I had the pleasure to work with and learn from during my first two years of my PhD. I would also like to thank **Dr Zhou Zou** for the scientific and critical discussions. My gratitude is extended to the rest of the lab members who have provided a friendly environment to work in: **Daniel Stark**, **Salma Srour**, **Nadia Baseer**, and **Michelle King**. I would also like to express my gratitude to **Professors Carl and Liz Smyth**, who have provided very beneficial advice in joint lab meetings.

I would like to thank **Dr Ben Phillips**, who taught me coding FIJI macros for image processing, and **Larissa Butler** who taught me CellProfiler for semi-automated analysis of DNA damage responses.

My deepest heartfelt appreciation goes to my outstanding colleagues and friends in Florey Building particularly, **Kate Kaloyanova**, **Hatoon Al Amri**, **Chris Munn**, **Andrew Wood**, **Pei Tseng** and **Laura Maple**, who have made my PhD the pleasant experience that it is. Thank you all for the smiles, laughs and the late-night/early-morning support. I would like to specially thank Kate for all the motivational conversations, walks, coffee hangouts and the funny memes, which have made my challenging days in the lab much more bearable.

I would like to thank my closest friends, **Ahmed ElSawaf**, **Fady Ghattas**, **Nada Adham**, **Salma Srour**, **Ola Shehata**, **Nagham Dous**, and **Moataz Swidan**. Thank you Ahmed and Moataz for the chill nights after exhausting days in the lab. Thank you Fady for all the phone calls you made to check on me when I was stressed. Thank you Salma and Nada for the advice and sympathetic ear. Thank you Nagham, Salma, and Ola for staying behind after work to keep me company during late-night experiments. On a side note, I would like to thank **Kevin** from Copper Pot who provided a friendly smile in his cafe during my thesis writing.

"Your education is our greatest investment."

This is a quote from my parents **Mr Tarek ElGhazaly**, and **Dr Azza Ahmed**, that will resonate with me for the rest of my life. I am the luckiest person in the world for having such supportive parents, who have been my greatest advocates for my learning and development to the scientist and the man I am today. I cannot express enough how thankful I am for my most amazing twin sister, **Hend ElGhazaly**. Hend has carried me throughout my worst times and celebrated with me my best times. She did not fail to be my backbone and the wall I lean on even remotely, and for that I am grateful. Love you Hend! I would also like to thank my grandma **Teeta Fatma** for her never ending prayers and love.

Finally, I would like to dedicate this PhD thesis to my late grandparents: **Gedo Abdel-Azim** and **Teeta Nawal**. Although, I would have loved to celebrate my accomplishment with you, I know that you are very proud of me.

Achievements during my PhD

My work throughout my PhD has been recognised by the following prizes:

- Fellow of the Higher Education Academy (2020)

- First Prize for an international online poster competition held by Scientistt.com (2020)

- First Prize in inter-departmental 3-Minute Thesis Talk (2019)

- Outstanding Poster Presentation in Faculty of Science Graduate Showcase, Sheffield. (2019)

- First Prize Poster Presentation in Cellular Microbiology Meeting in Francis Crick Institute, London (2019)

- First Prize for Departmental Talk in the University of Sheffield (2018)

Abstract

Cellular senescence is an innate physiological mechanism crucial in development, wound healing and tumour suppression. It is characterised by an irreversible cell cycle arrest, resistance to apoptosis, and an inflammatory secretome that remodels bystander cells, referred to as senescence-associated secretory phenotype (SASP). SASP acts in an autocrine or paracrine manner to reinforce senescence, transmit senescence to naive cells and activate immunosurveillance to remove cells of pathological potential. In ageing organisms, senescent cells accumulate, resulting in SASP-driven chronic inflammation, aberrant tissue homeostasis and immune functions, and age-related pathologies such as cancer. Ageing also comes with an increased susceptibility to infectious diseases but the cellular basis for this is unclear.

Salmonella Typhi causes more than 11 million cases of drug-resistant typhoid fever cases each year that are spreading intercontinentally, making it a global health concern. The typhoid toxin of *Salmonella* Typhi causes DNA damage, cell cycle arrest and cell distension, which are indicative of senescence. Toxin-induced DNA damage is associated with mortality, typhoid fever symptoms and chronic *Salmonella* carriage in animal models, which aids in pathogen shedding and disease transmission. Therefore, dissecting the typhoid toxin virulence mechanism is of utmost importance.

Using molecular and cellular biology, this thesis substantiates evidence that the typhoid toxin induces senescence *in vitro* marked by persistent DNA damage responses, increased senescence associated β-galactosidase, p21 activity, diminished lamin B1, and paracrine senescence via toxin-induced SASP (tox^{SASP}). Interestingly, previous work in our lab demonstrated that tox^{SASP} uniquely promoted *Salmonella* infection, while aphidicolin (APH), i.e. another senescence inducer, did not. This finding indicates that factors in the host secretome increase the susceptibility of bystander cells to *Salmonella* infection but the identity of the SASP factors are unknown. Using unbiased LC-MS/MS and GeneChip microarray transcriptomics, this thesis reveals tox^{SASP} constituents which were divergent from other senescence inducers, namely APH^{SASP} and ETP^{SASP}. Additionally, *in vitro* experiments implicate potential crosstalk between TGFβ and Wnt5a signalling pathway in toxin-induced senescence phenotypes. Indeed, purified Activin A, a TGFβ ligand, and Wnt5A contributed to tox^{SASP} paracrine senescence. Furthermore, TGFβ receptors knockdown via siRNAs ameliorated *Salmonella* invasion induced by tox^{SASP}.

In conclusion, this study reveals the first proteomic characterisation of a SASP induced by a bacterial toxin. The study represents a *Salmonella* hijacking mechanism via the TGFβ signalling pathway, which represents a novel host-pathogen interaction that may be of significance to invasive infections underlying typhoid fever and chronic carriage. This thesis is of broad significance as it reveals a way by which bacterial pathogens can reprogramme multicellular infection niches by hijacking the host secretome through DNA damage responses.

Table of Contents

List of Figures

List of Tables

Abbreviations list

53BP1 p53-binding protein 1

ACN Acetonitrile

ACTB Actin Beta

ACVR Activin A receptor

ADAM17 A disintegrin and metalloprotease 17

AHA L-Azidohomoalanine

ALK Activin-like kinase

AMR antimicrobial resistant

APH aphidicolin

APS ammonium persulfate

ATM Ataxia Telangiectasia Mutated

ATR Ataxia telangiectasia and Rad3 related

ATRIP ATR interacting protein

BMP Bone morphogenetic proteins

BONCAT Bio-Orthogonal Non-Canonical Amino acid Tagging

BSA bovine serum albumin

C/EBPβ CCAAT-enhancer-binding proteins beta

CCF Cytoplasmic chromatin fragments

CDK cyclin-dependent kinase

CDKi cyclin-dependent kinase inhibitor

CDT cytolethal distending toxin

CHAPS 3-((3-cholamidopropyl) dimethylammonio)-1-propanesulfonate

CM conditioned media

COVID Coronavirus

CTGF connective tissue growth factor

DALY Disability-adjusted life years

DAMP Damage-associated molecular patterns

DDR DNA damage response

DMEM Dulbecco's Modified Eagle Medium

DNA Deoxyribonucleic acid

DNA-PKc DNA-dependent protein kinase, catalytic subunit

DSB double-strand break

dsDNA double-stranded DNA

DTT Dithiothreitol

E. *Escherichia*

E8 Essential 8

EdU 5-Ethynyl-2-deoxyuridine

EGF Epidermal growth factor

ELISA enzyme-linked immunosorbent assay

ER endoplasmatic reticulum

ERAD Endoplasmic Reticulum-associated protein degradation

ERAD ER-associated degradation

ERK Extracellular signal-regulated kinase

ETP etoposide

FBS Foetal Bovine Serum

FGF Fibroblast growth factor

FST follistatin

FT flow through

g gram

GBD Global burden of Disease

GDF15 Growth Differentiation Factor 15

GnRHR Gonadotropin Releasing Hormone Receptor

GS Genotoxic senescence

GST glutathione S-transferase

H. *Haemophilus*

HCMV Human cytomegalovirus

HCV Hepatitis C virus

HDGF Hepatoma-derived growth factor

His histidine

HMG High mobility group

HMGA High mobility group proteins characterized by an AT-hook

HMGB1 High mobility group box 1 protein

HPLC High performance liquid chromatography

HQ toxin DNase inactive toxin harbouring H160Q mutation

IL interleukin

INHBA Inhibin Subunit Beta A

iNTS invasive non-typhoidal *Salmonella*

IPTG Isopropyl β- d-1-thiogalactopyranoside

IWP inhibitor of Wnt production

JNK c-Jun N-terminal kinases

KDa Kilo Dalton

KPSI kilo-pounds per-square-inch

LB Lysogeny broth

LC-MS/MS Liquid chromatography–mass spectrometry

LFQ Label-free quantification

LMIC low and middle income countries

LPS Lipopolysaccharides

M molar

m milli

MAPK Mitogen-activated protein kinase

MDR multidrug-resistant

MEF mouse embryonic fibroblast

MES 2-(N-morpholino)ethanesulfonic acid

MLN mesentric lymph nodes

MMP Matrix metalloproteinases

MOMP Mitochondrial outer membrane permeabilization

MOPS 3-(N-morpholino) propanesulfonic acid

MQ Milli-Q water

MRN Mre11-Rad50-Nbs1 complex

n nano

Neu5Ac N-Acetylneuraminic acid

Neu5Gc N-Glycolylneuraminic acid

NFκβ Nuclear Factor kappa-light-chain-enhancer of activated B cells

NiNTA Nickel-Nitrilotriacetic Acid

NK natural killer cells

ns non-significant

NT non-targeting

NTS non-typhoidal *Salmonella*

OBB Odyssey Blocking Buffer

OD Optical Density

OIS Oncogene-induced senescence

P/S Penicillin-Streptomycin

PAMP Pathogen-associated molecular pattern

PBS phospho-buffered saline

PBST PBS with 0.1% tween

PCA Principal Component Analysis

PDGF Platelet-derived growth factor

PFA paraformaldehylde

PIKK Phosphatidylinositol 3-kinase-related kinases

PLAUR Plasminogen Activator, Urokinase Receptor

PLK1 polo-like kinase 1

Plt pertussis-like toxin

psmad phospho-smad

PVDF polyvinylidene difluoride

RAW RAW 264.7 mouse macrophages

RING Response induced by a Genotoxin

RNA Ribonucleic acid

ROS Reactive oxygen species

RPA Replication Protein A

rpm Revolutions per minute

RS Replicative senescence

S. *Salmonella*

SA-β-gal Senescence Associated Beta Galactosidase

SAHF Senescence-associated heterochromatin foci

SASP Senescence Associated Secretory Phenotype

SCV *Salmonella* containing vacuole

SDF senescence DNA damage foci

SDS sodium dodecyl sulphate

SDS-PAGE sodium dodecyl sulphate–polyacrylamide gel electrophoresis

SF serum-free

Sif *Salmonella* induced filaments

SILAC Stable Isotope Labeling by/with Amino acids in Cell culture

siRNA short interfering Ribonucleic acid

SOC media Super Optimal broth

SPI *Salmonella* pathogenicity island

SSB single-strand break

ssDNA single-stranded DNA

T3SS Type 3 Secretion System

TBS Tris-buffered saline

TBST TBS with 0.1% tween

TCEP Tris(2 carboxyethyl)phosphine

TEAB Triethylammonium bicarbonate

TEMED tetramethylethylenediamine

TERT Telomerase Reverse Transcriptase

TFA Trifluoroacetic acid

TGF Transforming growth factor

TGFBR TGF beta receptor

TGFβ Transforming growth factor beta

TIMP1 TIMP Metallopeptidase Inhibitor 1

tox^{HQ-CM} conditioned media of cells treated with the typhoid toxin inactivated by a point mutation (H160Q)

tox^{SASP} or **tox^{WT-SASP}** SASP induced by the wild-type toxin

tox^{SEN} toxin-induced senescence

UN United Nations

UV Ultraviolet

VASN vasorin

VEGF Vascular endothelial growth factor

WHO World Health Organisation

WT wild-type

XF xeno-free

x g times gravity

γH2AX phosphorylated H2A histone family member X

μ micro

Part I

Literature Review

Chapter 1

Invasive infections of *Salmonella* enterica

1.1   Introduction

The United Nations has set out 12 global challenges we need to address to achieve a better and more sustainable future for all. UN sustainable development goal 3 is to end epidemics of neglected, communicable and water-borne diseases by 2030. High on this list is typhoid fever, one of our oldest killers, which affects many low-and middle-income countries where the most severely affected are children (~27%)[1]. World Health Organisation (WHO) reports that more than 2,000 children die each day of diarrhoeal diseases, which is more than HIV, measles and malaria combined, making it the second leading cause of deaths in children worldwide[2]. One of the top causes of diarrhoeal disease is *Salmonella*. *Salmonella enterica* subspecies *enterica* (henceforth *Salmonella*) is a species of rod-shaped Gram-negative bacteria that comprise more than 2500 serovars. *Salmonella* is transmitted from contaminated food and water via fecal-oral route. It is estimated that 1.8 billion people use a source of drinking water contaminated with faecal matter[3], which increases the risk of typhoid. With respect to human disease, *Salmonella* is grouped into i) typhoidal serovars which cause global epidemics of invasive enteric fever, also known as typhoid and paratyphoid fever, and ii) non-typhoidal serovars which result in a self-limiting non-invasive gastroenteritis.

1.2   Human diseases caused by *Salmonella* enterica

1.2.1   Non-typhoidal *Salmonella*

Non-typhoidal *Salmonella* (NTS) serovars (+2500) are zoonotic and have broad-host tropism[4]. NTS causes ~100 million causes of food poisoning and ~150,000 deaths per year worldwide, making it a global health concern. The most common NTS is *Salmonella* Typhimurium sequence type 19 (ST19), which infects humans and food-chain animals[4]. NTS results in self-limiting gastroenteritis

that is usually restricted to the terminal ileum and the colon by initiating a localised inflammatory response, i.e. non-invasive[5], with relatively mild symptoms such as diarrhoea and fever.

1.2.2 Invasive non-typhoidal *Salmonella*

The increasing number of immunocompromised individuals (e.g. through the AIDS pandemic, or the ageing population) has driven the evolution of NTS serovars that are adapted to the immunocompromised host where they cause a devastating invasive infection (iNTS disease; 535,000 cases/77,500 deaths in 2017)[6]. Individuals infected with iNTS typically present bacteraemia and a febrile illness with a clinical presentation similar to typhoid fever **(Section 1.2.3)**. The most dominant serovars with an invasive potential are currently *Salmonella* Typhimurium and and Enteritidis[7]. The prototype iNTS serovars *S.* Typhimurium ST313 is on the rise, has antibiotic resistance, and is associated with higher fatality rates than their non-invasive NTS counterparts, e.g. ST19[6,8]. Unlike non-invasive NTS, ST313 reduces inflammation, replicates in macrophages and results in systemic infections[9]

1.2.3 Typhoidal *Salmonella*

Enteric fever, or typhoid fever, is a systemic, lethal disease that is a result of an infection by the typhoidal *Salmonella* serovars Typhi, Paratyphi (A, B, and C), and Sendai which are human-specific pathogens and therefore unable to elicit disease in other animals[4]. Typhoid patients often suffer from high-grade fever (>39°C), constant fatigue, abdominal pain, diarrhoea, hepatosplenomegaly, rash, nausea, anorexia, constipation, headache and dry cough[10,11]. *Salmonella* can result in internal organ damage such as intestinal perforation, the most severe complication observed in *S.* Typhi infections. Typhoid fever is diagnosed in ∼10-20 million people worldwide and kills more than 200,000 people per year[12,13] **(Fig.1.1)**, which presents a lower disease burden but higher mortality rate than NTS. In addition, a recent Global Burden of Disease (GBD) study estimated that typhoid fever results in approximately 10 million cases with disability-adjusted life-years (DALYs) in 2017[6]. It is mainly prevalent in countries with scarce sources for clean food and water particularly in regions such as South Asia[6], southeast Asia[14], and sub-Saharan Africa[15]. The highest incidences of typhoid cases, and mortality is amongst children below 15 years old (∼56% of the cases, ∼59% of the deaths), which progressively decreases with age[6]. Infections with typhoidal *Salmonella* are not restricted to low- and middle-income countries (LMICs) countries, but also spreads to high-income countries through travel from endemic settings, or through chronic carriers of *Salmonella* who prepare food **(Section 1.3, Fig.1.1)**.

1.3 Chronic carriers of *S.* Typhi

During typhoid convalescence, 10% of individuals exhibit temporary *Salmonella* carriage (i.e. shedding *Salmonella* for less than 12-months), while 1-5% develop a chronic *S.* Typhi infection (*Salmonella*
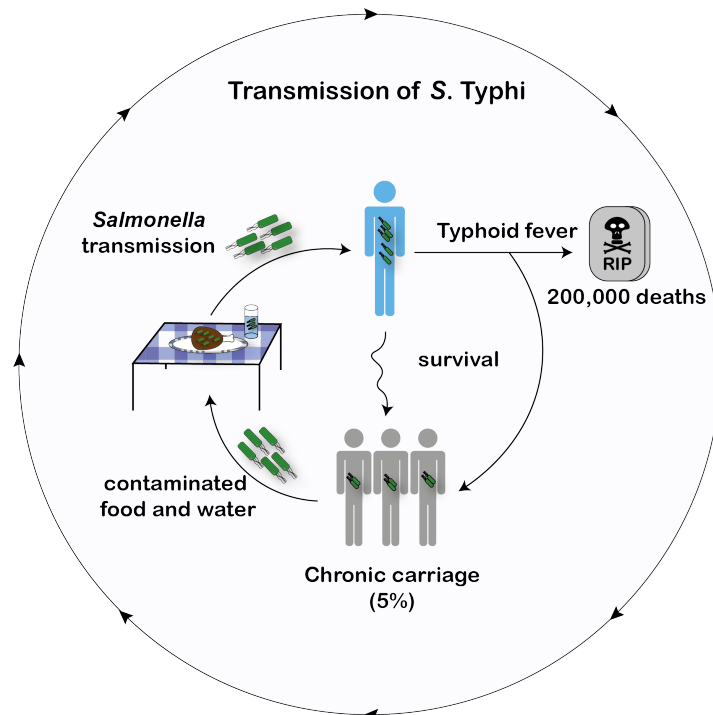
Figure 1.1|The transmission cycle of *Salmonella* Typhi. *Salmonella* is transmitted through contaminated food and water. Some of the infected develop severe typhoid symptoms and die, but some recover, retain the pathogen, and remain asymptomatic. Chronic carriers can then spread *Salmonella* undetected via shedding the bacteria in faeces, which can contaminate food and water sources and infect otherwise healthy individuals (e.g. sewage draining into drinking water).

carriage 12-months or more)[16]. Chronic carriage is not observed in NTS or iNTS infections, though temporary carriage ($\sim$ 55 days) is observed in 2% of cases[16,17]. In addition to these individuals, 25% of individuals do not develop any acute symptoms of typhoid fever, but shed *S.* Typhi in stools indicating asymptomatic chronic carriage[16] (**Fig.1.1**). The most infamous chronic carrier was Typhoid Mary who worked as a cook and passed the infection onto her customers in the 1850s, and Mr N the milker who infected farm products[18]. Interestingly, incidences of *S.* Typhi chronic carriage increased with age, and were more prevalent in females[16,19].

It is thought that chronic infection develops following dissemination to the reticuloendothelial system where *Salmonella* Typhi resides in the gallbladder[20]. From there, *Salmonella* can be excreted through bile into the gastrointestinal tract triggering relapse or shed in stools, which contributes to disease transmission[16]. Increasing evidence shows that *Salmonella* is evolutionarily adapted to thrive in the gallbladder[21,22,23]. *In vitro* studies indicated that *Salmonella* divide preferentially in gallbladder mimicking conditions[23], and specifically to cholesterol coated gallstones[24]. Gallstones aid in the formation of biofilms that protect bacteria from the immune system and allow them to thrive[25], making gallstones a suspected risk factor of persistent infection[26].

1.3.1 *Salmonella* and gallbladder cancer

A correlation between *S.* Typhi infections and gallbladder cancer is established [27]. The current notion is that alongside gallbladder stones, *S.* Typhi is a major risk factor in gallbladder cancer [26]. In Chile where *S.* Typhi is endemic, $\sim$44% of gallbladder cancer patients were positive for *S.* Typhi [27]. The majority of chronic carriers can be treated with a 4-week antibiotic therapy ($\sim$80% of the cases). However, if patients have gallstones, antibiotic treatment in addition to cholecystectomy (i.e. the removal of the gallbladder) might be necessary, to prevent complications and continued shedding of bacteria, which is invasive and expensive [28,29].

Salmonella is sufficient to induce carcinogenesis in mice and transform mouse embryonic fibroblasts that are genetically predisposed to develop cancer, e.g with mutated p53, amplified c-Myc [30]. As yet, the molecular basis for *Salmonella*-induced transformation is unknown. It is interesting to speculate that a virulence factor (e.g. typhoid toxin; **Section 1.8**) encoded by *Salmonella*, might contribute to oncogenesis.

The high fatality rate and the associated complications of invasive *Salmonella*, whether typhoidal or non-typhoidal, beg for research to examine their virulence in an effort to prevent lethal outbreaks.

1.4 Diagnostics, current treatments and preventions

1.4.1 Diagnosis

All diagnoses of enteric fever or invasive Salmonellosis begin with examining clinical signs and symptoms. However, systemic infections of both typhoidal *Salmonella* and iNTS, are often misconstrued for other febrile diseases such as dengue fever and malaria [8]. Symptoms can even include anaemia, pneumonia-like symptoms, and in some cases absence of diarrhoea, which could deflect from suspecting Salmonellosis. As a result, inappropriate treatments are administered to the patients and *Salmonella* is not directly tackled.

Typical diagnostics examine stool, blood or urine which measure shedding of *Salmonella* [31]. The most commonly used measures are bacterial cultures and Widal test [32]. Bacterial cultures are carried out with blood samples from patients and grown in controlled nutritious LB broth to examine for *Salmonella* growth. Widal tests utilise antigens from killed *Salmonella* and examine reactivity of circulating antibodies from patients sera with these antigens. Both tests are currently the gold standard and do not require expensive special lab equipment. However, they lack sensitivity, due to the low titre of *Salmonella* found in blood during bacteremia, or due to antibiotics that have been used prior to the test. In contrast, bone marrow test is the most sensitive as *Salmonella* Typhi has been reported to invade preferentially and resist antibiotic treatments in bone marrow cells [33,34]. However, it is very invasive, and requires trained specialists and state-of the art sterile medical equipment that is not

available in developing countries. Surveillance programmes and academic studies exploit genomics, proteomics, transcriptomics, *in vivo*-induced antigen and immunoaffinity proteomics-based technologies, which are fuelling novel diagnostic approaches though these may be better suited to surveillance monitoring rather than point-of-care diagnosis[35].

1.4.2 The rise in antibiotic resistant *Salmonella*

Untreated, typhoid fever historically had a mortality rate of up to 20% but this declined with the introduction of chloramphenicol in the 1940s[12,13,36,37]. With the appropriate antibiotic, mortality can be as low as 1%[12,37]. Antibiotics are usually the immediate treatment for patients infected with typhoidal *Salmonella*[4]. However, antibiotic treatment of NTS is restricted to immunocompromised patients and infections that have become invasive, due to the fact that it would prolong NTS excretion[4].

The emergence of multidrug-resistant (MDR) *Salmonella* has become a global health concern due to its potential to increase mortality to the alarming rates observed in the 1940s[37,38,39]. Additionally, MDR results in longer hospitalisation, force the use of more expensive drugs and hence increase health care costs in several countries[40,41].

Whole genomic sequencing of thousands of isolated *S.* Typhi revealed that the most dominant circulating *Salmonella* strain is H58, which is an MDR strain that is thought to have originated in South Asia and is now being transmitted intercontinentally to Africa and Southeast Asia[42]. Antimicrobial resistance (AMR) can also develop via gene transfer facilitated by transposon or plasmid exchange, or by chromosomal mutations[43]. In the case of H58 strain, AMR genes were initially associated with a self-transferrable IncHI1 plasmid that conferred multiple AMR genes resistant to previously prescribed antibiotics such as chloramphenicol, co-trimoxazole and ampicillin, making it a global threat[42,44,45]. A study by Wellcome Trust highlighted the disturbingly rapid spread of H58 typhoid cases demonstrated by the increase in AMR typhoid cases in Malawi from ∼7% to 97% between 2010 and 2014 only[45]. Whilst AMR arises naturally, it can also arise due to the misuse of antibiotics, for example through incomplete therapies, incorrect doses or incompatible antibiotics[4,46].

Currently, the first-line of antibiotics are fluoroquinolones, which block bacterial DNA replication via inhibiting the supercoiling activity of DNA gyrase. However, in 2017, the World Health Organisation declared fluoroquinolone-resistant *Salmonella* a high priority threat due to its prevalence and severity of the disease they cause[47]. The antibiotic resistance arose as a result of a mutation in the gyrase enzyme that has reduced its affinity to the drugs, and hence ameliorated their inhibition.

With increasing antimicrobial resistance, commonly used treatments are less effective. Thus, we need to advance understanding of disease mechanisms to develop new interventions and diagnostics.

1.4.3 Vaccination

Given the rise in MDR *Salmonella*, vaccines have been developed using various methods in an attempt to control outbreaks, and build herd immunity. Currently, there are no vaccinations for invasive *Salmonella* except for *S.* Typhi. There are two vaccines typically used: i) a live attenuated Ty21a and ii) unconjugated Vi capsular polysaccharide (Vi CPS), which is a capsule that coats *S.* Typhi and protects it from the host's immune system[48] (described in **Section 1.7.2.1**). Neither vaccinations are authorised for use in children younger than 2 years old, who represent a huge portion of the typhoid burden (∼30%). Recently, WHO authorised the use of a new typhoidal conjugated vaccine (TCV), where Vi capsule is conjugated with tetanus toxoid as a carrier protein[49], which has been shown to be safe and increase efficiency in children older than 6 months in phase III clinical trials[1,50,51]. The characteristics of each vaccine is summarised in **Table 1.1**.

Vaccines					
	Vaccine	**Properties**	**Advantages**	**Disadvantages**	**Efficacy**
Authorised	**Ty21a**[48]	• live attenuated • oral • developed using non-specific mutagenesis • Vi capsule absent	• allows for cross-reactivity with other typhoidal strains that do not express Vi e.g. Paratyphi • 7 years protection	• 3-4 doses • Not authorised for <6 years • Difficult to swallow for children	50-80%
Authorised	**Vi CPS**[48]	• unconjugated Vi capsular polysaccharide • intramuscular injection • purified from *S.* Typhi	• 1 dose • Low reactogenicity	• short-term protection • Protection against *S.* Typhi only • Not authorized <2 years old • 2 years protection	50-80%
In development	**TCV**	• Vi capsule conjugated with tetanus toxoid as a carrier protein[49] • intramuscular injection	• safe in children >6 months[1,50,51]	• 3 years protection (less than Ty21) • Still in trials	80%

Table 1.1|Effective typhoidal vaccines currently authorised or in development.

Modelling predicts that vaccination alone is insufficient to eradicate typhoid[52], and thus integrated control strategies are required with improved antibiotic therapies, diagnostics, and education programmes. Therefore, there is still current need to develop existent or alternative strategies to treat and prevent invasive *Salmonella* from establishing disease. To do this, the virulence of *Salmonella* and its pathogenesis is currently a major focus of the field.

1.5 Pathogenesis of *Salmonella*

1.5.1 Bacterial entry into host cells

Both typhoidal and NTS serovars enter the body via ingestion of contaminated food and/or water (**Fig.1.1**). The first contact with the host is with non-phagocytic cells, such as gut epithelial cells (**Fig.1.2**). They adhere to the surface of gut epithelial cells via adhesins, which facilitate bacterial attachment to the host cell[4,53]. The *Salmonella* genome contains pathogenicity islands that encode important virulence factors for cellular invasion[54]. Notably, expression of *Salmonella* pathogenicity
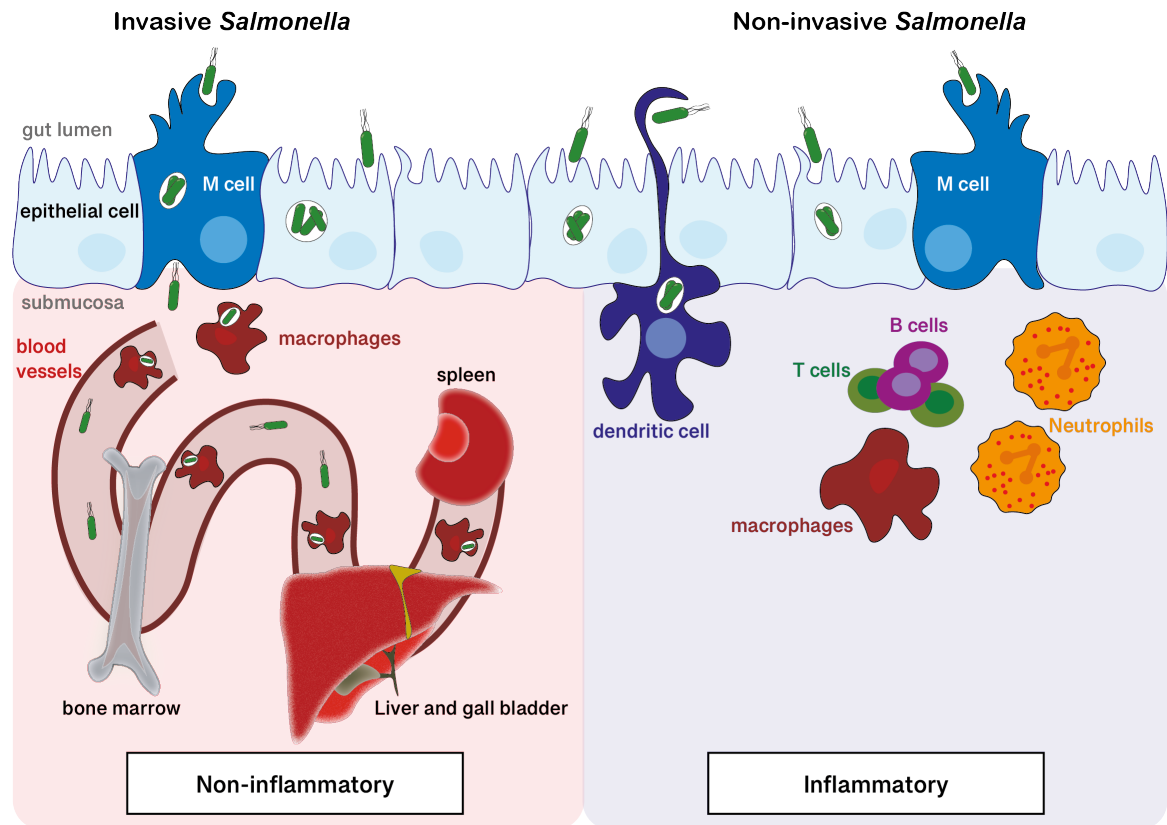
Figure 1.2| Pathogenesis of invasive and non-invasive *Salmonella*. *Salmonella* can infect gut epithelial cells, macrophages, M cells, and dendritic cells. Invasive *Salmonella* breach the gut epithelial barrier, evade any immune responses, and infect macrophages or remain free in the blood stream (i.e. bacteraemia), where it spreads to sterile systemic sites such as the bone marrow, liver, and/or spleen (left panel). In contrast, non-invasive *Salmonella* elicits a localised inflammatory response marked by neutrophil transmission (right panel).

island 1 (SPI1) is activated in the high salt environment of the host gut and encodes a needle-like assembly protein, the type 3 secretion system (T3SS1), that delivers virulence effector proteins directly into the cells, forcing *Salmonella* internalisation into host cells[55]. The virulence effectors then hijack the actin cytoskeleton indirectly (e.g. SopE activation of Rho GTPases) or directly (e.g. SipA binding of actin filaments), which promote membrane ruffling and macropinocytosis of *Salmonella*[55] **(Fig.1.3)**.

1.5.2 Survival in host cells

Intracellular *Salmonella* then resides in a phagosome-like compartment known as the *Salmonella* containing vacuole (SCV) within cells of the intestinal epithelium[56]. The SCV enters the lysosomal pathway and the acidification of the SCV activates expression of *Salmonella* pathogenicity island (SPI2) that encodes T3SS2 which delivers virulence effectors that sustain intracellular survival **(Fig.1.3)**. For example, *Salmonella*-induced filaments (Sif) redirect nutrients into the vacuole to allow for a nutrient rich niche suitable for replication[57,58]. Additionally, SifA and SopD2 produced by *Salmonella* maintain the vacuolar membrane and its integrity[59]. Mutant SifA *S.* Typhimurium led
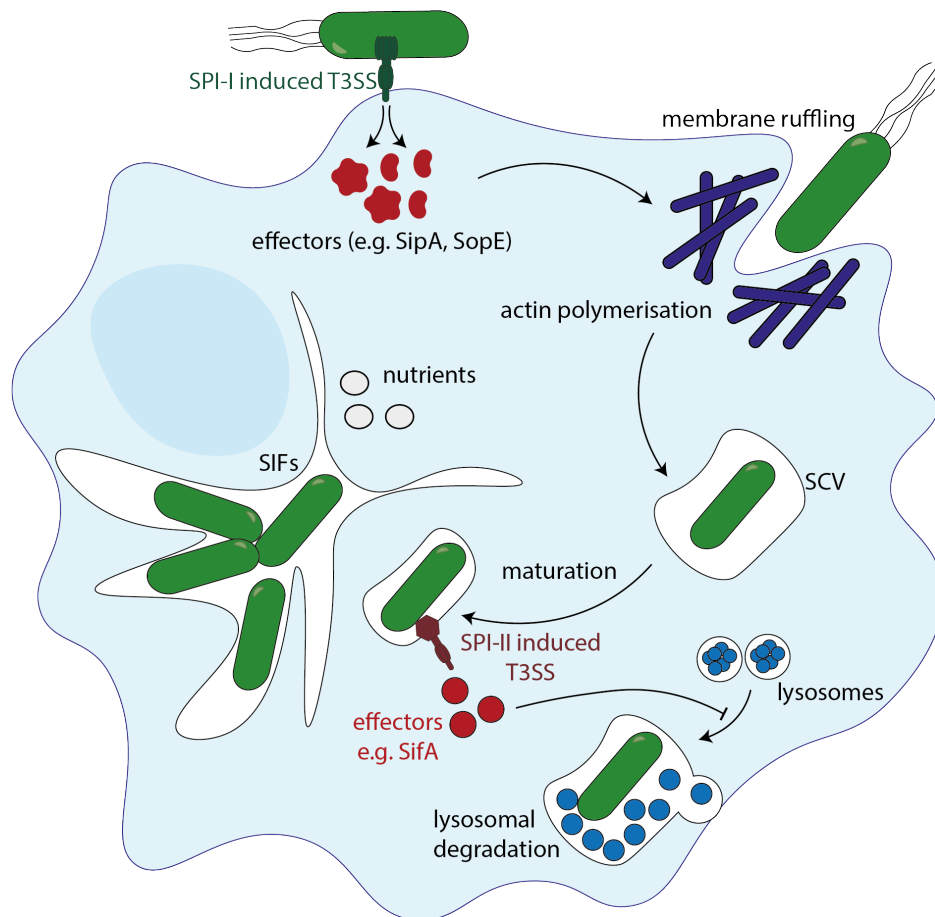
Figure 1.3| *Salmonella* **entry into the cell.** *Salmonella* utilises its needle-like type 3 secretion system (T3SS) encoded by SPI-1 to inject effectors that polymerise actin and promote *Salmonella* engulfment. Initially *Salmonella* resides in an endosome which is referred to as a *Salmonella* containing vacuole (SCV). Once in the SCV, *Salmonella* utilises T3SS encoded by SPI-2 to release effectors necessary for maintenance of the SCV.

to the bacterial escape into the cytosol of macrophages and promoted *Salmonella* killing[60] **(Fig.1.3)**. Unlike other phagosomes, SCV evades lysosomal degradation, which promotes its survival[61,62]. Interestingly, the T3SS2 effector SifA sequesters Rab39-mediated retrograde trafficking of SCV into lysosomes thereby preventing lysosomal degradation[63]. Next, *Salmonella* alongside the SCV divide, until there is one bacterium per SCV in the host cell[64] **(Fig.1.3)**.

1.5.3 Interactions with intestinal innate immunity key to dissemination

The distinct diseases caused by NTS and typhoidal *Salmonella* are determined by a critical interaction with intestinal innate defences. For example, host cell inflammasomes sense virulence factors of NTS (e.g. flagella, T3SS of prototype NTS serovar *S.* Typhimurium ST19) triggering pyroptosis of infected epithelial cells and macrophages that recruits neutrophils. As a result, neutrophils kill NTS, prevent dissemination and restrict disease to a localised non-invasive infection in the intestinal mucosa **(Fig.1.2)**[65,66,67,68]. In contrast, typhoidal serovars (e.g. *S.* Typhi, *S.* Paratyphi A) evade inflammasome defences and disseminate within infected macrophages to cause invasive infections[69]. Similarly, iNTS *S.* Typhimurium ST313 also evades the inflammasome, which is thought to

contribute to immune evasion and dissemination from the intestinal mucosa[70]. Immune evasion by invasive serovars of typhoidal and iNTS *Salmonella* is partly facilitated by degradation of genes that encode pro-inflammatory virulence factors, which are actively expressed in the non-invasive serovar NTS serovar *S.* Typhimurium ST19[71].

1.5.4 Systemic infection

Unlike NTS, typhoidal *Salmonella* usually do not elicit an inflammatory response at the early stages of infection. Whilst *S.* Typhimurium has evolved to flourish in inflammatory conditions to outcompete the gut microbiota, it is thought that *S.* Typhi lost that ability to thrive systemically[4,72,73]. The lack of an inflammatory response allows typhoidal *Salmonella* to evade the immune system and become systemic where it reaches liver, gallbladder and spleen[4]. For the typhoidal strain and in keeping with a lack of inflammation, there is no neutrophil transmission across the intestinal epithelium in comparison with NTS which are restricted by infiltrating neutrophils **(Fig.1.2)**[74]. Invasive strains such as *S.* Typhi disseminate within mononuclear phagocytic cells including macrophages or dendritic cells, via three routes[75]: (i) *Salmonella* can infect macrophages resident in the underlying gut-associated lymphoid tissue (GALT) that contain immune effector sites such as Peyer's patches, which are distributed across the lamina propria within the intestinal mucosa, or (ii) *Salmonella* can drain from the Peyer's patches into mesenteric lymph nodes (MLNs) where they can infect macrophages and other mononuclear phagocytes, and finally, (iii) free *Salmonella* can invade the bloodstream from the MLNs causing a transient primary bacteraemia characteristic of typhoid fever. In the blood, *Salmonella* moves out of the circulation by mononuclear phagocytes. Regardless of the mechanism, infected macrophages migrate to organs of the reticuloendothelial system (e.g. liver, spleen) where *Salmonella* survives intracellularly, as described in **Section 1.5.2**[56,63] **(Fig.1.3)**. *S.* Typhi resides at these systemic sites until onset of typhoid fever (8-14 days), which is typically accompanied by sustained, albeit low level (1–10 organisms/mL), secondary bacteremia lasting several weeks[76] **(Fig.1.2)**.

1.6 Modelling *Salmonella* infection and typhoid fever

Given that *S.* Typhi is human-specific, there is no animal model that faithfully recapitulates typhoid fever in humans. *S.* Typhimurium causes human disease but is a pathogen that causes a systemic typhoid-like infection in mice, which has been exploited to provide information on *Salmonella* invasion, transmission and dissemination[77,78,79]. However, there are a number of important differences between *S.* Typhi and *S.* Typhimurium **(Fig.1.4)**. For example, (i) SPI2 is required for intracellular survival of *S.* Typhimurium but not *S.* Typhi[80], (ii) *S.* Typhimurium and *S.* Typhi genomes share 11 common SPIs but some are specific to *S.* Typhi (SPI-7, 15, 17, and 18) or *S.* Typhimurium (SPI-14)[71], and (iii) *S.* Typhi has unique virulence factors implicated typhoid, e.g. Vi capsule, typhoid toxin[81]. Much attention has been focussed on developing animal models that are permissible for *S.* Typhi. For instance, Toll-like receptor 11 (TLR11) is present in mice but not in humans and recognises the
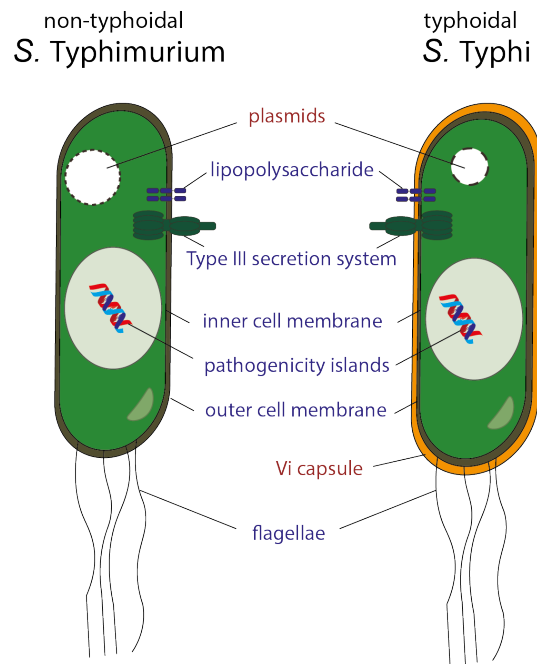
Figure 1.4| Structural comparison between *S.* Typhimurium and *S.* Typhi. Similarities between both serovars are indicated by blue text and differences are indicated by red text. The small plasmid in *S.* Typhi depicts genomic degradation (Inspired by diagram from de Jong et al 2012[71]).

Salmonella flagellin, which is a pathogen-associated molecular pattern (PAMP). Knocking out TLR11 disrupts PAMP detection allowing systemic *S.* Typhi and *S.* Typhimurium infections[82]. Having allowed *S.* Typhi to enter the vascular system, effects on the liver, gall bladder and other usual targets of the pathogen could be studied in mice.

Another approach was to humanize mice by engrafting human immune cells including B cells, NK cells, monocytes, CD4+ and CD8+ cells into immune-deficient mice. The engraftment allowed *S.* Typhi to replicate normally in mice and assisted in modelling long-term persistent infection[77,83]. After a few days, the infection becomes similar to human typhoid and leads to lethality.

1.7 *S.* Typhi adaptation to the human host (Fig.1.4)

1.7.1 Genomic degradation

S. Typhi is a human-restricted pathogen while *S.* Typhimurium infects a broad-range of animal hosts[4]. 90% of genes are identical in *S.* Typhi and *S.* Typhimurium ST19[84]. Of the 4,000 genes in *S.* Typhi, 200 are functionally disrupted but these genes are actively expressed in *S.* Typhimurium ST19[71]. *S.* Typhi's genome degradation is thought to contribute to its human host restriction. Similarly, *S.* Typhimurium ST313, which was identified in 2009 as causing a typhoid-like bacteraemia in immunocompromised HIV-infected individuals, is also undergoing genome degradation in genes that are expressed in *S.* Typhimurium ST19 but degraded in *S.* Typhi[85]. Some of the virulence factors that were degraded in *S.* Typhi include motility, chemotaxis factors and the type III secretion system

effectors that are usually found in *S.* Typhimurium and have been shown to promote infection of animal hosts[86]. One such factor is GtgE, a type III secretion system effector, found in *S.* Typhimurium but not *S.* Typhi. GtgE degrades Rab32, which is responsible for lysosomal biogenesis and bacterial killing in animals[87]. Therefore, GtgE-mediated Rab32 degradation allows the survival of intracellular *S.* Typhimurium in deficient lysosomes within animal hosts. Spanò and Galán (2012) demonstrated that the expression of GtgE in engineered *S.* Typhi enabled the normally human-specific pathogen to survive in a mouse and thus demonstrated an example of how host specificity is controlled[87].

1.7.2   Gene Acquisition

1.7.2.1   Vi capsule and immune evasion

S. Typhi also encodes unique virulence factors, e.g. Vi antigen. Vi is a polysaccharide antigen that forms the capsule surrounding *S.* Typhi (**Fig.1.4**). It is thought that Vi masks *S.* Typhi from the immune system, inhibiting an immune response in comparison with *S.* Typhimurium[88]. Infecting mice with *Salmonella* Typhi lacking the Vi capsule allowed host immune deposition of complement proteins (C3) on *Salmonella*, resulting in *Salmonella* clearance from mouse tissues[89]. However, typhoidal serovars *S.* Paratyphi and *S.* Sendai do not express Vi, but can still cause enteric fever. Additionally, *S.* Typhi with Vi mutation still causes a typhoid-like illness[90]. Therefore, it is likely that virulence factors of *S.* Typhi work in combination to cause typhoid fever.

1.7.2.2   The typhoid toxin.

A major focus of the field has been understanding how *S.* Typhi causes invasive typhoid fever while the highly-related NTS serovars cause non-invasive gastroenteritis. Genomic analysis of *S.* Typhi and *S.* Typhimurium revealed a novel toxin encoded only in *S.* Typhi[91] (**Fig.1.5a, 1.5c**). Similarly, other typhoidal strains encode the typhoid toxin such as *S.* Paratyphi which highlights its importance[92]. Although the typhoid toxin is largely absent in 2000+ NTS serovars, 15 NTS serovars were found to encode typhoid toxin homologues, the best-characterised being *S.* Javiana, which encodes Javiana toxin[93,94].

1.8   The role of the typhoid toxin in disease

At the outset of my PhD, the typhoid toxin had been identified as a novel chimeric exotoxin secreted by typhoidal *Salmonella*[81,95,96]. In a seminal Nature paper in 2013, intravenous injection of purified typhoid toxin into a mouse was shown to induce the deadly symptoms of typhoid fever including 100% lethality, which followed weight loss and decreased number of monocytes and neutrophils[81,97]. In contrast, the typhoid toxin facilitated host survival in a mouse model infected with *S.* Typhimurium engineered with the toxin islet[78]. The toxin suppressed intestinal inflammatory responses, promoted

host survival and established chronic bacterial carriage whereby only animals infected with toxigenic *Salmonella* were viable at 6 months. Similarly, the NTS strain, *S.* Javiana, encodes the Javiana toxin with an identical CdtB subunit to the typhoid toxin. Mice infected with wild-type *S.* Javiana exhibited reduced pathology, intestinal inflammatory responses, and increased systemic spread relative to infection with *S.* Javiana ΔCdtB[98,99]. These mouse infection studies indicated that the toxin plays an immune-evasive role important in suppressing innate immune responses and establishing systemic infections, which contrasted with studies using purified toxin that indicated a role in acute typhoid symptoms. Indeed, human infection challenge with wild-type *S.* Typhi and the toxin null mutant showed that the toxin was not involved in initiating acute typhoid fever but instead reduced human pathology and played a significant role in systemic phenotypes such as bacteraemia[100]. The toxin-induced phenotypes during infection, i.e. survival, bacteraemia and chronic carriage[78,99,100], and the increased mortality observed with intravenous injection of the toxin[81], represent the conflicting disease outcomes of typhoid fever patients (**Fig.1.1**).

Since its discovery the typhoid toxin has been considered one of the main virulence factors of *S.* Typhi and became at the forefront of the research on typhoid fever. This thesis specifically addresses the effects of the typhoid toxin on host human cells. The next part of this chapter described the typhoid toxin in more detail.

1.9   Typhoid toxin structure and function

1.9.1   AB toxins

The typhoid toxin belongs to a large family of potent proteins known as the AB toxin family[81,101], which encompasses many plant and bacterial toxins. The family's name is derived from their composition of two subunits, A and B[102]. The "A" subunit is for "active" and usually refers to enzymatically active subunits that exert an effect on host cells. The "B" subunit refers to proteins which mediate "binding" to the receptor. The typhoid toxin was discovered by virtue of its similarity to cytolethal distending toxins (CDTs). CDTs are tripartite proteins (i.e. consist of 3 subunits) secreted by a variety of Gram-negative bacteria including *Haemophilus ducreyi*, *Escherichia coli* and *Shigella*[97] and usually adopt an AB_2 structure. The three subunits are CdtA, CdtB and CdtC[103], where CdtB is the A subunit, and CdtA and CdtC are the B subunits. However, interestingly *Salmonella* Typhi did not encode CdtA and CdtC but still induced toxigenic effects dependent upon CdtB[91]. In 2008, Spano and colleagues found that the CdtB of typhoid toxin formed a complex with PltA and PltB[96], which are homologues of pertussis toxin (**Fig.1.5a, 1.5c**), an AB_5 toxin (i.e. 1 PltA is the A subunit bound to 5 PltB) that contributes to whooping cough during *Bordetella pertussis* infection[104].
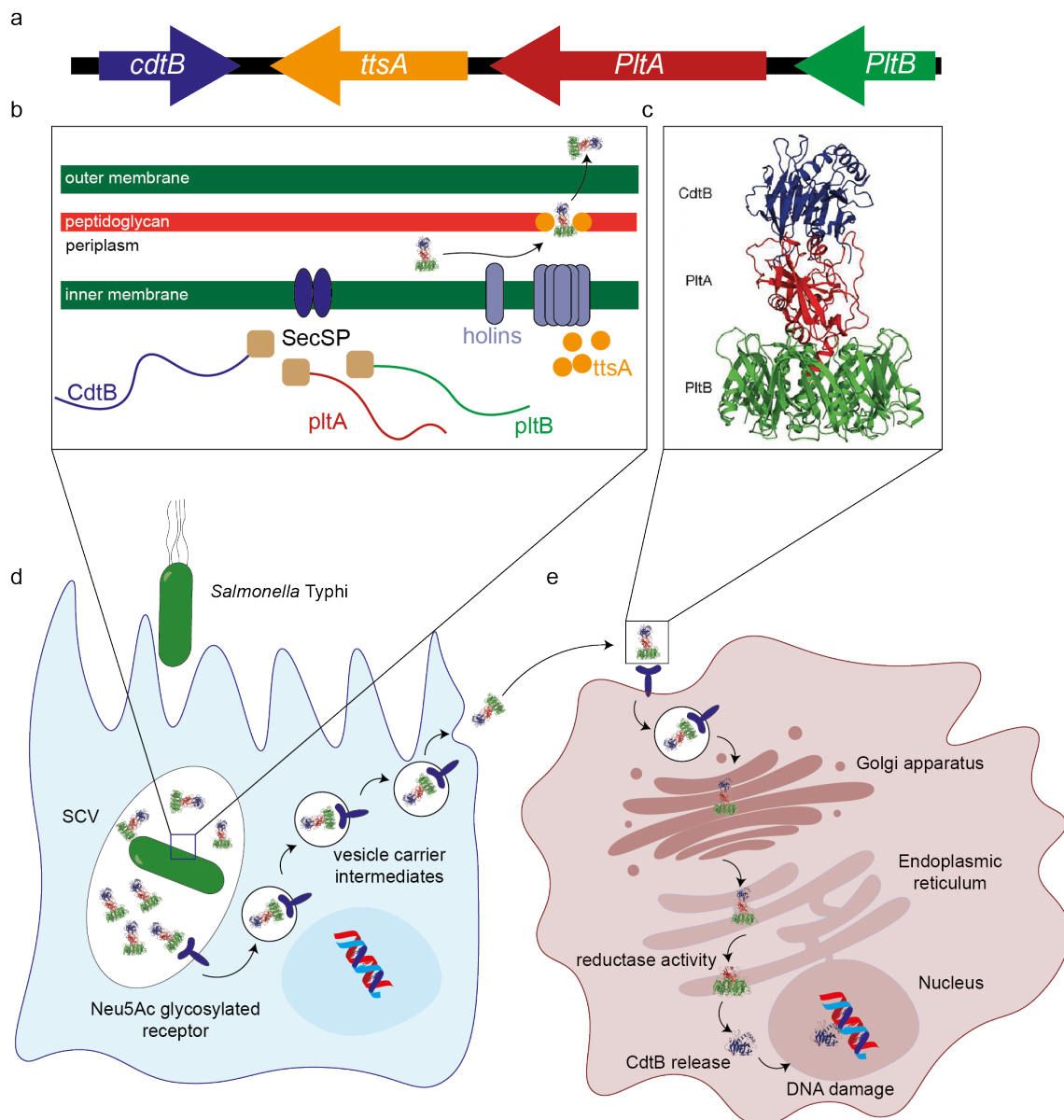
Figure 1.5|The typhoid toxin synthesis and transport. a, The typhoid toxin encoding island depicting the three subunits and a murmidase, ttsA. **b,** Illustration of the *Salmonella* membrane showing assembly of the toxin subunits in the periplasm. Potential holins and ttsA collaborate to allow for the holotoxin to be secreted out of *Salmonella*. **c,** The 3D structure of the typhoid toxin[81]. **d,** Only when *Salmonella* is in the SCV, does it secrete the typhoid toxin. The toxin is then sorted into vesicle carrier intermediates via its PltB subunit that binds to the Neu5Ac receptors, trafficked to the membrane and exocytosed. **e,** Retrograde trafficking of the typhoid toxin in an autocrine and/or paracrine manner.

1.9.2 Evolution of the structure of the typhoid toxin

The typhoid toxin is a unique chimeric toxin that adopts an A_2B_5 architecture[81,92]. The "A" subunits are composed of PltA (pertussis toxin) and CdtB (cytolethal distending toxin), which are usually independent bacterial toxins[105]. The "B" subunit is composed of five PltB (Pertussis-like toxin B) subunits, a homologue of one of the components of the heteropentametric B subunits in pertussis toxin **(Fig.1.5a, 1.5c)**.

1.9.3   CdtB of the typhoid toxin

In the typhoid toxin, the CdtB has structural and functional homology to mammalian DNase[97]. Early studies characterised the function of CdtB through experiments using other bacterial CDTs that constitute CdtB homologues[97].

Structure alignment of *H. ducryei* CdtB with DNase I revealed two conserved catalytic histidines (H160 and H274) critical for toxicity. Similar to DNase, wildtype CDT showed cell cycle arrest and plasmid relaxation *in vitro*. In fact a point mutation on the catalytic position histidine 160 to glutamate (i.e. H160Q or tox^{HQ}) abolished toxicity *in vitro*[97]. However, in comparison to bovine DNase I, CdtB only retains 0.01% activity *in vitro*, which has been attributed to the presence of Valine at position 118 in CdtB in place of a glutamate in DNase[97]. In addition, three DNA substrate binding residues, Arg 144, Asn 201, Arg117 were found in CdtB at the equivalent 3D positions in DNase (Arg11, Asn170, and Arg41 respectively)[97]. Triple-mutant of these domains diminished toxic activities but did not abolish it, providing insight into CdtB and DNA interaction.

The CdtB of typhoid toxin showed $\sim$50% sequence identity to the CdtB of *H. ducryei* whereby the catalytic and DNA binding residues were conserved[81]. Regardless of the structural differences to DNase, comet assays performed *in vivo* and *in vitro* indicate that the typhoid toxin causes DNA fragmentation via its CdtB subunit[106,107].

Indeed, when the typhoid toxin was applied to cultured cells, it resulted in a DNA damage response, cell cycle arrest and cell distension[81,96,106], which have become the established readouts for assaying toxicity. Interestingly, all observed effects of the typhoid toxin described in **Section 1.8** were dependent on eliciting a DNA damage response (DDR) by the CdtB nuclease activity. Deleting or rendering the CdtB subunit inactive via H160Q point mutation, reversed all these effects of the typhoid toxin. This implicates the DNase activity of the typhoid toxin in the disease phenotypes of *S.* Typhi. Most recently, our lab[106] implicated the CdtB-induced DNA damage response in senescence (discussed in **Chapter 2**), which enhanced *Salmonella* infections in host human cells.

CdtB is bound to PltA by disulphide bonds mediated by C-terminal cysteines in PltA (Cys214) and CdtB (Cys269) **(Fig.1.5c)**[81,105]. These cysteine residues are specific to the typhoid toxin subunits and missing from their respective homologues in other species, i.e. pertussis toxin in *Bordetella pertussis*, and CDTs in a broad range of Gram negative bacterial pathogens. When the toxin is exposed to a reducing environment, e.g. the cytosol of the cell, the disulphide bond is broken and CdtB is free to translocate to the nucleus via the Golgi and ER complexes **(Fig.1.5e)**[105], where it exerts its DNase activity.

1.9.4 PltA subunit

PltA has ADP-ribosyl transferase activity with unknown targets. When intestinal epithelial cells were infected with a PltA mutant *S*. Typhi, the toxin lost its intoxication ability. Mutating its catalytic residue however showed no difference to the wild type toxin, demonstrating that PltA is only required for CdtB-mediated toxicity, i.e. by linking CdtB to the receptor binding subunit PltB (**Fig.1.5c**)[96].

1.9.5 PltB subunit

The typhoid toxin has five PltB subunits arranged in a pentameric structure with a central channel. PltB subunits are thought to have a binding site that bind oligosaccharides in a location similar to subunits in other toxins that are known to bind glycoproteins[81]. The linear arrangement of the subunits within the typhoid toxin dictate that there would be no interaction between CdtB and PltB, since PltA is located between these two subunits (**Fig.1.5c**).

1.10 Production and secretion of the typhoid toxin

S. Typhi is thought to invade intestinal epithelial cells, M cells, and immune cells such as macrophages by adhering to their surface and getting internalised. It is only when *S*. Typhi invades human cells and resides in the SCV does it start to express the typhoid toxin from ~3h post-infection[91,96] (**Fig.1.5d**).

The genome islet of the typhoid toxin encodes the toxin subunits pltB, pltA and cdtB plus the sty1889 gene, also known as ttsA (**Fig.1.5a**). The proximity of ttsA to the genes that code for the toxin indicated functional relevance. TtsA is a muramidase and belongs to a class of bacteriophage endolysins, which when knocked out led to the disruption of toxin secretion[95]. Although bacteriophage muramidase activity usually leads to bacterial lysis, it is thought that TtsA has been adapted to secrete the typhoid toxin in *S*. Typhi. In this context, it is thought that TtsA is transported by unidentified holins that form a channel through the inner bacterial membrane, where it leads to small holes in the bacterial membrane (particularly the peptidoglycan) to allow for toxin to be released[92] (**Fig.1.5b**). Each PltB/PltA/CdtB subunit peptide has a secretion signal that allows its secretion via sec machinery from the bacterial cytoplasm into the periplasm between the inner and outer membrane of *Salmonella*. The toxin is then assembled in the periplasm before being secreted into the SCV[92] (**Fig.1.5b**).

Once the toxin is synthesised and secreted from the pathogen, it traffics via small carrier intermediate vesicles derived from the SCV (**Fig.1.5d**). As the SCV is a compartment created from the host cell membrane, it was hypothesized that the toxin is sorted via its receptor-binding subunit PltB. Indeed mutating the PltB prevented the packaging of the toxin in the vesicle intermediate, and the subsequent exocytosis, providing yet another role for PltB in toxin packaging in the host cell[108]. Next, the carrier intermediates are targeted to the invaded cell membrane where they fuse and exocytose the toxin. The toxin then either acts on the same host cell where the *Salmonella* resides (autocrine)

or on a neighbouring cell (paracrine)[96].

1.11   Typhoid toxin interactions with cell surface receptors

Co-immunoprecipitation of purified typhoid toxin revealed that all toxin receptors were glycosylated[109], which allows the toxin to bind to diverse receptors on different cell types. Mutations affecting the N-glycans of these receptors rendered cells more resistant against the toxin. Protein-protein interaction arrays[81] and glycan microarray experiments[109] found that the toxin preferentially binds to receptors associated with the glycan consensus Neu5Ac on glycoproteins which is predominant in humans **(Fig.1.5c, 1.5d)**. In contrast, other mammals express sialylated glycans terminated with Neu5Gc instead[109]. Human cells that were grown in Neu5Gc rich media conferred resistance to the toxin, indicating that Neu5Ac might be a factor that confers toxin specificity to humans[109]. The expression of either Neu5Ac or Neu5Gc in humans is dictated by the CMAH gene. In humans CMAH is absent leading to the up-regulation of Neu5Ac, while other mammals, such as chimpanzees express CMAH more prominently, resulting in the up-regulation of Neu5Gc.

Consistent with the fact that chimpanzees express Neu5Gc, *S.* Typhi only caused mild symptoms that are similar to the NTS[110]. On the other hand, mice express Neu5Ac in most of their tissues due to low level activation of Neu5Gc, and demonstrate typhoid fever symptoms upon intoxication, making them a suitable model to examine the toxin *in vivo*.

1.12   Internalisation of toxin in the host cell.

The process of the toxin internalisation was only recently examined via fluorescently tagged typhoid toxin[111]. After binding to the host cell receptors, the typhoid toxin undergoes receptor-mediated endocytosis, retrograde trafficking into the Golgi apparatus, and then trafficks to the ER where reductases break the disulphide bond between the CdtB and PltA subunits **(Fig.1.5e)**. Genome-wide screen using CRISPR/cas9 technology revealed that the release of the subunits into the cytosol is mediated by proteins involved in the Endoplasmic-reticulum-associated protein degradation (ERAD) pathway that usually targets misfolded proteins. This internalisation process is analogous to other AB$_5$ toxins[112,113,114,115,116], whereby the toxin is disassembled into its functional subunits using the host cell's own machinery. As a result, free CdtB is released into the cytosol where it targets the nucleus and causes DNA damage, cell cycle arrest and cell enlargement[81,106]. The CdtB DNAse activity was required to achieve the conflicting diseases outcomes i.e. mortality, and survival of the host, described in **Section 1.8**.

Prior to discussing the DNA damage induced by the toxin, it is prudent to introduce DNA damage responses and the differential cellular fates that result as a consequence.

Chapter 2

Senescence and host-pathogen interactions

2.1 Introduction

One of the most vital components of every eukaryotic cell is its nuclear DNA. DNA is a complex macromolecule in the form of a double helix that is responsible for encoding all proteins necessary for survival and the function of the cells and organisms. A double membraned nuclear envelope surrounds DNA to organise and protect it from damage. Everyday our genomic DNA is subjected to thousands of intrinsic (e.g. reactive oxygen species as a result of metabolism) and extrinsic (e.g. UV radiation) inducers of DNA damage. Therefore, it is necessary for the cell to resolve the damage in order to sustain its survival and functional integrity, which is achieved via a DNA damage response (DDR). The DDR stalls or arrests the cell cycle to prevent the propagation of corrupted genetic information into daughter cells. This is important to prevent aberrant phenotypes such as cancer cell formation. Throughout the past few decades, scientists unveiled evolutionarily conserved mechanisms to repair the damage that occur, which have become the centre of many research fields particularly oncology and gerontology. This chapter will focus on the DDR mechanisms and the resulting cell fate if the DNA damage is unresolved, with particular focus on senescence responses.

2.2 Cellular organisation of DNA

Most human cells, excluding spermatozoa and ova, are diploid, i.e. contain two copies of 23 chromosomes per nucleus, containing ~3 billion base pairs[117]. In order to compact the lengthy DNA in the small nuclear structure, the double helix is coiled around proteins known as histones forming a nucleosome[118]. Each nucleosome consists of a core octamer made of two copies of each histone: H2A, H2B, H3, H4, to which the DNA coils around. Histones are positively charged which allow tight binding to the negatively charged DNA[119]. The formation of multiple nucleosomes results in the commonly known structure, chromatin, which forms chromosomes[120]. Histones are susceptible to
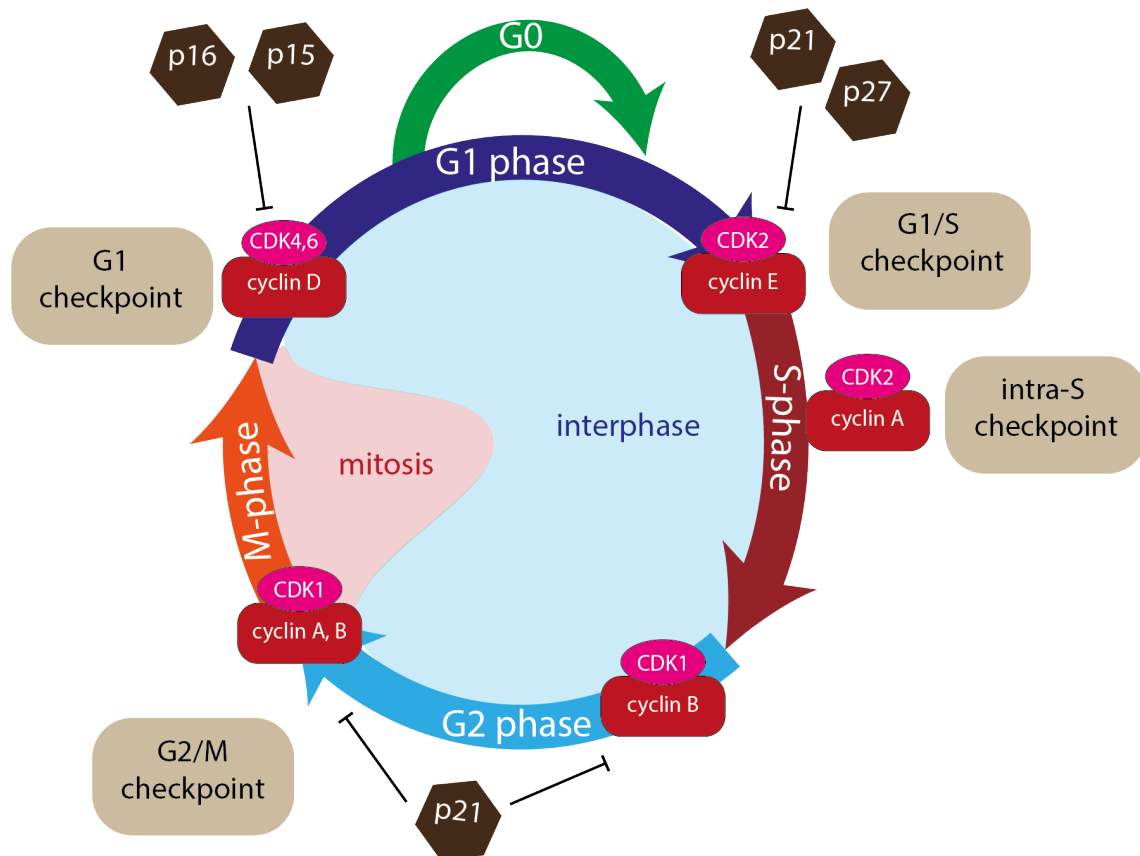
Figure 2.1|The cell cycle. Illustration of the various stages of the cell cycle. At certain stages, the cell deploys checkpoints to ensure that DNA replication is error free via recruitment of cyclins and cyclin dependent kinases (CDK). If damage occurs, CDK inhibitors, such as p16, p15, p21, and p27 ensure cell cycle arrest until damage is repaired.

post-translational modifications such as ubiquitination, methylation, acetylation and phosphorylation, which play a pivotal role in the chromosome structures, chromatin remodeling and transcription[121]. Chromatin is subdivided into euchromatin, which are gene-dense and accessible for transcription, and heterochromatin, which are inaccessible and hidden from transcription machinery[120]. The complex organisation of DNA allows for diverse regulatory processes involving cell division, DNA repair pathways and epigenetic changes that dictate cellular fates.

2.3   The cell cycle

Undifferentiated cells undergo DNA replication to generate copies of the same genetic material and allow for cell division, which is essential in processes such as embryogenesis, wound healing and regeneration. The cell goes through a cell division cycle that is subdivided sequentially into G1, S, G2, (collectively interphase) and M phase **(Fig.2.1)**. DNA replication occurs during the S (or synthesis) phase, which is preceded by a gap phase (G1) that prepares for DNA synthesis and succeeded by another (G2) which prepares the cell for cytokinesis and cell separation[122]. When a cell becomes differentiated or adopts what is known as 'quiescence', the cell exits the cell cycle and enters a G0 phase **(Fig.2.1)**. The cell cycle is a carefully regulated process governed by 'checkpoints'
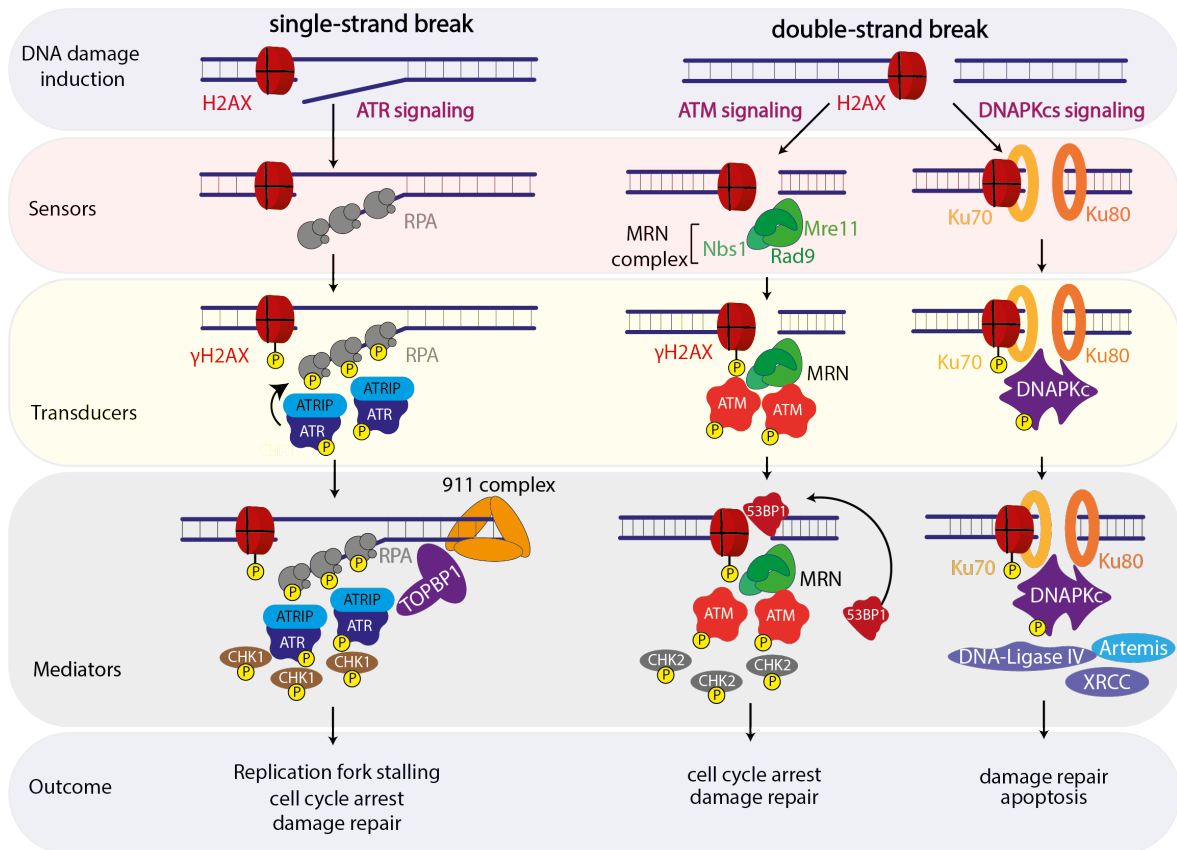
Figure 2.2|DNA damage pathways activated upon single-strand or double-strand DNA damage.
Simplified drawing depicting sensors, transducers, mediators and differential outcomes of each pathway. Upon
DNA damage all the three signalling pathways can converge to repair DNA damage or decide cell fate.

that ensure that replication is error-free. These checkpoints lie between G1/S or G2/M phase and are
monitored by cyclins and their substrate cyclin-dependent kinases (CDK) that start a phosphorylation
cascade promoting progression through the cell cycle. Occasionally, where DNA damage occurs, CDK
inhibitors such as p21, which is a target of p53, prevent the formation of cyclin-CDK complex, lead to
cell cycle arrest and begin a DNA damage response[123] **(Fig.2.1)**. Another cell cycle modulator is p16,
which inhibits CDKs and cyclins (e.g. CDK4 and cyclin D), thereby preventing the phosphorylation
of retinoblastoma tumour suppressor protein (Rb). Rb forms a complex with E2F an elongation factor
required for cell division, and arrests the cell cycle at G1 phase[124].

2.4   The DNA Damage response

Depending on the form and extent of DNA damage, our cells elicit an appropriate DNA damage
response to maintain normal function and survival. One of the most significant forms of DNA damage
include single strand breaks (SSB), which if unresolved can develop into double strand breaks (DSB),
thus resulting in genomic instability[125]. Master regulators of the DDR are the phosphatidylinositol-3-
kinase related kinases (PIKK): Ataxia Telangiectasia Mutated protein (ATM), Ataxia Telangiectasia
and Rad3 related protein (ATR), and DNA-dependent protein kinase (DNA PKcs) **(Fig.2.2)**. In

response to DNA damage breaks, histone H2AX is phosphorylated by kinases to phospho-H2AX (i.e. γH2AX) at position serine 139[126]. γH2AX then acts as a signal hub for recruitment of repair proteins[127], transcription factors or cell cycle regulator to mediate repair[128,129]. Though redundancy exists, ATM, ATR and DNA-PKcs principally phosphorylate H2AX in response to two distinct types of DNA damage: ATM and DNA PKc recognise DSB while ATR responds to SSB at DNA replication forks[130,131,132,133]. Recognition of DNA damage activate PIKK[134], which then recruit mediator proteins by phosphorylating diverse substrates to (i) pause the cell cycle, (ii) mediate repair, and (iii) decide on cell survival[135] (**Fig.2.2**).

2.4.1 Single-strand break repair pathway

SSBs are by far the most common form of DNA damage that occur in the mammalian cell, usually due to intrinsic stresses by metabolites such as reactive oxygen species (ROS)[136]. It can also occur as a result of a malfunctioned replication fork. For instance, during S-phase, DNA topoisomerase 1 nicks one DNA strand, to relax and unwind the double helix transiently, allowing access of replication machinery. As a result, a single-stranded DNA (ssDNA) forms. However, if topoisomerase fails to reseal the ssDNA, for example by colliding with DNA polymerases or RNA transcription machinery, this can result in a SSB and replication fork stalling, known as replication stress[137].

To prevent SSB formation, Replication Protein A (RPA), a tripartite protein consisting of 60KDa, 32KDa, and 14 KDa subunits[138], binds and coats exposed ssDNA. Next, ATR-interacting protein (ATRIP) recognises ssDNA-RPA complexes and results in the recruitment and autophosphorylation of ATR[139,140] (**Fig.2.2**, left panel). Activated ATR subsequently phosphorylates RPA at serine 33 (RPApS33) and threonine 21 (RPApT21)[141] to mediate DNA synthesis and repair[139]. Next, ATR mediates repair locally and prevents further global replication firing until the SSB is repaired, by phosphorylating its substrate CHK1 which diffuses to exert action in the nucleus[142]. The ATR kinase signal is then amplified by a trimer complex known as 9-1-1 (RAD9, RAD1 and HUS1) and TOPBP1[143,144]. CHK1 is a checkpoint surveillance protein which controls the cell cycle through recruitment of p53[145,146], which is a transcription factor that activates cyclin-dependent kinase inhibitors such as p21[147]. As a result, replication is halted until the damage is resolved. Inhibiting ATR leads to failed repair locally and causes unscheduled global replication origin firing resulting in the accumulation and persistence of ssDNA across the genome. This was termed "replication catastrophe", where the finite pool of RPA is exhausted by excess substrate ssDNA that can become unprotected resulting in fork collapse, double-strand breaks and permanent exit of the cell cycle[148].

2.4.2 Double-strand break repair pathway

The production of DSB is the most lethal form of DNA damage a cell can encounter. Its effects can sometimes be deleterious of genes that might be important for cell survival[149]. They can form as

a result of collapsed replication forks or other exogenous sources such as the chemotherapeutic agent, aphidicolin (APH), that inhibits DNA polymerase α activity and results in replication stress (Glover et al 1984).

At the site of DSB, the MRN complex which constitutes (Mre-11 Rad50, Nbs1) detects the damage and recruits ATM[150] which is the main driver of DSB repair signalling (**Fig.2.2**, right panel). Experiments with APH-induced replication stress revealed that the activation of ATM is also partially dependent on ATM-interacting protein, ATMIN[129]. ATM is activated by auto-phosphorylation and subsequently activates various effectors such as CHK2, another cyclin and checkpoint regulator. In contrast to ATR, ATM leads to recruitment of the p53-binding protein, 53BP1 which tethers ATM to the double strand breaks and initiates a recruitment cascade for DSB repair. Similar to ATR, ATM-dependent activation of 53BP1 can also prime the activation of p53 which results in cell cycle arrest, making 53BP1 a tumour suppressor protein[151]. During DSB repair, ssDNA forms which can activate ATR signaling in conjunction with ATM kinase activity at the same damage site[152]. When ATM was knocked down in irradiated cells, low levels of γH2AX were detected. Blocking DNA-PKc but not ATR via wortmannin abrogated the low level of DNA damage observed in ATM knockout cells, indicating that DNA-PKc is secondary to ATM as a sensor of DSB[128]. DNA-PKcs autophosphorylates after binding to Ku proteins, which are sensors of DSB to initiate repair. Whilst DNA-PKc plays an important role in DSB repair, its activity dominated over ATM particularly in apoptotic cells[131] (**Fig.2.2**, right panel).

Although the cell has a DNA damage contingency plan in place, extensive DNA damage might not always be successfully repaired. At this stage, the cell must eliminate the problem to prevent aberrant DNA replication and oncogenic phenotypes. The cell either adopts apoptosis or senescence.

2.4.3   Apoptosis

Apoptosis is non-inflammatory programmed cell death which is initiated after extensive, unrepaired DNA damage[153]. Apoptotic cells are marked by DNA fragmentation, chromatin condensation, and nuclear shrinkage due to a cascade of signalling involving activation of caspases that carry out mass proteolysis. In terms of DDR, studies showed that the phosphorylation of H2AX by DNA-PKcs, but not by ATM, is required for apoptosis[131]. In early apoptosis, γH2AX which is typically observed as foci, migrates to the periphery of the nucleus, forming an 'apoptotic ring', while maintaining a pan distribution of H2AX[154]. Localised with this ring are ATM, Chk2 and DNA-PKc. In late stages of apoptosis, γH2AX becomes distributed across the whole nucleus. If the DNA damage is persistent but not fatal, the cell can adopt senescence as a measure to contain the damage, while allowing for cell survival.

2.4.4   Senescence

Senescence is a phenomenon whereby the cell exhibits several key features, namely irreversible cell cycle arrest, resistance to cell death signalling and production of a characteristic secretion profile called the senescence-associated secretory phenotype (SASP)[155]. The cell decision between senescence and apoptosis is an unclear process. Recent findings implicate High mobility group box-1 (HMGB1) and the degree of p53 activation as a contributing factor to these cell fates. Indeed after treating cells with the topoisomerase 2 inhibitor doxorubicin, senescent cells showed elevated HMGB1 and p21, whilst apoptotic cells showed diminished levels of both proteins[156]. Although senescence and quiescence are terms that are sometimes misused interchangeably, they vary molecularly and morphologically. Quiescence is a reversible cell-cycle arrest state that can be triggered due to lack of nutrients (such as serum-starvation) or differentiation. Given favourable environmental or molecular signals, the cell can resume the cell cycle. In contrast, senescence is an irreversible stress-response that normally accumulates during the ageing process of an organism or induced by extensive DNA damage[157].

At the outset of my PhD, we discovered that the typhoid toxin induction of DNA damage via the CdtB subunit resulted in a senescence-like response[106]. Therefore, before describing these results, the rest of the literature review will discuss hallmarks of senescence, the benefits and drawbacks of senescence, and provide insight into host-pathogen interactions with cellular senescence.

2.5   Characteristics of cellular senescence

As the development of cellular senescence is temporal and occurs in stages, there is not a single gold standard universal marker of senescence to this day. To identify senescent cells, researchers utilise various markers of senescence in combination. These include morphological changes, DDR pathways, metabolic changes and other molecular changes[155](**Fig.2.3**).

Permanent cell cycle arrest. The most established marker of senescence is irreversible cell cycle arrest often mediated by a sustained p53 activity and activation of different CDK inhibitors such as $p21^{WAF/Cip1}$, $p16^{INK4A}$, and $p15^{INK4b}$[158,159]. This is supported by colony forming assays and experiments showing that senescence cells are unable to incorporate thymidine analogues (e.g. EdU) added to cell culture media, signifying inability to divide[160].

Morphology and lysosomal activity. Senescent cells typically display an enlarged, flattened, and granular phenotype, which is easily observed using light microscopy. Perhaps the most commonly used marker is the up-regulation of the lysosomal marker senescence-associated β-galactosidase activity (SA-β-gal)[161]. However, the limitation of SA-β-gal is that quiescent cells can sometimes display SA-β-gal. For example, healthy macrophage cells show intrinsically high levels of SA-β-gal in the absence of genotoxic stresses during polarisation in response to immune signals[162]. Alternatively,

---

***Fig.2.3** was published as part of Humphreys et al 2020 (Cells). Access via this link.
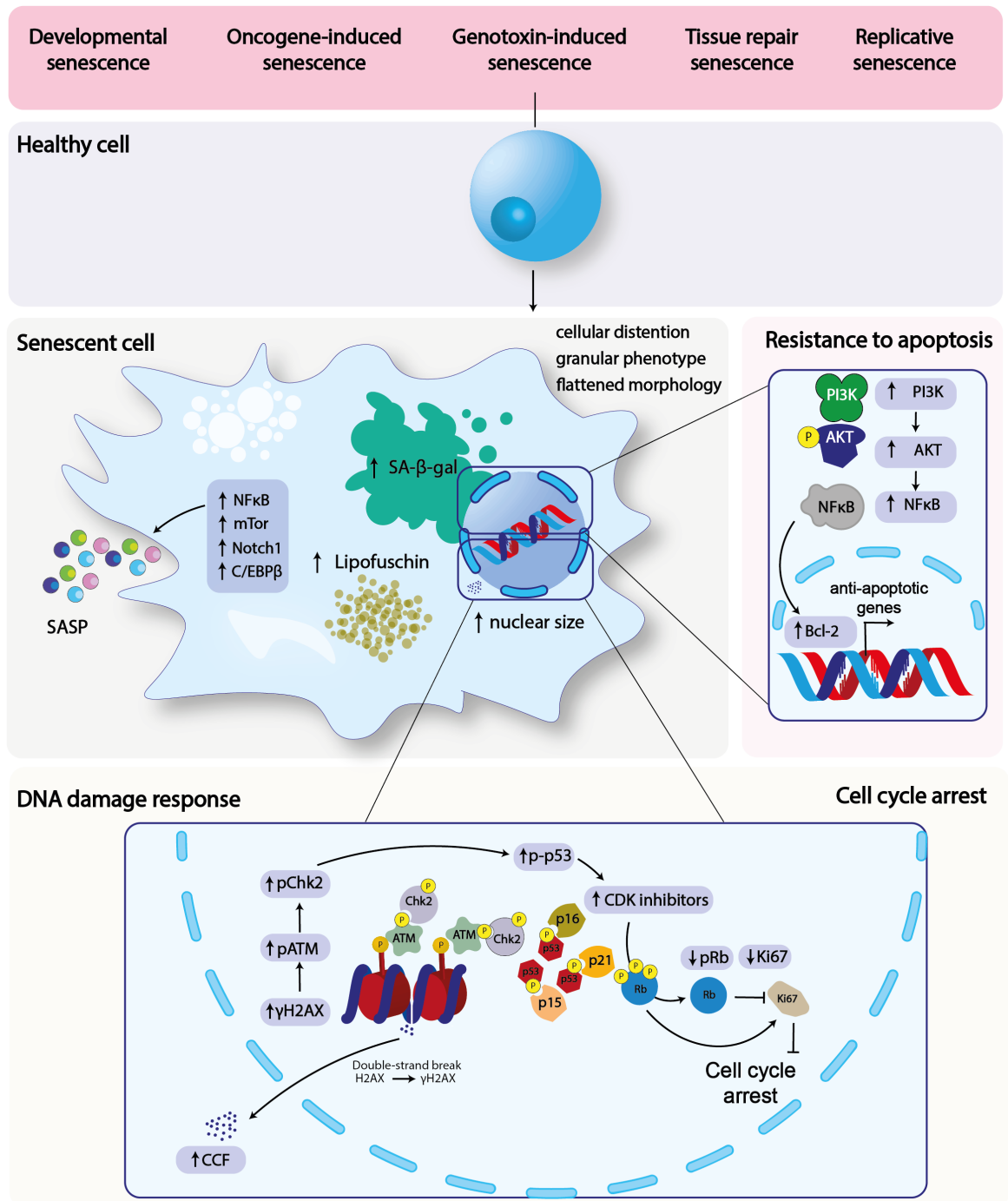
Figure 2.3| Hallmarks of senescence. The figure demonstrates different types of senescence and the most common features of senescent cells. *

lipofuschin, which is an aggregate of proteins and lipids that represents residues of lysosomal digestion, is used[58].

DDR and nuclear structure. As previously described, senescent cells can display a chronic DDR marked by persistent γH2AX foci and downstream effectors such as ATM and ATR. However, DDR is often triggered independently of a senescence response, and in some cases, is absent in senescent cells. Therefore, this marker is not used solely to identify senescent cells[163]. Nuclear size can also

increase, and senescent cells sometimes display multi-nucleation that is a result of failed mitosis in G2/M phase (i.e. presence of 2 copies of each chromosome; 2N to 4N)[164,165].

Lamin B1 down-regulation. Other nuclear changes that occur in senescence is the down-regulation of the nuclear envelope protein, lamin B1. This was observed in various types of senescence including irradiated cells, constitutive ras-oncogene activation and replicative senescence[166]. In contrast, over-expressing lamin B1 improved proliferation rate and delayed onset of senescent phenotypes[167]. Interestingly, loss of lamin B1 was also reported to be essential for the development of a full senescent phenotype[168]. In addition, it resulted in global chromatin remodelling and cytoplasmic chromatin fragments (CCF)[169].

Chromatin remodelling. In normal cells, chromatin is composed of euchromatin, which allow for transcription, and heterochromatin, which is hidden from transcription machinery[120]. One of the observable changes in chromatin structure of senescent cells is the generation of senescence-associated heterochromatin foci (SAHF), which is mainly reported in oncogene-induced senescence[170,171]. SAHF constitutes repressive histone marks such as methylation H3K9me3 that is different from facultative heterochromatin mark H3K27me3[172]. SAHF formation results in repressing proliferative genes, such as E2F, and prevents accessibility of DDR proteins causing resistance to apoptotic pathways[172].

Anti-apoptotic properties. In addition to suppressing extensive DDR, senescence cells display increased signalling of pro-survival genes such as BCL2 which is activated due to up-regulation of transcription factor NFκB[173]. As a result, senescent cells can resist cellular death and survive for an extended duration regardless of initial DNA damage induction.

Senescence Associated Secretory Phenotype (SASP). SASP is a cohort of molecules, typically inflammatory molecules, growth factors, cytokines and chemokines that are secreted by senescent cells. SASP constituents vary depending on the senescence inducer and the cell type[174]. Therefore, a 'gold standard' SASP signature is still not discovered, especially *in vivo*. However, a recent library of its constituents, namely "SASP Atlas", revealed core SASP proteins that were secreted by senescent epithelial and fibroblast cells using different senescence induction methods, and matched with blood plasma analysed from an ageing population[174]. The top candidates included GDF15, SERPINs and MMP. Interestingly, senescent fibroblasts that resume cell proliferation due to an inactivation in p53, still retain most SASP constituents, which indicates that SASP is a more permanent characteristic of senescence than cell cycle arrest[175].

2.6 Senescence - The Bright and Dark Sides

Senescence has been typically acknowledged as an anti-tumorigenic phenomenon and represents a defence mechanism against pathologies that require cell proliferation. Normally, senescent cells accumulate as the organism ages, resulting in age-related pathologies such as osteoarthritis, diabetes,

Alzheimer's and cardiovascular diseases[176]. Indeed, transplanting senescent cells in young mice led to physical weaknesses as measured by their grip endurance, maximal speed and hanging endurance[177]. In contrast, ablating senescent cells (via senolysis) improved their health and strength, and prolonged the life span of ageing mice[177]. Since senescence has anti-tumorigenic properties, but is the basis of age-related diseases, is senescence beneficial or detrimental?

Different types of senescence have been identified: i) replicative senescence ii) oncogene-induced senescence, iii) genotoxin-induced senescence, iv) developmental senescence, v) tissue repair senescence, and vi) paracrine senescence.

Replicative senescence (RS). This type of senescence was the basis of the discovery that cells undergo a finite amount of cycle before they undergo permanent cell cycle arrest[178]. At every chromosomal replication, telomeres, which are nucleotide sequences found at the end of each chromosome, get shorter. This process is known as telomere attrition and is due to incomplete chromosomal replication. Since telomeres are non-coding they prevent deletion of important genes within the chromosome. However, critically short telomere lengths are detected as DNA damage and elicit a DDR that activates a senescence-like response to prevent further replication and damage to coding genes[143,179].

Oncogene-induced senescence (OIS). Independent of RS, OIS is triggered upon activation of aggressive oncogenes, such as RAS[180]. Oncogene activation results in replication stress, the formation of multiple DSB and the activation of DDR[181]. It is thought that OIS together with RS is adopted to prevent the uncontrolled cell division and the carcinogenesis of normal cells by arresting the cell cycle in G1 phase[182].

Genotoxic-induced senescence (GS). Similarly to OIS, GS is elicited by subjecting cells to external DNA damage inducing agents such as irradiation, chemotherapeutic drugs (e.g. aphidicolin or etoposide, a topoisomerase II inhibitor), and bacterial toxins, or internal agents such as ROS generated due to aberrant metabolism[183,184]. DNA damage induction results in DSBs which orchestrate a stabilised DDR leading cells into senescence[184,185].

Developmental and tissue repair senescence. These two types are not as well-addressed as RS, OIS, and GS. It is evident that senescence is an intrinsic mechanism used in non-disease contexts as well, for example, during embryogenesis. Given their high secretion profile, it is thought that SASP might contribute to cell fate and stem cell control. Similarly in wound healing, secretion of growth factors such PDGFAA recruit immune cells that aid the process of tissue regeneration[186].

Paracrine senescence. Also known as transmissible senescence, this type of senescence is induced via secretions of senescent cells, SASP, that transmit senescence to neighbouring cells that are otherwise healthy. It is usually less potent than primary induced senescence but can confer beneficial and detrimental effects, which are discussed in the following sections[155,187].

2.7 Senescence Associated Secretory Phenotype (SASP) – Friend or Foe?

SASP is capable of altering the tissue microenvironment by inducing transmissible senescence in surrounding naïve cells[188]. SASP can be composed of soluble factors that act on receptors, non-soluble factors secreted via exosomes, and secreted proteases. Proteases can then cleave membrane bound receptors, break down the extracellular matrix or inhibit secreted soluble molecules thereby modulating the tissue microenvironment[189]. Many of the benefits and drawbacks of senescence in the literature have been mainly attributed to the composition, timing and duration of SASP[190]. Paradoxically, SASP is a sword with two-edges depending on organismal context. It can be beneficial, e.g. in tumour suppression, wound healing and immune clearance or it can be detrimental, e.g. chronic inflammation and cancer promotion[191].

2.7.1 SASP as a friend

SASP is important to maintain normal physiological functions of mammals and other organisms. As described in developmental and tissue repair senescence in **Section 2.6**, SASP is imperative from embryonic stages into adulthood. In embryos, SASP recruits immune cells that eliminate senescent cells in order to balance cell populations in each organ. In p21 knockout mice, that are incapable of undergoing senescence, apoptosis compensates, albeit resulting in embryonic deformities[192]. SASP can also cue for tissue development via growth factors essential for organogenesis such as TGF and FGF[193].

Progressing into adulthood, SASP has a clear impact on important homeostatic processes such as wound healing. At the site of wound infliction in mice, senescent fibroblasts and endothelial cells were observed. Interestingly, double knockout mice (p21/p16) displayed a lack of PDGF-AA, which is a prominent SASP factor, resulting in delayed wound closure[191]. In addition, SASP was shown to limit liver deterioration following injury. In mice primed to develop liver fibrosis, senescent cells enhanced degradation of the extracellular matrix and immune cell recruitment, via SASP, which were essential in liver repair[194].

Furthermore, SASP can reinforce senescence in an autocrine manner via chemokine signalling, to prevent tumorigenesis[195]. Chemokine signaling recruits immune cells such as natural killer cells, neutrophils, monocytes, macrophages, dendritic cells, B cells and T cells to eliminate senescent cells and prevent their chronic accumulation[196,197], which is essential in development and wound healing. Interestingly, although SASP has important functions in physiologically healthy organisms, it can have detrimental effects if senescent cells accumulate and SASP becomes chronic.

2.7.2   SASP as a foe

In an ageing organism, senescent cells accumulate, for example due to telomere attrition (discussed in **Section 2.6**), resulting in immuno-senescence, i.e. senescence of immune cells and a chronic pro-inflammatory SASP known as 'inflamm-aging'[198]. Inflammaging was correlated to many age-related diseases such as cardiovascular disease, Alzheimer's and cancer[190,199].

SASP has been implicated in the development, invasion and metastasis of many cancers including breast cancer and melanoma amongst others[189]. When senescent fibroblasts were incubated with pre-malignant cells, tumorigenesis was induced[200]. When they were incubated with malignant cells, cancer progression was accelerated[201]. As SASP is rich in pro-angiogenic factors such as vascular endothelial growth factors (VEGF), tumours *in vivo* were highly vascularised in presence of senescent cells compared to non-senescent cells. Given the pro-tumorigenic effects of SASP, its impact drives chemo-therapy resistance *in vivo*[184,202].

Although short-term exposure to SASP was described as beneficial in wound healing, chronic SASP on the contrary ameliorates it. SASP transmits senescence to stem and progenitor cells required for differentiation, and thereby preventing their normal function of tissue regeneration[203].

2.8   The complex regulation of SASP

SASP regulation involves a complex interplay of intrinsic and extrinsic signaling pathways. The most recognized transcription factors involved in a pro-inflammatory SASP are CCAT/Enhancer Binding Protein (C/EBPβ) and NFκB[204].

C/EBPβ, is a transcription factor able to promote expression of inflammatory SASP proteins such as IL-1β, GROα and IL-6[195]. Indeed, studies have shown that C/EBPβ binds to IL-6 promoter in OIS[205]. Interestingly, the action of C/EBPβ is further modulated by an alternative isoform, C/EBPγ which heterodimerizes with C/EBPβ to suppress SASP gene transcription[206]. Furthermore, sustained DDR in senescent cells were shown to increase NFκB signaling activity that was activated by IL-1β expression[207] and enhanced by p38 MAPK signaling[208]. Indeed, inhibiting NFκB signaling via metformin resulted in a significant reduction of CXCL5, IL-6 and IL-8[209]. Conversely, JAK2/STAT3 activation resulted in secretion of anti-inflammatory proteins such as IL-10 and IL-13. Inhibiting JAK2/STAT3 signaling pathways in PTEN-null mice, favoured an NFκB-induced inflammatory phenotype and immune cell filtration[210].

SASP is also regulated on an epigenetic level via chromatin remodelling, triggered by lamin B1 downregulation[169]. For instance, senescent cells lose the repressive histone modification H3K27me3 which results in activation of SASP genes[169]. Additionally, the nuclear protein, HMGB2 is enriched in OIS cells, and excludes relevant SASP genes from SAHF to allow for their transcription during
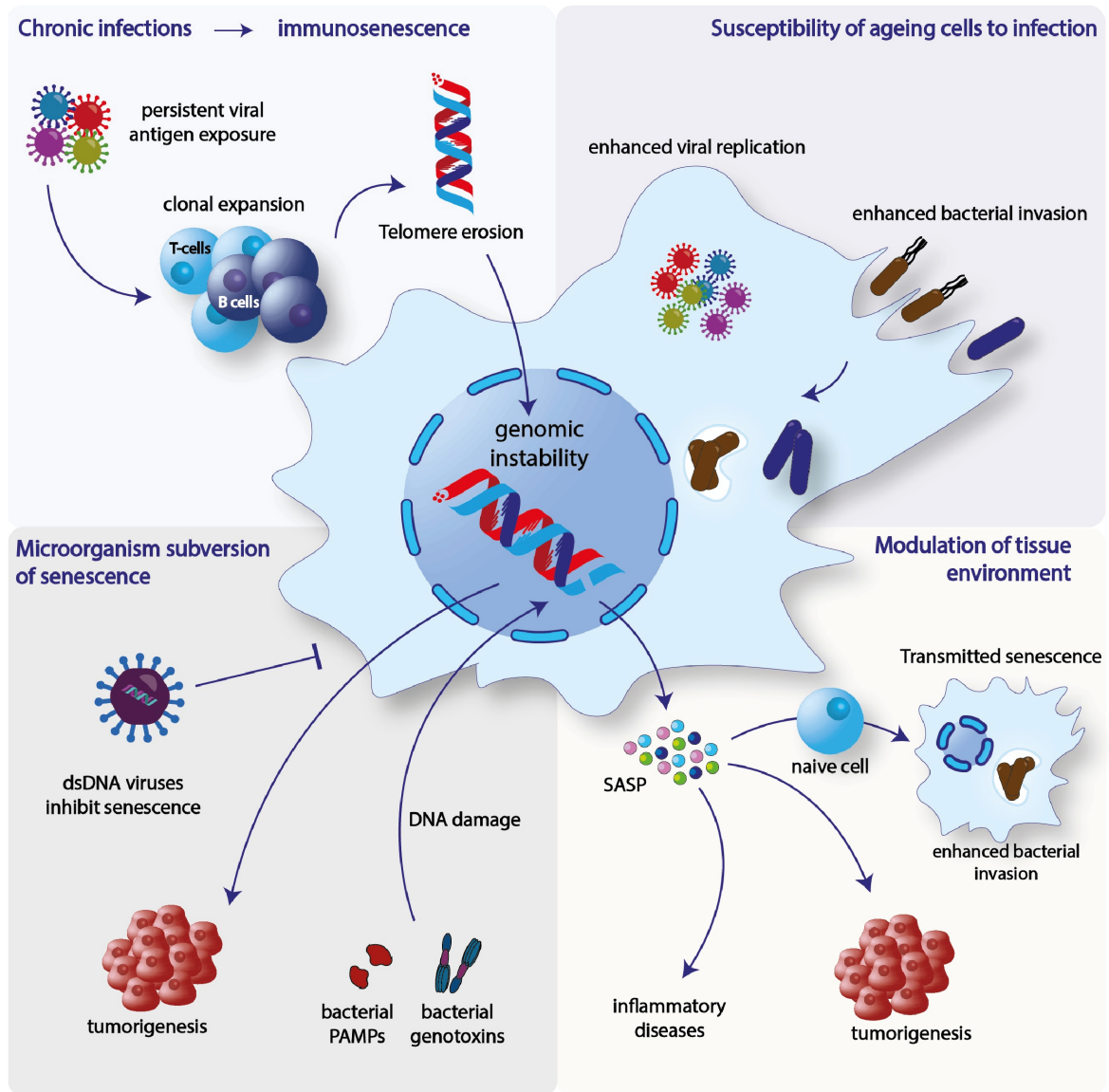
Figure 2.4| Senescence and host-pathogen interactions. Illustration of the diverse interactions between viruses/bacteria and senescent host cells.*

senescence[211], and promoted by NFκB and p38 MAPK signalling[212].

2.9 Senescence and Host-pathogen interactions

Given the regulation of inflammation and immune system in senescence, it is not surprising that there are emerging roles for senescence in viral and bacterial pathogenesis. In some cases, pathogens can subvert senescence in their favour, while in other cases senescence is a host-defence mechanism against pathogens or a driver of pathogen-associated oncogenesis. This section will highlight some examples of senescence as a host-defence mechanism and other examples as a pathogen-subversion mechanism in favour of infections[213] **(Fig.2.4)**.

****Fig.2.4** was published as a graphical abstract for Humphreys et al 2020 (Cells). Access via this link.

Viruses can induce senescence via replication stress. Chronic viral infections can lead to immunosenescence, a process whereby immune cells show decreased function and adopt senescence[213]. For instance, human cytomegalovirus (HCMV) is a double stranded DNA virus that causes herpes and results in latent infections. Continuous antigen exposure of HCMV results in T lymphocytes clonal expansion, possibly leading to telomere shortening and replicative senescence[214,215,216]. It is thought senescence might be induced to allow these cells to sustain viral burden and prevent apoptosis. This is indeed the case for the human hepatitis C virus (HCV) where chronic infections of the liver are common, and leads to liver fibrosis and cirrhosis[217]. Memory T-cells exhibited significantly shorter telomeres compared to uninfected individuals, which is indicative of immunosenescence (**Fig.2.4**, top left panel)[218]. This phenomenon aids the promotion of chronic viral infections[219].

Bacteria can induce senescence via genotoxic stress. Increasing evidence shows that bacteria have evolved virulence mechanisms to induce premature senescence. This could be via eliciting a chronic inflammatory response indirectly via pathogen-associated molecular pattern (PAMPs) such as lipopolysaccharide (LPS)[220] or via the secretion of genotoxins (**Fig.2.4**, bottom left panel)[106,221]. One example includes *E. coli*, a Gram-negative bacterium that produces colibactin, a genotoxin. Colibactin causes DNA interstrand crosslinks, resulting in DNA SSB and subsequent DSB fromation[221] thereby activating ATR and ATM signalling, respectively[221]. Extensive damage led to apoptosis, whilst other intoxicated cells survived and demonstrated senescence markers such as SA-β-gal, SAHF, and inflammatory SASP. However, colibactin-induced SASP, triggered the proliferation of bystander cancer cells and promoted oncogenesis (**Fig.2.4**, bottom right panel)[222].

Of more relevance to the typhoid toxin are cytolethal distending toxins (CDTs), which were described in **Chapter 1, Section 1.9**. Briefly, CDTs possess a DNase homologue called CdtB that induces SSBs and DSBs. CDT-intoxicated cells display distended flattened morphology similar to what is observed in senescence. There are very few examples in the literature of CDT-induced senescence. Namely, cells infected with *H. ducreyi*, a Gram-negative bacterium that secretes CDT, demonstrate persistent γH2AX, 53BP1 signalling, and SASP that comprises cytokines such as IL6, IL8, IL24. Interestingly, *in vivo* experiments with CdtB showed increased tumour invasion and endoreplication, which are key in cancer progression (**Fig.2.4**, bottom left panel)[223].

2.10 Is senescence a host defence mechanism or a pathogen-induced virulence mechanism?

Elderly individuals are the most vulnerable age group to infections by bacteria and viruses[224,225]. Indeed, experiments with influenza virus and varicella zoster virus show that senescent cells allowed for enhanced viral infection as measured by increased virus titre and gene expression (**Fig.2.4**, top right panel)[226]. Similar to viruses, aged organisms are more susceptible to many bacterial infections. Experiments *in vivo* show that aged mice are more susceptible to *S.* Typhimurium which causes
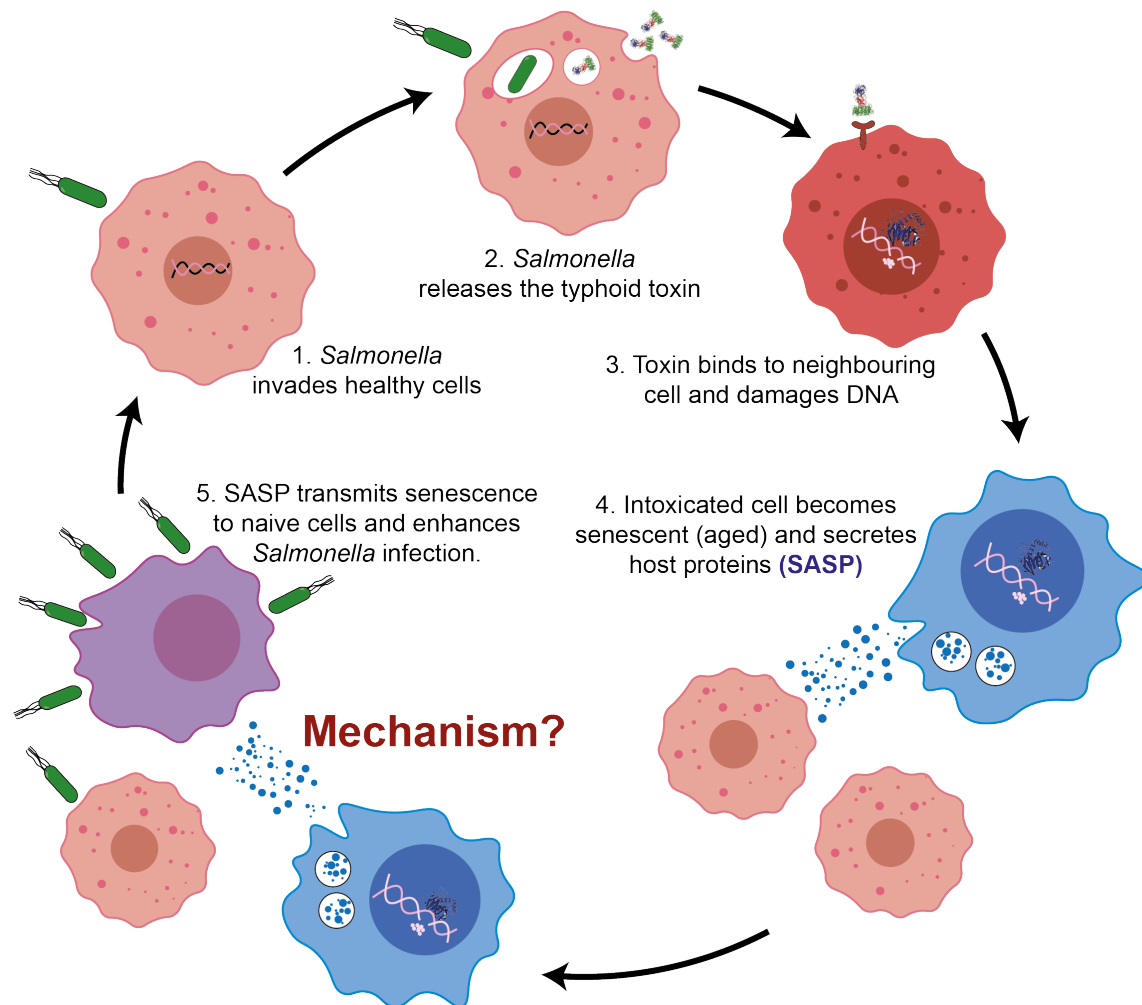
Figure 2.5| The typhoid toxin proposed mechanism of disease. This diagram demonstrates how *Salmonella* hijacks the host human cells via SASP to enhance invasion in bystander cells. This model was developed based on Ibler et al 2019[106] findings alongside some of the results presented in the first results chapter.

gastroenteritis[227]. Another example include the increased susceptibility of senescent cells *in vitro* and *in vivo* to *Streptococcus pneumoniae* which is thought to invade better due to the inflammatory profile of senescent cells[228]. These examples describe pathogens that exploit senescence in their favour (**Fig.2.4**, top right panel). On the other hand, double stranded DNA viruses, such as human papilloma virus, inhibit senescent phenotypes by degrading p53 to combat protective senescence-induced cell cycle arrest resulting in cervical cancer (**Fig.2.4**, bottom left panel)[229].

In contrast, viruses that exploit the human host cell replication machinery to divide would be incapable to replicate if it resides in a senescent cell. For instance, vesicular stomatitis virus, a negative-sense single-stranded RNA virus, displayed a reduced titre of the virus in senescent MEFs cells *in vitro* or in lungs of chemically-aged mice *in vivo* after administering bleomycin, a senescence-inducer[230]. Unlike viruses, bacteria are self-sufficient and do not require the host replication machinery to survive and replicate. So is the senescence phenotype induced by the genotoxic effects of bacterial toxins, such as colibactin and CDTs, a mechanism of host-defence or pathogen subversion?

2.11 The typhoid toxin of *Salmonella* proposed mechanism of disease

At the outset of my PhD, injected toxin had been shown to induce typhoid fever in a mouse[81] but how the typhoid toxin contributed to invasive infections was unclear. Given the DNase activity of the typhoid toxin of *Salmonella*, my lab colleague, Dr Angela Ibler examined the DNA damage response induced in a CdtB-dependent manner. Interestingly, she discovered a novel DNA damage phenotype, which was termed as RING (a response induced by a genotoxin) marked by the localisation of γH2AX at the nuclear periphery (discussed and examined in **Chapter 3**), which was similar to the apoptotic ring. However, RING cells survived and the phenotype was persistent for at least 48h post intoxication. This non-canonical response was marked by induction of ssDNA breaks, activation of ATR signalling and exhaustion of the RPA response resulting in replication fork collapse and replication stress. In addition, canonical DDR was also elicited and marked by γH2AX foci which was ATM-dependent. As a result of toxin-induced DDR, cells showed a senescence-like phenotype including cell cycle arrest, cell enlargement, and unidentified SASP that transmitted cells to and enhanced *Salmonella* invasion in naive bystander THP1 monocytes and fibroblast-like HT1080 cells. Interestingly, conditioned media from another chemical senescence inducer, aphidicolin, did not enhance invasion, indicating a specific phenotype induced by the typhoid toxin. This suggests that *Salmonella* has evolved a senescence hijack mechanism to modulate the microenvironment in favour of infection and potential persistence[106] (**Fig.2.5**).

2.12 Aims and hypothesis

Given the molecular role of the toxin, this thesis aims to:

1. Further characterise the senescence-like phenotype induced by the toxin.

2. Identify the toxin-induced host secretome underlying senescence responses.

3. Resolve the SASP factors mediating transmissible senescence and *Salmonella* invasion

I hypothesise that the typhoid toxin induces a unique SASP that reprograms the infection niche in favour of *Salmonella* invasion. Understanding the senescence-like stress response induced by the toxin and identifying SASP molecules that are potentially toxin-specific are key to i) elucidate on the role of typhoid toxin during infection, ii) provide insight into potential biomarkers of chronic carriers, and iii) identify potential targets for therapeutic intervention. Since this project also includes studying DNA damage, senescence and *Salmonella*, it will not only contribute to the knowledge-base of aging-research, but also have an impact on pathology, cell and molecular biology fields.

Part II

Results

Chapter 3

Typhoid toxin-induced DNA damage and senescence responses

Uniting the diverse phenotypes observed *in vivo*, systemic spread of *Salmonella*[78,99], suppressed inflammation[78,81,99,231], bacteraemia[100], and chronic *Salmonella* carriage[78] is the key role of the toxin's nuclease activity and the host DDR. Thus, understanding how the toxin manipulates host cell DDR has the potential to reveal important host-pathogen interactions and shed light on the role of the typhoid toxin. Upon starting my PhD, my laboratory colleague Dr Angela Ibler had discovered that purified recombinant typhoid toxin induced the RING phenotype[106]. I was first tasked with substantiating these findings in different cell lines using recombinant typhoid toxin and examining whether they occur during *Salmonella* infection. Next, I investigated the cell fate of intoxicated cells, which centred on a senescent-like response that became the focus of my PhD.

3.1 The purification of the typhoid toxin

Different techniques have been adopted to examine the typhoid toxin activity *in vitro* and *in vivo*. For instance, cell cultures or animal models were infected with *S.* Typhi or *S.* Javiana, or with *S.* Typhimurium engineered to encode the typhoid toxin[78,79,107]. Using *Salmonella* best reflects a natural infection but resolving whether damage has occurred from intoxication, infection or a mixture of both in the same cell makes interpretation more challenging. To uncouple the toxin from other *Salmonella* virulence factors, *Salmonella* can be induced to express and secrete the typhoid toxin when cultured in minimal media that mimics the *Salmonella*-containing vacuole, e.g. pH 5.8, but the yields are very low[232]. However, the most common method is the heterologous expression of recombinant toxin in *E. coli*[81,94,106,109,111]. The approach has been used effectively to study the typhoid toxin in our laboratory and has been broadly adopted in the field.

To purify the typhoid toxin, *E. coli* C41 was transformed with the T7 expression vector pETDuet1-pltB-HIS/pltA-MYC/cdtB-FLAG. *E. coli* C41 is engineered with T7 RNA polymerase whose expres-
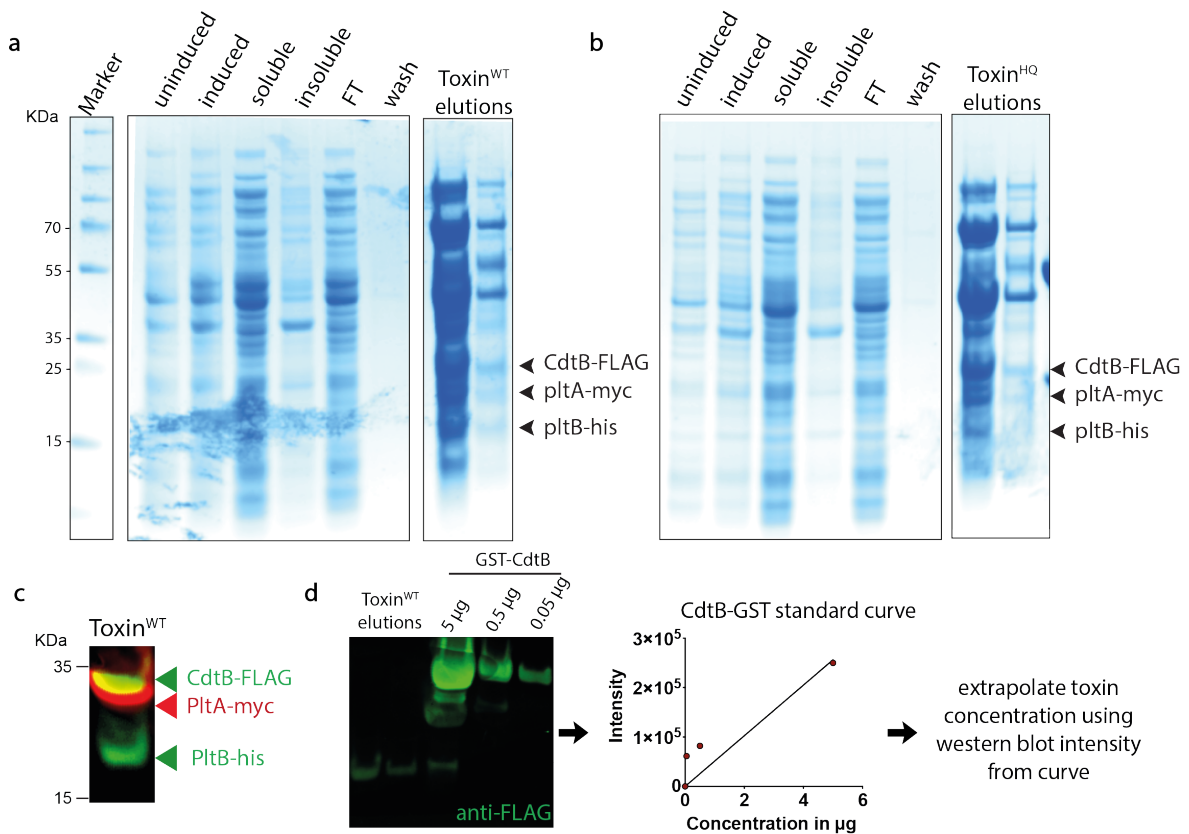
Figure 3.1| Toxin purification and concentration measurement. **a-b,** Commassie stains of each fraction of the purification of **a,** toxin^{WT} and **b,** toxin^{HQ}. Uninduced and induced fraction depict *E. coli* before and after IPTG treatment. Soluble and insoluble fractions are proteins in bacteria after lysis. FT=flow through of the soluble fraction through the Ni-NTA column. Wash fraction is the buffer used to wash the column before eluting bound proteins to the Ni-NTA beads. Arrows indicate the different subunits of the toxins. **c,** Western blot of the toxin^{WT} subunits with anti-FLAG (CdtB^{FLAG}), anti-Myc (PltA^{Myc}), anti-His (PltB^{His}). **d,** Purified GST-CdtB of known concentrations was used to create a standard curve to extrapolate the concentration of the toxin^{WT} fraction using intensities measured in ImageStudio.

sion is induced using IPTG that drives expression of wild-type (toxin^{WT}) subunits: CdtB-FLAG, PltA-Myc, and PltB-His. In contrast to *Salmonella* , which encodes TtsA that facilitates toxin secretion[95], the toxin is not secreted by *E. coli* and accumulates in the periplasm. Therefore, the holotoxin was purified from lysed *E. coli* using NiNTA affinity chromatography of PltB-His. As a consequence, any CdtB present should be bound to PltB via PltA.

The purification efficiency was examined using Coomassie stained gels **(Fig.3.1a)**. The typhoid toxin subunits, CdtB, PltA and PltB were faintly observed at the relevant protein sizes, after induction with IPTG and elution from columns. Additionally, western blot against FLAG, Myc and His tags confirmed that the holotoxin has been purified **(Fig.3.1c)**. As expected, the yield was low, which is evidenced by the high abundance of *E. coli* contaminants, and only a crude preparation of toxin was harvested **(Fig.3.1a-b)**. Indeed, researchers have previously omitted affinity chromatography and opted to use a whole extract instead[103,233]. To control for *E. coli* contaminants, such as LPS, in downstream host-pathogen interaction experiments, mutant toxin H160Q (toxin^{HQ}) was purified from *E. coli* expressing pETDuet1-pltB-HIS/pltA-MYC/cdtB-H160Q- FLAG **(Fig.3.1b)** to examine
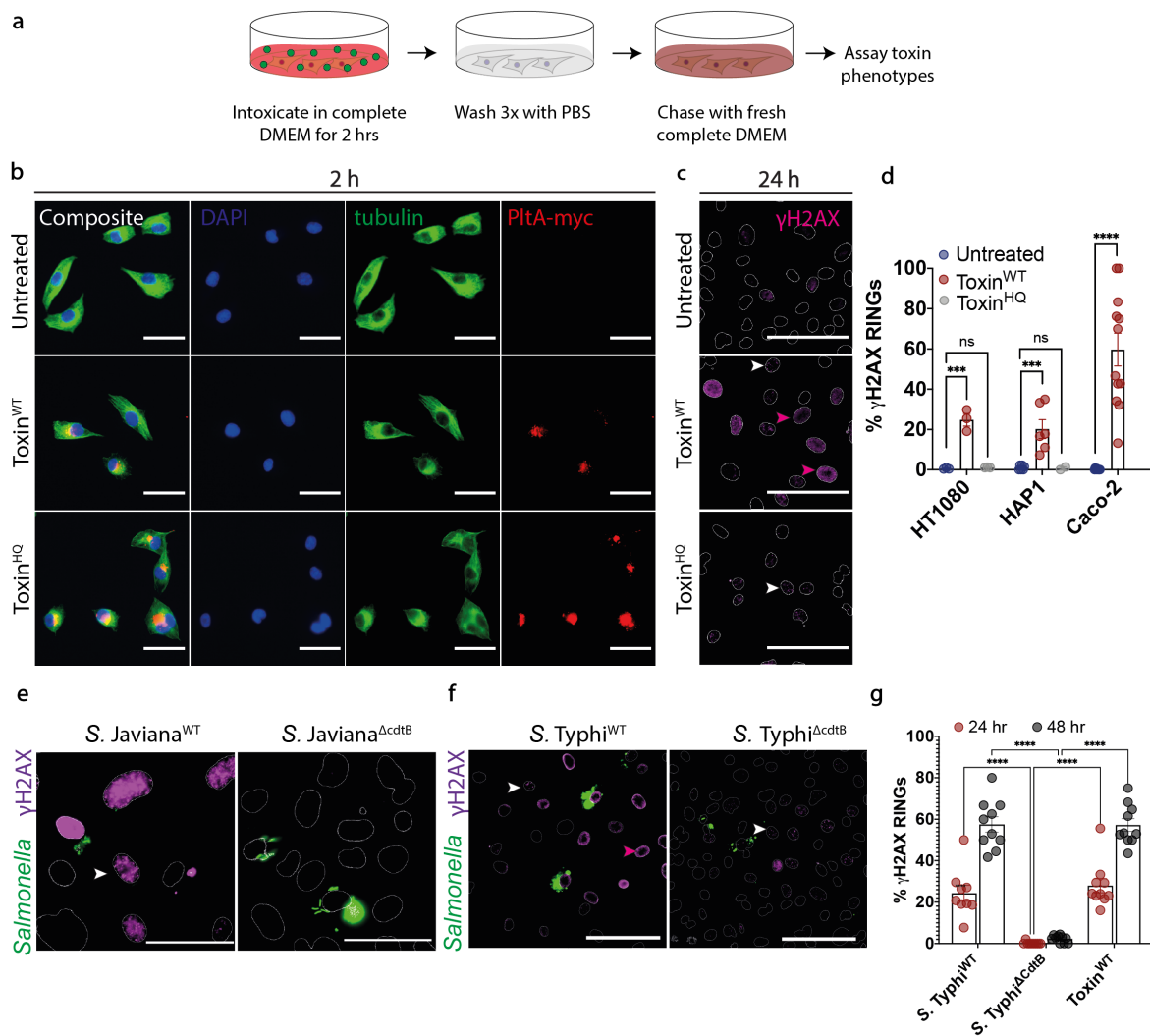
Figure 3.2| Intoxication and the DNA damage response (DDR). a, Schematic demonstrating the methodology used to intoxicate cells. **b,** Immunofluorescence of toxin pltA subunit (anti-myc, red) inside the cells marked by tubulin (green) and DAPI (blue) after a 2h treatment in HT1080 cells. **c,** DNA damage response in HT1080 cells marked by γH2AX (magenta). **d,** Quantification of γH2AX RINGs in three different cell lines after 24h after toxin wash for HT1080 (3 biological replicates; ∼600-1000 nuclei/condition), HAP1 (6 biological replicates; ∼150-1000 nuclei/condition) and CACO-2 (2 biological replicates; 550-1800 nuclei/condition) Each circle is a biological replicate for HT1080 and HAP1, and a field of view for CACO-2. **e and f**, Representative immunofluorescence images of the DDR of HT1080 to infection at 24h with **e,** *Salmonella* Javiana (MOI 16) **d,** *Salmonella* Typhi (MOI 8) expressing the wild-type toxin or mutant toxin with the deleted active subunit, CdtB subunit (ΔCdtB). Nuclei are displayed as white outlines, *Salmonella* in green and γH2AX in magenta. **c, e and f,** Arrows indicate nuclei with γH2AX RINGs (magenta arrow), and γH2AX foci (white arrow) phenotypes **g,** Quantification of H2AX RINGs in **f** at 24h and 48h of infection from one biological replicate. Each circle represents a field of view (∼400 nuclei/condition). Scale bars denote 50 µm **(b)** and 100 µm **(c, e and f)**. Two-way ANOVA with Sidak multiple comparisons test was carried out to test for statistical significance **(d and g)**. Error bars indicate SEM.[*]

the effect of CdtB DNase activity. Subsequently, the toxin concentration was estimated by creating a standard curve using western blot intensities of known concentrations of purified GST-CdtB-FLAG and extrapolating the concentration of purified typhoid toxin's CdtB intensity **(Fig.3.1d)**.

---

[*]**Fig.3.2d, f and g** were published as part of Ibler et al 2019 (Nat Comms). Access via this link.

3.2 The typhoid toxin induces the novel DNA damage phenotype, RINGs.

Previously, human HT1080 fibrosarcoma cells, which have wild-type p53 alleles, have been used to study diverse DDRs including responses to the typhoid toxin[106,234,235]. Thus, HT1080 cells were intoxicated using established protocols to confirm that the purified typhoid toxin was functional[106].

Briefly, the toxin was pulsed on cells for 2 hours to allow for its endocytosis, before washing the cells with PBS to remove any extracellular toxin. The cells were then chased in fresh complete growth media for the remainder of the experiment (**Fig.3.2a**). After 2h pulse, PltA subunits were observed inside the cells, particularly at the perinuclear microtubule organising centre where endosomes accumulate (**Fig.3.2b**), providing evidence of toxin uptake.

Consistent with Ibler et al 2019, 2h incubation with toxin^{WT} induced γH2AX foci and RING at 24h (**Fig.3.2c**; white and magenta arrows respectively)[106]. The induction of RINGs was reproducible in different cell lines including HT1080, HAP1 (haploid) and Caco-2 (colorectal adenocarcinoma) cells (**Fig.3.2d**; $\sim$25%, $\sim$20% and $\sim$60%, respectively)[106]. This DNA damage response was not observed for untreated and toxin^{HQ}. To examine whether the same DNA damage phenotype is observed during infection, cells were infected with *S.* Javiana and *S.* Typhi encoding the wild-type toxin (WT) and toxin with deleted CdtB subunit (ΔCdtB) then assayed for DNA damage at 24h. *S.* Javiana and *S.* Typhi both induced γH2AX in a CdtB-dependent manner. However, unlike *S.* Javiana, which only demonstrated γH2AX foci (**Fig.3.2e** white arrows) *S.* Typhi displayed the RING phenotype (**Fig.3.2f,** magenta arrows) observed with the purified recombinant typhoid toxin (**Fig.3.2c**). RING positive nuclei increased from $\sim$20% to $\sim$60% after 48 h infection or intoxication (**Fig.3.2g**). Interestingly, γH2AX was induced in non-infected cells surrounding both *S.* Javiana- and *S.* Typhi-infected cells supporting the fact that the toxin is secreted from infected cells and can act in a paracrine fashion (**Fig.3.1e-f**).

3.3 The typhoid toxin induces replication stress leading to RPApT21 exhaustion.

The typhoid toxin has been previously implicated in cell-cycle arrest in G2/M phase[91,92]. Therefore, it was hypothesised that it induces DNA damage in a replication-dependent manner (e.g. during S-phase). To test this hypothesis, cells were serum-starved to arrest their cycle at G1, before intoxicating in serum-free growth media and assaying for DNA damage. Immunofluorescence of intoxicated cells abolished RING formation in serum-starved cells, but instead demonstrated predominantly γH2AX foci phenotype that was independent on replication (**Fig.3.3a, white arrows; 3.3b**). Since RINGs appeared to be replication-dependent, and the CdtB's nickase activity was hypothesised to cause ssDNA breaks[97,236,237,238], replication stress was examined. During replicative stress, RPA binds and
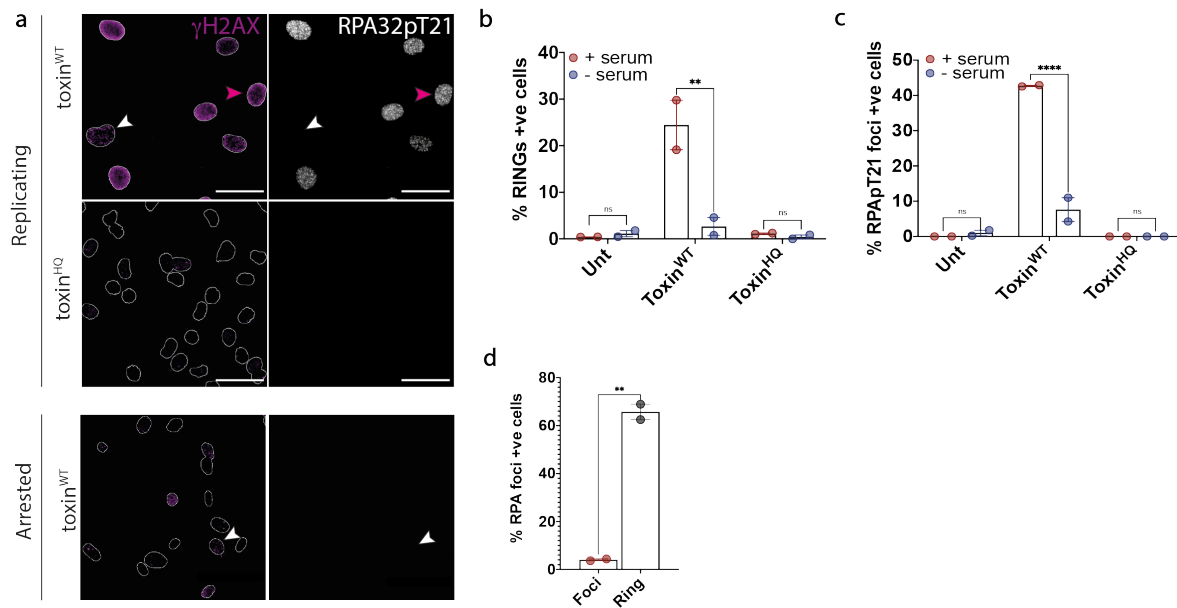
Figure 3.3| DNA damage response in replicating and cell-cycle arrested HT1080 cells. a, Representative immunofluorescence images of nuclear outlines of intoxicated cells at 24h with γH2AX (magenta) and the replication stress marker, RPApT21 (white) with serum (replicating) and serum-starved (arrested). Arrows indicate nuclei with γH2AX RINGs (magenta arrow), and γH2AX foci (white arrow) phenotypes. Scale bars denote 50 µm. **b-d,** Quantification of **b,** RING positive nuclei (∼300-600 nuclei/condition), **c,** RPApT21 foci positive nuclei (∼350-600 nuclei/condition), and **d,** nuclei that display RPApT21 with either γH2AX RINGs or foci from all conditions at 24h (∼1500 nuclei/phenotype) across two biological replicates (circles on the graph). Error bars indicate SEM. Two-way ANOVA with Sidak multiple comparisons test **(b and c)** and an unpaired t-test **(d)** were used to test for statistical significance.*

persists on ssDNA of stalled replication forks and recruits ATR to signal a DNA damage checkpoint, and phosphorylates RPA at theronine 21 position (RPApT21)[148]. Indeed, toxin^WT led to an increase in RPApT21 positive nuclei **(Fig.3.3a, 3.3c)**, that specifically localised with RING-positive nuclei **(Fig.3.3a, 3.3d**; magenta arrows**)**, which was not the case with toxin^HQ and untreated cells. These results support that the toxin induces replication stress.

3.4 Intoxicated cells demonstrate a senescence-like phenotype.

It was previously shown that the exposure of cells to cytolethal distending toxins leads to apoptosis and senescence[239,240,241], but the fate of cells targeted by the typhoid toxin is unclear. When cell proliferation was examined in toxin^WT-treated cells, no colonies were observed, unlike untreated and toxin^HQ treated cells **(Fig.3.4a**, top panel**)**, which confirmed previously reported toxin^WT-induced cell-cycle arrest[91,92]. Upon higher magnification imaging of the plates, intoxicated cells appear to have survived. They displayed astonishing enlargement and distension of cells, which is a typical morphology induced by cytolethal distending toxins **(Fig.3.4a**, exemplified by cells in the bottom panel**)** and a hallmark of senescence[155,163]. The result in **Fig. 3.4a** favoured the hypothesis that the typhoid toxin induces senescence rather than apoptosis. To investigate this further, cells were assayed for the lysosomal senescence-associated beta-galactosidase activity (SA-β-gal). If cells have elevated

---

***Fig.3.3a,** (top panel) **and d** were published as part of Ibler et al 2019 (Nat Comms). Access via this link.
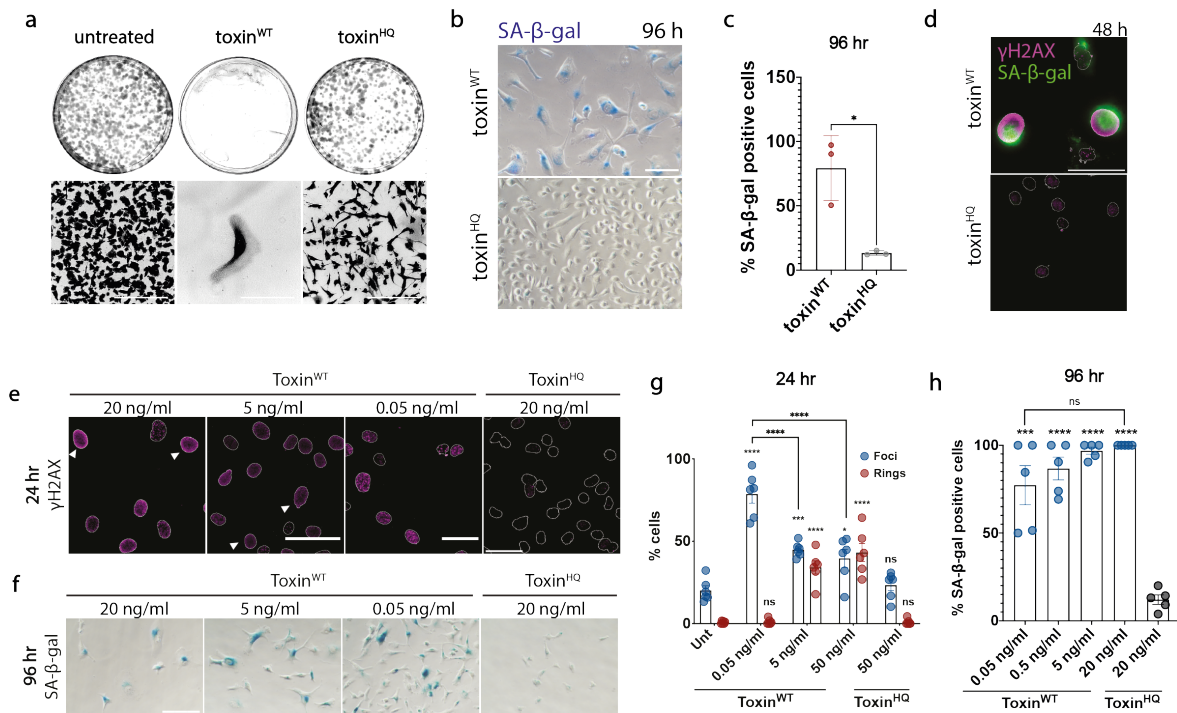
Figure 3.4| Senescence-like phenotype induced by the typhoid toxin in HT1080 cells. a, Clonogenic assay to examine cell division by intoxicated cells and imaged on day 8 post-intoxication (top panel), and the magnified plates using 20X objective (bottom panel). **b,** Representative images of intoxicated cells histologically stained for senescence-associated β-galactosidase activity at 96h post-intoxication. **c,** Quantification of b from 2 biological replicates (circles represents 3 technical replicates; 300-750 nuclei/condition). **d,** Representative image of SpiDER gal localising with RING positive nuclei. **e,** Representative images of the DNA damage responses to titrated toxin^{WT} concentrations marked by γH2AX at 24h. **f,** Representative images of a senescence response to titrated toxin^{WT} concentrations marked by SA-β-gal at 96h. **g,** Quantification of **e**. Each circle is a field of view (1 biological replicate, ∼200-500 nuclei/condition). **h,** Quantification of **f**. Each circle is a field of view (1 biological replicate,∼80-200 cells/condition). One-way ANOVA test was used with Tukey's multiple comparison carried out for **g**. Unpaired t-test was used for **h**. Asterisks indicate significance compared to untreated counterpart unless otherwise indicated by brackets. Error bars indicate standard error of the mean (SEM). All toxin concentrations are at 20 ng/ml unless indicated. Scale bars are 50 µm **(e)**, 100 µm **(a, b and d)**, 300 µm **(f)**.*

SA-β-gal activity, cells can convert the substrate (X-gal) into a blue precipitate under sub-optimal pH6, in contrast to physiological β-gal which is active at pH4[242]. As predicted, toxin^{WT}-treated cells showed a statistically significant increase in the percentage of SA-β-gal positive cells 96h post intoxication compared to the negative control **(Fig.3.4b, 3.4c)**, which was reproducible in other cell lines including retinal epithelial RPE-1 cells **(Fig.3.6g)** and IMR90 lung fibroblast cells **(Fig.3.7b, 3.7g**; marked by reduction of EdU positive nuclei**)**. SA-β-gal in intoxicated cells was also observed by fluorescence microscopy **(Fig.3.4d)**, which also revealed SA-β-gal in RING-positive cells. Thus, the typhoid toxin induces several traits characteristic of senescence, namely (i) cell cycle arrest, (ii) cellular distention, and (iii) increased lysosomal SA-β-gal activity.

To further examine the DDR responsible for the senescence phenotype, SA-β-gal and γH2AX were investigated with different concentrations of toxin. Titration of the toxin from 20 ng/ml to 0.05 ng/ml reduced the proportion of RING-positive cells, which corresponded with an increase in γH2AX foci

---

*****Fig.3.4d, and part of g** were published as part of Ibler et al 2019 (Nat Comms). Access via this link.
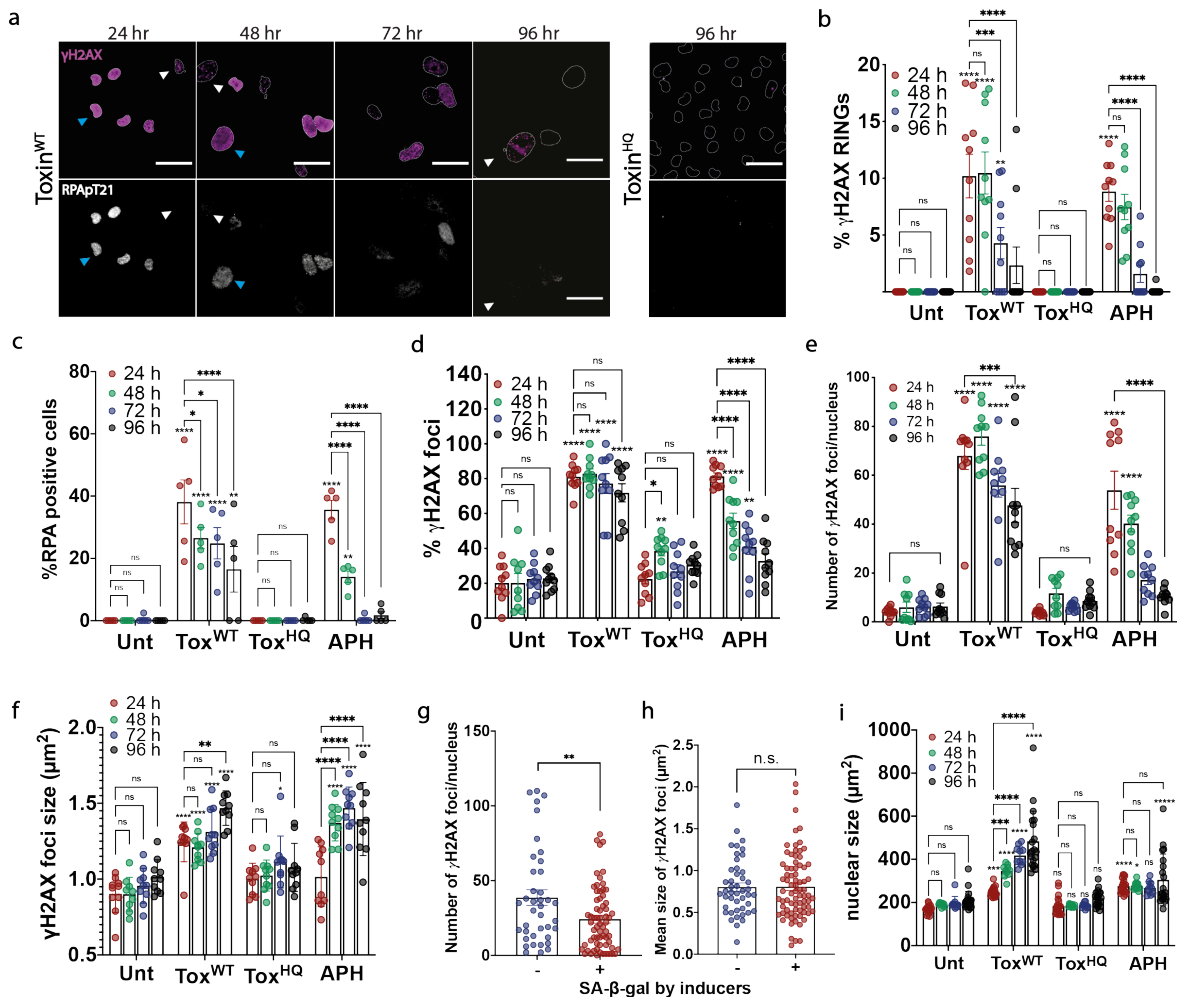
Figure 3.5| Time course of the DNA damage response and replication stress to the typhoid toxin from early to late senescence. a, Representative images of a time-course experiment of DNA damage responses marked by γH2AX (magenta) and replication stress marker RPApT21 (white) stained at 24h intervals. Arrows indicate nuclei with γH2AX RINGs (magenta arrow), and γH2AX foci (white arrow) phenotypes. **b,** Percentage of γH2AX RINGs positive nuclei. Each circle represents a field of view (2 biological replicates, ∼140- 1300 nuclei/condition) **c,** Percentage of nuclei positive for phosphorylated RPA (RPApT21). Each circle represents a field of view (2 biological replicates, ∼170-920 nuclei/condition). **d,** Percentage of γH2AX foci positive nuclei. Each circle represents a field of view (2 biological replicates, ∼140-1300 nuclei/condition). **e,** Number of γH2AX foci per nucleus including foci in RING cells. Each circle is the average number of foci/nucleus per field of view (2 biological replicates, ∼140-1300 nuclei/condition). **f,** Size of γH2AX foci induced. Each circle is the average size per field of view (2 biological replicates ∼3000-22000 foci measured/condition). **g and h,** Number and size of foci/nucleus in SA-β-gal positive and negative cells by senescence inducers. Each circle depicts a nucleus after outliers were removed using GraphPad ROUT (Q=1%). **i,** Nuclear sizes changes across 4 days. Each circle is the average nuclear size per field of view (3 biological replicates, ∼160-1500 nuclei). Quantification was using CellProfiler **(b, d-g)** and the MATLAB code from Ibler et al, 2019 **(c)**. Two-way ANOVA test was used with Tukey's multiple comparison carried out for **b-f, i**. Unpaired t-test was used for **g-h**. Asterisks indicate significance compared to untreated counterpart unless otherwise indicated by brackets; if not indicated it is not significant. Error bars indicate SEM. Scale bars of representative images are 50 µm.

(Fig.3.4e, 3.4g). Despite the loss of RINGs with low concentrations of toxin^{WT} (0.05 ng/ml), SA-β-gal was apparent in ∼75% of cells mirroring the proportion of cells with γH2AX foci **(Fig.3.4f-h)**. Thus, the data suggest that toxin-induced γH2AX foci and RINGs can both drive cellular senescence, which may reflect damage in G1 (γH2AX foci) and S phase (RINGs).

3.5 Toxin-induced γH2AX foci drive cellular senescence

The data in **(Fig.3.4d)** and **(Fig.3.4e)** show that RINGs cause cellular senescence but RINGs were only apparent at ng concentrations (>5ng/ml), which suggests relatively high doses of toxin are required for RING-driven senescence. Differences in toxin dose may also explain why RINGs were observed with *S.* Typhi but not *S.* Javiana **(Fig.3.2e, 3.2f)**. Thus, we extended our analysis of γH2AX RINGs and foci to examine their relative contribution to toxin-induced senescence responses between 24h and 96h **(Fig.3.5a)** . Surprisingly, the number of RING-positive cells decreased between 24h and 96h **(Fig. 3.5a, 3.5b**: ∼10% to ∼2%**)**. Consistent with this, the reduction in RINGs was concomitant with a reduction in RPApT21-positive cells **(Fig.3.5a; 3.5c**: ∼40% to ∼15%**)** In contrast, there was no significant difference in the proportion of cells with γH2AX foci between 24h and 96h **(Fig.3.5d**: ∼80% at 24h vs 70% at 96h**)**. Deeper inspection of the toxin^{WT}- induced γH2AX foci in **Fig.3.5a** revealed further evolution of DDRs whereby the number of γH2AX foci per nucleus decreased by the 96h point **(Fig.3.5e)**, which was coincident with an increase in the size of γH2AX foci **(Fig.3.5f)**. Treatment of cells for 24h with the inducer of DNA replication stress aphidicolin (APH) also triggered RINGs and RPApT21 that decreased between 24h and 96h **(Fig.3.5b**: ∼9% to 0%, **3.5c**: ∼35% to 1%**)**. In contrast to the toxin^{WT}, APH-induced γH2AX foci also decreased between 24h and 96h **(Fig.3.5d**: ∼80% to 30%**)**, which likely reflects significant DNA repair due to removal of APH at 24h while intracellular toxin^{WT} persists until presumably degraded by host proteases. No DDRs were observed in negative control cells that were either untreated or treated with toxin^{HQ} **(Fig.3.5b-d)**. Interestingly, examination of SA-β-gal positive cells by toxin^{WT} and APH (i.e. senescence inducers) were associated with significantly fewer γH2AX foci per nucleus **(Fig.3.5g)**, regardless of their size **(Fig.3.5h)**. Despite the loss of RINGs **(Fig.3.5a, 3.5b)**, nuclei of toxin^{WT}-treated were increasingly distended **(Fig.3.5i)**, which is an indicator of cellular senescence[243]. These data suggest that senescence is predominantly associated with persistent γH2AX foci.

3.6 Toxin induced DDR in caspase-deficient Retinal Epithelial Cells (RPE-1)

RING cells were not observed after 48 h **(Fig.3.5a, 3.5b)** in HT1080 cells and their fate is unclear. γH2AX at the nuclear periphery has been observed at early stages of apoptosis in a caspase-dependent manner[154,244]. To investigate whether RING cells become apoptotic despite showing signs of senescence **(Fig.3.4d)**, RPE-1 cells, which resist apoptosis by expressing low levels of caspase-8[245], were intoxicated and assayed for γH2AX, RPApT21, and SA-β-gal. Unconventionally, at the standard intoxication concentration (i.e. 20 ng/ml), RING cells were absent **(Fig.3.6a, 3.6b)**, which indicates that RING formation is potentially caspase-8 dependent. However, increasing the toxin concentration 10-fold in RPE-1 cells (20 ng/ml to 200 ng/ml) induced RINGs and RPApT21 positive nuclei in a dose-dependent manner **(Fig.3.6a**, magenta arrows; **3.6b**, ∼0% to ∼8%; **3.6c**, ∼10% to 20%**)**.
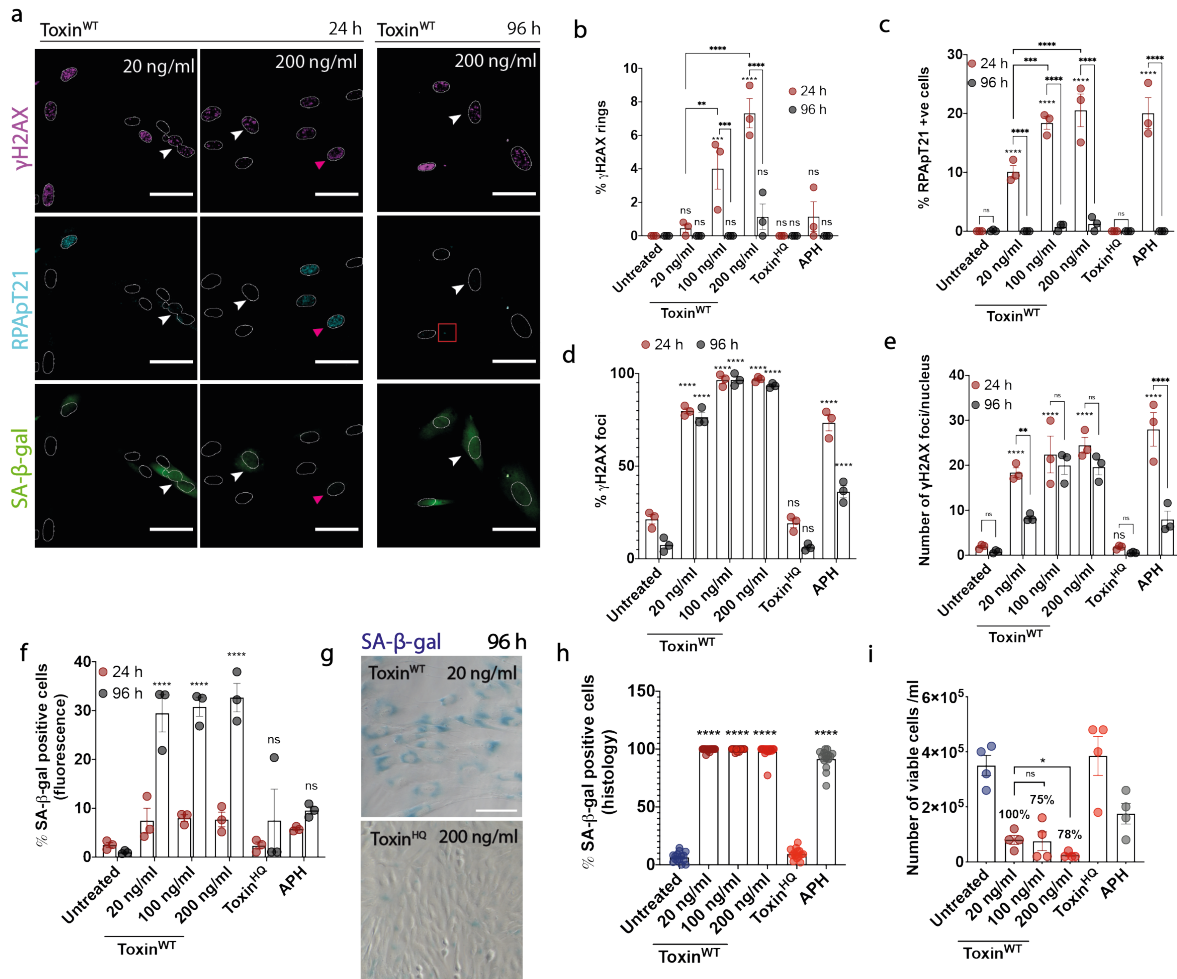
Figure 3.6| DNA damage response in caspase-8 deficient cell line, RPE-1 cells. a, Representative images of DNA damage responses in RPE-1 cells at early (24h) and late (96h) time-points experiment marked by γH2AX (magenta), replication stress marker RPApT21 (white), and SA-β-gal (green) stained at 24h and 96h at different concentrations. Arrows indicate nuclei with γH2AX RINGs (magenta arrow), and γH2AX foci (white arrow) phenotypes, and red box highlights cytosolic RPApT21. **b-d,** Percentage of **b,** γH2AX RING-, **c,** RPApT21-, **d,** γH2AX foci-positive nuclei. **e,** Number of γH2AX foci per nucleus including foci in RING cells. **f,** Percentage of RPE-1 cells expressing fluorescent CellEvent Green Probe for SA-β-gal. **b-f,** Each circle represents technical replicates (1 biological replicate, ∼300-1700 nuclei/condition). **g,** Representative image of intoxicated RPE-1 cells histologically stained for senescence-associated β galactosidase activity at 96h post-intoxication. **h,** Quantification of **g** with toxin[HQ] concentration at 200 ng/ml. (1 biological replicate; 600-3000 cells/condition). **i,** Number of viable cells as assayed using Trypan blue and hemocytometer. Average percentage viability is denoted on each bar. Each circle represents a technical replicate from 1 biological replicate. Two-way **(b-f)** and one-way **(h)** ANOVA test were used with Tukey's multiple comparison to test for statistical significance. Asterisks indicate significance compared to untreated counterpart unless otherwise indicated by brackets. Error bars indicate SEM. Scale bars of representative images are 50 μm **(a)** and 100 μm **(g)**.
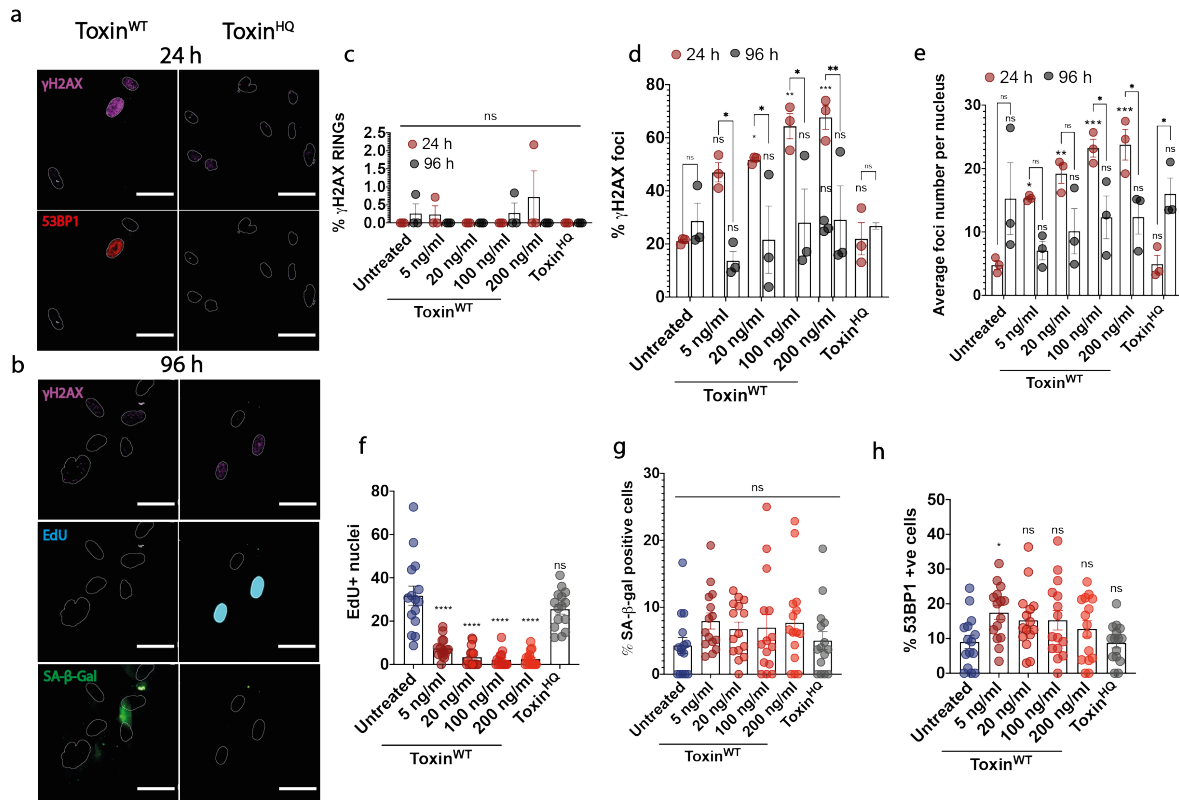
Figure 3.7| DNA damage response in primary fibroblast cell line, IMR90 cells. a and b, Representative images of DNA damage responses in IMR90 cells at **a,** early (24h) and **b,** late (96h) time-points experiment marked by γH2AX (magenta), repair protein 53BP1 (red), EdU (cyan) and SA-β-gal (green) stained at 24h and 96h at 100 ng/ml of toxin^{WT} and 200 ng/ml toxin^{HQ}. **c-e,** Percentage of **c,** γH2AX RING- **d,** γH2AX foci-positive nuclei and **e,** number of foci per nucleus at 24 and 96h post treatment at different toxin concentrations. Each circle represents biological replicates (∼350-750 nuclei per variable). **f-h,** Percentage of, **f,** EdU **g,** SA-β-gal and **h,** 53BP1-positive cells from 3 biological replicates (∼350-750 nuclei per variable). Each circle represents a field of view. SA-β-gal of toxin-treated cells was thresholded using images of untreated cells. Two-way **(c-e)** and one-way **(f-h)** ANOVA test with Dunnett's and Sidak multiple comparison tests were carried out to test for significance. Asterisks indicate significance compared to untreated counterpart unless otherwise indicated by brackets. Error bars indicate SEM. Scale bars of representative images are 50 μm.

Consistent with HT1080s, RING and RPApT21 positive nuclei were induced at 24h but disappeared by 96h post-intoxication. Notably, RPE-1 displayed cytosolic RPApT21 at high concentration at 96h **(Fig.3.6a;** red boxes), which might indicate leakage of DNA fragments into the cytosol, a marker of senescence[155,246]. RPE-1 cells showed an increase in γH2AX foci positive nuclei at 24h **(Fig.3.6d,** ∼80-100%) that were persistent at 96h for RPE-1 **(Fig.3.6d)**. As with HT1080 cells **(Fig.3.5a, 3.5e)**, the number of γH2AX foci per nucleus was significantly reduced between 24 and 96h for both cell lines particularly at low concentrations in RPE-1 **(Fig.3.6e)**.

Toxin^{WT} induced up-regulation of SA-β-gal at all concentrations in RPE-1 cells at 96h **(Fig.3.6f-h;** ∼30% fluorescence and ∼100% histology). However, at RING-permissive concentrations at 24h in RPE-1 cells **(Fig.3.6b)**, the number of viable cells **(Fig.3.6i)** and the extrapolated percentage viability of RPE-1 cells were slightly reduced **(Fig.3.6i;** ∼100% to 75% n.s.) at 96h, which suggests potential apoptosis that was delayed due to senescence responses.

3.7 Toxin induced DDR in primary lung fibroblast cells, IMR90

Previously, RING formation had been observed in seven cell lines tested, including U2OS, HAP1, HT1080, THP1, Caco-2, RAW, MEF cells **(Fig.3.2)**[106]. Thus, the lack of RINGs in RPE-1 cells was surprising **(Fig.3.7)**. Similarly, a lack of RINGs was observed in primary IMR90 fibroblast cells **(Fig.3.7a-c)**, which is an established senescence model and has been used to study senescence induced by cytolethal distending toxins[240,247,248]. The observation with RINGs warranted further investigation. Like RPE-1 cells **(Fig.3.6)**, IMR90 cells showed an increase in γH2AX foci positive nuclei at 24h **(Fig.3.7d**, ∼50-70%**)** but the effect was modest relative to HT1080 and RPE-1 cells **(Fig.3.5, Fig.3.6)**. Moreover, while γH2AX foci positive cells were persistent at 96h for HT1080 **(Fig.3.5d)** and RPE-1 **(Fig.3.6d)**, γH2AX foci positive cells were reduced in IMR90s **(Fig.3.7d,** ∼10-20%**)**. The number of γH2AX foci per nucleus was significantly reduced between 24 and 96h in all cell lines **(Fig.3.5e, Fig.3.6e, Fig.3.7e)**. Though the toxin caused cell-cycle arrest in IMR90 cells as determined by EdU labelling **(Fig. 3.7b, Fig.3.7f)**, the modest effect of the toxin in IMR90 cells was reflected by no significant difference in 53BP1-positive cells and SA-β-gal **(Fig.3.7g, Fig.3.7h)**, which are hallmarks of senescence. In summary, both RPE-1 and IMR90 cells do not display RINGs, and while RPE-1 cells show hallmarks of senescence in toxin-treated cells, this was not the case for IMR90 cells.

3.8 Characteristics of toxin-induced senescence.

While characteristics of oncogene-induced senescence and replicative senescence are well established, bacterial-induced senescence remains a relatively uncharacterised phenomenon with very few examples cited in the literature[213,222,240]. Thus, senescence responses to the typhoid toxin were further investigated.

A hallmark of senescence is the p53 effector p21, which is a CDK inhibitor[249]. Relative to negative control cells, p21 expression was upregulated in toxin^WT- or APH-treated cells, which was coincident with induction of γH2AX **(Fig.3.8a)**. Persistent DDRs in senescent cells can lead to enlarged senescence DNA damage foci (SDF) identified by co-localisation of γH2AX and 53BP1[179,250,251,252]. At 96h, γH2AX foci were found enlarged in 80% of toxin^WT-treated cells **(Fig.3.5e, 3.5f)**. Similarly, 53BP1 was found co-localised in enlarged foci with γH2AX in 80% of cells at 96h **(Fig.3.8b, 3.8c)**, which were also SA-β-Gal positive indicating senescence **(Fig.3.8b)**. Indeed, relative to untreated cells, toxin^WT significantly increased the proportion of 53BP1-positive cells at 24h, which was not the case with toxin^HQ, APH and the topoisomerase inhibitor, etoposide (ETP) **(Fig.3.8c)**. By 96h, toxin^WT, toxin^HQ, APH and ETP had increased the proportion of 53BP1-positive cells **(Fig.3.8c)**, albeit to a lesser extent with toxin^HQ, which has been observed before[106]. The modest effect of toxin^HQ was reflected by the number of 53BP1 foci per nucleus, which mirrored untreated cells and contrasted with the significant effects mediated by toxin^WT, APH and ETP **(Fig.3.8d)** The increase
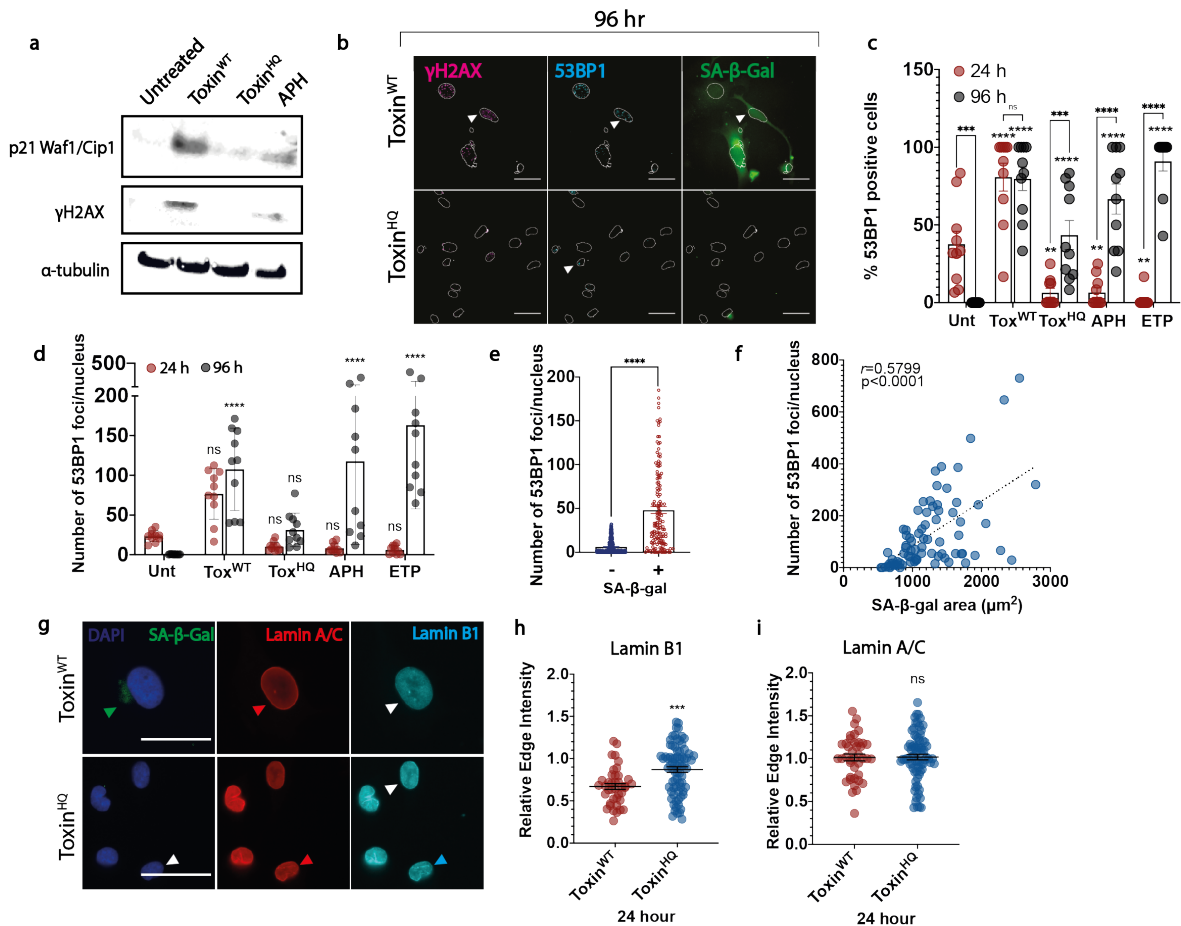
Figure 3.8| Senescence hallmarks induced by toxin^WT. a, Western blot of whole-cell lysates collected at 48 h post-removal of the senescence-inducer from one biological replicate. **b,** Representative images of intoxicated cells at 96h stained for γH2AX (magenta), 53BP1 (cyan), and SA-β-gal (green). White arrows indicate 53BP1 positive cells. **c,** Quantification of 53BP1-positive nuclei from **b** using cell profiler and untreated as minimum threshold. **d,** Number of 53BP1 foci per nucleus using CellProfiler. **c and d,** Each circle is a field of view (1 biological replicate, ∼30-180 nuclei/condition). **e,** Number of 53BP1 foci in cells that are either positive or negative for SA-β-gal from all conditions. **f,** Pearson's correlation of the number of 53BP1 foci and area of SA-β-gal occupying the corresponding cell. Each circle represent cells of senescence inducers positive for SA-β-gal after outliers were removed using GraphPad ROUT (Q=1%). **g,** Representative images of intoxicated cells at 24h stained for lamin A/C and lamin B1, and their contribution to SA-β-gal. Red arrows indicate nuclei positive for lamin A/C. Cyan arrows indicate nuclei positive for lamin B1. White arrows indicate nuclei with absent lamin B1. Green arrow indicates nucleus positive for SA-β-gal. **h,i,** Relative edge intensity of the **h,** lamin B1 **i,** lamin A/C calculated by creating a ratio of intensity on the nuclear membrane and intensity inside the nucleus. Each circle represents a nucleus (10 fields of view, 1 biological replicate, ∼40-140 nuclei/condition). All toxin concentrations are at 20 ng/ml. Asterisks indicate significance compared to untreated at the same time-point unless otherwise indicated by brackets. Two-way ANOVA with Sidak and Dunnet's multiple comparisons test (c and d respectively), and unpaired t-test **(e, h and i)** were used to test for statistical significance. Asterisks indicate significance compared to untreated counterpart unless otherwise indicated by brackets. Error bars indicate SEM. Scale bars of representative images are 50 μm.

in the number of 53BP1 was associated with SA-β-gal-positive cells (**Fig.3.8e**) and the increase in the area occupied by SA-β-gal activity in the cell (**Fig.3.8f**), indicating that 53BP1 is coincident with toxin-induced senescence.

Lamin B1 downregulation has been proposed to drive the establishment of a full senescence phenotype, thereby triggering chromatin remodelling to induce SASP[249]. When the nuclear envelope was examined, lamin B1 was down-regulated by toxin^WT relative to toxin^HQ (**Fig.3.8g, 3.8h**: lamin B1),

while other nuclear lamina components remained unchanged (**Fig.3.8g, 3.8i**: lamin A/C). These results show that the toxin induces a p21-driven senescence phenotype characterised by SDFs and downregulation of lamin B1.

3.9 Typhoid toxin induces a host senescence-associated secretory phenotype (SASP)

The typhoid toxin has demonstrated various senescence-associated phenotypes. Senescent cells are typically metabolically active with a senescence-associated secretory phenotype that modulates the surrounding environment[253,155]. Conditioned media (CM) harvested from intoxicated HT1080 cells at 96h post intoxication, transmitted senescence as exemplified by cellular distension and up-regulation of SA-β-gal in naive HT1080 cells (**Fig.3.9a, 3.9b**; ∼50%), suggesting toxin-induced SASP (tox^{SASP}). Analysis of tox^{SASP} at 24h intervals indicated a gradual increase in transmissible senescence that reached maximum potency between 24-48 h (**Fig.3.9c**, ∼80%). Transmissible senescence was not limited to cells of the same type. IMR90 SASP induced transmissible senescence in naive IMR90 (**Fig.3.9d-f**; ∼95%) and naive HT1080 (**Fig.3.9g, 3.9h**; ∼70%).

Previous literature described that SASP of various senescent cell types retained the ability to induce DNA damage[254]. Indeed, tox^{SASP} showed 30% increase in γH2AX-positive HT1080 cells (**Fig.3.9i, 3.9j**; ∼40%) with negative control CM and ∼70% with tox^{SASP}). Transmissible senescence was also observed during infection by CM harvested from cells treated for 2h or 24h with toxin^{WT} secreted from cells infected by wild-type *S.* Javiana but not *S.* Javiana$^{\Delta tox}$ (**Fig.3.9k-m**; ∼80% SA-β-gal positive cells). Importantly, this shows that *Salmonella* -infected cells transmit SASP in a toxin-dependent manner.

To examine whether the paracrine effect in cells treated with recombinant toxin is due to contaminating toxin in the conditioned media, intoxication was carried out using the third wash fraction (wash^{toxWT}) after intoxication as illustrated in (**Fig.3.10a**). If any toxin remains, it would be able to induce γH2AX in untreated cells. However, cells treated with wash^{toxWT} showed significantly reduced DNA damage compared to intoxicated cells and mirrored negative controls (**Fig.3.10b, 3.10c**). Additionally, CM harvested from toxin^{WT}- and toxin^{HQ}-treated cells was analysed by mass spectrometry. Whilst all subunits were detected in the purified toxin^{WT}, only the PltB subunit was detected in the CM (**Fig.3.10d, 3.10e**). Interestingly, PltB is known to bind cell surface receptors so its presence may indicate that intoxication can induce shedding of PltB-loaded receptors that have been recycled to the cell surface. Nevertheless, it is well-established that only the holotoxin comprising PltB-PltA-CdtB is toxigenic and drives toxin-induced phenotypes[78,81,96].

****Fig.3.9l and m** were published as part of Ibler et al 2019 (Nat Comms). Access via this link.
****Fig.3.10c** was published as part of Ibler et al 2019 (Nat Comms). Access via this link.
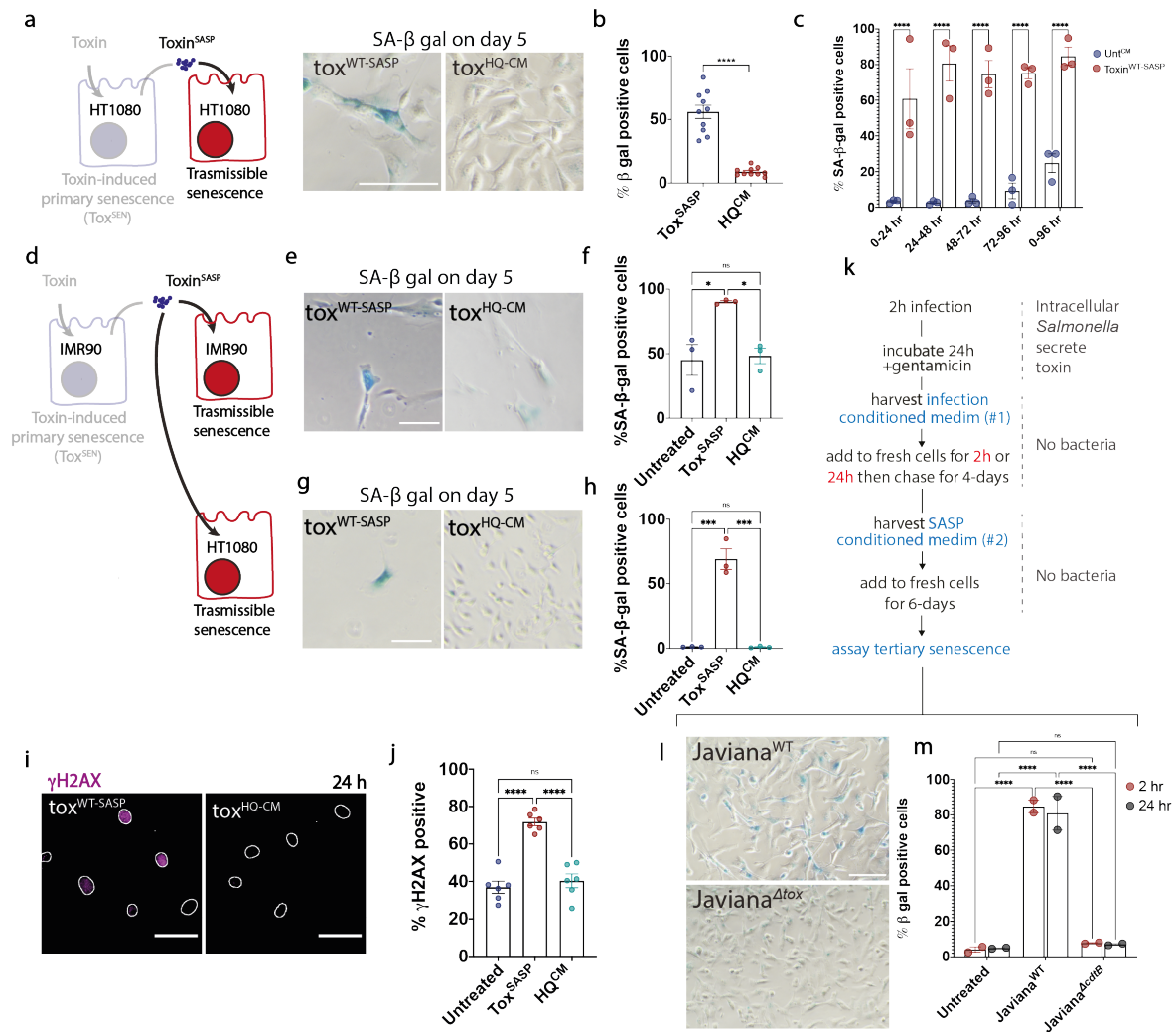
Figure 3.9| Transmissible senescence by the typhoid toxin. a, Representative images of naive HT1080s treated for 5 days with either toxin^{WT}-SASP or the tox$^{HQ\text{-}CM}$ harvested from intoxicated HT1080s at day 4, before histologically stained for SA-β-gal. **b,** Quantification of **a**. Each circle is a field of a view (2 technical replicates, 1 biological replicate; ∼1000-3000 cells/condition). **c,** Percentage of SA-β-gal-positive cells treated with 24h fractions of conditioned media collected from intoxicated cells across 4 day. Each circle represents a field of view (1 biological replicate; ∼50-1800 cells/variable). **d-g,** Representative images of naive **e,** IMR90 cells or **g,** HT1080 cells, treated for 5 days with either toxin^{WT}-SASP or the tox$^{HQ\text{-}CM}$ from intoxicated IMR90s at day 4, before histologically stained for SA-β-gal. **f and h,** Quantification of e and g respectively. Each circle represents a biological replicate. (∼400 cells/condition for **f;** ∼400-3800 cells/condition for h). **i,** Representative images of DNA damage (γH2AX; magenta) induced in HT1080 cells after 24h of treatment with toxin^{WT}-SASP or the tox$^{HQ\text{-}CM}$ harvested from intoxicated HT1080s at day 7. Each circle is a field of view (1 biological replicate, ∼250-350 nuclei/condition). **k-m, k,** Workflow of conditioned media harvest from *Salmonella* infected HT1080, **l,** Representative images of naive HT1080s stained for SA-β-gal after conditioned media treatment, and **m,** Quantification of **l** of cells subjected to conditioned media after 2h or 24h treatment with toxin harvested from *Salmonella* . Each circle is a technical replicate (1 biological replicate, 160-7000 cells/condition). Unpaired t-test **(b)**, two-way ANOVA with Tukey's multiple comparison tests **(c and m)**, one-way ANOVA with Tukey's multiple comparison tests **(f, h, j)** were carried out to test for significance. Error bars indicate SEM. Scale bars of representative images are 50 μm **(i)** and 100 μm **(a, e, g, and l)**.*

3.10   Discussion

The typhoid toxin-induced DNA damage has been implicated in typhoid fever and chronic *Salmonella* carriage, which is mediated by manipulation of host cell functions through unknown mechanisms[78,81,96].
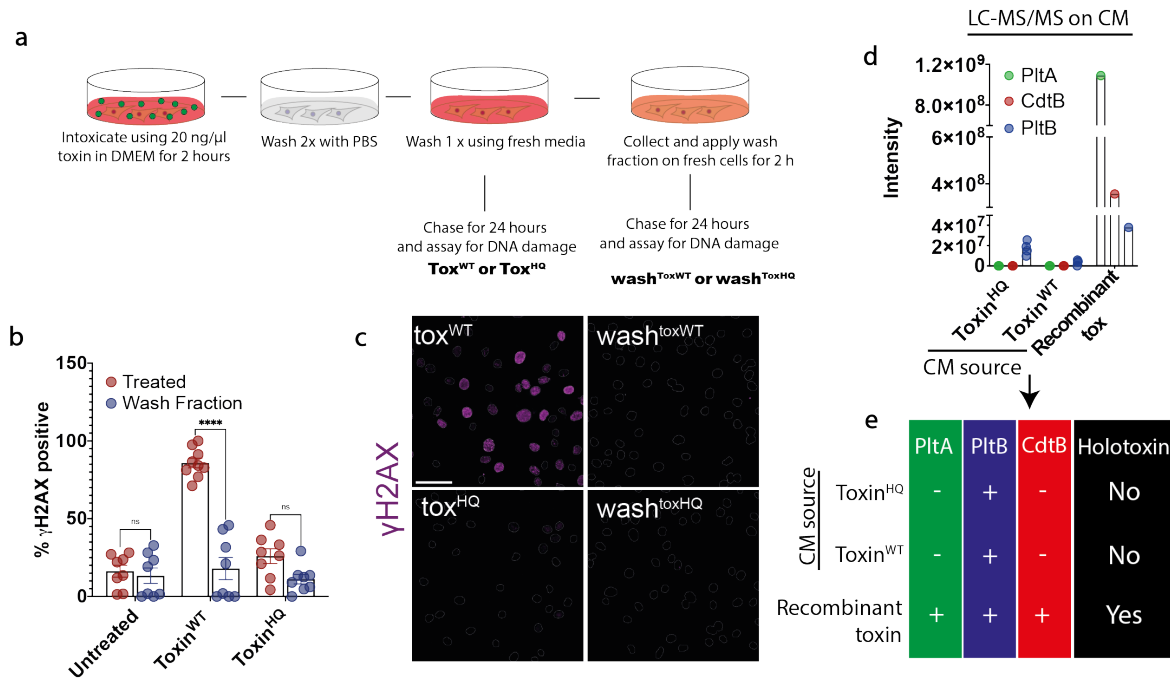
Figure 3.10| Transmissible senescence is due to host proteins. a, Experimental schematic to test whether toxin is contaminating the conditioned media collected. **b and c,** representative image and quantification of γH2AX (magenta) positive nuclei of HT1080 cells treated directly with the toxin, or treated with the third wash post-intoxication at 24h. **d and e,** LC-MS/MS analysis of conditioned media harvested from toxin-treated cells (4 biological replicates) with the recombinant purified typhoid toxin as a positive control. Intensities of each toxin subunit detected is depicted in **d** and summarised in **e**. + denotes presence and - denotes absence. Scale bars of representative images are 50 μm.[*]

Little was explored into the DNA damage responses to the toxin in host cells and how this facilitates invasive *Salmonella* systemic infections leading to typhoid and chronic bacterial carriage[78,81,99,231]. This chapter presents evidence of a novel toxin-induced DNA damage phenotype localised at the periphery of the nucleus we called RINGs that is replication-dependent. The RING phenotype was observed with the recombinant toxin, and during infection in multiple cell lines, concurrent with RPApT21 foci (**Fig.3.11**). Healthy human cells have a finite amount of RPA in the nucleus that protects ssDNA during replication. Ibler et al (2019) showed that toxin nuclease activity caused excessive SSBs that exhausted the cellular pool of RPA resulting in massive DNA damage manifesting as RINGs[106]. The data in **Fig.3.3** were presented in Ibler et al (2019) and support the view that the toxin causes RPA exhaustion directing the cell to a senescence-like phenotype. Similar to the typhoid toxin, *E. coli* CDT has been shown to result in ssDNA and RPA activation[236].

Senescence is a normal physiological process that increases in aging organisms. Emerging research implicates senescence in both host-protection and pathogen hijacking mechanisms[213]. However, it is unclear whether the senescence phenotypes induced by toxin are mechanisms of host defence or pathogen attack.

This chapter presented evidence that toxin results in senescence phenotypes including persistent
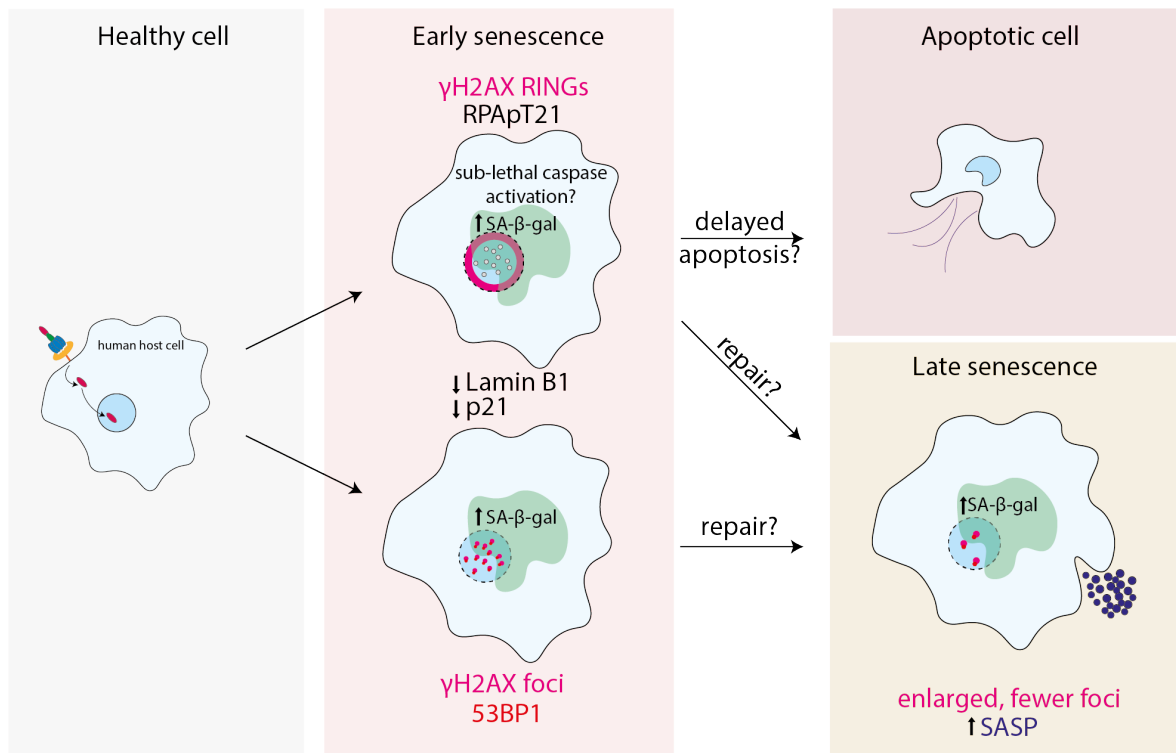
Figure 3.11| Proposed cell model. The typhoid toxin binds to the cells via the PltB subunit. The toxin's CdtB subunit translocates to the nucleus where it causes two distinct DNA damage phenotypes: foci and RINGs. γH2AX foci localise with 53BP1, and RINGs lead to the exhaustion of RPA in the nucleus in early senescence. In late senescence, γH2AX foci increase in number and decrease in size signifying potential repair. RINGs disappear over time and potentially undergoes apoptosis or repair into γH2AX foci positive cells.

γH2AX foci localised with 53BP1 foci, up-regulation of p21, down-regulation of lamin B1, and SASP that transmits senescence to naive cells (**Fig.3.11**). The experiments using RPE-1 cells indicate that caspase-8 plays a key role in RING formation. γH2AX has previously been observed at the nuclear periphery at early stages of apoptosis further suggesting a role for caspases in peripheral γH2AX localisation[154,244,255]. However, neither cleavage of caspase-3 or apoptosis marker PARP1 was observed in intoxicated cells, and the pan caspase inhibitor ZVAD-OMe-FMK had no effect on toxin-induced γH2AX RINGs[106]. How can the role of caspase-8 be explained? Sublethal activation of caspases has previously been shown to resist apoptosis in a mechanism called minority-MOMP[256], which has also been implicated in host cell infections by diverse pathogens[257]. Thus, sub-lethal activation of caspase-8 may contribute to RING formation and senescence. In contrast, RING cells' disappearance could be a result of repaired DNA damage that developed into γH2AX foci. Nevertheless, the lack of RINGs and the high proportion of senescent RPE-1 cells suggests that RINGs are not required for toxin-mediated senescence, which can in fact be driven by γH2AX foci (**Fig.3.11**).

Aged animals are more susceptible to infections by CDT secreting bacteria, such as *Salmonella* Typhimurium[258] and *Staphylococcus aureus*[259]. Similarly, the typhoid toxin might be exploiting the senescence phenotype in favour of *S.* Typhi infections. Indeed, research in the Humphreys lab[106] showed that conditioned media harvested from intoxicated cells enhance infection in naive cells, providing a novel role to toxin-induced senescence. Additionally, in the context of infection, *Salmonella*

-induced secretion of host survival proteins as part of SASP, would sustain host cell survival, creating a safe haven to evade the immune system and establish more chronic infections. Therefore, it is prudent to characterise the constituents of toxin$^{\text{SASP}}$ and examine their role in invasion. The next chapter presents the optimisation of conditioned media harvest and analysis by mass spectrometry in an effort to identify constituents of toxin$^{\text{SASP}}$.

Chapter 4

Metabolic labelling of toxin$^{\text{WT-SASP}}$

Cell culture secretomes are typically analysed using pre-determined antibody arrays, ELISA, or western blotting of conditioned media analyses[175,195,205,260]. Whole-cell transcriptomic analysis is attractive because it represents an unbiased approach but this would not resolve the host secretome[189,261]. LC-MS/MS is an unbiased quantitative approach for analysing the conditioned media and identifying the host secretome. The aim of this chapter is to optimise methodology for identifying the host secretome in cells undergoing toxin-induced senescence through conditioned media analysis using LC-MS/MS. This will build towards understanding transmission of senescence and how this enhances *Salmonella* invasion.

The main challenge of analysing conditioned media using mass spectrometry is the abundance of foetal bovine serum (FBS) in the culture medium, which will mask less abundant proteins. This chapter summarises an approach, which uses a methionine analogue, known as bio-orthogonal non-canonical amino acid tagging (BONCAT), that enables LC-MS/MS analysis of the toxin-induced secretome in conditioned media.

4.1 Optimisation of cell survival with the methionine analogue, AHA.

BONCAT exploits the methionine analogue L-Azidohomoalanine (AHA), which can be used to label newly synthesised proteins and identify secreted proteins[262]. BONCAT is a popular quantitative method due to its non-radioactivity, and sensitivity which makes it ideal for secretome analysis by mass spectrometry. This method has been recently used to identify proteins involved in autophagy in cell cultures[263] and translationally active populations of cystic fibrosis microbiota[264].

After incubating cells with AHA, conditioned media containing labelled (SASP$^{\text{AHA}}$) and unlabelled SASP (SASP$^{\text{untagged}}$) were harvested before AHA-tagged proteins were immobilised on an
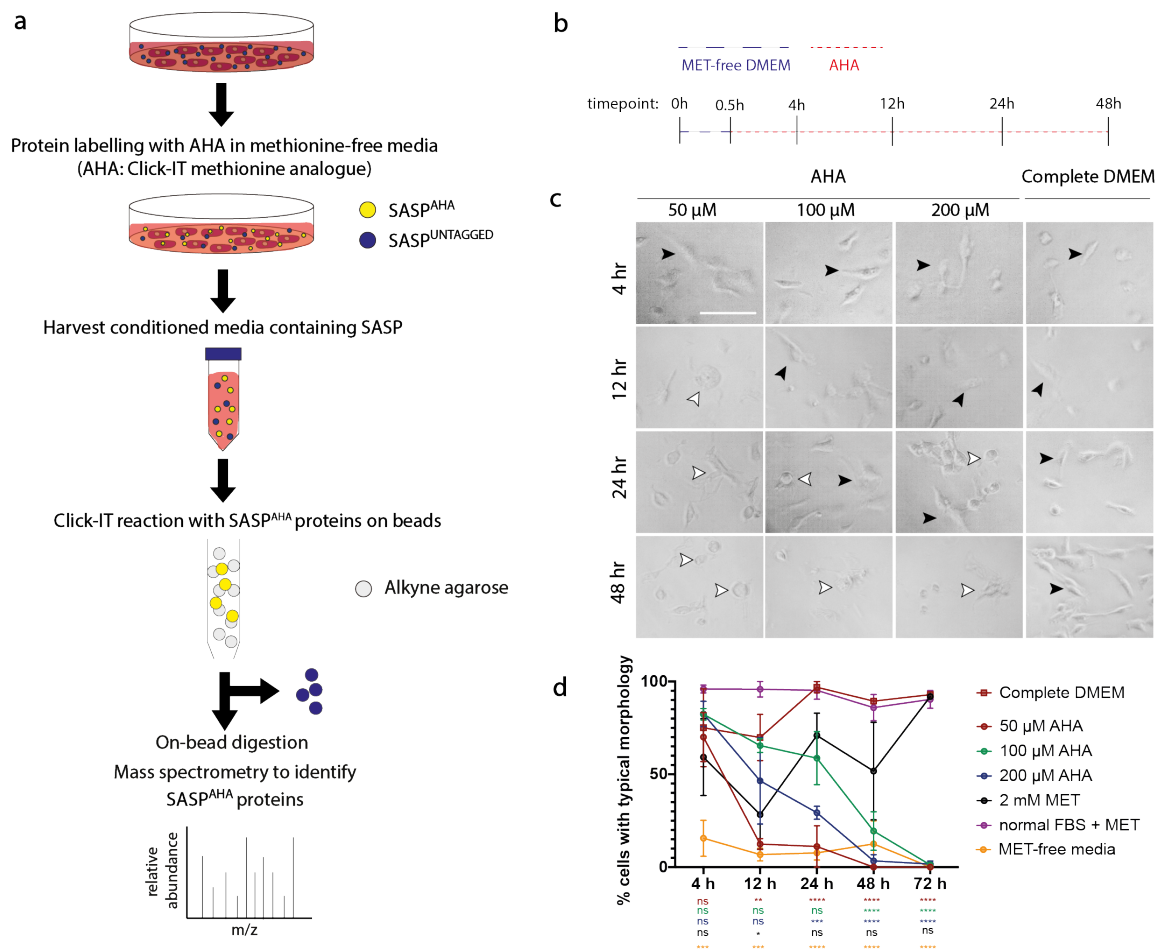
Figure 4.1| HT1080 cell morphological response to methionine analogue AHA. a, Schematic of the BONCAT experimental concept. AHA in methionine-free media is incubated on cells. Cells would then incorporate AHA in the newly synthesised proteins. Next, Click-iT reaction is performed where the alkyne on the agarose beads binds with the azide to the AHA tag. Untagged proteins subsequently flow through and SASP[AHA] proteins are digested on bead. Peptides of SASP[AHA] are then analysed using mass spectrometry. **b-d,** Different concentrations of AHA were tested on HT1080 and images of the cell morphology was taken at indicated time intervals. **b,** Timeline of the experiment with AHA. Cells were starved of methionine (blue line) before incubating with AHA (red line) for 4h, 12h, 24h and 48h. **c,** Representative images of the cells at indicated concentrations and timepoints. White and black arrows depict dysmorphic cells and healthy cells, respectively. Scale bar is 100 μm. **d,** Percentage of healthy cells from total cells counted in each well. Circles indicate conditions that required pre-starvation, dialysed FBS, and methionine-free media unless otherwise stated. The square indicates the usual culture conditions without any of the aforementioned conditions. Two-way ANOVA of all conditions compared to complete DMEM was carried out to test for significance. Data was collected from 1 biological replicate (3 technical repeats; ∼20 to 500 cells/condition). Asterisks under the time-points are colour coded similarly to the legend. Error bars are SEM.

alkyne-beads column. The azido moiety binds to the alkyne moiety via a chemoselective ligation reaction called Click-iT. Untagged abundant proteins flow through the column, then bound proteins are digested into peptides on beads and analysed by LC-MS/MS (**Fig.4.1a**).

Methionine is an essential amino acid for protein synthesis and almost all research that uses BONCAT, labels cells with AHA for a short duration e.g. 4h[262,263,264]. Thus, the proliferation and morphology of cells was examined in the presence or absence of AHA after starving cells of methionine (**Fig.4.1b**). HT1080 cells grown in complete DMEM had an extended morphology, typical of fibroblast-like cells, which was observed at all timepoints (**Fig.4.1c**, black arrows; **Fig.4.1d**). In
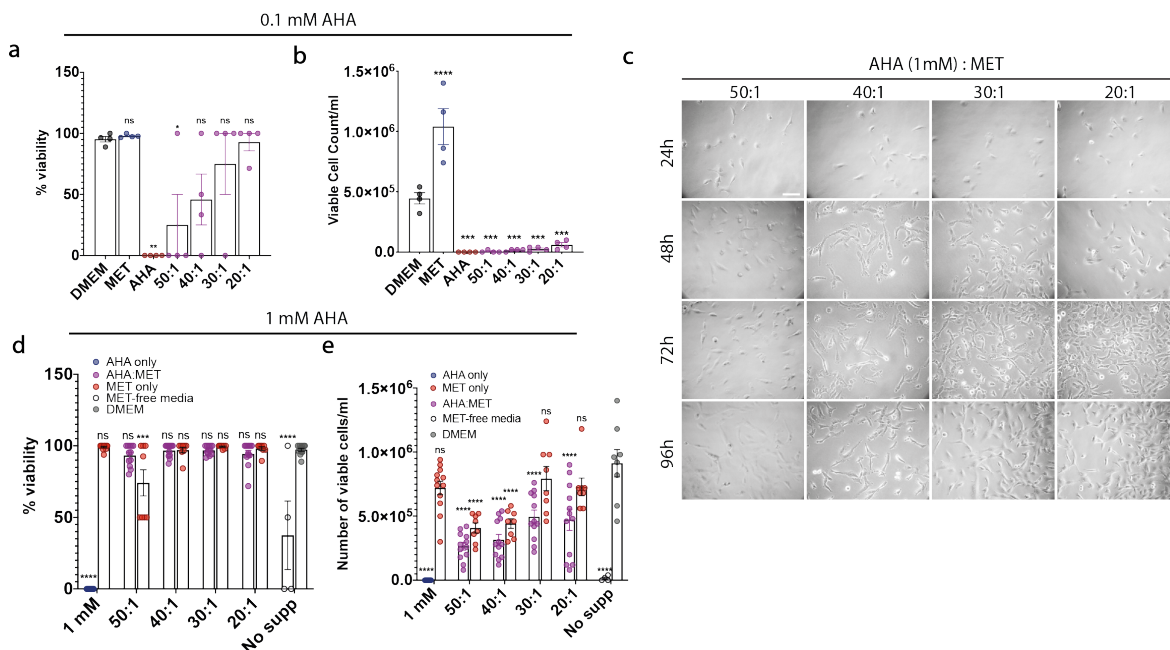
Figure 4.2| Influence of AHA:Methionine combinations on HT1080 cell viability. a and b, Trypan blue survival assay was used to assess **a,** cell viability and **b,** number of viable cells in various ratios of 0.1 mM AHA to methionine at 96h. **c,** Representative images of cell morphology incubated with various ratios of 1 mM AHA to methionine, at different time-points. Scale bar is 100 µm. **d and e,** Trypan blue survival assay was used to assess **d,** cell viability and **e,** number of viable cells in various ratios of 1 mM AHA and methionine mixtures at 96h. **a-e,** Data was collected from three biological repeats, except methionine incubation on its own was from two biological repeats and methionine-free DMEM negative control was from one biological repeat. Each circle represents a technical replicate. One-way ANOVA with Dunnett's multiple comparisons test compared with complete DMEM was used to test for statistical significance. Error bars indicate SEM.

contrast, atypical cell morphology was observed in the presence of AHA from 12h incubation, which was exemplified by cell rounding (**Fig.4.1c**; white arrows). Interestingly, increasing the concentration of AHA from 50 µM to 100 µM prolonged the typical fibroblast morphology from 12h to 24h (**Fig.4.1c**). However, increasing AHA concentration to 200 µM seemed to increase cell rounding (**Figs.4.1c, 4.1d**). Thus, it was clear that cells were susceptible to cell rounding in the absence of L-methionine and prolonged exposure to AHA regardless of its concentration (**Fig.4.1b**, 0% fibroblast morphology at 72h in all concentrations). This correlated with a reduction in HT1080 cells with typical morphology in methionine-free conditions with or without AHA (**Fig.4.1d**). In contrast, supplementing methionine-free media with L-methionine, in place of AHA, sustained typical morphology as observed with complete DMEM. In summary, while methionine-starvation appeared toxic to cells, experiments suggest that AHA sustained a typical morphology of HT1080 cells at 100 µM up to 24 hours. This suggests utilisation of AHA in place of L-methionine for less than 24 hours. Thus, further AHA optimisation experiments were initiated to improve cell homeostasis over a longer period of time.

Cell rounding in **Fig.4.1** indicated cell death in response to AHA. To enable long incubations with AHA while maintaining cell survival at the cost of sensitivity, Bagert and colleagues (2014) recommended a mix of 1 mM AHA and L-methionine in a 30:1 ratio[265]. Therefore, trypan blue staining of cells was used to assay cell viability directly following incubation with indicated AHA:MET ratios in methionine-free media at 96h **Fig.4.2**.

As 100 μM seemed to be the optimal concentration in terms of morphology **(Fig.4.1)**, the effect of different L-methionine ratios was examined on cell morphology and survival at a later time-point (96h). As expected, cells did not survive in AHA alone **(Fig.4.2a**, 0%). However, increasing concentration of L-methionine, i.e. from ratios of 50:1 up to 20:1 seemed to be positively promoting cell survival and division to levels observed for complete DMEM and methionine-free media supplemented with L-methionine alone **(Fig.4.2a)**. However, the number of viable cells were quite low for all AHA-containing media **(Fig.4.2b)**. To maintain both cell viability and growth, the concentration of AHA was increased to 1 mM, as recommended by Bagert and colleagues (2014)[265]. A 10-fold increase to 1 mM AHA was able to maintain both cell survival and growth **(Fig.4.2c-e)**. However, by maintaining the same AHA:MET ratios, the relative concentration of methionine was also increased in comparison to **(Fig.4.2a, 4.2b)**. The higher concentrations of methionine used in combination with 1 mM AHA, were sufficient for cell growth even in the absence of AHA **(Fig.4.2c-e)**, indicating that the cells preferably use L-methionine rather than AHA for protein synthesis. As a result, concentration of AHA-containing SASP proteins in the secretome might be reduced, which might impact the analysis by mass spectrometry.

4.2 The typhoid toxin induces senescence and transmissible senescence in AHA-containing media.

Though cells did not survive for long periods of time, e.g. 96h in **Fig.4.2**, without L-methionine, even with AHA, cells appeared closer to control during short incubation periods, e.g. 12h with 100 μM AHA in **Fig.4.1**. Thus, cells were incubated with AHA then complete DMEM growth media in cycles of 8h (day time) and 16h (overnight) for 96h as depicted in **Fig.4.3a**. As observed in **Fig.4.3c**, at 96h, there was cell survival and no cell rounding. Next, the ability of the typhoid toxin to induce senescence in AHA-containing media was examined. Indeed, the typhoid toxin and APH induced significant senescence **(Fig.4.3b-d**; >80% SA-β-gal positive cells). They also induced cell enlargement compared to untreated and toxin[HQ] **(Fig.4.3c)**. Untreated and toxin[HQ] cells also induced a relatively high number of SA-β-gal cells in AHA-treated cells **(Figs.4.3a**, red arrows; **4.3c**, **4.3d)**. However, it seems that SA-β-gal was reduced during the recovery period **(Figs.4.3a**, black arrows; **4.3c**; **4.3d)**. These results indicate that even though AHA induces a stress response exemplified by up-regulation of SA-β-gal, this effect is reversible, and does not induce permanent senescence-like phenotype.

Next, transmissible senescence by conditioned media (CM[AHA]) collected from the experiment in **Fig.4.3c** was examined **(Fig.4.3e-g)**. Since APH is present in the first 24h of positive control experiments, transmissible senescence was tested for all conditions using CM[AHA] fractions harvested between 24h-96h **(Fig.4.3f**; fractions) for comparison. For controls, transmissible senescence was assayed using complete DMEM harvested from untreated cells or cells treated with toxin[WT] or APH **(Fig.4.3e-g)**. Cells proliferated and exhibited no SA-β-gal activity when treated with unt[CM] **(Fig.4.3g)**. This
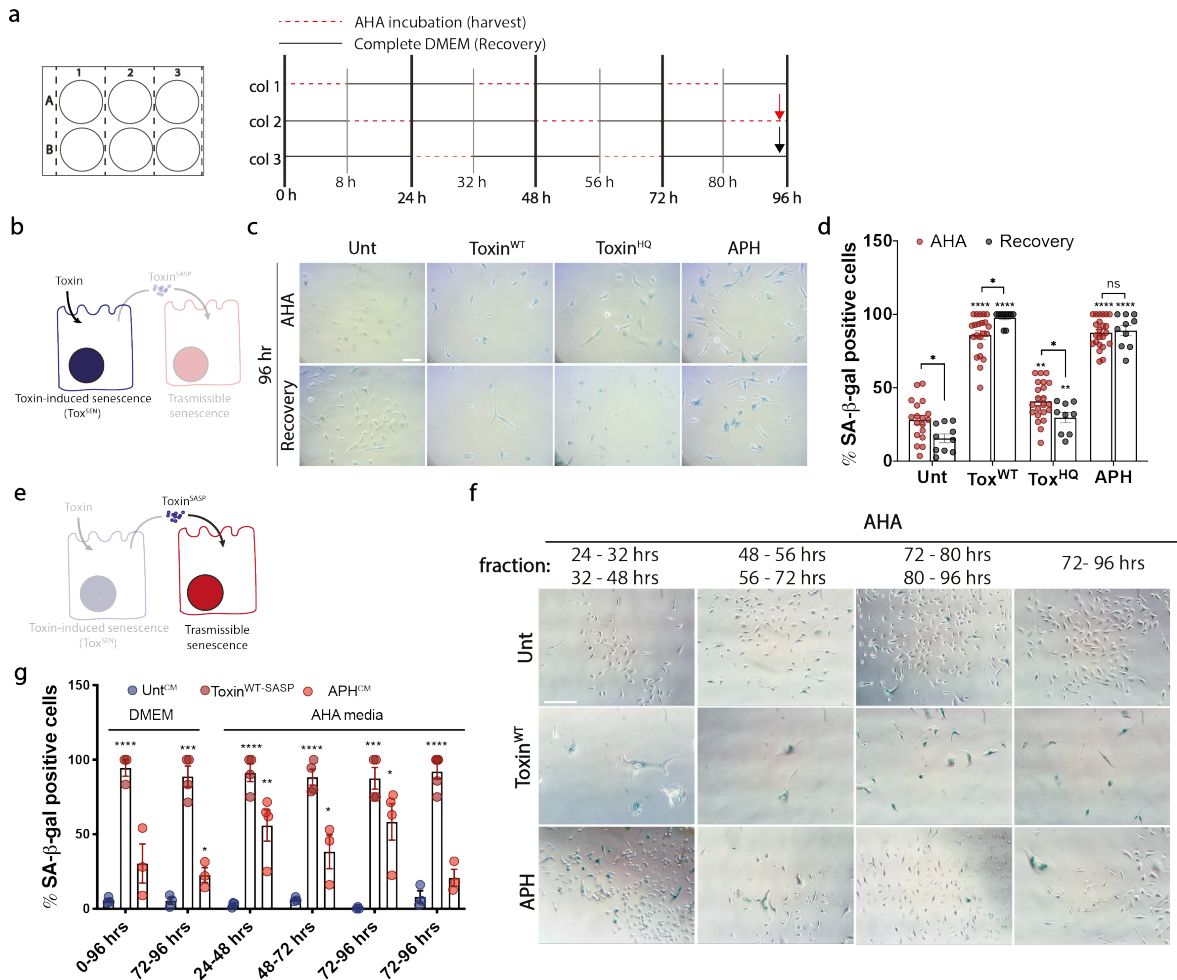
Figure 4.3| Senescence and transmissible senescence induced by typhoid toxin in AHA-containing media. a, Experimental design to label proteins with AHA over 96h, while maintaining a healthy state of cells. cells in column 1 of a 6 well plate were treated with AHA post intoxication. Meanwhile, cells in column 2 and column 3 were incubated in fresh DMEM. After 8h, CM^{AHA} was collected, washed and replaced with fresh DMEM. Simultaneously, labelling of cells in column 2 began for the overnight duration (i.e. 16h), and third column remained in fresh DMEM that was not replaced with AHA until the 24 hour time-point. The process was repeated until the end of the 96hour period and fractions collected were pooled in together. This experimental design allowed cells to incubate in AHA for a maximum of 16h and at least a 24-hour period of cell recovery in normal DMEM before re-incubating in AHA. The red arrow indicate the end of the AHA experiment and the black arrow indicate recovery cells in **c. b-d,** Primary senescence of cells marked by SA-β-gal at the end of the 96hour time-point from wells subjected to the last AHA incubation in the series (col. 2) and cells undergoing the last recovery in complete DMEM incubation (col. 3). **d,** Quantification of **c** from 2 biological repeats for AHA (∼300-800 cells/condition), and 1 biological repeat for recovery (∼80-400 cells/condition). **e-g,** Transmissible senescence on naive HT1080, using conditioned media in complete DMEM or conditioned media labelled with AHA (CM^{AHA}) that were harvested and combined at indicated time-points. CM^{AHA} was diluted 1:1 with complete DMEM before cell treatments. **f,** Representative images of transmissible senescence assayed by SA-β-gal after 5 day treatment with conditioned media. **g,** Quantification of **f** from 1 biological replicate (∼20-500 cells/condition). **d and g,** Each circle represents a field of view. Unpaired student's t-test were carried out between each condition and its untreated counterpart unless otherwise indicated. Error bars indicate SEM. **c and f,** Scale bars are **c,** 100 and **f,** 200 μm

contrasted with tox$^{WT-SASP}$ induced transmissible senescence (**Fig.4.3**g; ∼95%). Interestingly, CM from APH-treated cells, only induced modest SA-β-gal (**Fig.4.3**g; ∼25%). Consistent with this, results from Ibler et al (2019) showed that APH induced γH2AX RINGs and primary senescence, yet transmissible senescence was reported to be ∼40% relative to ∼80% for the toxin[106]. The transmissible senescence phenotypes observed in control experiments with complete DMEM were mirrored in
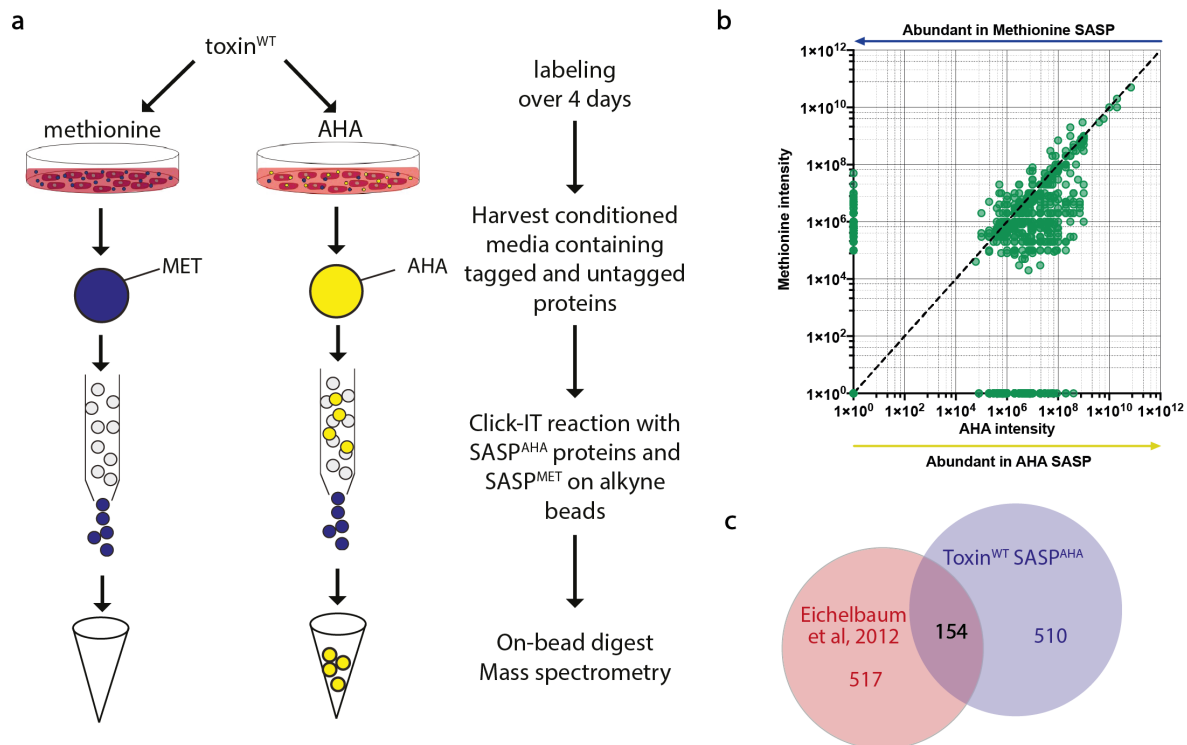
Figure 4.4| Pilot mass spectrometry analysis. a, HT1080 cells were intoxicated and labelled with either the methionine analogue, AHA, or cold L-methionine. Protein enrichment was carried out to select for AHA-tagged proteins and samples were analysed by mass spectrometry. **b,** A plot of L-methionine intensity against AHA intensity to visualize the specificity of AHA labelling. Each dot represents a protein. Proteins under the dotted line depict proteins AHA-specific, and proteins above the line depict methionine-specific proteins. **c,** Venn diagram of the mutual and exclusive proteins identified in this pilot experiment compared to the compendium of secreted proteins[262].

conditions with AHA media **(Fig.4.3e-g)**. Thus, the toxin induces both primary and transmissible senescence in -methionine/+AHA conditions.

4.3 Pilot experiment shows toxin-induced secretome was successfully labelled by AHA.

In order to confirm that proteins collected incorporated AHA, a pilot mass spectrometry experiment was carried out. Intoxicated cells were incubated with either AHA or L-methionine for 96h. Click-iT reaction was then carried out on conditioned media to immobilise AHA-containing proteins before on-bead digestion and mass spectrometry **(Fig.4.4a)**.

If cells incorporated AHA, proteins in AHA samples should show higher intensity relative to L-methionine samples. Indeed, 295 out of 944 proteins detected were solely found in the AHA samples (AHA-specific) compared to 80 proteins solely in L-methionine samples (Met-specific). Additionally, 738 proteins were found more abundantly in the AHA samples **(Fig.4.4b)**, 662 of which were human proteins. Eichelbaum et al. (2012) published a study where they mapped out a compendium of secreted proteins from various different cell lines using BONCAT[262]. They used PC3, WPMY-1,
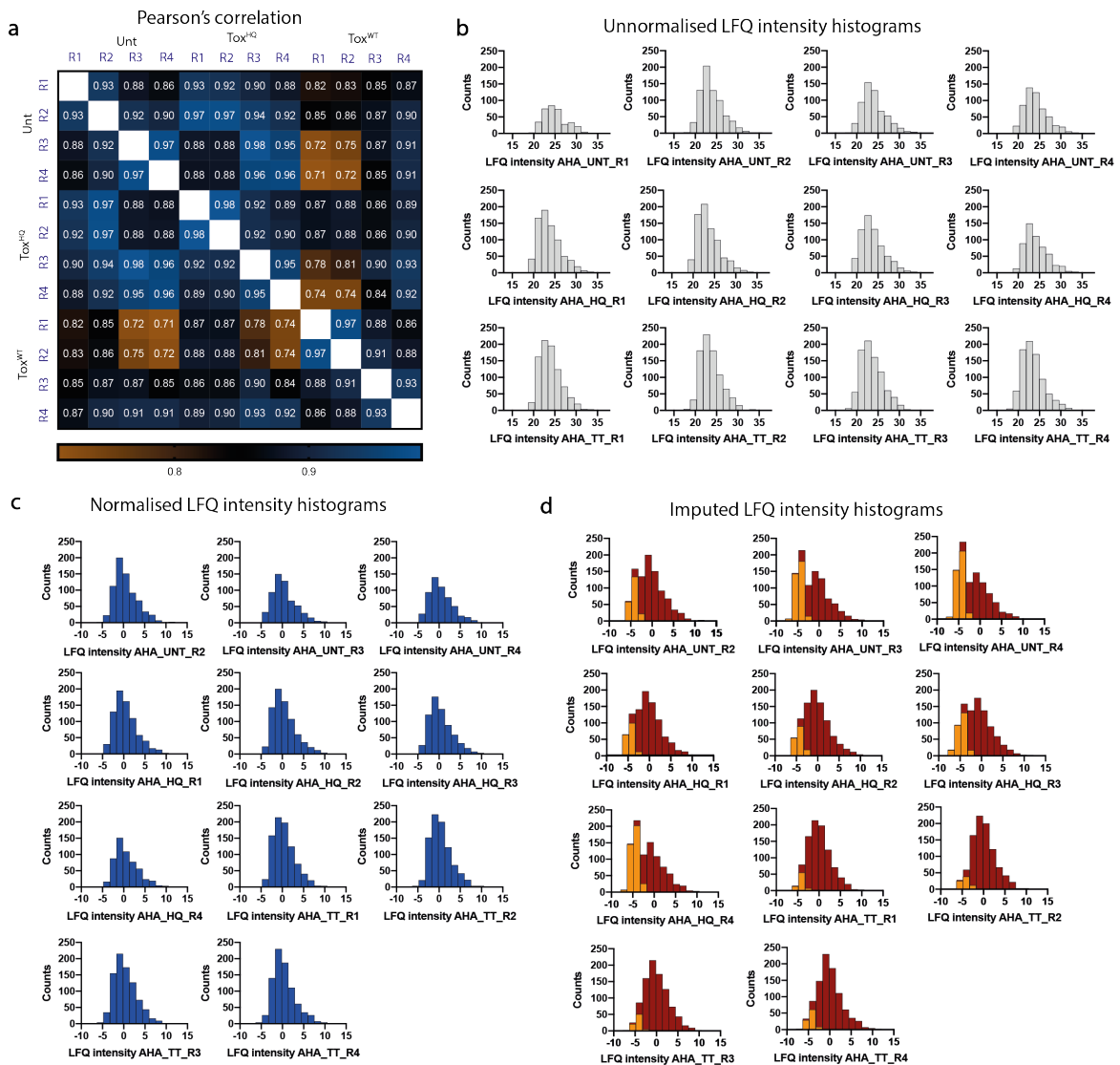
Figure 4.5| Raw data analysis exported from MaxQuant and processed using Perseus bioinformatics analysis of AHA conditioned media. a, Heat map summarising the column Pearson's correlation analysis comparing LFQ intensities of samples with each other. **b-d,** Frequency distribution histograms of the different samples analysed by mass spectrometry of **b,** unnormalised, **c,** normalised and **d,** imputed LFQ values. **c and d,** untreated repeat 1 was excluded due to the low LFQ intensity shown in b.

RAW, PHC, Hepa1c1 and Hepa1-6 cell lines. Comparative analysis between human proteins identified from the AHA experiment, and proteins identified in Eichelbaum et al (2012)[262], showed 154 proteins in common **(Fig.4.4c)**. This data provides further evidence on the feasibility of AHA-labelling SASP proteins for identification and elucidating the host cell secretome in response to toxin^{WT}.

4.4 Newly translated proteins that are secreted in response to toxin^{WT}

Collection of CM^{AHA} was harvested from 4 biological repeats of untreated, tox^{WT}, tox^{HQ} and APH-treated cells over 96h using the protocol described in **Fig.4.3a**, and validated for transmissible
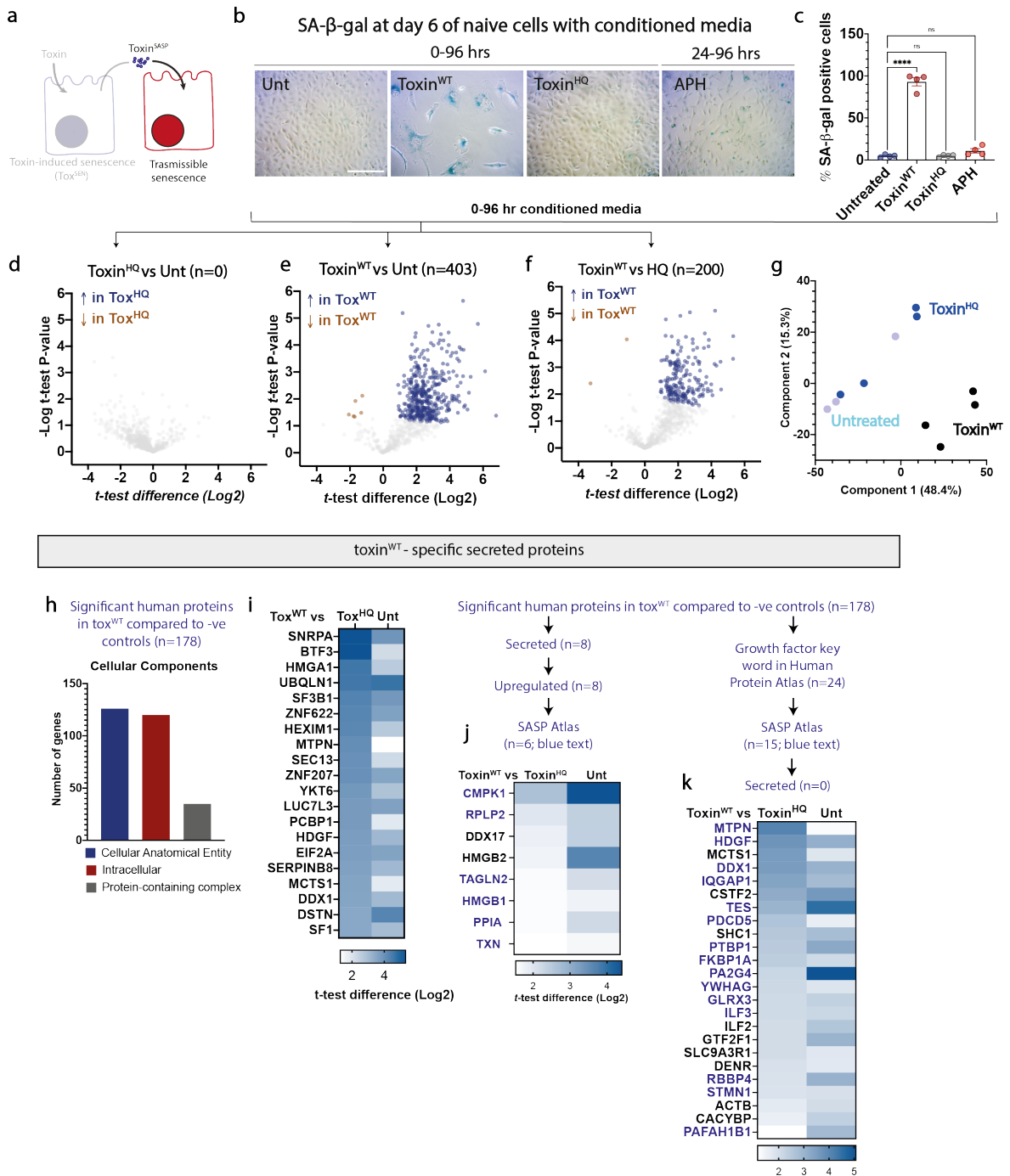
Figure 4.6| Newly synthesised proteins in toxin^WT-induced secretome. a, Conditioned media from untreated, intoxicated cells (toxin^WT and toxin^HQ), and APH were harvested and validated for transmissible senescence prior to mass spectrometry analysis. **b,** Representative images and **c,** quantification of transmissible senescence induced in naive HT1080 cells by Unt^CM, toxin^WT-SASP, tox^HQ-CM and APH^CM (0-96hr) for 6 days then assayed for SA-β-gal. Each circle is a biological replicate of the samples analysed by mass spectrometry (at least 10 fields of view per replicate, ~300-2800 cells/condition per replicate). Scale bar is 200 μm. One-way Anova with Tukey's multiple comparison test was carried out to test for significance. Error bars denote SEM. **d-f,** Volcano plots of secretomes induced between 0h and 96h post removal of toxin and analysed using Perseus two-sample t-test (s0=0.01 and FDR=0.05) from at least 3 biological repeats/condition. Number of significant proteins between **d,** toxin^HQ and unt, **e,** toxin^WT and unt, and **f,** toxin^WT and toxin^HQ, are indicated. Brown dots indicate down-regulated proteins and blue dots indicate up-regulated proteins relative to each other. **g,** Principal component analysis on the different CM^AHA harvested at 96h post-intoxication. **h,** Toxin-specific proteins compared to negative controls were analysed for their cellular localisation using Panther analysis of the 178 gene names **i,** Heat map of the highest 20 secreted proteins in response to intoxication compared to toxin^HQ and Unt. **j,** Toxin-specific proteins that were shortlisted using the flowchart on the top. Heat map lists gene names of significant different proteins in toxin^WT-SASP compared to Unt^CM, tox^HQ-CM. **k,** Potential candidates for enhancing *Salmonella* invasion as filtered using the flowchart on the left.

Gene name were cross referenced with proteins involved in growth factor signalling as dictated by a search of the Human Protein Atlas. **h and i,** Blue text indicates proteins up-regulated in the SASP Atlas as well. Gene names displayed were matched with the Human Secretome Atlas and the compendium of secreted proteins [262,266].

senescence **(Fig.4.6a, 4.6b)**. As expected, CM^{AHA} from $toxin^{WT}$-treated cells showed ~100% SA-β-gal, whilst APH^{SASP} did not show a significant increase in percentage of SA-β-gal positive cells compared to the negative controls **(Fig.4.6c)**. Given these observations, it was decided that the best samples to carry forward for further analysis were untreated, tox^{HQ}, and tox^{WT}. MaxQuant analysis and Perseus-generated multi-scatter plots and Pearson's correlation analysis of the samples demonstrated that even though untreated replicate 1 showed good correlation with replicate 2 (0.934), the correlation to replicate 3 and 4 were not as high (0.878 and 0.864 respectively) **(Fig.4.5a)**. Furthermore, the analysis showed relatively good protein count of label-free quantification (LFQ) intensities for all conditions analysed **(Fig.4.5b)**. However, untreated replicate 1 showed lowest counts of proteins **(Fig.4.5a)**. As a result, untreated replicate 1 was excluded from further analysis. LFQ intensities were then normalised and missing values from the MaxQuant analysis were imputed from the normal distribution to provide complete normalised proteomics data **(Fig.4.5c, Fig.4.5d)**.

There was no difference in secretomes of untreated and $toxin^{HQ}$ treated control cells **(Fig.4.6d)**, but a divergent secretome was induced by $toxin^{WT}$-treated cells compared to untreated **(Fig.4.6e, n=403)** and $toxin^{HQ}$ **(Fig.4.6f, n=202)**. This was further consolidated by principal component analysis (PCA) that showed clustering of the negative control replicates together, which were divergent from $toxin^{WT}$ **(Fig.4.6g)**. Strikingly, the majority of proteins detected were up-regulated in tox^{WT} compared to the negative controls.

There were a sum of 920 proteins cumulatively in all samples[*]. Peptides identified from the samples contained both human and bovine sequences. Proteins that had bovine sequences are likely to be due to the presence of dialysed FBS in the methionine-free media **(Materials and Methods; Section 10.1.1)**. Therefore, bovine peptide sequences were eliminated, which revealed 692 human proteins (i.e. ~75% of all proteins identified). To identify enhancers of infection, the $toxin^{WT}$-induced secretome was filtered against both negative controls **(Fig.4.6h)**, which implicated 178 proteins. However, PANTHER cellular component analysis indicated the majority of the proteins identified in tox^{SASP} are intracellular (~120 proteins). Closer examination of the top 20 factors increased in tox^{WT} compared to tox^{HQ} included: SNRPA, UBQLN1, and BTF3 all of which execute intracellular functions [267,268,269,270] **(Fig.4.6i)**.

To identify $toxin^{SASP}$ proteins previously reported as secreted, two databases were used: i) Eichelbaum et al 2012 Compendium of Secreted Proteins, which was identified using BONCAT on diverse cell lines [262], and ii) The Human Secretome Atlas [266]. The Human Secretome Atlas is a database of 2641 proteins (i.e. ~13% of all human coding genes) created by a) annotating transcriptomics analysis for the presence of a secretion signal peptide, b) including proteins annotated as secreted

---

[*]Click here to access the whole dataset extracted and used for BONCAT analysis

on Uniprot, c) validating secretion using antibody- and mass spectrometry based-analyses on blood plasma samples[266].

Only 4.5% (i.e. 8 proteins) of the toxin-specific proteins were previously reported as secreted in one or both of secretome databases used[262,266], 6 of which have been reported in the SASP Atlas[174] **(Fig.4.6j)**. Curiously, top factors in tox^{SASP} included nuclear protein factors from the High-mobility group (HMG) superfamily e.g. HMGA1, HMGB1, and HMGB2, which were recently implicated in extracellular functions as well[271]. Notably, HMGB1 is a damage-associated molecular pattern (DAMP), also known as an alarmin, which has been reported to be a core SASP component of fibroblast senescence[174]. Similarly, extracellular HMGA1 was reported to mediate tumorigensis and metastasis[272], and work in conjunction with NOTCH to regulate chromatin organisation and SASP[170]. Curiously, HMGB2, was not reported as an alarmin, but is involved in chromatin remodeling and SASP regulation[211]. Interestingly, extracellular DAMPs have been implicated in ageing and inflammation and are used as a biomarker for infectious diseases, malignant tumours, and other diseases[273].

Growth factors have been previously reported to increase membrane ruffling[274]. Therefore, to examine putative candidates that might be synthesised to enhance *Salmonella* invasion, proteins were searched for any link with growth factor using "growth factor signalling" as a key word on the Human Protein Atlas[275]. Out of 178 proteins, ∼13.5% of toxin-specific proteins were involved in growth factor signalling **(Fig.4.6k)**. Although, none of these proteins have been reported in the Human Secretome or Eichelbaum et al 2012 **(Fig.4.6k)**[262,266,276], 15 of the growth factor signalling proteins have been reported in the SASP Atlas[174], perhaps providing an insight into contextually-secreted proteins. For instance, HDGF, which was up-regulated significantly in toxin^{WT}-treated cells, is a growth factor that is recently discovered to be secreted in cancer cell lines and has anti-apoptotic properties[277], but was not found in either atlases **(Fig.4.6k)**. There were also conventionally abundant intracellular proteins such as ACTB which might have been detected due to apoptotic cells.

4.5 Discussion

This chapter explored late senescence secretome using a novel approach, BONCAT, and revealed newly synthesised proteins in response to the typhoid toxin. BONCAT is a very powerful technique as it is safe, reliable, easy and non-radioactive compared to other proteomic techniques[263]. It has been previously used in many temporal and spatial experiments providing great sensitivity[262,263,265].

This approach revealed a unique secretome induced by the nuclease activity of toxin^{WT} in comparison with the negative controls. It also identified previously reported SASPs, which validates the senescence phenotypes induced by the toxin and provide potential factors involved in toxin-induced phenotypes[174]. Nevertheless, there was a large amount of intracellular proteins that are reasoned to be an apoptotic release due to the stress of the BONCAT protocol on the cells, which is exemplified

by Panther Cellular Component analysis, the high presence of DAMPs such as HMG proteins, and the few matches to the Human Secretome Atlas **(Fig.4.6h-j)**. This suggests that secretomes analysed might have included SASP as well as the secretome of cells undergoing cell death. It is worth-noting that some intracellular factors identified, such as EIF2A and HMG proteins, can be secreted in exosomes or in unconventional protein secretion pathway[278,279,280], without bearing a secretion signal peptide. Therefore, the secretome databases used may not be entirely inclusive. The abundance of intracellular proteins and the scarcity of proteins reported as secreted in the examined SASP, reduced the reliability of these results.

Moreover, the lack of senescence positive control (e.g. aphidicolin) **(Fig.4.6c)** hindered the ability to narrow down the hits to the best toxin-specific SASP proteins for further examination.

Furthermore, even though toxin^{WT}-induced senescence in the presence of AHA, there was a larger percentage of senescence in untreated cells and toxin^{HQ} treated cells than normal DMEM as depicted by SA-β-gal. Additionally, the recovery period in complete DMEM added to the protocol might include latent AHA-tagged protein secretions that were not analysed, which could have reduced sensitivity and inclusiveness. All together, these results suggest that alternative approaches to identify tox^{SASP} should be explored.

Chapter 5

The typhoid toxin-induced host secretome

In Chapter 4, BONCAT was used to identify newly synthesized proteins in response to the typhoid toxin, which presented some challenges and disadvantages. In contrast, many research groups that aimed to identify secretomes have cultured cells in serum-free media to restrict FBS contaminants from masking low abundance proteins[174,281,282,283,284,285]. The aim of this chapter is to characterise tox[SASP] via two complementary approaches using LC-MS/MS: (i) conditioned Essential 8 (E8) stem cell minimal media, and (ii) serum-free DMEM.

5.1 HT1080 cell growth in diverse serum-free media

HT1080s cells were cultured with serum-free, xeno-free cancer cell line medium (XF; PromoCell), Essential 8 (E8) and DMEM serum-free (SF) and compared with complete growth DMEM media with 10% FBS **(Fig.5.1a)**. XF is a commercially available xeno-free, serum-free, cancer cell line media that was advocated as a better alternative to DMEM. Essential 8 media (E8) is a stem cell media comprising of only 8 essential components: DMEM:F12, L-ascorbic acid-2-phosphate magnesium (64 mg/L), sodium selenium (14 µg/L), FGF2 (100 µg/L), insulin (19.4 mg/L), NaHCO3 (543 mg/L), transferrin (10.7 mg/L), and TGFβ1 (2µg/L), or NODAL (100 µg/L). SF has been previously used by Basisty et al, 2019 to identify SASP in fibroblasts and epithelial cells[174].

Cells were seeded at a low density (i.e. 1×10^3) and their morphology, growth and number were examined across 4 days in indicated media **(Fig.5.1)**. In all conditions, cells looked healthy and similar to complete DMEM media at 24h. However, serum-free DMEM showed a distensive, string-like morphology at 96h, indicating cell stress, whilst cells in XF and E8 had a similar morphology to control **(Fig.5.1a)**. When growth was quantified, cells doubled within each 24h interval in the presence of DMEM. XF media showed an initial statistically significant lag in growth but followed a similar trend to complete DMEM media starting from 48h. E8 also only supported growth from 48h
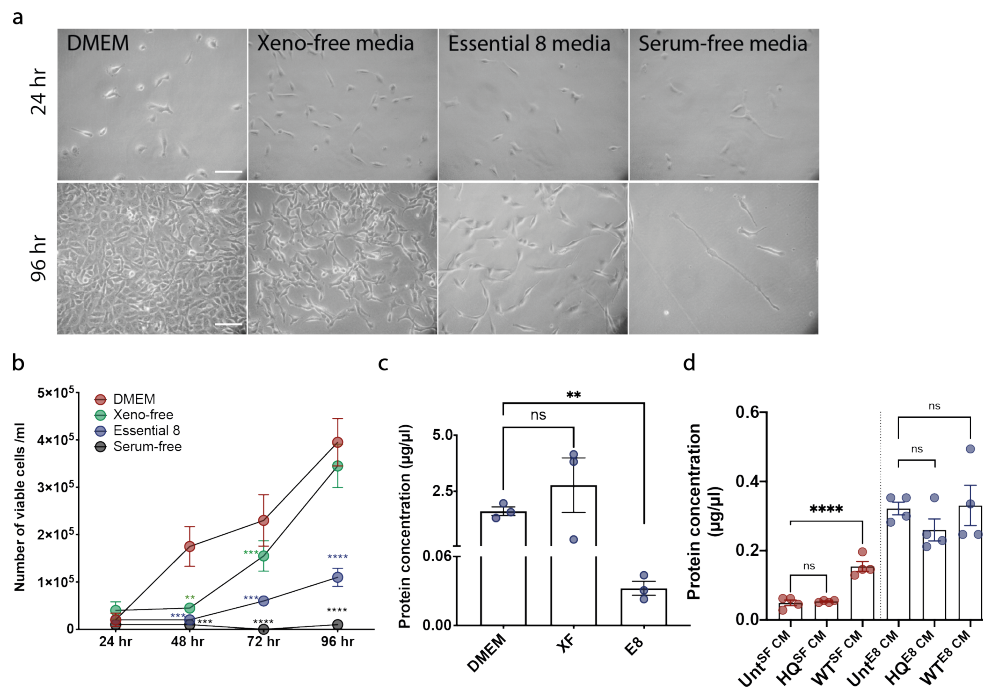
Figure 5.1| Cells survival and protein concentration of different cell culture media. Cells were seeded at 2500 per well and growth monitored for 96h. **a,** Representative images of HT1080s grown in each culture medium at 24h and 96h. Scale bar is 100 µm. **b,** Number of viable cells over time showing growth or cell cycle arrest assayed using trypan blue. **c,** Protein concentration of unconditioned media as assessed by Bradford assay. **d,** Protein concentration of conditioned SF DMEM and E8 media of cells treated with tox^{WT} and tox^{HQ} as assessed by Bradford assay at 48h post intoxication. **c** and **d** concentrations should not be compared due to technical differences with the BSA standard curve, which is a limitation of this method. **b,** Two-way ANOVA with Dunnett's multiple comparison's, **c,** an unpaired t-test were carried out for each time point in comparison with DMEM of the same time-point. **d,** One-way ANOVA with Dunnett's multiple comparison's was carried out in comparison to untreated of each medium. Where it is unindicated it is non-significant difference. Each circle represents a technical replicate. **b-c,** are one biological replicate each with 3-4 technical replicates. **d** each circle represents a biological replicate, which was later analysed by mass spectrometry.

but at a much slower rate than DMEM **(Fig.5.1b)**. Cells incubated in serum-free DMEM remained at a low cell number and viability decreased after 48h as determined by a reduction in cell number exemplified at the 72h timepoint.

To further examine which growth media supported production of a host secretome, protein concentration of conditioned and unconditioned media were quantified. Although XF media is serum-free, it contained a higher concentration of proteins than complete DMEM and therefore was excluded from further experiments **(Fig.5.1c)**. In contrast, E8 media showed significantly lower protein concentration than both DMEM and XF media. No proteins were detected in unconditioned serum-free DMEM (data not shown).

Next, protein concentrations of $tox^{WT\text{-}CM}$ and $tox^{HQ\text{-}CM}$ were compared to unt^{CM} in both SF and E8 conditions. In comparison to the negative controls, $tox^{WT\text{-}CM}$ showed a significant increase in secretions in SF media, but no change in E8 media **(Fig.5.1d)**. This suggests that E8 supplements might confer high background protein level relative to SF, which might mask differences in secretions between conditions. Since Basisty and colleagues used serum-free conditions to identify the secre-
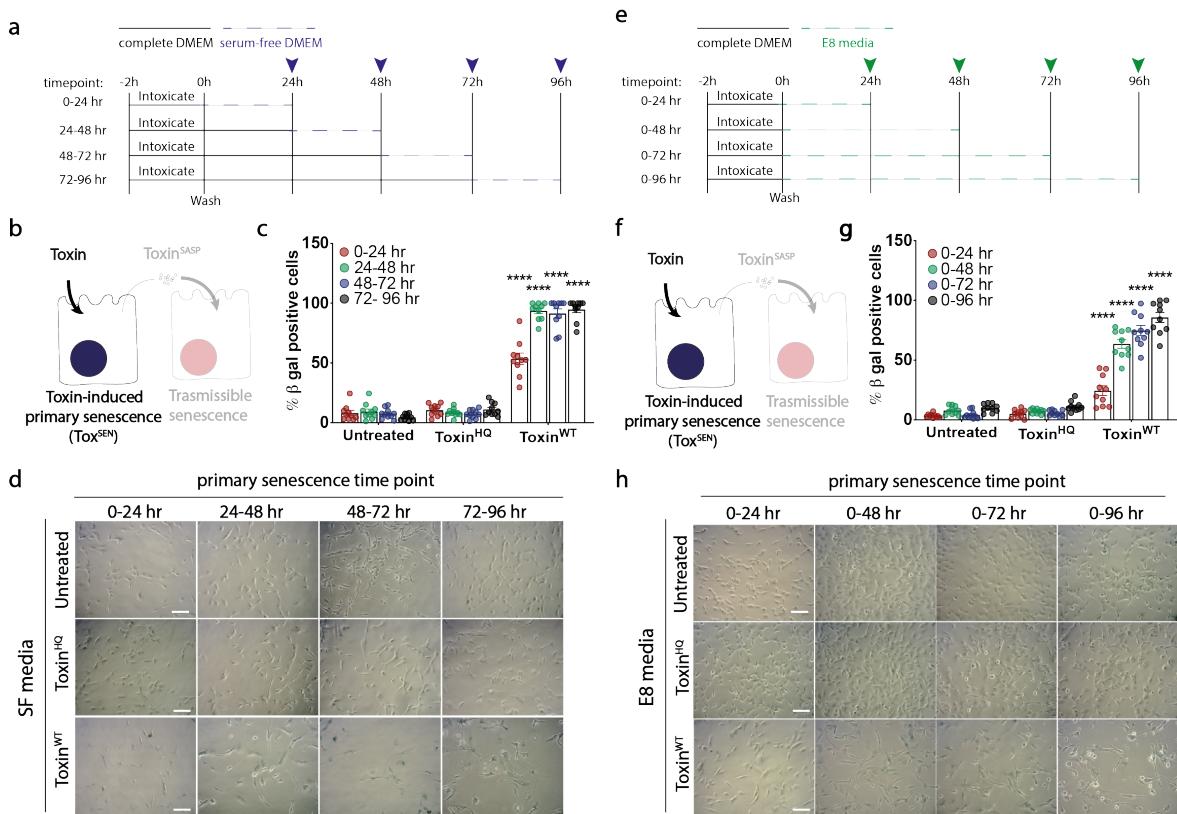
Figure 5.2| Senescence induced by typhoid toxin in serum-free and Essential 8 (E8) media. a, Experimental schematic demonstrating the timeline of serum-free media application and collection timepoints across 4 days. Each batch of cells were seeded differently to account for cellular replication every 24h in complete media and cell cycle stalling in serum-free media. ($2x10^4$ cells for 0-24h, $1x10^4$ for 24-48h, $5x10^3$, $2.5x10^3$ cells in a 24-well format. **b-d,** Primary senescence induced in HT1080s at the end of each incubation with serum-free media (blue arrow in **a**). **c,** Quantification of SA-β-gal positive cells at the end of each incubation with serum-free media. **d,** Representative images of **c**. **e,** Experimental schematic demonstrating the timeline of E8 media application and collection timepoints across 4 days. Each batch of cells were seeded differently to account for cellular replication every 24h as per the growth curve in **Fig.5.1**. Cells were seeded in 6-well format at $1x10^5$ (0-24h, 0-48h), $8x10^4$ (0-72h), and $4x10^4$ (0-96h). **f-h,** Primary senescence induced in HT1080s at the end of each incubation with E8 media (green arrow in **e**). **g,** Quantification of SA-β-gal positive cells at the end of each incubation with E8 media. **h,** Representative images of **g**. **c and g,** One-way ANOVA with Tukey's multiple comparisons test was carried out against the corresponding time-point for untreated and toxin[HQ] treated cells. Each circle represents a field of view (1 biological repeat, ∼300-2500 cells per variable). Error bars indicate SEM. **d and h,** Scale bar is 100 µm.

tome of fibroblast and epithelial cells[174] and E8 showed potential in terms of viability and cellular replication, both media were further tested for toxin-induced senescence phenotypes.

5.2 Primary senescence in cells cultured in SF and E8.

The ability of a 2h toxin treatment to induce primary and transmissible senescence in serum-free DMEM (henceforth SF) and E8 was examined at different timepoints across 96h **(Fig.5.2)**. Cells incubated in SF media, hereafter SF cells were viable in the first 24h **(Fig.5.1)**. Thus, intoxicated cells were cultured in complete DMEM for up to 72h and the conditioned media was harvested following a 24h incubation in SF at the relevant timepoints, as depicted in **(Fig.5.2a)**. Upon harvesting the conditioned media, cells undergoing toxin-induced primary senescence (tox[SEN]) were assayed for
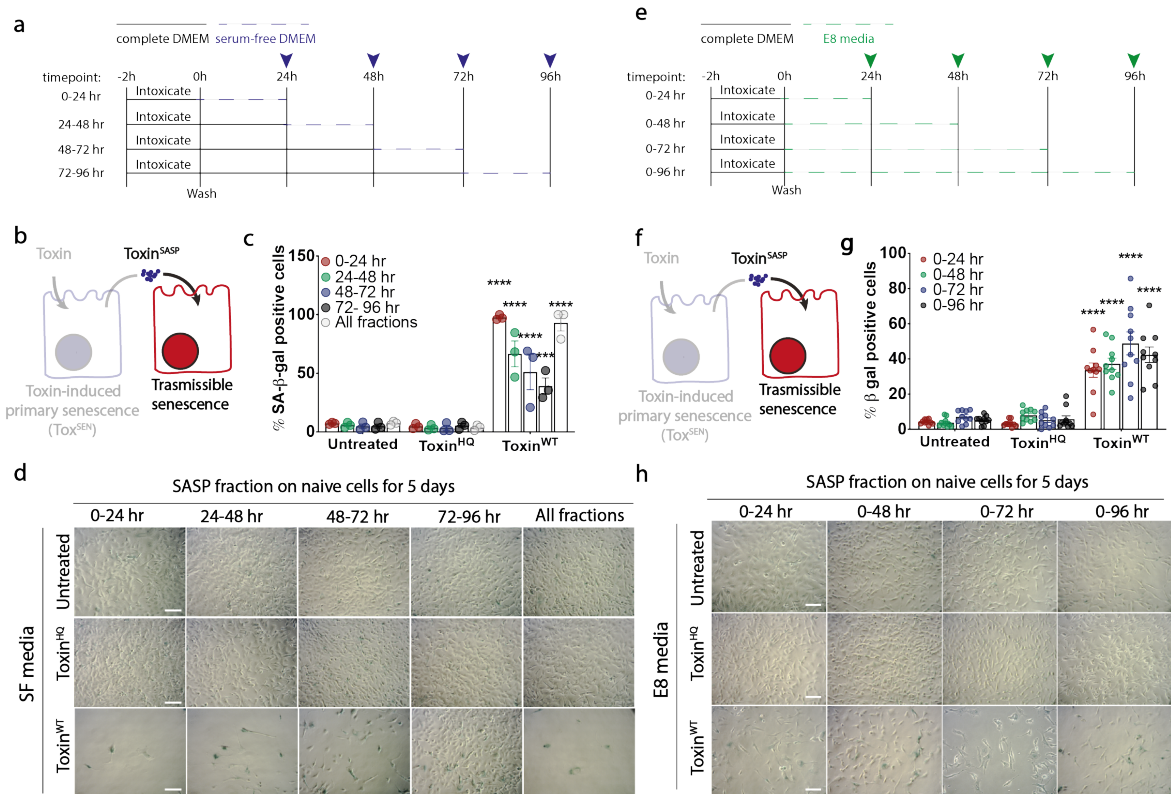
Figure 5.3| Transmissible senescence induced by typhoid toxin in serum-free and Essential 8 (E8) media. a, Experimental schematic demonstrating the timeline of serum-free media application and collection timepoints across 4 days. Cells were seeded at 1000/well. **b-d,** Transmissible senescence induced in naive HT1080s using each fraction of serum-free media collected (blue dotted lines). **c,** Quantification of SA-β-gal positive cells induced by each serum-free conditioned media fraction in naive HT1080s. **d,** Representative images of **c. e,** Experimental schematic demonstrating the timeline of E8 media application and collection timepoints across 4 days. **f-h,** Transmissible senescence induced in naive HT1080s using each fraction of E8 media collected (green dotted lines). **g,** Quantification of SA-β-gal positive cells induced by each E8 conditioned media fraction in naive HT1080s. h, Representative images of **g. c and g,** Two-way ANOVA with Dunnett's multiple comparisons test was carried out against the corresponding time-point for untreated and toxin[HQ] treated cells. Each circle represents a biological replicate ($\sim$200-7500 cells/condition) for **c,** and technical replicates ($\sim$600-2500 cells/condition) for **g**. Error bars indicate SEM. **d and h,** Scale bar is 100 μm.

senescence by SA-β-gal **(Fig.5.2a**; blue arrows**)**. Senescence was observed in 50% of cells at 24h, which increased to $\sim$100% thereafter **(Fig.5.2b-d)**. This contrasted with cells treated with toxin[HQ], which was equivalent to untreated cells. Parallel experiments using E8 media, which unlike SF was incubated with toxin-treated cells throughout (e.g. 0-24h, 0-48h)**(Fig.5.2e**; green arrows**)**, mirrored the trend observed in SF cells with maximal primary senescence observed at 96h **(Fig.5.2e-h**: $\sim$20% at 24h to $\sim$80% at 96h**)**.

5.3 Transmissible senescence in cells cultured with SF and E8 media.

Each fraction of conditioned SF or E8 media harvested at 24h intervals was assayed for its ability to transmit senescence into naive cells **(Fig.5.3a**, blue lines; **Fig.5.3e**, green lines**)**. Relative to un-
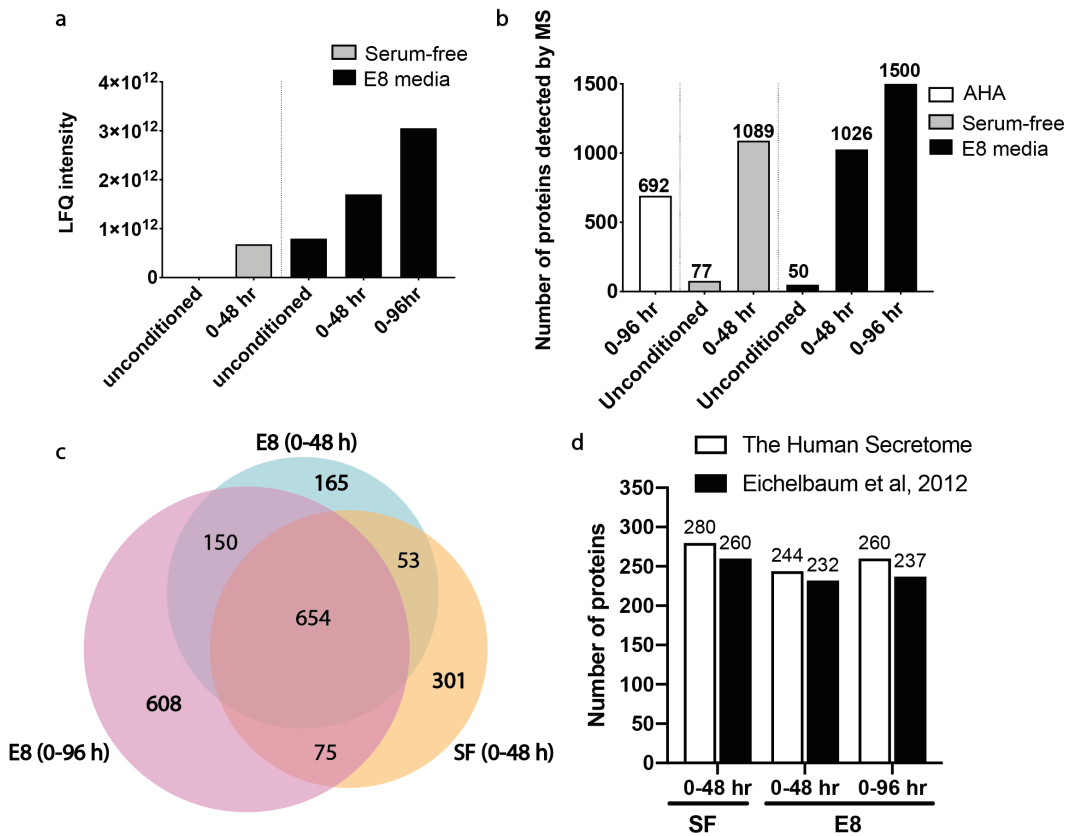
Figure 5.4| Pilot mass spectrometry experiment comparing proteins from serum-free and E8 conditioned media of intoxicated cells. a, Comparison of label-free quantification intensity of proteins detected in serum-free conditioned media from 0 to 48h post intoxication, and E8 conditioned media from 0 to 48h and 0 to 96h post intoxication. **b,** Number of proteins detected in each conditioned media from different methodologies in comparison with BONCAT method that uses the methionine analogue, AHA to label newly synthesised proteins. **c,** Venn diagram showing the number of proteins that are common and unique to each conditioned media collection method using BioVenn. **d,** Number of gene names of each method that matched with The Human Secretome, or the compendium of secreted proteins in human cell lines.[262,266]

treated and toxin^{HQ}, only toxin^{WT} (toxin^{SASP}) retained the ability to induce transmissible senescence **(Fig.5.3b-d)**. SF fraction 0-24h showed the highest percentage of SA-β-gal positive cells in SF conditions. The subsequent toxin^{SASP} fractions (24-48h, 48-72h, 72-96h) weakened progressively to ∼40% SA-β-gal positive cells **(Fig.5.3c-d)**. However, when all SF fractions were combined, the transmission of senescence mirrored the first 24h. This suggests that toxin^{SASP} elicits an acute senescence response due to a factor present in the 0-24h SF fraction. When SF was compared to E8, all 0-24h, 0-48h, 0-72h and 0-96h E8 fractions consistently showed ∼40-50% transmissible senescence compared to the negative controls **(Fig.5.3g-h)**. In summary, cells cultured in both SF and E8 media induced tox^{SEN} and tox^{SASP}. As tox^{SEN} and toxin^{SASP} in SF were maximal in the first 48h, subsequent experiments were carried out using 0-24 and 24-48h fractions. Since E8 fractions showed similar phenotypes in all timepoints, 0-48h and 0-96h were analysed in a pilot mass spectrometry experiment.

5.4 Pilot mass spectrometry analysis of host cell secretomes.

To examine the difference between SF and E8, three samples were analysed by mass spectrometry: tox^{SASP} in E8 (0-48h), E8 (0-96h) and SF (0-48h comprising 0-24h and 24-48h in combination) (**Fig.5.4**).

Label-free quantification (LFQ) intensity is an indicator of the relative amount of proteins in the samples. SF unconditioned media showed almost no LFQ intensities compared to E8 media which shows a higher intensity (**Fig.5.4a**). Even though the LFQ intensity was higher in E8 tox^{SASP} than SF tox^{SASP} at 0-48h (**Fig.5.4a**), SF analysis revealed the highest number of proteins (**Fig.5.4b**: SF, n=1089 / E8, n=1026). Tox^{SASP} from E8 conditioned media between 0-96h showed the highest LFQ intensity and identified the most proteins (**Fig.5.4a-b**). Interestingly, there were 654 proteins that were common between all three samples (**Fig.5.4c**) whilst also revealing significant differences at 0-48h (**Fig.5.4c**: SF, 301 unique proteins / E8, 165 unique proteins). This suggests that growth media composition regulates the secretome, as well as incubation time since the most significant difference was observed between E8 0-48h and E8 0-96h (**Fig.5.4c**). Mass spectrometry on SF and E8 conditioned media led to the detection of more than ~50% additional proteins relative to AHA-labelled proteins using BONCAT methodology (**Fig.5.4b**), which highlights BONCAT's limitations. Comparative analysis with the Human Secretome[266] and the compendium of secreted proteins[262] showed that even though E8 incubation for 96h has the highest LFQ intensity (**Fig.5.4a**) and the most number of proteins detected (**Fig.5.4b**), conditioned media in SF for 48h has the highest number and percentage of secreted proteins matches (n=280, ~26%) compared to to E8 48h (n=244, 24%) and 96hr (n=260, ~11%) (**Fig.5.4d**). Given the higher sensitivity of both approaches compared to BONCAT, and to examine tox^{SASP} in different growth media, quantitative LC-MS/MS on both E8 and SF conditioned media were used to identify the proteins secreted by intoxicated cells.

5.5 Mass spectrometry of toxin-induced host secretome in E8 media.

Tox^{SASP} and APH^{SASP} both transmitted senescence to naive cells indicating a common mechanism, but only tox^{SASP} enhanced *Salmonella* invasion by macropinocytosis into bystander cells[106]. This suggests the toxin induces a secretome customised for infectious disease. To investigate the molecular basis of these divergent SASPs, tox^{SASP} was compared to SASP generated by chemical inducers of DNA double-strand breaks and senescence, APH and ETP[286] and negative controls. A minimum of 3 biological replicates of conditioned media from untreated, toxin^{WT}-, toxin^{HQ}-, APH-, and ETP-treated cells cultured in E8 media (0-48h) were harvested and assayed for transmissible senescence. Toxin$^{WT-SASP}$ induced senescence in ~70% of cells relative to ~20% in negative controls (**Fig.5.6a-c**). Similarly, APH induced significant senescence (~40%), but ETP only induced ~25% senescence, which was not statistically significant.
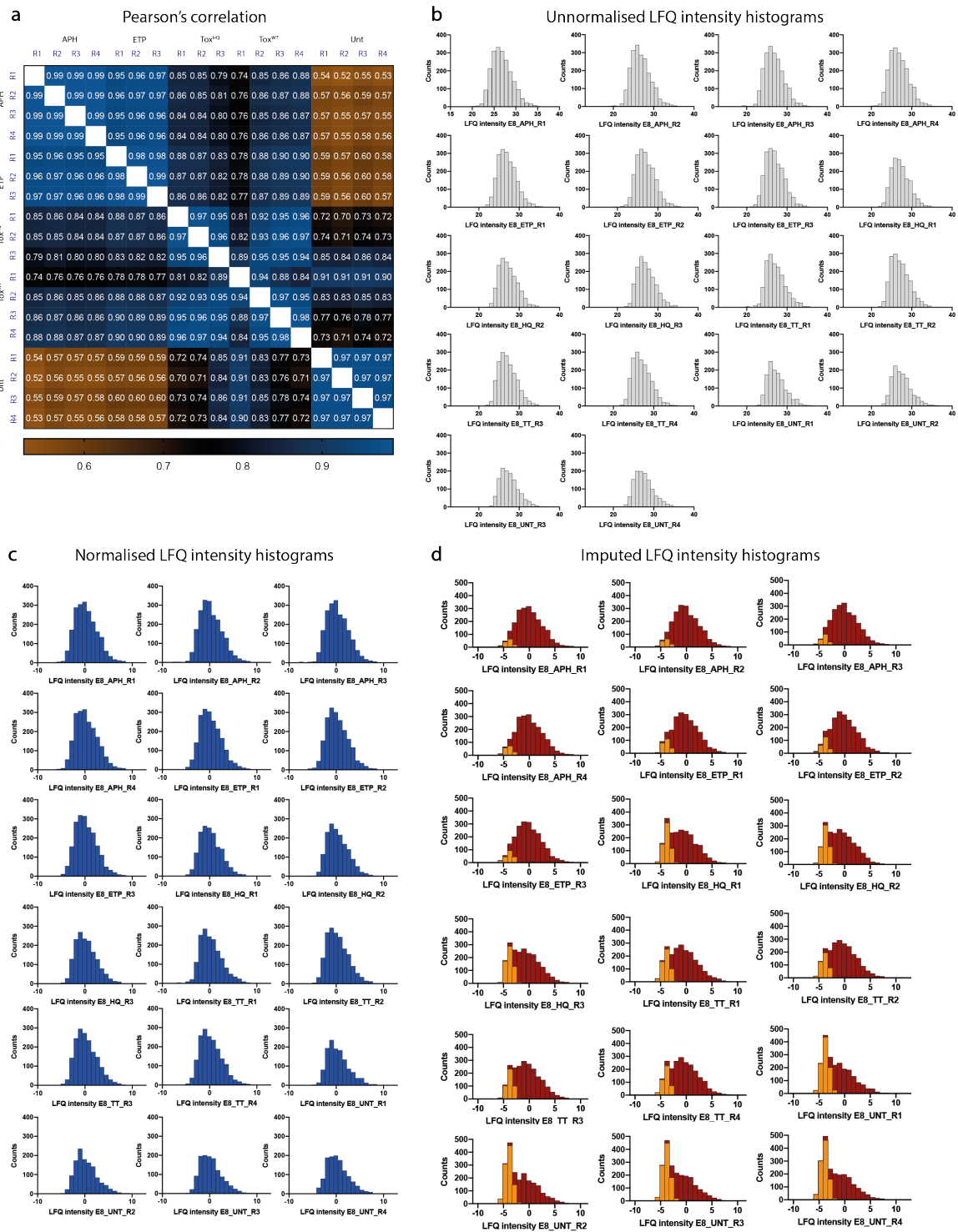
Figure 5.5| Raw data analysis exported from MaxQuant and processed using Perseus bioinformatics analysis. a, Heat map summarising the column Pearson's correlation analysis comparing LFQ intensities of E8 samples with each other. **b-d,** Frequency distribution histograms of the different E8 samples analysed by mass spectrometry of **b,** unnormalised, **c,** normalised and **d,** imputed LFQ values.

Pearson's column correlation analysis showed high correlation between the different biological replicates of each condition (**Fig.5.5**a, r>0.84), which indicates high reproducibility. Surprisingly, toxin[HQ] replicates had low correlation with untreated samples (**Fig.5.5**a, r<0.8), but a high correlation with toxin[WT] samples (**Fig.5.5**a, r>0.9). This indicates a technical error following assaying of
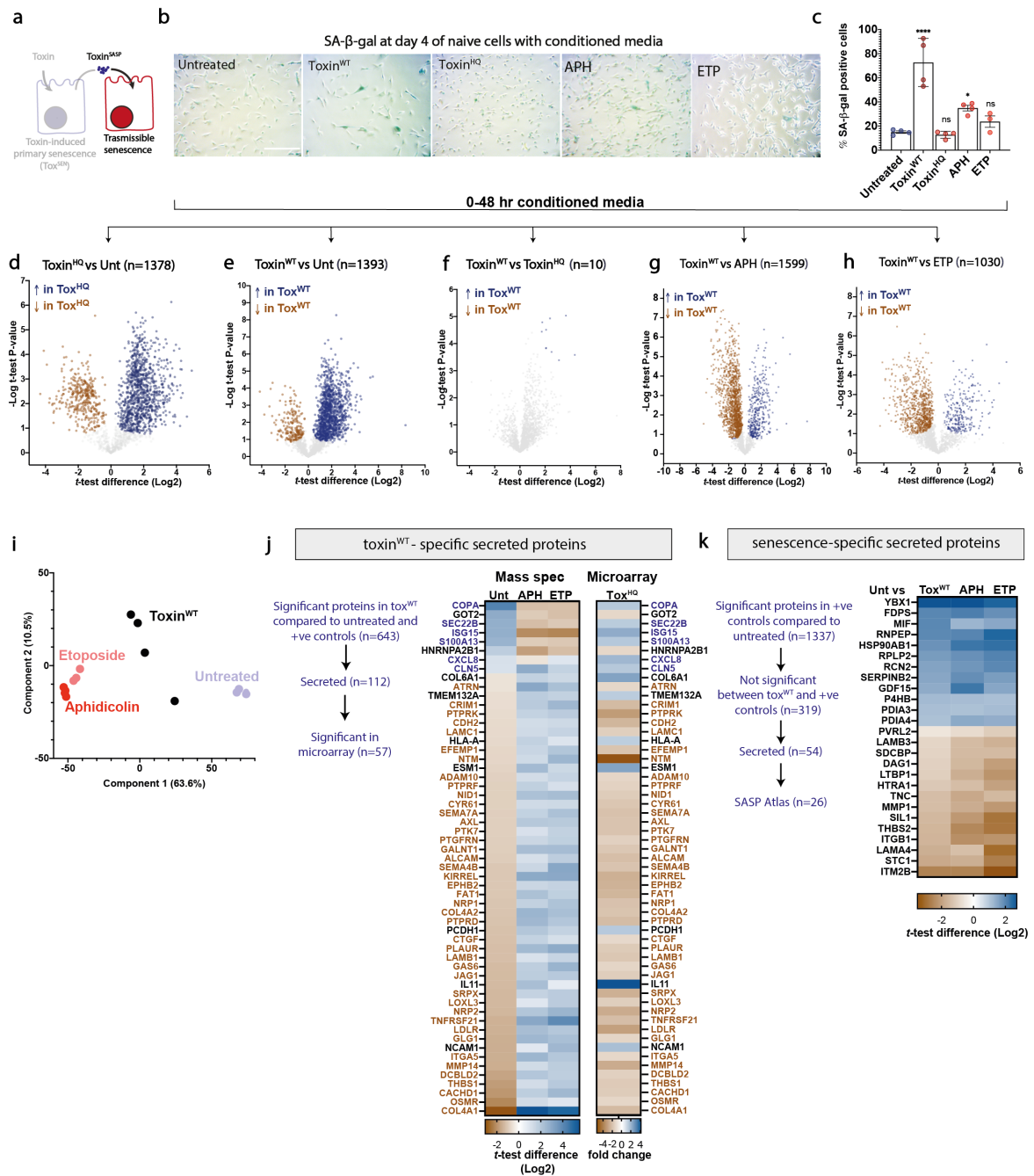
Figure 5.6| Analysis of typhoid toxin-induced secretome in E8 media. a, Conditioned media from untreated, intoxicated cells (toxin[WT] and toxin[HQ]), and other senescence inducers (APH and ETP) were harvested and validated for transmissible senescence prior to mass spectrometry analysis. **b,** Representative images and **c,** quantification (right) of transmissible senescence induced in naive HT1080 cells by unt[CM], toxin[WT-SASP], tox[HQ-CM], APH[CM] and ETP[CM] (0-48hr) for 4 days then assayed for SA-β-gal. Each circle is a biological replicate of the samples analysed by mass spectrometry (at least 10 fields of view per replicate, ∼300-2800 cells/condition per replicate). Scale bar is 200 μm. One-way Anova with Tukey's multiple comparison test was carried out to test for significance. Error bars denote SEM. **d-h,** Volcano plots of secretomes induced between 0h and 48h post removal of toxin and analysed using Perseus two-sample t-test (s0=0.01 and FDR=0.05) from at least 3 biological repeats/condition. Number of significant proteins between **d,** toxin[HQ] and unt, **e,** toxin[WT] and unt, **f,** toxin[WT] and toxin[HQ], **g,** toxin[WT] and APH, and **h,** toxin[WT] and ETP are indicated. Brown dots indicate down-regulated proteins and blue dots indicate up-regulated proteins relative to each other. **i,** Principal component analysis on the different E8 SASP and conditioned media collected after 48h post removal of inducer after excluding toxin[HQ]. **j,** Heat map listing gene names of significant different proteins in toxin[WT-SASP] compared to both unt[CM], APH[CM] and ETP[CM]. Flowchart of the filtering steps (left). The list was compared to GeneChip microarray data (p<0.05), and matches are displayed. Blue text indicates up-regulated genes, brown text indicates down-regulated genes, and black text indicates opposing fold changes in both mass spectrometry and microarray analyses.

k, Proteins identified to be significantly increased or decreased in a senescence-specific manner compared to the unt[CM]. Flow chart of the filtering steps used (left) to reach the list of candidates (right) potentially responsible for transmitting senescence. **j and k,** Gene names displayed were matched with the Human Secretome Atlas and the compendium of secreted proteins[266,262].

transmissible senescence in **Fig.5.6b, 5.6c** and mass spectrometry of toxin[HQ] samples, e.g. toxin[WT] contamination of toxin[HQ]. LFQ intensities of the samples were normalised **(Fig.5.5b-c)** and missing values imputed **(Fig.5.5d)** from the normal distribution before carrying out Student's t-test for comparative analysis of the secretomes. Consistent with the Pearson's correlation analysis, volcano plot analysis revealed significant differences between tox[HQ-CM] and unt[CM] **(Fig.5.6d**, n=1378**)**, but almost no difference with toxin[WT] **(Fig.5.6f**, n=10**)**[*]. Given the marked difference in transmissible senescence **(Fig.5.6b-c)**, volcano plot analysis further indicates a technical error during sample preparation for Orbitrap analysis. Therefore, toxin[HQ] samples were excluded from further E8 analysis.

Similar to the data extracted using BONCAT, toxin[WT] showed a significantly divergent secretome compared to unt[CM] and the positive controls in E8 media **(Fig.5.6e, 5.6g-h)**, which was exemplified with the PCA clustering analysis **(Fig.5.6i)**. To compensate for the lack of toxin[HQ] data in E8 media analysis, toxin-specific proteins were compared to the GeneChip microarray of toxin[WT] vs toxin[HQ] **(Fig.5.6j)**. E8 and microarray analysis revealed co-regulation in both the secretome and transcriptome. Half of the significant proteins identified in toxin[WT] compared to negative and positive controls were also significant in the microarray analysis **(Fig.5.6j**, 57 out of 110**)**.

Interestingly, the top significant candidates included COPA and SEC22B which were up-regulated and essential in vesicle trafficking, indicating potential exosomal release of proteins[287,288]. Of interest, the ubiquitin-like protein ISG15, a regulator of the Type I interferon pathway was up-regulated in toxin[WT]-treated cells **(Fig.5.6j)**. ISG15 has previously been shown to constitute anti-viral properties[289]. Additionally, in *Listeria monocytogenes* infections, free ISG15 was up-regulated and resulted in restricted infection[290]. Interestingly, the typhoid toxin also induced inflammatory constituents, previously associated with senescence phenotypes **(Fig.5.6j)**. The toxin positively regulated the inflammatory protein CXCL8, which reinforces senescence through ROS and p53 activation[195,205], but negatively regulated anti-inflammatory metalloproteases such as MMP14. Downregulation of MMP14 was shown to induce senescence in mice[291]. Additionally, the toxin upregulated S100A13, which is a DAMP that drives inflammation[292] **(Fig.5.6j)**. In fact, cell stimulation using S100A13 showed induction of NF-κB which drives senescence phenotypes[293,294]. To identify mediators of transmissible senescence, the secretomes of all senescence inducers (toxin[WT], APH[SASP] and ETP[SASP]) were filtered against unt[CM] **(Fig.5.6k**; n=319**)**, then cross examined with secretome atlases[262,266] and the SASP Atlas[174] **(Fig.5.6k**, n=26**)**. Interestingly, GDF15, also known as macrophage inhibitory cytokine-1, and a TGFβ family member was up-regulated **(Fig.5.6k)**. TGFβ signaling pathways have been previously reported as pivotal in transmissible senescence[187], which hints at TGFβ signaling activation by the typhoid toxin.

---

[*]Click here to access the whole dataset extracted and used for E8 analysis

Although E8 conditioned media provided a more inclusive secretome compared to BONCAT, the lack of toxin[HQ] control was not ideal. In addition, SF showed a higher percentage of secreted proteins in the pilot experiment. Therefore, conditioned media collected from SF was analysed by LC-MS/MS and controlled for DNA damage phenotypes, as well.

5.6 Toxin-induced host secretome underlying tox[SASP] in SF media.

Prior to analysing the SF conditioned media by mass spectrometry, the DNA damage responses to the typhoid toxin were investigated at 24h and 48h when SF conditioned media was harvested (**Fig.5.7**a, red arrows). As expected, in serum-free conditions no RINGs were detected, and the majority of cells displayed a γH2AX foci phenotype (**Fig.5.7**b-f, ~90%). Cells showed a decrease in RPApT21 positive nuclei, (**Fig.5.7**g, 16% to 8%) but a sustained 53BP1 response across timepoints (**Fig.5.7**h, 70-80%). Other senescence inducers, i.e. aphidicolin and etoposide, displayed a similar γH2AX foci phenotype but less significant RPA and 53BP1 responses in serum-free conditions.

Conditioned SF media fractions 0-24h and 24-48h from the experiment in **Fig. 5.7** were combined and 4 biological replicates were validated for their ability to transmit senescence (**Fig.5.9**a, 5.9b). Next, LC-MS/MS was used to identify the protein constituents of each secretome. Perseus column correlation analysis showed high correlation between the different biological replicates of each condition (**Fig.5.8**a, r>0.90), which indicates the samples' high quality. Label-free quantification of the samples were normalised (**Fig.5.8**b, 5.8c) and missing values imputed (**Fig.5.8**d) from the normal distribution before carrying out Student's t-test for comparative analysis of the secretomes (**Fig.5.9**c-e). Similar to BONCAT, there was very little difference in the secretomes of untreated and toxin[HQ]-treated negative control cells (**Fig.5.9**c, n=65 significant proteins), which contrasted with the secretome of toxin[WT]-treated cells that was significantly divergent from untreated (**Fig.5.9**d,n=1153) and toxin[HQ] (**Fig.5.9**e, n=1186)[*]. Interestingly, previous literature provided evidence that SASP proteins were predominantly upregulated in response to irradiation- and oncogene-induced senescence[174]. Similarly, the majority of significant secreted proteins were upregulated in response to the toxin (**Fig.5.9**e, 954 out of 1186). **Fig.5.9**f reveals the toxin[WT]-induced secretome defined by proteins in the Human Secretome and Eichelbaum et al 2012 compendium of human secreted proteins that were differentially regulated relative to untreated and toxin[HQ]-treated negative controls[262,266] (P<0.05, n=133 significant proteins).

To further investigate the toxin[WT] secretome, global changes in transcription were determined by GeneChip microarray analysis of cells at 48h following 2h treatment with toxin[WT] or toxin[HQ] (**Fig.5.9**g). Of the 133 proteins comprising the toxin[WT]-induced secretome (**Fig.5.9**f), 65 proteins were identified as significant by both mass spectrometry and microarray analyses (**Fig.5.9**g).

---

[*]Click here to access the whole dataset extracted and used for SF analysis
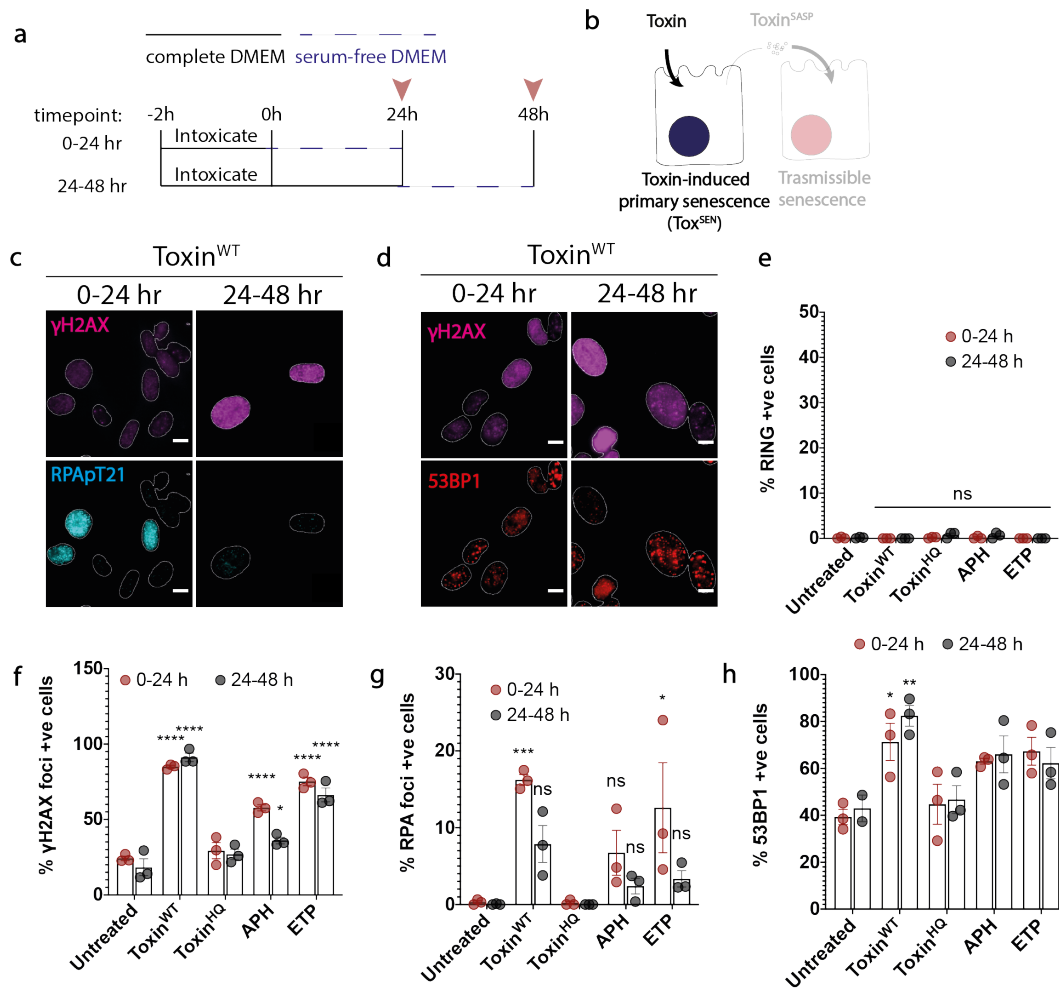
Figure 5.7| DNA damage responses of intoxicated cells in serum-free conditions during conditioned media extraction. a, The experimental protocol of serum-free conditioned media extraction for mass spectrometry analysis. Arrows indicate cells fixed at the end of 0-24h (red) and 24-48h (black) incubation with serum-free media time point for DNA damage assays. **b,** Experiments shown are toxin-induced senescence. c, Representative images of toxin-induced γH2AX (magenta) and RPApT21 (cyan) response at the end of the 0-24h and 24-48h serum-free incubation. d, Representative images of toxin-induced γH2AX (magenta) and 53BP1 foci (red) at the end of the 0-24h and 24-48h serum-free incubation. **c and d,** Scale bars on representative images denote 50 μm. **e,** Percentage of RING positive nuclei detected using the RING tracker. **f,** Percentage of γH2AX foci positive nuclei quantified using CellProfiler. **g,** Percentage of RPApT21 positive nuclei quantified using CellProfiler. **h,** Percentage of 53BP1 positive nuclei quantified using Cell-Profiler. **e-h,** RPApT21 positive nuclei were determined using CellProfiler by thresholding the amount of RPA occupying each nucleus. γH2AX and 53BP1 foci were counted using CellProfiler, and positive cells were determined using the cut-off value derived from number of foci in untreated cells between 0-24h. Each circle on the graphs represents a biological replicate (30 fields of view, ~500 nuclei/condition). Two-way ANOVA with Sidak multiple comparisons test was carried out to test for significance. Error bars denote SEM.

Panther analysis of the matches between SF mass spectrometry and microarray analyses showed that the proteins identified are involved in various pathways most notably the gonadotropin-releasing hormone receptor pathway (GnRHR), TGFβ signalling pathway, angiogenesis and notch signaling pathway **(Fig.5.9g, Supplementary Fig.S1)**. TGFβ signalling pathway was the only pathway to have all the three proteins involved upregulated, hinting at an activation of the pathway in paracrine senescence signaling. INHBA (i.e. activin βA), GDF15 and BMP1, which activate the TGFβ signalling pathway, a major axis in transmissible senescence[187,295], was also found upregulated in both
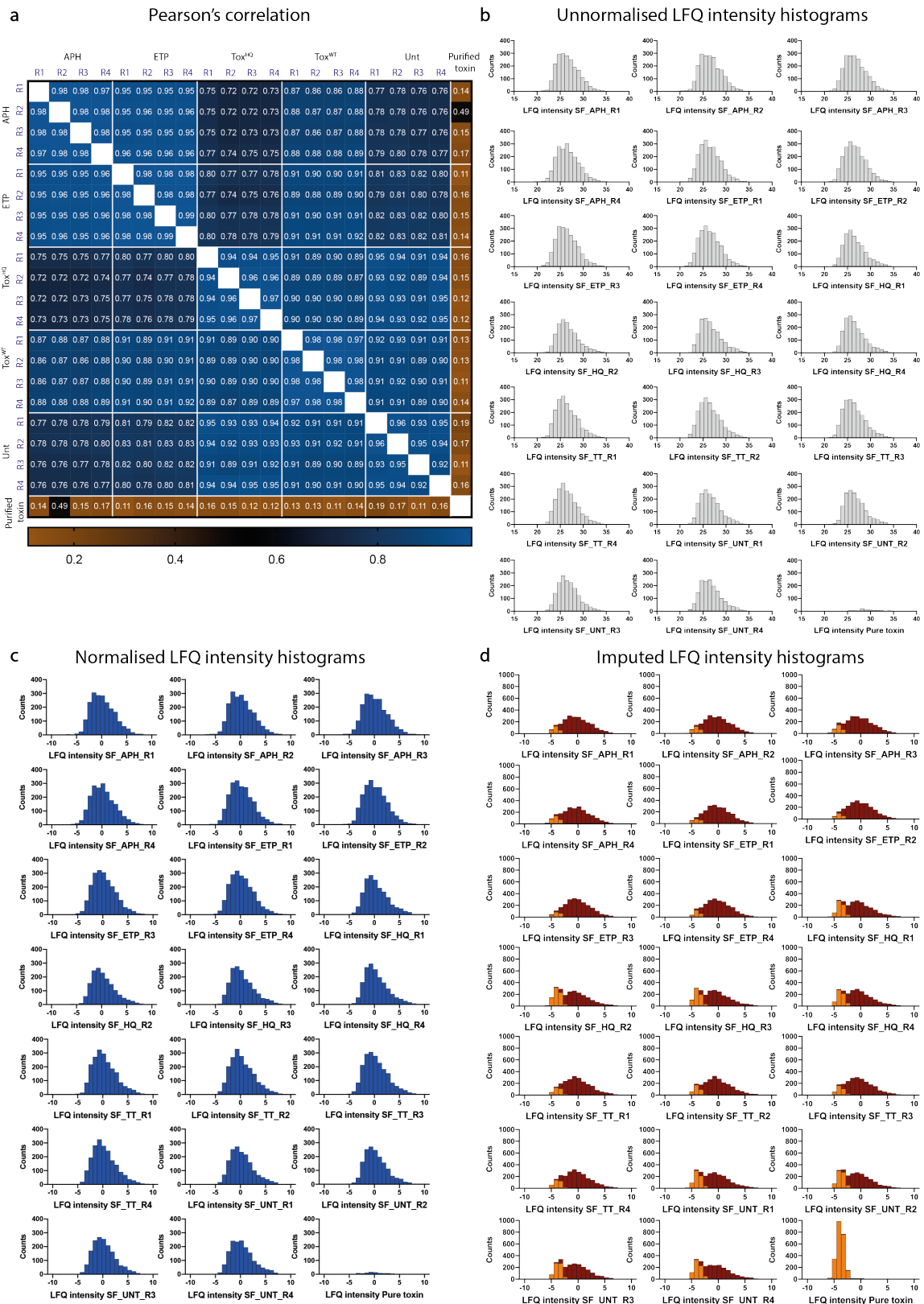
Figure 5.8| Raw data analysis exported from MaxQuant and processed using Perseus bioinformatics analysis. a, Heat map summarising the column Pearson's correlation analysis comparing LFQ intensities of samples with each other. **b-d,** Frequency distribution histograms of the different samples analysed by mass spectrometry of **b,** unnormalised, **c,** normalised and **d,** imputed LFQ values.
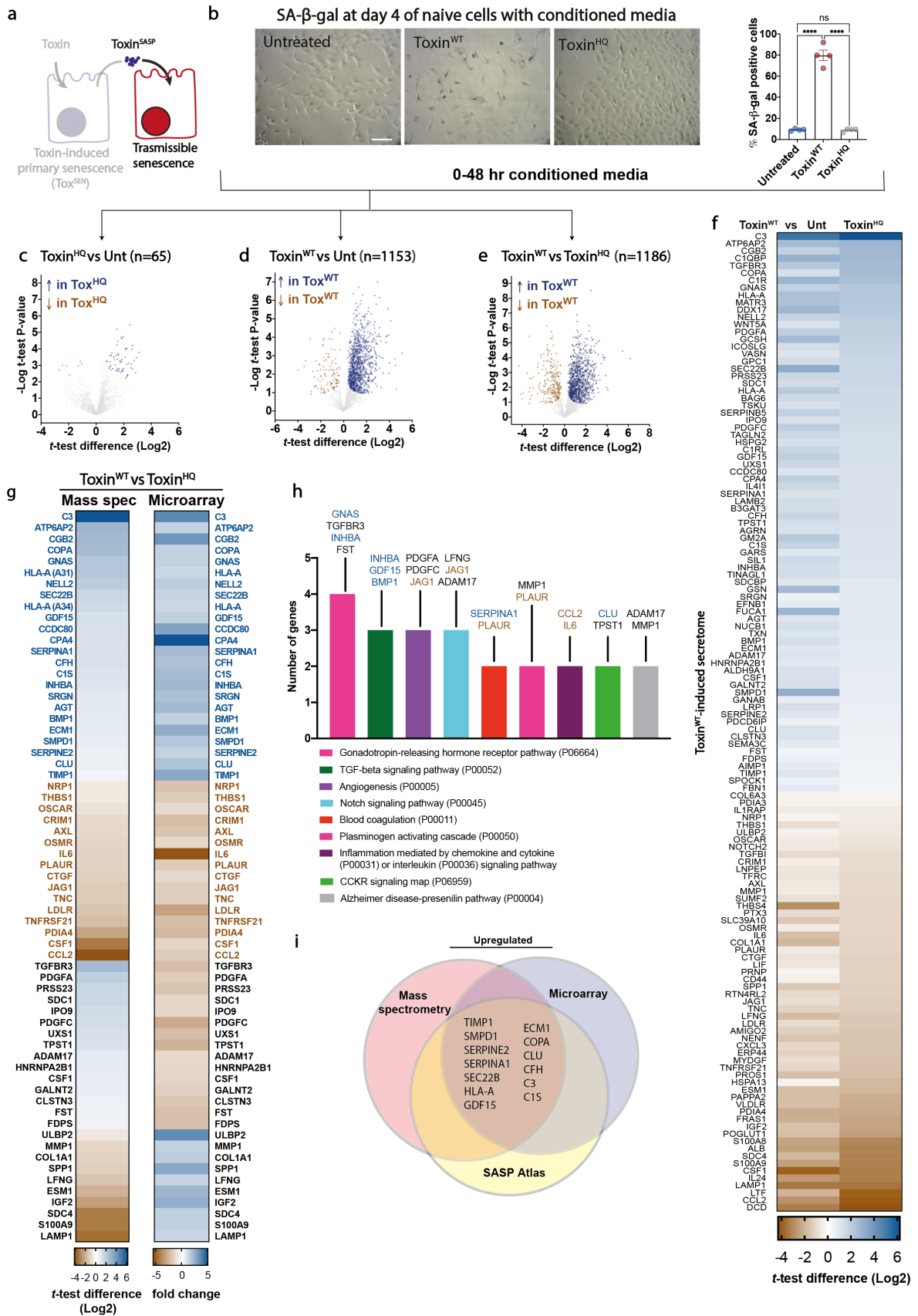
Figure 5.9| The typhoid toxin-induced secretome. a, Conditioned media from untreated and intoxicated cells with toxin$^{\mathrm{WT}}$ and toxin$^{\mathrm{HQ}}$ were collected and validated for transmissible senescence before mass spectrometry.

b, Representative images (left) and quantification (right) of transmissible senescence induced in naive HT1080 cells by unt^{CM}, toxin$^{WT-SASP}$ and tox^{HQ-CM} (0-48hr) for 4 days then assayed for SA-β-gal. Each circle is a biological replicate of the samples analysed by mass spectrometry (40 fields of view, ∼500 and 2500 cells per condition). One-way Anova with Tukey's multiple comparison test was carried out to test for significance. Error bars denote SEM. **b,** Scale bar is 100 µm. **c-e,** Volcano plots of secretomes induced between 0h and 48h post removal of toxin and analysed using Perseus two-sample t-test (s0=0.01 and FDR=0.05) from 4 biological repeats per condition. Number of significant proteins between **c,** toxin^{HQ} and unt, **d,** toxin^{WT} and unt, and **e,** toxin^{WT} and toxin^{HQ} are indicated. Brown dots indicate down-regulated proteins and blue dots indicate up-regulated proteins relative to each other. **f,** Heat map listing gene names of significant different proteins that increase or decrease in toxin$^{WT-SASP}$ compared to both unt^{CM} and tox^{HQ-CM}. Gene names displayed were matched with the Human Secretome Atlas and the compendium of secreted proteins[262]. Proteins that showed opposing secretion profile in toxin$^{WT-SASP}$ vs unt^{CM} and toxin$^{WT-SASP}$ vs tox^{HQ-CM} are not displayed. Genes were sorted from highest to lowest t-test difference in toxin$^{WT-SASP}$ vs tox^{HQ-CM} **g,** Heat map of a comparative analysis between the toxin-induced secretome displayed in **f,** and GeneChip microarray data (p<0.05). Blue text indicates up-regulated genes, brown text indicates down-regulated genes, and black text indicates opposing fold changes in both analyses. **h,** Panther pathway analysis of genes listed in **g**. Blue text indicates up-regulated genes, brown text indicates down-regulated genes, and black text indicates opposing fold changes in both mass spectrometry and microarray analyses. **i,** Venn diagram displaying the gene names of proteins that were found (i) in the Human Secretome[266], (ii) up-regulated in the mass spectrometry, (iii) up-regulated in the microarray and (iv) up-regulated in the SASP Atlas[174].

analyses (**Fig.5.9h,**; blue labelling). Interestingly, inhibitors of Activin βA-driven TGFβ signalling, TGFBR3 and FST, which are constituents of the GnRHR (**Fig.5.9g, 5.9h**), were found upregulated in mass spectrometry but downregulated in the microarray (black labelling). This perhaps suggests that the receptor TGFBR3, for example, is shed from senescent cells rather than overexpressed.

Other factors identified were notably regulators of blood coagulation and blood vessel formation (**Fig.5.9h, Supplementary Fig.S1**). PDGFs, which were upregulated in the secreted proteins are pro-angiogenic[296], whilst JAG1, which is also pro-angiogenic, was downregulated in both E8 secretome, SF secretome and microarray analyses[297] (**Fig.5.6j; 5.9g, 5.9h**). Additionally, SERPINA1 which is a positive regulator of blood coagulation[298] was upregulated in both analyses, whilst PLAUR, which is an anticoagulant[299] was downregulated, indicating potential toxin-induced blood coagulation (**Fig.5.9g,5.9h**). Of the proteins that were downregulated in both mass spectrometry and microarray analyses (brown labelling), the most striking were the interleukins, IL6 and CCL2, which are a hallmark of pro-inflammatory SASP (**Fig.5.9g, 5.9h**).[174,189,300] The secretome included known SASP proteins such as effectors of innate immunity (e.g. complement C3, C1S) that were upregulated in both analyses (indicated by blue labelling), as were GDF15, SERPINA1, SERPINE-2, ECM1, and TIMP1 amongst others that were identified in the SASP Atlas database[174] (**Fig.5.9i**).

To examine the factors that contribute to the tox^{SASP}-specific phenotypes, APH^{SASP} and ETP^{SASP} constituents were also compared to tox^{SASP} (**Fig.5.10a-c**). Conditioned media from each senescence inducer was validated for their ability to transmit senescence before analysing the secretomes by LC-MS/MS (**Fig.5.10b**). PCA analysis of the secretomes displayed 3 distinct clusters grouping senescence-inducers APH^{SASP} and ETP^{SASP}(red), the negative controls secretomes (blue), and tox^{SASP}, which generated an independent cluster establishing that the toxin has the most divergent
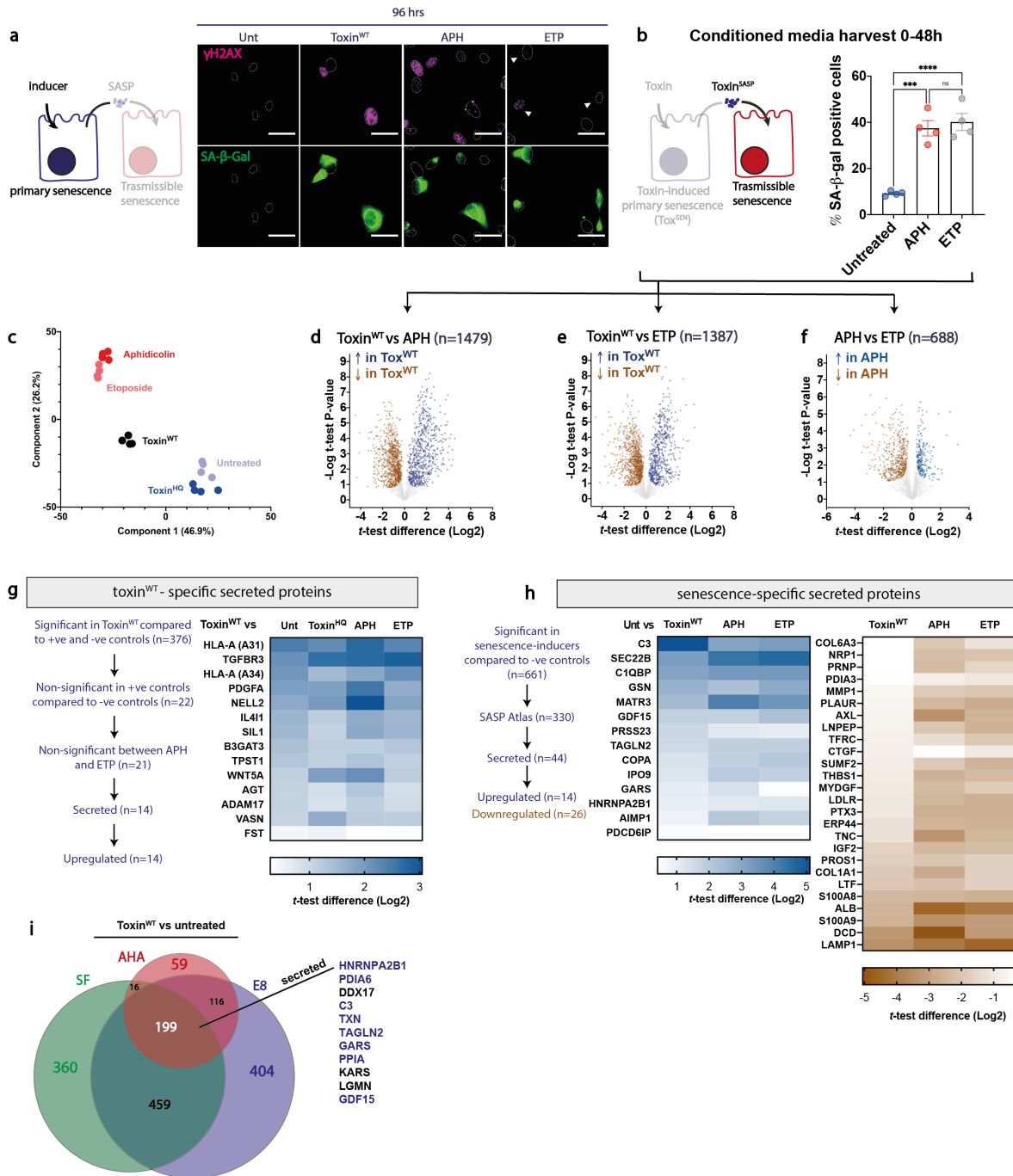
Figure 5.10| The unique toxin-induced secretome relative to other senescence inducers. a, Representative images of DNA damage (γH2AX - magenta) and primary senescence (SA-β-gal - green) responses induced by toxin^WT, aphidicolin (APH) and etoposide (ETP) at 96h. White arrows indicate γH2AX-positive nuclei for ETP-treated cells. Scale bar is 50 μm. **b,** Quantification (right) of transmissible senescence induced in naive HT1080 cells by unt^CM, APH^SASP and ETP^SASP (0-48hr post removal) for 4 days then stained for SA-β-gal. Each circle is a biological replicate of the samples analysed by mass spectrometry (40 fields of view; ~500 and 2500 cells/condition). One-way Anova with Tukey's multiple comparison test was carried out to test for significance. Error bars denote SEM. **c,** Principal component analysis on the different SASP and conditioned media collected after 48h post removal of inducer. **d-f,** Volcano plots of secretomes induced between 0h and 48h post removal of toxin analysed using Perseus two-sample t-test (s0=0.01 and FDR=0.05) from 4 biological repeats per condition. Number of significant proteins between **d,** toxin^WT and APH, **e,** toxin^WT and ETP, and **f,** APH and ETP indicated. Brown dots indicate down-regulated proteins and blue dots indicate up-regulated proteins relative to each other. **g,** Proteins identified to be significantly increased in a toxin^WT-specific manner compared to all negative and positive controls.

Flowchart of the filtering steps (left) to reach toxin-specific list including proteins that are potentially involved in enhancing *Salmonella* invasion (right). **h,** Proteins identified to be significantly increased or decreased in a senescence-specific manner compared to the negative controls. Flow chart of the filtering steps used (left) to reach the list of candidates (right) potentially responsible for transmitting senescence. **i,** Venn diagram of proteins that were consistently significantly up-regulated in toxin^WT-SASP compared to unt^CM from all three mass spectrometry techniques (SF, E8 and AHA). Genes listed are the proteins detected as secreted by the Human Secretome Atlas and the compendium of secreted proteins[262,266]

secretome of the senescence-inducers **(Fig.5.10c)**. Upon closer inspection, tox^SASP was significantly divergent from APH^SASP **(Fig.5.10d**, 1479 significant proteins**)** and ETP^SASP **(Fig.5.10e**, 1387 significant proteins**)**. Interestingly, most proteins were upregulated in toxin^SASP compared to APH^SASP (646 out of 1479) and downregulated compared to ETP (848 out of 1387). Consistent with PCA, ETP and APH were less divergent to each other only showing 688 significant proteins **(Fig.5.10f)**.

To identify enhancers of infection, the toxin^WT-induced secretome was filtered against all significant secretome proteins in unt, toxin^HQ, APH^SASP and ETP^SASP **(Fig.5.10g**, left flowchart**)**. All toxin-specific proteins identified were upregulated. Putative enhancers of infection included regulators of TGFβ signalling TGFBR3, FST, the transmembrane protein vasorin (VASN) and metalloprotease ADAM17. ADAM17 liberates the extracellular domain of vasorin, which negatively regulates TGFβ pathways[301]. ADAM17 is the prototype sheddase liberating membrane-bound growth factors (e.g. TGFβ and EGF ligands) that makes ADAM17 an important regulator of growth factor signalling and membrane ruffling[302]. Interestingly, n-EGF-like 2 (NELL2) was identified, as was the ADAM17 activator PDGF[303]**(Fig.5.10g, Supplementary Fig.S1)**. Thus, the data implicates growth factor signalling in tox^SASP-driven infection into bystander cells.

Another putative candidate of infection was Wnt5a **(Table 5.1)**. Strikingly, Wnt5a was amongst 33 proteins identified only in toxin^WT-treated cells prior to any Perseus analysis **(Table 5.1)** indicating toxin-specificity. Wnt5a was previously shown to increase macrophage uptake of bacteria and increased bacterial survival[304]. Additionally, Wnt5a reportedly activated TGFβ to mediate intestinal repair post-injury, demonstrating a crosslink between Wnt5a signaling and TGFβ pathway[305]. This suggests a potential collaborative action of TGFβ and Wnt ligands in toxin-induced senescence.

Proteins detected only in toxin^WT samples prior to Perseus analysis										
Gene names										
C1RL	LTBP4	RAB35	NUP85	**WNT5A**	SULF2	NELL2	CD99L2	SEC24B	SIRT5	ACVR1
ATP2B4	RHOG	TOR4A	RPL23A	TAF15	TPST1	MYADM	OSTF1	CFH	ADGRL2	THTPA
BABAM1	POMGNT1	ARRB1	ARFGAP2	PHLDB1	TRIM21	UBE2C	RAB13	ACTB	NOG	STRN

Table 5.1|List of 33 gene names of proteins that were detected by LC-MS/MS exclusively in toxin^WT-SASP, in at least 3 out of 4 replicates, after MaxQuant analysis and before importing into Perseus for statistical analysis.

To identify mediators of transmissible senescence, the secretomes of all senescence inducers (toxin^WT,

APH^{SASP} and ETP^{SASP}) were filtered against negative controls (unt, toxin^{HQ}) **(Fig.5.10h**, n=661**)** then cross-examined with the SASP Atlas and the secreted protein databases. Out of the 14 upregulated protein, the TGFβ family member GDF15 was immediately striking, as it was also identified in E8 and SF toxin^{WT}-induced secretome **(Fig.5.6k, 5.9f-i)**. GDF15 was previously reported to be differentially expressed during ageing, negatively regulates IL6 expression (observed in **Fig.5.9f-h**), and has been identified as a SASP component[306,307,308].

Similarly to the tox^{SASP}, APH^{SASP} and ETP^{SASP} showed a reduction in MMP1, and growth factors such as Myeloid-derived growth factor (MYDGF), insulin growth factor 2 (IGF2), and connective tissue growth factor (CTGF) **(Fig.5.10h)**. Interestingly, CTGF remodels tissues during fibrosis by modulating pathways, for instance through inhibiting BMP and Wnt pathways, and activating TGFβ[309]. The most downregulated secretions include Dermcidin (DCD), S100A9, and S100A8. DCD is a peptide that displays antimicrobial activity. Furthermore, S100 proteins are considered Damage-Associated Molecular Pattern (DAMP) proteins which are released from unhealthy cells to elicit immune cell driven inflammation[292]. The fact that DCD, S100A9 and S100A8 are downregulated the most in toxin^{WT}-induced SASP suggests a host pro-survival and a *Salmonella* protective environment by suppressing antibacterial activity or immune activation by DAMPs.

Given that there were diverse secretomes induced by the typhoid toxin in SF, E8 and BONCAT, the common proteins that were up-regulated were examined using BioVenn **(Fig.5.10i)**. Interestingly, 199 proteins were found consistently significant in toxin$^{WT-SASP}$ compared to unt^{CM} from the three secretomes, but only 12 proteins were reported as secreted **(Fig.5.10i)**. The most intriguing was GDF15, which implicated the TGFβ pathway using three diverse mass spectrometry methods at acute and chronic SASP.

5.7 Discussion

This chapter, together with **Chapter 4** reveals an unbiased analysis of the human cell secretory responses to a bacterial toxin for the first time using three different approaches. It also establishes a road map for understanding the molecular mechanisms by which diverse genotoxic agents remodel bystander cells to induce transmissible senescence, which represents a powerful innate defence against the proliferation of cells with pathological potential (e.g. cancer, virus-infected). Counter to its role in innate defence, tox^{SASP} was shown to enhance *Salmonella* invasion, induce transmissible senescence and DDRs in bystander cells through unidentified factors[106]. In disease, SASP is known to evolve from a good servant into a bad master when deregulated, and is implicated in age-related pathologies such as cancer, cardiovascular disease, and neurodegenerative disorders[249]. The contribution of senescence and SASP to bacterial infection is not understood.

Whilst some toxin-induced significant proteins in SF matched E8 (e.g. COPA, SEC22B, JAG1, PLAUR, CTGF, GDF15), there was very little overlap in secretomes, which indicates an important
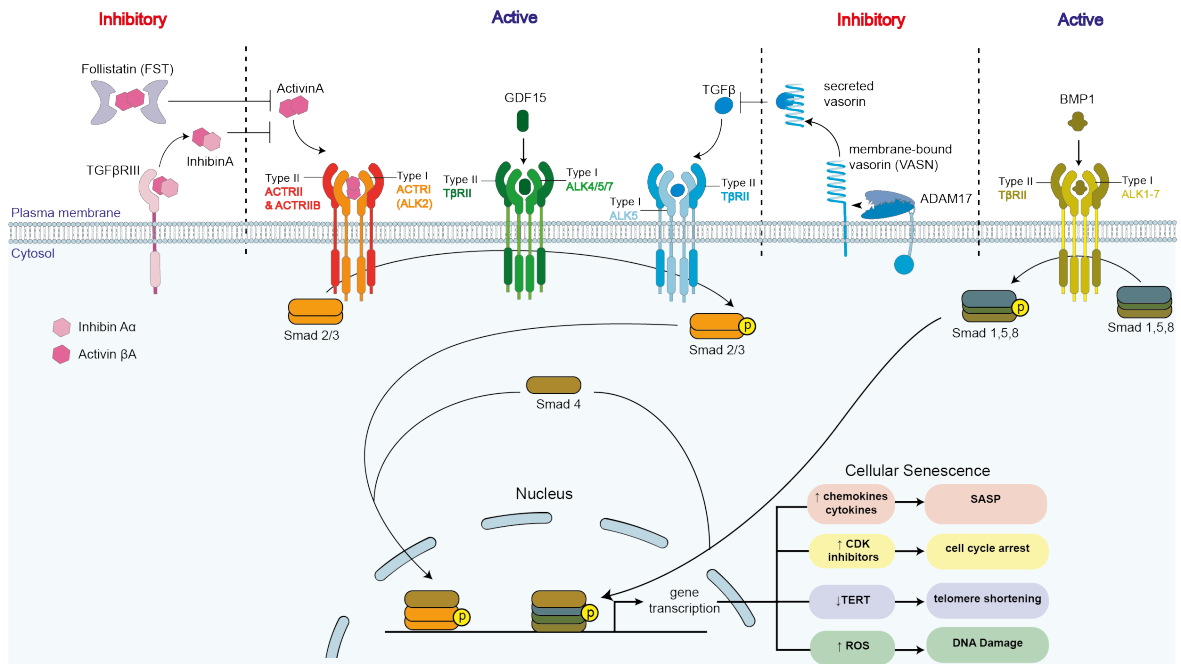
Figure 5.11| Role of TGFβ network identified in the toxin-induced secretome. Schematic representation of the different toxin-specific proteins involved in the TGFβ pathway. The different players identified are either involved in activating the pathway or inhibiting it. Ligands that activate the pathway include Activin A, TGFβ, GDF15 or BMP1 binding to their respective receptors and activating a cascade of phosphorylated smad transcription factors that leads to the production of various proteins involved in establishing a senescence phenotype. These ligands are inhibited via follistatin that sequesters Activin A, TGFBRIII that delivers inhibinA and negatively regulates the activin pathway, and ADAM17 that cleaves membrane-bound vasorin into a soluble secreted protein that sequesters TGFβ. The inhibitory pathway thus prevents the cascade of smad phosphorylation and the senescence-associated gene transcription.

role of growth media in influencing the secretome. E8 showed intriguing candidates such as ISG-15, which could be activated in response to the typhoid toxin as an innate host defence mechanism[289,290]. Interestingly, ISG15 is an interferon-stimulated gene, which modifies host proteins in a manner similar to ubiquitination, i.e. ISGylation[310]. It would be interesting to examine whether ISG15 in the secretome was free, or in fact ISGylated a host factor in a senescence-dependent manner. Interestingly in E8, the toxin had a more inflammatory phenotype, which could be due to the prior priming of cells using E8 components. The differential regulation of tox$^{\text{SASP}}$ constituents in different growth media is fitting with the reported dynamic properties of SASP, which is context-dependent[174,187,189]. However, SF mass spectrometry was the most-controlled experiment out of the three growth media used. Therefore, for the purposes of this thesis, information was mainly inferred from SF analysis.

The secretome analysis from acute senescence responses identified tox$^{\text{SASP}}$ candidates that potentially drive infection and senescence. The most prominent upregulated proteins included TGFβ family members (**Fig.5.9f-i**), which are major players in transmissible senescence driving cancer (**Fig.5.11**)[187,311]. **Fig.5.11** demonstrates the potential mode of action of the identified TGFβ ligands.

While other potential candidates in this study also present themselves as possible players in infection and senescence, the TGFβ network represents an interesting starting point. The TGFβ pathway

is further implicated by toxin^{WT}-induced increases in TGFβ1 (relative to untreated, APH^{SASP} and ETP^{SASP}) and TGFβ2 (relative to APH^{SASP} and ETP^{SASP}) (data not shown). However, it is unclear whether the toxin would activate or inhibit the TGFβ pathway (**Fig.5.11**), which will be an important step in understanding its significance in the mechanisms underlying toxin-driven transmissible senescence and infection (henceforth toxin^{SASP} phenotypes). Interestingly, the downregulation of IL6 and CCL2 and the implication of NOTCH signaling (**Fig.5.9g,5.9h**) suggest that pro-inflammatory SASP is downregulated in the toxin in favour of a TGF-rich secretome[295]. Other proteins of interest that were shown to be implicated directly in increased phagocytosis of bacteria and their survival in macrophage is Wnt5a[312], which also retains the ability to activate TGFβ signaling[305].

Moreover, this study demonstrated the modulation of pro-angiogenic host proteins in response to intoxication (namely PDGF and JAG1) (**Fig.5.9h**). Interestingly, other pathogens have also been observed to modulate these pathways for survival[313]. For instance, *Mycobacterium tuberculosis* induces host proangiogenic factors that ease its spread to systemic sites, whilst *Aspergillus fumigatus* attenuates angiogenesis to allow for its persistence. Therefore, it is unsurprising that the typhoid toxin might modulate angiogenic host factors to regulate systemic infections and *Salmonella* persistence. Furthermore, the increase of blood coagulants potentially implicates the typhoid toxin in the appearance of blood clots in *Salmonella* Typhi patients[314].

A comparative analysis with other senescence inducers provided insight into the similarities to tox^{SASP}. These included down-regulation of inflammatory proteins such as MMPs, S100A8, and S100A9, which could be hypothesized to be pro-infection and allows for *Salmonella* immune evasion. Together with data from BONCAT and E8 conditioned media, SF confirmed the divergent and unique secretome induced by the typhoid toxin. BONCAT and E8 also confirmed that the common denominator regardless of the growth medium or the time-point is the up-regulation of GDF15, a TGFβ pathway activator. All in all, the three mass spectrometry techniques provided inclusive and diverse methods to explore the toxin-induced secretome, and confirmed that *Salmonella* is likely hijacking the TGFβ pathway.

The use of HT1080s, a fibrosarcoma cell line, is a limitation of this analysis. However, as the toxin^{SASP} phenotypes were demonstrated using conditioned media from intoxicated HT1080s, it was prudent to use this cell line to identify putative, responsible host proteins[106]. Other suitable cell lines include IMR90s, the cell line of choice in most senescence studies[187] or primary colonic cell lines such as HIEC-6, and CCD-112CoN.

Interestingly, whilst the serum-free approach is commonly used to characterise secretory phenotypes[174,281,282,283,284,285], a recent publication suggested that cells cultured in serum using BONCAT in combination with pulsed-SILAC, i.e. stable non-radioactive isotopes, provides a higher secretion profile compared to serum-free media[315]. Indeed, TGFBI, TGFB2, and MMPs amongst others were much more highly secreted in serum-containing media than serum-free media[315]. This approach allows to examine secretomes in serum-containing media, and avoids affecting replication and secretion

rates of SF cells[315].

In summary, *Salmonella* hijacking of the TGFβ and Wnt signalling pathway would represent a novel host-pathogen interaction that may be of significance to invasive infections underlying typhoid fever and chronic carriage.

5.8 Supplementary figure

Pathway	Gene	Pathway	Gene
■ Histamine H2 receptor mediated signaling pathway (P04386)		■ Insulin/IGF pathway-protein kinase B signaling cascade (P00033)	
■ Cortocotropin releasing factor receptor signaling pathway (P04380)		■ Insulin/IGF pathway-mitogen activated protein kinase kinase/MAP kinase cascade (P00032)	IGF2
■ Enkephalin release (P05913)			
■ Endothelin signaling pathway (P00019)	GNAS	■ Pyridoxal-5-phosphate biosynthesis (P02759)	
■ Beta1 adrenergic receptor signaling pathway (P04377)		■ Serine glycine biosynthesis (P02776)	AGT
■ Beta2 adrenergic receptor signaling pathway (P04378)		■ Angiotensin II-stimulated signaling through G proteins and beta-arrestin (P05911)	
■ Beta3 adrenergic receptor signaling pathway (P04379)			
■ 5HT4 type receptor mediated signaling pathway (P04376)		■ PDGF signaling pathway (P00047)	PDGFA
■ Heterotrimeric G-protein signaling pathway-Gi alpha and Gs alpha mediated pathway (P00026)		■ Axon guidance mediated by semaphorins (P00007)	NRP1
		■ Cholesterol biosynthesis (P00014)	FDPS
■ Interleukin signaling pathway (P00036)	IL6	■ p53 pathway (P00059)	THBS1
■ Alzheimer disease-presenilin pathway (P00004)	MMP1	■ Integrin signalling pathway (P00034)	COl1A1
■ Alzheimer disease-amyloid secretase pathway (P00003)	ADAM17		

Figure S1| Panther pathway analysis for the rest of the genes. Gene names and their relevant pathways from **Fig.5.9g** that are not displayed in **Fig.5.9h**.

Chapter 6

TGFβ pathway and Wnt5a contribution to toxin phenotypes

6.1 Introduction

The TGFβ superfamily constitutes a plethora of multifunctional cytokines that are master regulators of diverse cellular processes, including proliferation[316,317], survival[318], differentiation[319], wound healing[320], angiogenesis[316,321] and senescence[187,322]. There are over 30 members of the TGFβ family in humans, e.g. BMPs, Activins and GDFs[323]. Structural differences confer the diversity and differential actions of the TGFβ members[324]. For instance, Activin A is a homodimer of activin βA (INHBA) subunits, whilst its antagonist, inhibin A is a heterodimer of activin βA (INHBA), and Inhibin Aa (INHA) subunits **(Chapter 5, Fig.5.11)**[325].

As illustrated in **Fig.5.11 (Chapter 5)**, canonical TGFβ signalling is initiated upon binding of ligands to membrane-bound serine/threonine kinase receptors, forming a complex[326]. Type II kinase activity phosphorylates and activates type I kinase receptors. Subsequently the signal is transduced intracellularly via phosphorylation of Smad transcription factors that translocate to the nucleus and regulate TGFβ target genes in collaboration with DNA-binding co-factors (activators and repressors).

The human genome encodes seven type I receptors (Activin-like kinases, ALK1-7), five type II receptors (TβRII, ActRIIA, ActRIIB, BMPRII, and AMHRII) and eight Smad proteins (smad1-8)[327,328,329]. The different combinations of type I and type II receptors confer ligand specificity and as a result, also confers differential R-smad signal transduction, and target gene transcription[330]. Furthermore, there are three classes of Smad proteins: regulatory smads (R-smad1,2,3,5,8), co-smad (C-smad4) and inhibitory smads (I-smad6,7). Upon positive activation of the TGFβ pathway, phosphorylated R-smads (psmad) form a transcriptional complex with co-smad4 which is necessary for gene transcription. Conversely, I-Smads are post-translationally modified to be either degraded or stabilised by multiple accessory proteins (e.g. ubiquitin ligases). I-smads can inhibit the pathway by competing with smad 4 to bind with R-smads, or prevent trafficking of receptors to the membrane to

receive less activatory signals[331].

Increasing evidence has implicated activated TGFβ signaling in senescence responses. It was reported the TGFβ can induce reactive oxygen species (ROS) from mitochondria[332,333], up-regulates SA-β-gal and CDK inhibitors such as p21, leads to cell-cycle arrest in G1 phase[334], and down-regulates telomerase reverse transcriptase (TERT) in fibroblasts, colon and breast cancer cells[335,336,337]. It was also shown to be a pivotal component of SASP that acts in an autocrine manner to reinforce senescence elicited via the inflammasome[187]. TGFβ can trigger these responses canonically (via phosphorylation of R-smads) or in a non-canonical manner via smad-independent pathways[311,338], such as p38MAPK[339], JNK[340], and ERK pathways[341]. It can also influence Ras, RhoA, Rac and Cdc4[342], which are all regulators of membrane ruffling[343].

The cellular responses to TGFβ stimulation are context-dependent and require fine tuning of three main determinants: i) the intensity of the signal (ligand concentration, receptor abundance, and extracellular regulators); ii) downstream activation of smad classes; iii) epigenetic modifications of the receiving cell that would open or hide genes from transcription factors[324].

Several papers propose that the TGFβ ligands are excellent therapeutic targets, as well as diagnostic and prognostic markers of disease[344]. Given that the toxin[SASP] leads to transmissible senescence and increases *Salmonella* invasion, potentially due to increased membrane ruffling, and TGFβ regulators were amongst the most up-regulated SASP components, the aim of this chapter is to examine their contribution to the senescence phenotype and *Salmonella* infection.

6.2 The typhoid toxin activates downstream effectors of the TGFβ signalling pathway

It was next examined whether toxin-induced senescence is transmitted through factors upregulated or down-regulated in the secretome. Toxin[WT-SASP] conditioned media was combined with unt[CM] or tox[HQ-CM] to replenish down-regulated factors before assaying transmissible senescence by remaining upregulated factors in the secretome (**Fig.6.1a, 6.1b**). Toxin[WT-SASP] alone or in combination with unt[CM] and tox[HQ-CM] increased SA-β-gal indicating that factors upregulated in the secretome mediate transmissible senescence (**Fig.6.1a, 6.1b**, ∼40% SA-β-gal positive cells), and were thus prioritised for investigation. Up-regulated proteins in toxin[WT-SASP] included both inhibitors (e.g. FST) and activators (e.g. GDF15, BMP1, and Activin A) of the TGFβ signalling pathway (**Fig.5.9, 5.10, in Chapter 5**). To investigate if the toxin activates the TGFβ pathway, phosphorylated smad2 (psmad2) and smad1/5 (psmad1/5) were examined using mean psmad intensity of untreated cells as a threshold. Indeed, toxin[WT] induced nuclear localisation of psmad2 (**Fig.6.1c, 6.1d**) and psmad1/5 (**Fig.6.1e, 6.1f**) in ∼90% of the cells, which was similar to APH and ETP, but more statistically significant than 10 ng/ml TGFβ3 on its own (**Fig.6.1d**). Phospho-smad positive nuclei displayed either near pan-staining phenotype, or foci of varying intensities (**Fig.6.1e**). There was also high
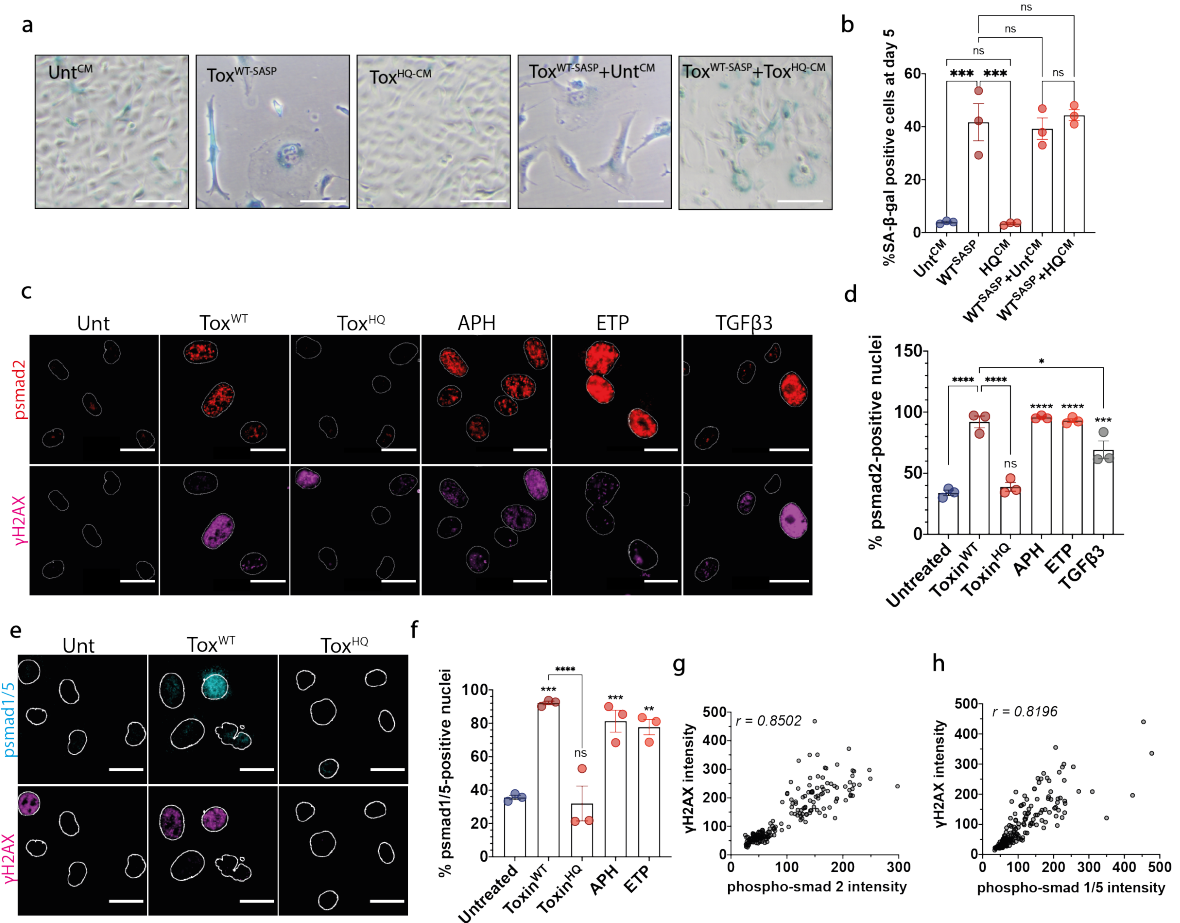
Figure 6.1| Toxin^WT induction of TGFβ signalling. a, Transmissible senescence in naive HT1080 cells treated with serum-free conditioned media harvested 48 h post intoxication and supplemented with 10% FBS before assaying for SA-β-gal after 5 days. Toxin^WT-SASP was combined with negative control conditioned media to examine whether factors of interest are up- or down-regulated. **b,** Quantification of a from 3 biological replicates (∼1000-6500 cells/condition per replicate). **c and e,** Representative images of intoxicated cells in primary senescence at 48 h post intoxication assayed for γH2AX (magenta) and **c,** psmad2 (red), **e,** psmad1/5 signaling (cyan). **d and f,** Quantification of **c and e** respectively from three biological replicates (**c,** ∼100 to 400 cells/condition per replicate; **e,** ∼50-200 cells/condition per replicate). **g and h,** Pearson's correlation of γH2AX and **g,** psmad2 and **h,** psmad1/5 intensity in each cell. Each circle represent a field of view. Quantification of immunofluorescence images was carried out using CellProfiler. Mean intensity of untreated cells were used to sort psmad-positive nuclei. One-way ANOVA with **b,** Tukey's or, **d and f,** Dunnett's multiple comparisons test were carried out to test for statistical significance. Error bars denote SEM. Scale bars are **a,** 100 µm and **c and e,** 25 µm.

correlation between DNA damage induction in cells and elevated levels of psmad2 (**Fig.6.1g**, r=0.85) and psmad1/5 (**Fig.6.1h**, r=0.82), indicating an increased level of psmad2 with increased γH2AX intensity.

6.3 Toxin^SASP transmits senescence via TGFβ ligands

Previous research has demonstrated that TGFβ ligands induce senescence phenotypes[322]. To ensure that the same phenotype occurs in HT1080, purified recombinant TGFβ3 control, and toxin^SASP components Activin A and GDF15 were examined for induction of senescence phenotypes (**Fig.6.2**). At a relatively low concentration (10 ng/ml), TGFβ3 showed an increased level of SA-β-gal positive
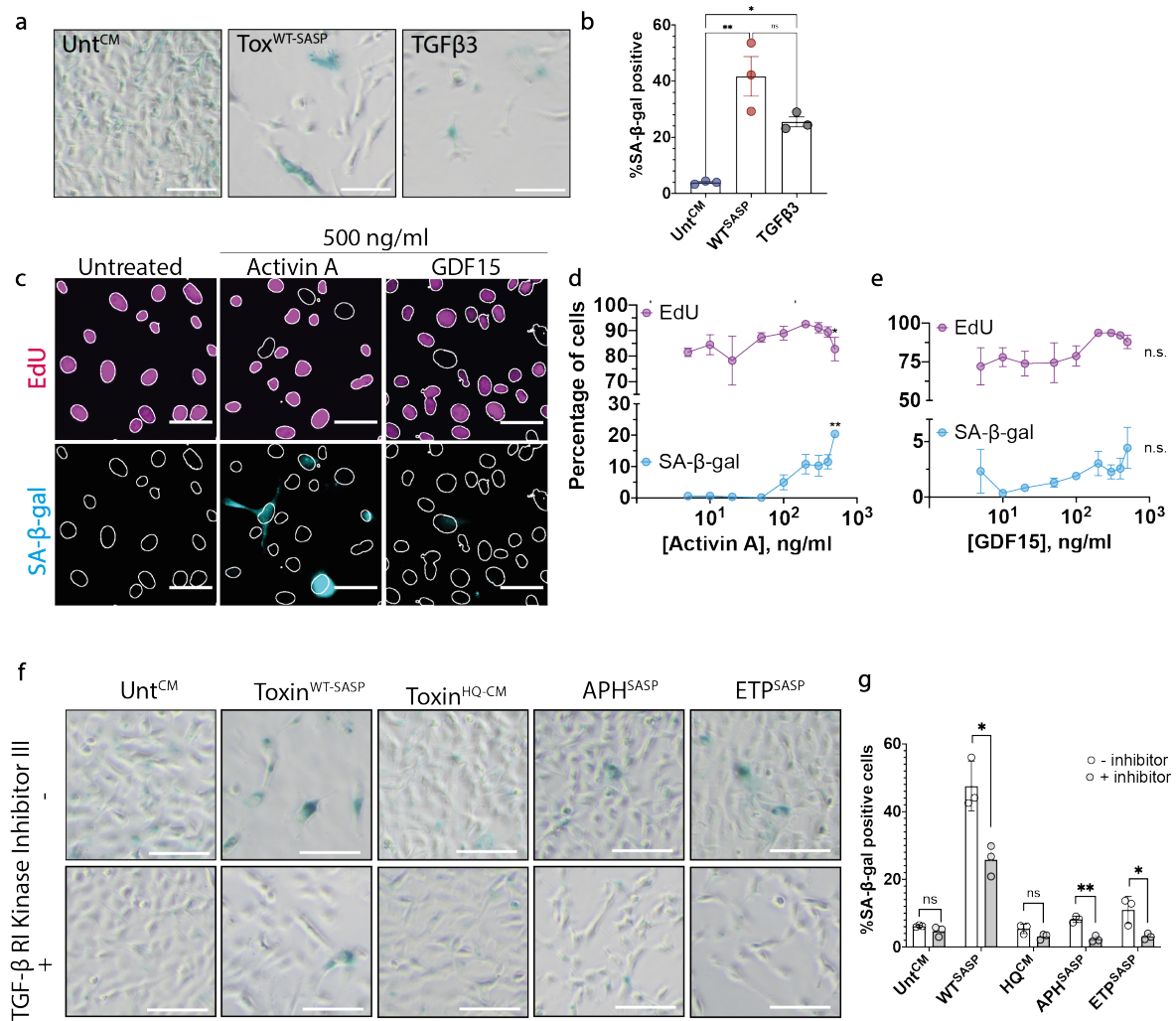
Figure 6.2| Contribution of TGFβ family ligands to senescence. a, Representative images of HT1080 cells assayed for SA-β-gal after 5 days treatment with TGFβ3 (10 ng/ml) compared to toxin[SASP]. **b,** Quantification of a from 3 biological replicates (∼1500-6500 cells/condition per replicate). **c,** Immunofluorescence images of cells treated with high concentrations of Activin A and GDF15 (500 ng/ml) for 5 days before assaying for EdU (magenta) and SA-β-gal (cyan). **d and e,** Quantification of EdU- (magenta line) and SA-β-gal (cyan line) positive nuclei after 5 days incubation with **d,** Activin A and **e,** GDF15 at various concentrations (5, 10, 20 ,50 ,100, 200, 300, 400, 500 ng/ml) and compared to untreated cells using CellProfiler from 3 biological replicates (300-1300 nuclei/condition per replicate). **f,** Representative images and **g,** quantification of cells treated +/- TGFBRI kinase inhibitor (1 μM) and serum-free conditioned media harvested at 48 hrs post-intoxication and supplemented with 10% FBS before assaying for SA-β-gal (3 biological replicates; ∼600-3500 cells/condition per replicate). One-way ANOVA **b,** with Tukey's or **d and e,** Dunnett's multiple comparisons compared to untreated cells, and **g,** Two-way ANOVA with Sidak multiple comparisons test were carried out to test for statistical significance. Error bars denote SEM. Scale bars are **a and f,** 100 μm and **c,** 50 μm.

cells **(Fig.6.2a, 6.2b,** ∼25%) compared to untreated cells, which was concurrent with elevated psmad2 positive nuclei **(Fig.6.1d)**. However, only high concentrations (500 ng/ml) of Activin A led to the up-regulation of SA-β-gal **(Fig.6.2c, 6.2d,** cyan) and cell cycle arrest marked by decreased EdU positive nuclei **(Fig.6.2c, 6.2e,** magenta). Although there were mild observable differences between GDF15-treated and untreated cells, all concentrations used for GDF15 were not sufficient to mirror TGFβ3 **(Fig.6.2c, 6.2e)**.

To examine the significance of TGFβ ligands in transmissible senescence induced by toxin[SASP], in-

hibitor of TGFβ type I Kinase was used at 1µM according to previous studies examining TGFβ-driven senescence[187]. Astonishingly, blocking receptor kinase activity reduced transmissible senescence by all SASPs, and was observed significantly in toxin[WT-SASP] (**Fig.6.2f, 6.2g**). These findings were exemplified by the reduced SA-β-gal positive cells, and increased cell number per field of view (**Fig.6.2f**). Together with the activation of psmad2, and psmad1/5 signaling, evidence suggests that toxin[WT] hijacks the TGFβ signalling pathway to transmit senescence in naive cells.

6.4 The typhoid toxin-induced Activin A causes DNA damage.

TGFβ induces ROS, which contributes to its senescence induction[332,333]. Although the typhoid toxin's CdtB subunit has high DNase homology, research has shown that it acts as a weak nuclease *in vitro*[106]. Therefore, the effect of TGFβ signalling on toxin-induced DNA damage phenotype was examined by knocking down smad2 and INHBA.

To determine the optimal cell density and lipid reagent (Lipofectamine RNAiMax) for efficient knockdown, siRNA against Polo-Like Kinase-1 (PLK1) was used. PLK1 is a protein that regulates cell cycle transition and its decreased expression leads to apoptosis[345]. Lipofectamine was titrated from 1.5 µl, which is the advised volume in a 24-well plate format, to 2.5 µl and applied on cells of various seeding densities with or without siPLK1. All concentrations of lipofectamine with siPLK1 at all cell densities showed high levels of apoptosis compared to the same volume of lipofectamine without siPLK1 (**Fig.6.3a**). Therefore, subsequent experiments used 0.25-0.5 µl of Lipofectamine on 0.5×10^4 cells density to allow for cells to reach 60-70% confluency before toxin treatments.

Next, the role of Activin A during toxin-induced senescence was examined. Immunofluorescence of toxin[WT]-treated cells validated the up-regulation of Activin A intracellularly compared to the negative control toxin[HQ] (**Fig.6.3b-d**). Following a 48h INHBA knockdown, toxin[WT]-treated cells (48h) showed similar levels of Activin A to that observed in the negative control toxin[HQ] (**Fig.6.3c, 6.3d**), 50% knockdown). Astonishingly, siINHBA significantly reduced γH2AX foci induction by toxin[WT] (∼70%) relative to non-targeted siRNA (**Fig.6.3e**). However, a much larger proportion of siINHBA cells were positive for SA-β-gal (**Fig.6.3f**), which was more intense than non-targeted intoxicated cells (**Fig.6.3c**), with no change to nuclear size (**Fig.6.3g**). This could be attributed to the fact that INHBA acts as a subunit in the Inhibin A/Inhibin B heterodimer which antagonises Activin A activity, i.e. homodimer of Inhibin A[325], leading to a more intense SA-β-gal activity (**Fig.6.3c**). Like Activin A (**Fig.6.3c, 6.3d**), intoxication also increased production of pSmad2 (**Fig.6.1c**). Thus, γH2AX foci were examined in cells transfected with siSmad2 (**Fig.6.3h**). The increase in pSmad2 following intoxication (**Fig.6.1c, 6.1d**) was reduced by siSmad2 (**Fig.6.3h, 6.3i**, 40% knockdown) to the levels observed for negative controls (**Fig.6.1c, 6.1d**). Remarkably, relative to the siNT negative control, siSmad2 led to significant halving of γH2AX foci by the toxin[WT] (**Fig.6.3j**) but this had no
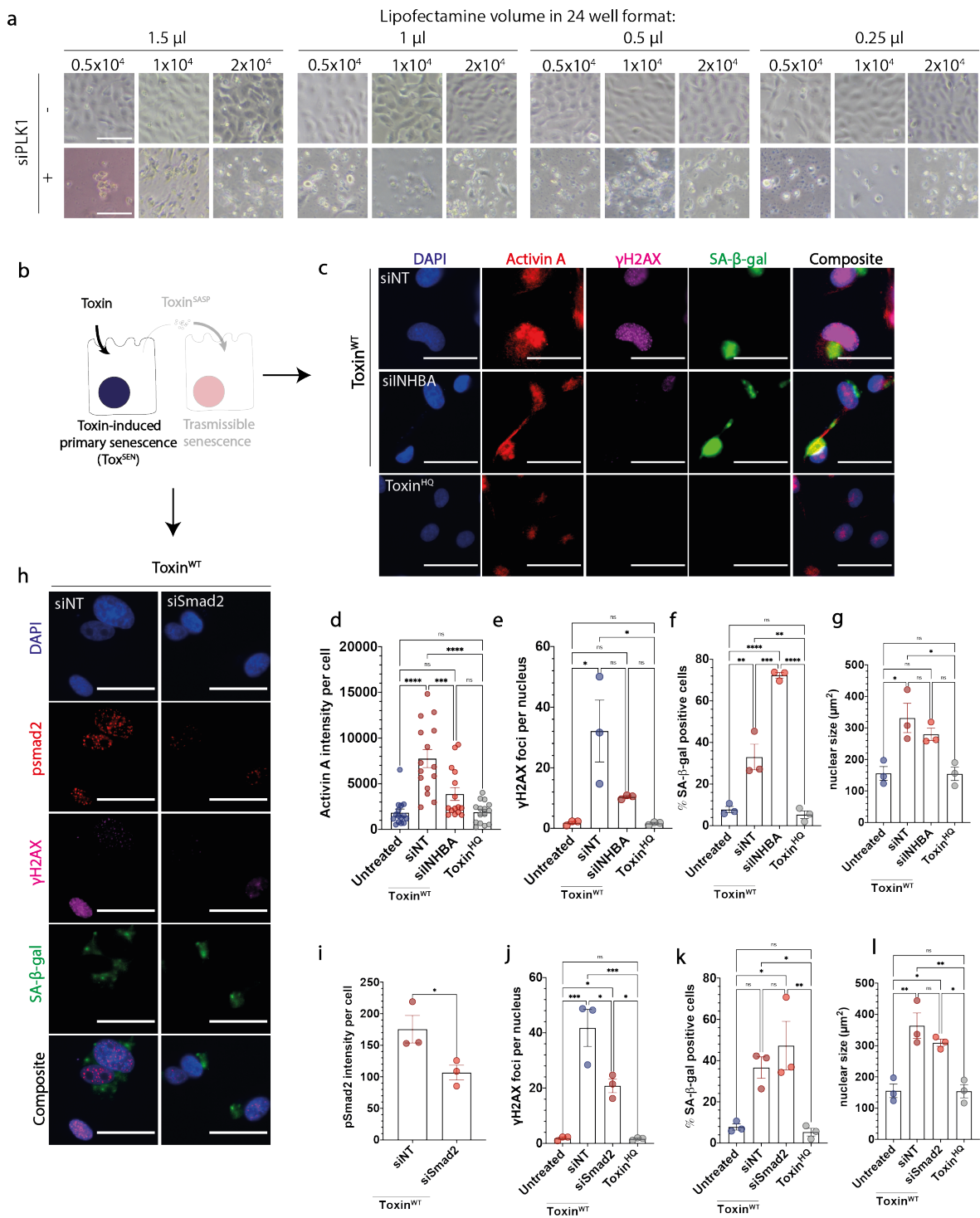
Figure 6.3| Influence of TGFβ signalling on DNA damage and senescence. a, Optimisation experiment to develop a functioning protocol for Lipofectamine RNAiMAX as a lipid reagent to deliver siRNA. Viability of HT1080 cells was examined using light microscopy after 48 h PLK1 knockdown to assay for knockdown efficiency at different cell densities and Lipofectamine RNAiMAX volumes in a 24-well format. **b-i,** Representative images and quantification of intoxicated HT1080 cells that were assayed for DNA damage (magenta) and SA-β-gal (green) after knocking down **c-g,** Activin A (red) and h-l, psmad2 (red). Quantification was carried out using CellProfiler and included d, Activin A intensity, **e,** number of γH2AX foci per nucleus, **f,** percentage of SA-β-gal positive cells and **g,** nuclear sizes after knockdown of INHBA (3 biological replicates, ∼30-500 nuclei/condition per replicate). Quantification also included **i,** psmad2 intensity per cell (circles represent fields of view), **e,** number of γH2AX foci per nucleus, **f,** percentage of SA-β-gal positive cells and g, nuclear sizes after knockdown of psmad2 (3 biological replicates, ∼50-500 nuclei/condition per replicate). NT=non-targeting. **e-l,** One-way ANOVA with Tukey's multiple comparison test and **i,** unpaired t-test, were carried out to test for statistical significance. Error bars denote SEM. Scale bars are **a,** 100 µm and **c and h,** 50 µm.

effect on the proportion of SA-β-gal positive cells (**Fig.6.3k**) or nuclear size (**Fig.6.3l**).

This data potentially uncouples toxin-induced DNA damage responses from toxin-induced senescence.

6.5 Wnt5a contributes to toxin-induced transmissible senescence

Mass spectrometry analysis showed that Wnt5a was specifically up-regulated in toxin[SASP], but not in the secretomes of positive and negative controls (**Chapter 5**). Several studies have shown that TGFβ signalling led to up-regulation of Wnt5a[346,347]. Wnt5a is a pro-survival secreted protein[348] that belongs to the Wingless protein family (Wnt) and mainly activates the non-canonical Wnt signalling pathway[349]. It is increasingly apparent that TGFβ and Wnt proteins work collaboratively to establish multiple disease states such as cancer progression and fibrosis[324,347,350,351,352].

To confirm that Wnt5a is induced in other non-cancer cell lines in a toxin-specific manner, intoxication experiments were performed in IMR90 cells, which have also demonstrated a strong transmissible senescence phenotype (**Chapter 3, Fig.3.9**). Western blot of whole IMR90 lysates confirmed that Wnt5a was up-regulated in toxin[WT]-treated, but not by other senescence inducers or the negative controls (**Fig.6.4a, 6.4b**), which confirmed that it is not cell-line specific. This was further consolidated by immunofluorescence of Wnt5a/b in HT1080s, which showed an increased expression in toxin[WT] but not toxin[HQ] treated cells (**Fig.6.4c**).

Wnt ligands were previously shown to induce senescence stress responses[187,353,354,355]. Indeed, augmenting concentrations of the Wnt signalling agonist CID11210285 from 0.1 nM to 100 nM, increased SA-β-gal positive cells in a dose-dependent manner at 48h (**Fig.6.4d-e**). To examine the relevance of Wnt5a specifically, recombinant Wnt5a was applied on cells at increasing concentrations, as well. Similarly to CID11210285, Wnt5a induced up-regulation of SA-β-gal at varied concentrations (**Fig.6.4f, 6.4g**), albeit to a lesser extent than the agonist, and showed maximal effect at 500 ng/ml (**Fig.6.4g**, ∼30-40%). To test whether Wnt is involved in toxin-induced transmissible senescence mediated by the toxin, inhibitor of Wnt production (IWP-2) was incubated with toxin[WT-SASP]. IWP-2 acts on Porcupine, a membrane-bound acyltransferase that palmitoylates Wnt allowing for its secretion[356]. However, IWP-2 did not cause any observable change to EdU incorporation (**Fig.6.4h, 6.4i**; magenta) or SA-β-gal (**Fig.6.4h, 6.4j**, cyan) in intoxicated cells at 48h.

As IWP-2 is a generic Wnt inhibitor and does not isolate the effects of Wnt5a, siRNA of Wnt5a was examined for toxin-induced DNA damage, senescence and SASP (**Fig.6.5a**). In intoxicated cells, Wnt5a expression was observed following siNT but this was markedly reduced in siWnt5a cells (**Fig.6.5b, 6.5c**, 84% knockdown). Similar to Activin A, siWnt5a reduced toxin-induced γH2AX foci by 70% relative to siNT cells, which was still statistically more significant than the untreated
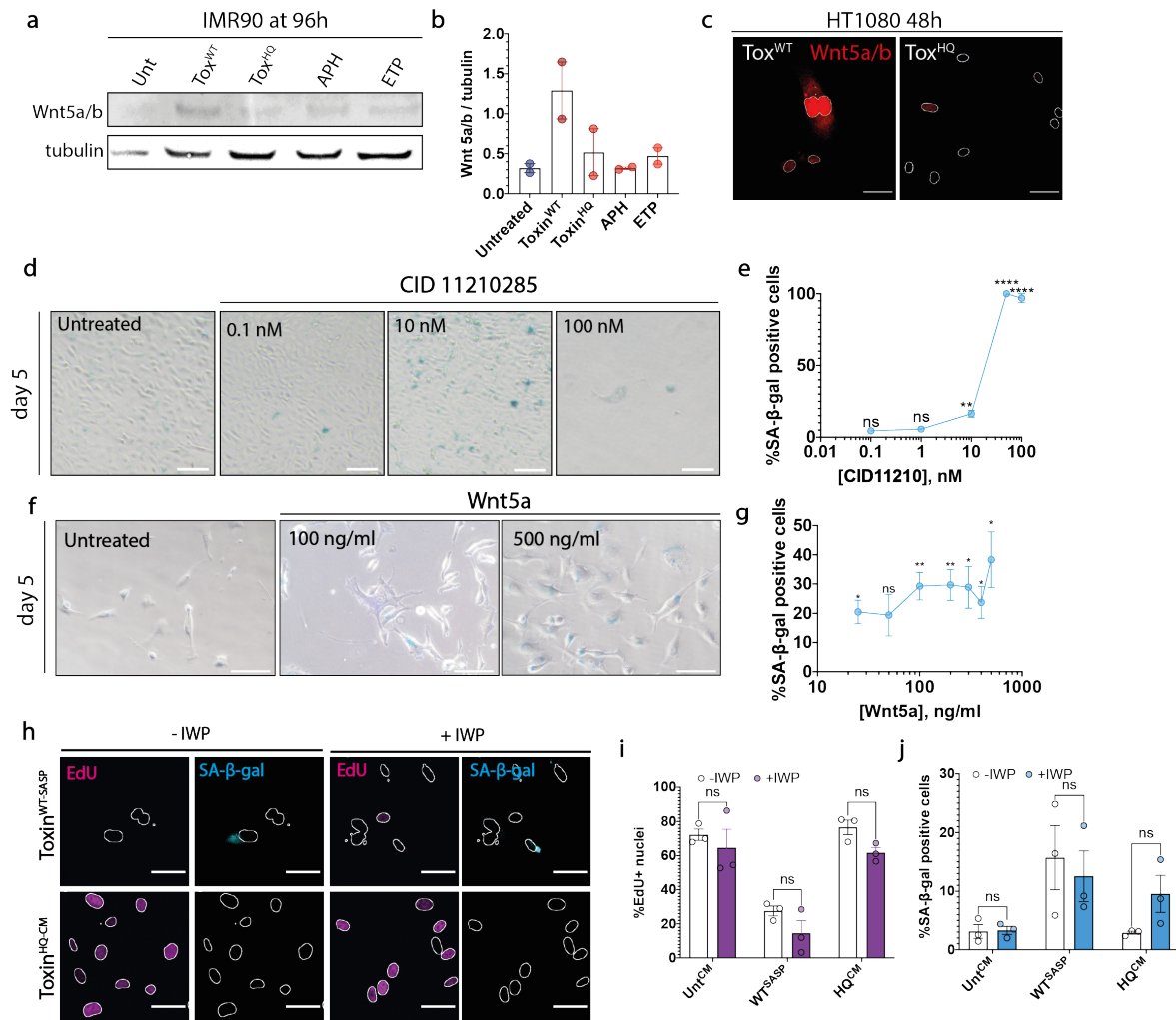
Figure 6.4| Contribution of Wnt signalling to senescence. a, Western blot of IMR90s whole-cell lysates 96h post-treatment. **b,** Quantification of Wnt5a/b intensity relative to tubulin from two biological replicates using ImageStudio Lite. **c,** Immunofluorescence image of Wnt5a/b in intoxicated HT1080 cells at 48h. **d,** Representative images of HT1080 cells assayed for SA-β-gal after 5 days treatment with Wnt agonist, CID11210 at different concentrations (0.1, 1, 10, 50, 100 nM), and **e,** its quantification from 3 biological replicates (∼5-3000 cells/condition per replicate). **f,** Representative images of HT1080 cells assayed for SA-β-gal after 5 days treatment with Wnt5a at different concentrations (25, 50, 100, 200, 300, 400, 500 ng/ml) and **g,** its quantification from one biological replicate (∼300-500 cells/condition). **h,** EdU (magenta) and SA-β-gal (cyan) in naive HT1080 cells treated for 5 days with conditioned complete media harvested from intoxicated HT1080 cells at incubated with 2 µM of inhibitor of Wnt production (IWP2) at 48h. **i and j,** Percentage of **i,** EdU- and **j,** SA-β-gal positive cells +/-IWP2 from 3 biological replicates (∼60-350 nuclei/condition per replicate). **e and g,** One way ANOVA with Dunnett's multiple comparisons test compared to untreated and **i and j,** Two-way ANOVA Sidak multiple comparison tests were used to test for statistical significance. Error bars denote SEM. Scale bars are **c and h**, 50 µm and **d and f,** 100 µm.

and toxin$^{\text{HQ}}$ negative controls **(Fig.6.5d)**. Although this was consistent with previous reports of Wnt5a inducing ROS[357], other research groups demonstrated that Wnt5a inhibits ROS in a context-dependent manner[358]. Equally, no major difference to percentage of SA-β-gal positive cells **(Fig.6.5e)** or intoxicated nuclear size **(Fig.6.5f)** were observed. The reduction in DNA damage by the toxin was also confirmed using western blot of HT1080 lysates at 48h **(Fig.6.5g)**. Interestingly, Wnt5a knockdown halved the transmissible senescence induced by tox$^{\text{SASP}}$ **(Fig.6.5h-j)**, which provided evidence of Wnt5a contribution to toxin-induced senescence phenotypes.
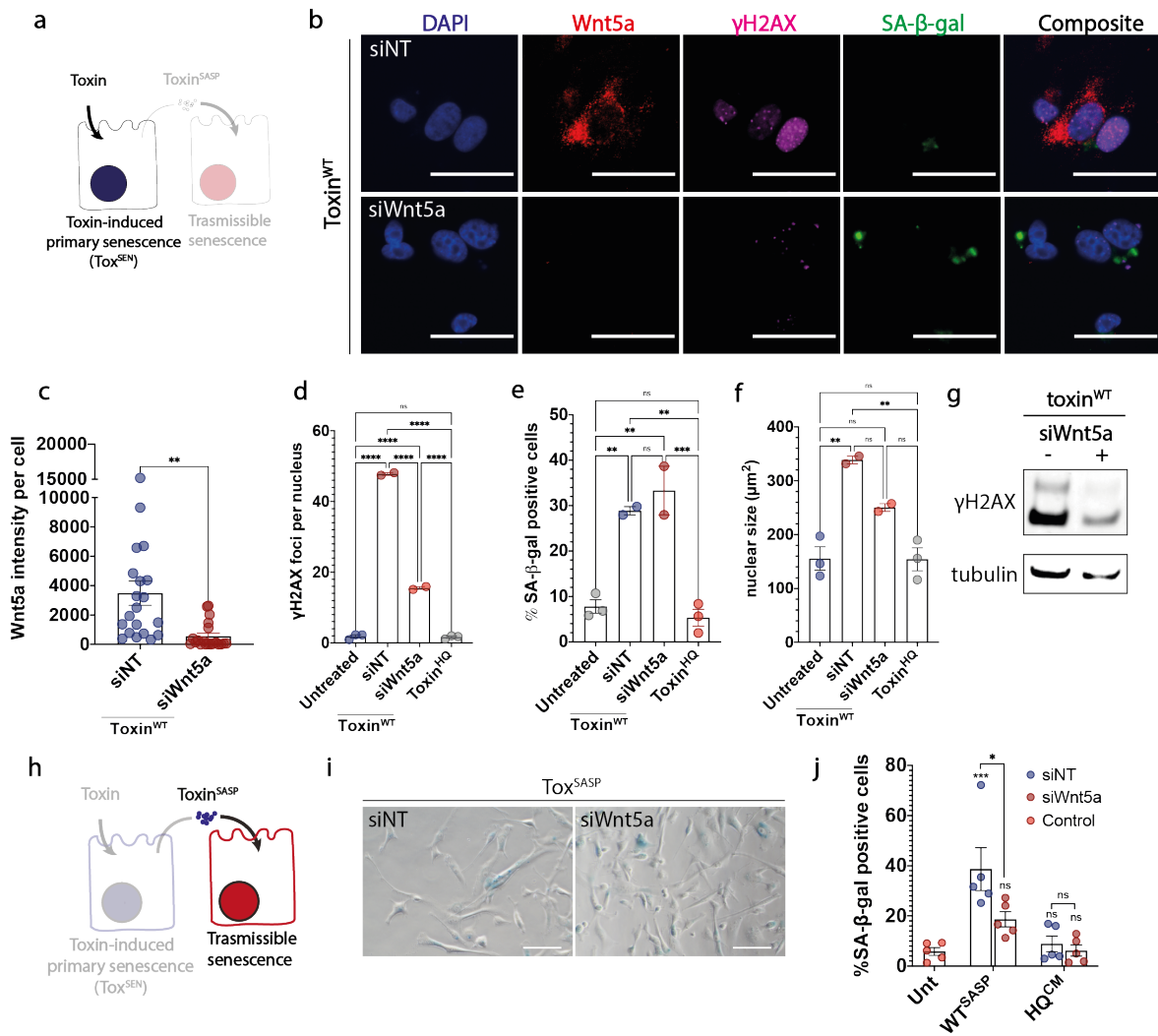
Figure 6.5| Influence of Wnt5a on DNA damage and senescence. a-f, Representative images and quantification of intoxicated HT1080 cells that were assayed for DNA damage (magenta) and SA-β-gal (green) after knocking down Wnt5a (red). **c-f,** Quantification was carried out using CellProfiler and included **c,** Wnt5a intensity (each circle represents a field of view), **d,** number of γH2AX foci per nucleus, **e,** percentage of SA-β-gal positive cells and **f,** nuclear sizes after knockdown of Wnt5a (2 biological replicates, ∼90-140 nuclei/condition per replicate). **g,** Western blot with anti-γH2AX of whole-cell lysates knocked down of Wnt5a 48 hours post intoxication. **h-j,** Transmissible senescence induced in naive HT1080s by complete conditioned media harvested Wnt5a knocked down at 48 h. NT=non-targeting. **j,** Quantification of **i** from 5 biological replicates (∼800-2000 cells/condition per replicate). **c,** Unpaired t-test, and **d-f,** and **j,** One-way ANOVA with Tukey's multiple comparison test were carried out to test for statistical significance. Asterisks denote significance compared to untreated unless otherwise indicated by brackets. Error bars denote SEM. Scale bars are **b,** 50 µm and **i,** 100 µm.

In summary, Smad2, Activin A and Wnt5a facilitate toxin-induced DDRs but despite this they did not influence primary senescence in toxin-treated cells (tox$^{\text{SEN}}$). Nevertheless, Wnt5a promotes toxin-induced transmissible senescence in naive cells, which validates its role in tox$^{\text{SASP}}$.

6.6   Activin A and Wnt5a in combination phenocopy tox$^{\text{SASP}}$

Several studies show that TGFβ and Wnt signalling pathways work synergistically to cause disease[319,324,347,350,351,352]. To test their synergy in transmissible senescence, tox$^{\text{HQ-CM}}$ was supple-
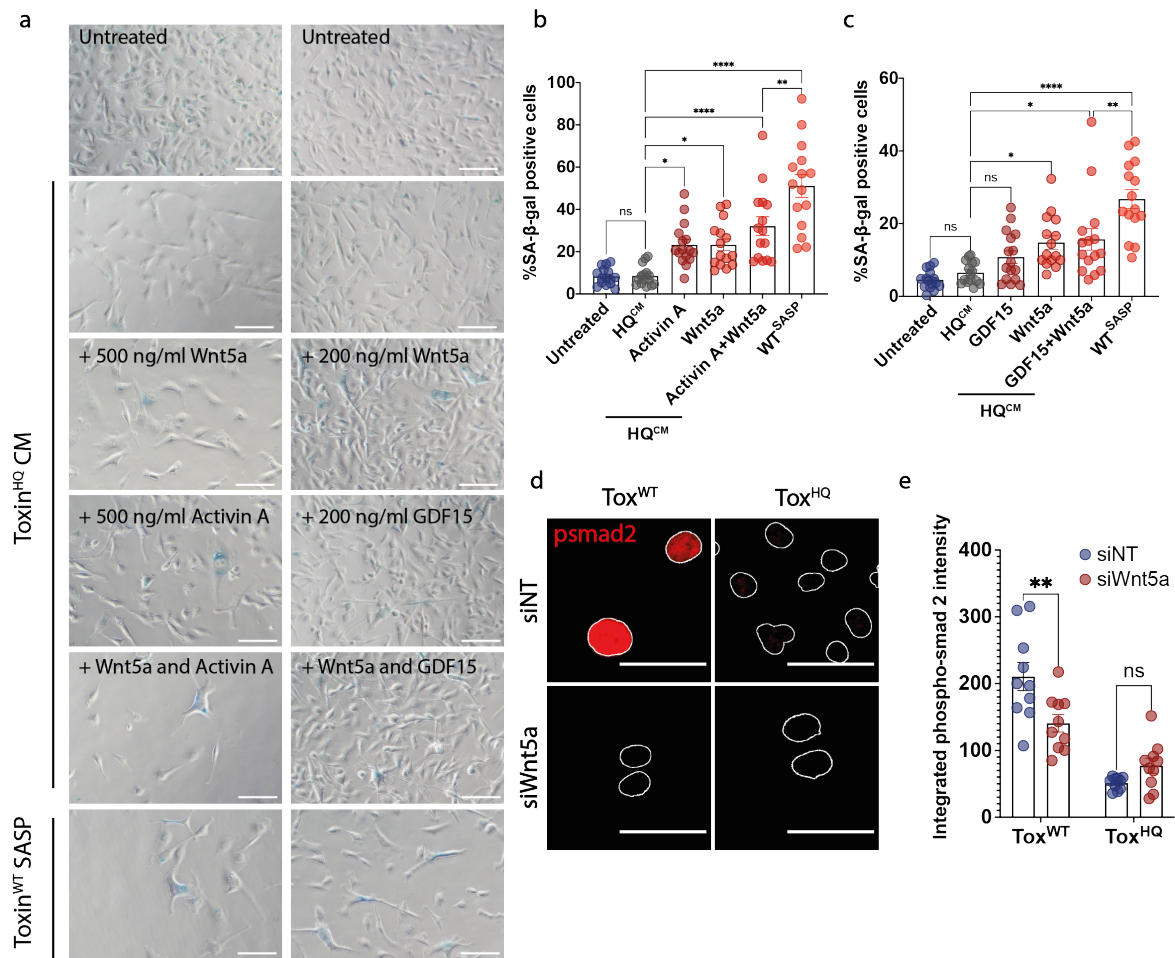
Figure 6.6| Potential cross-talk between Wnt5a and TGFβ signalling pathways. a, Transmissible senescence induced by tox[HQ-CM] supplemented with Activin A, or GDF15 with or without the equivalent concentration of Wnt5a in HT1080 cells. **b and c,** Quantification of **b,** Wnt5a and Activin (500 ng/ml) and **c,** Wnt5a and GDF15 (200 ng/ml). Each circle represents a field of view (**b,** 250-1400 cells **c,** 750-2200 cells /condition per replicates). **d,** Immunofluorescence of psmad2 signaling (red) in Wnt5a knocked-down intoxicated cells. NT=non-targeting. **e,** Quantification of d from 1 biological replicate. Each circle represents a field of view (2 technical replicates, ∼50-220 cells/condition). **b and c,** One-way ANOVA with Tukey's multiple comparisons test and **e,** two-way ANOVA with Sidak multiple comparsions test were used to test for significance. Error bars denote SEM. Scale bars are **a,** 100 µm and **d,** 50 µm.

mented with either Activin A, Wnt5a, or in combination. Consistent with previous data **(Fig.6.2c-d, 6.4f-g)**, each of Activin A and Wnt5a enabled transmissible senescence by tox[HQ-CM] **(Fig.6.6a, 6.6b,** ∼20%**)**. Interestingly, tox[HQ-CM] supplemented with both Activin A and Wnt5a had an additive effect and pheno-copied tox[SASP] with significant transmissible senescence **(Fig.6.6a, 6.6b)**. Nevertheless, SA-β-gal positive cells were more abundant when treated with tox[SASP] and there were observable cell cycle arrest and distension **(Fig.6.6a)**. This suggests additional factors in tox[SASP] play a role. Thus, synergy between GDF15 and Wnt5a was also examined. However, tox[HQ-CM] supplemented with GDF15, was not enough to cause senescence on its own **(Fig.6.6a, 6.6c)**. Although in combination with Wnt5a, there was more induction of senescence, the number of senescent cells did not increase beyond that observed for Wnt5a alone **(Fig.6.6c)**.

TGFβ ligands can mediate their effects through smad-driven signalling[187,322]. To test whether

the synergy between Activin A and Wnt5a centres on smad signalling, Wnt5a was knocked down and psmad2 examined **(Fig.6.6d)**. Wnt5a knockdown led to the reduction of nuclear psmad2, **(Fig.6.6e,** 34% reduction**)**, which was consistent with Borcherding et al 2015[352]. This suggests that Activin A and Wnt5a cooperate to augment smad-driven signalling induced by toxin[WT].

6.7 Effect of Wnt5a, Activin A, and GDF15 on *Salmonella* invasion and replication.

Ibler et al (2019) described that tox[SASP] enhanced *Salmonella* infection of mouse embryonic fibroblast (MEF) cells relative to APH in complete media[106]. However, drivers of the enhanced invasion remain unexplored.

As HT1080 cells have mutated Ras activation[359], they continuously undergo high basal levels of membrane ruffling. Therefore, an experimental protocol was established to examine the rate of *Salmonella* invasion in NIH/3T3 cells, which are mouse embryonic fibroblasts **(Fig.6.7a)**. To assay *Salmonella* invasion, serum-starved cells are infected in the absence of antibiotics for 30min before aspiration of extracellular bacteria then cell incubation with gentamicin, which kills any extracellular *Salmonella*. After 2h, whole-cell lysates are cultured on agar plates and *Salmonella* colony forming units are quantified.

To begin with, serum-starved cells were primed for 1h with conditioned media before infecting with *Salmonella*. Toxin[WT-SASP] showed a subtle but significant increase in invasion compared to unt[CM], whilst tox[HQ-CM] and APH[SASP] showed no significant change **(Fig.6.7b, 6.7c)**. Interestingly, unlike APH[SASP], ETP[SASP] showed an increase in *Salmonella* colony forming units (CFUs) **(Fig.6.7b)**.

Next, to further remodel the target cells prior to infection, cell incubation with conditioned media was extended from 1h to 24h. Whilst toxin[WT-SASP], tox[HQ-CM], and ETP[SASP] showed an increased invasion compared to short incubation (1h) with conditioned media, APH[SASP] showed decreased invasion rates **(Fig.6.7d)**, showing diverse cell remodelling abilities of the different SASPs within an infection niche.

To examine the effects of SASP components on *Salmonella* invasion, tox[HQ-CM] was supplemented with recombinant Activin A, GDF15 or Wnt5a for 1h prior to infection. Although previous experiments showed that Activin A, but not GDF15, and Wnt5a work collaboratively to induce transmissible senescence, invasion rates were increased when tox[HQ-CM] was supplemented with Wnt5a or GDF15 but not Activin A **(Fig.6.7e)**. Supplementing tox[HQ-CM] with both Wnt5a and Activin A, increased invasion to levels similar to Wnt5a alone. To validate the role of Wnt5a, neutralising antibodies were added to tox[SASP] before assaying invasion. If tox[SASP] enhances invasion via these factors, then the antibodies would decrease invasion rates. Curiously, anti-Wnt5a and anti-Activin A led to increased invasion **(Fig.6.7f)**. Similar findings were made when Wnt5a and Activin A were knocked down
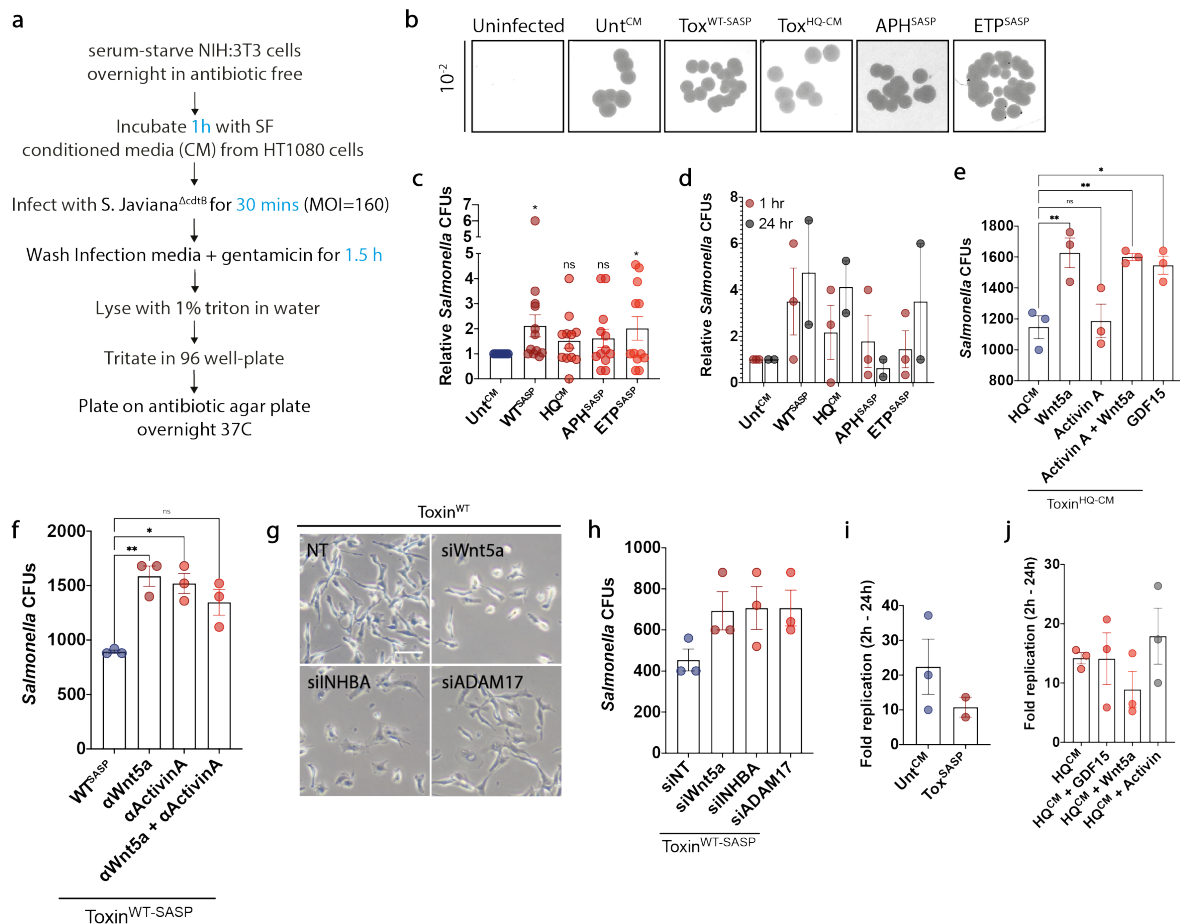
Figure 6.7| Effect of Wnt5a and TGFβ ligands on *Salmonella* invasion. a, Experimental protocol for assaying *Salmonella* invasion. All experiments were carried out with 1h incubation with conditioned media prior to infection unless otherwise stated. **b,** Representative pictures of *Salmonella* colony forming units (CFUs) on agar plates after a 2 hr infection from 5 µl of a 10-2 dilution. **c,** Quantification of b depicting *Salmonella* CFUs relative to cells treated with unt^{CM} (3 biological replicates). **d,** *Salmonella* CFUs that invaded naive 3T3 cells with 1h or 24h pretreatment with conditioned media prior to infections (1 biological replicate). **e,** *Salmonella* CFUs in 3T3 cells pretreated with tox^{HQ-CM} supplemented with Wnt5a (500 ng/ml), Activin A (500 ng/ml), both, or GDF15 (200 ng/ml) for 1h prior to infection (1 biological replicate). **f,** *Salmonella* CFUs after treating conditioned media with neutralising antibodies 1:500 for 1 hour prior to applying them on 3T3 cells and carrying out the invasion protocol (1 biological replicate). **g,** Morphology of intoxicated cells at 48 h in serum-free media after 48 hour knockdown of Wnt5a, INHBA, and ADAM17 in complete media. Scale bar is 100 µM. **h,** Invasion assay with 3T3 cells pretreated with conditioned media for 1h from Wnt5a, INHBA, and ADAM17 knocked down cells before infection (1 biological replicate). **i and j,** Fold change of *Salmonella* replication at 24h relative to 2h *Salmonella* infection post treatment with indicated conditioned media. (1 biological replicate). **c-f and h-j,** Each circle represents technical replicates. **c,** Unpaired t-test compared to unt^{CM} cells and **e and g** one-way ANOVA with Tukey's multiple comparisons test were used to test for statistical significance. All other graphs showed no statistical significance. Error bars denote SEM.

(**Fig.6.7**h). Interestingly, the conflicting observations for Wnt5a was previously reviewed[360], where both Wnt5a knockout mice and treatment with recombinant Wnt5a show heightened responses to β-catenin[361]. While purified Wnt5a retains the ability to activate or repress canonical Wnt signalling by competing with Wnt3a, knocking down Wnt5a also leads to heightened sensitivity to Wnt3a[362].

As stated in **Chapter 5**, the tox^{SASP} constituent ADAM17 is a sheddase that liberates growth factors from the cell surface and represents an important regulator of TGFβ[301] and other growth

factors involved in membrane ruffling[302]. To examine whether a disruption in TGFβ modulation would impact on infection, ADAM17 was knocked-down **(Fig.6.7g-h)**. Consistent with Activin A knockdown, conditioned media from siADAM17 intoxicated cells also increased invasion **(Fig.6.7g-h)**.

Next, *Salmonella* intracellular replication was examined after 1h incubation with conditioned media supplemented with the different ligands by examining intracellular *Salmonella* following a 24h infection relative to a 2h infection. The most striking observation was that cells subjected to tox[SASP] limited *Salmonella* replication **(Fig.6.7i)**. Interestingly, tox[HQ-CM] supplemented with Wnt5a also limited *Salmonella* intracellular replication, but not GDF15 or Activin A, indicating that Wnt5a might restrict *Salmonella* replication **(Fig.6.7j)**. It is also worth noting that the cell morphology of siWnt5a intoxicated cells showed a more round-up appearance, which is indicative of either defected adhesion, or cellular death **(Fig.6.7g)**.

6.8   Discussion

Salmonella subversion of the human secretome presents a novel, unexplored area of research. This chapter examined a few up-regulated proteins implicated in TGFβ in the toxin-induced secretome identified by mass spectrometry in **Chapter 5**. Consistent with previous findings[187], inhibiting TGFβ receptor ameliorated transmission of senescence. Data suggest that Activin A and Wnt5a work separately and in combination to enhance senescence-phenotypes. Evidently, both ligands induce DNA damage, potentially via ROS, in directly intoxicated cells. This matches previous reports[332,333,357] that SASP proteins induce DNA damage in bystander cells. These observations present a novel method of toxin-induced DNA damage, by which it subverts the host secretome to indirectly consolidate the DNA damage. Not only do TGFβ ligands release ROS from mitochondria, they also suppress antioxidants allowing for ROS accumulation[363]. Although the majority of research implicated Wnt5a in inhibiting ROS production, knocking down Wnt5a in intoxicated cells showed decreased DNA damage foci. This could be due to the fact that TGFβ genes are also targets of the Wnt5a pathway, which was observed in colonic crypts[305]. The notion of indirect DNA damage mandates examining ROS generation in intoxicated cells via fluorescent probes such as dihydroethidium (cellular) and mitoSOX (mitochondrial)[364].

Data presented in this chapter, showed that even though Activin A induced senescence, it did not necessarily enhance invasion. In contrast, GDF15 was shown to drive *Salmonella* invasion regardless of its ability to induce senescence. As previously mentioned, reports provide evidence that TGFβ ligands regulate membrane ruffling by activating Ras, RhoA, Rac and Cdc4[343,342] in smad-independent pathways such as MAPK, JNK, ERK and p38 pathways as well[338,339,341,340]. Additionally, Wnt5a was also observed to modulate the actin cytoskeleton in stem cells[365]. Interestingly, my results showed that too much Wnt5a (applying purified protein), or too little Wnt5a (knockdown) enhanced invasion. As *Salmonella* uptake is an actin-dependent process[366], it seems that the typhoid toxin might exploit

Wnt5a secretion levels to influence actin-mediated membrane ruffling and hence modulate bacterial burden to promote host survival, and bacterial persistence. Therefore, it would be interesting to visualise how my proteins of interest affect membrane ruffling and actin cytoskeleton assembly via immunofluorescence.

Preliminary experiments explored the effect of ALK2,4,5,7 receptors knockdown individually or knockdown of all receptors on *Salmonella* invasion (data not shown). When tox$^{\text{WT-SASP}}$ was applied on ALK-receptor deficient cells, invasion was ameliorated in ALK2 and ALK7 knockdown cells, and invasion was halved when all receptors were partially knocked down (data not shown). There was no change to invasion rate with tox$^{\text{HQ-CM}}$-treated cells. This gave preliminary insight into a potential mechanism by which *Salmonella* manipulates the host. However, it is worth noting that a knockdown control confirming RNAi targeting was not carried out, but is still required to corroborate the observations.

As it currently stands, there is no direct link between transmitting senescence to naive cells and enhancement of invasion. It appears that Wnt5a (a toxin-specific protein) and GDF15 (senescence-specific protein) would bring about both toxin$^{\text{WT}}$ phenotypes independently. Many of the invasion experiments are preliminary and require more biological replicates. Investigating toxin$^{\text{WT}}$ senescence phenotypes are yet to be explored in GDF15 knockdown cells.

TGFβ ligands are important immuno-modulators[367]. For instance, Activin A is produced by immune cells such as macrophages and regulates both inflammatory and anti-inflammatory responses depending on context[368]. Follistatin (a toxin-specific protein, and unexplored in this thesis) has been previously reported as an important regulator of Activin A and can ameliorate inflammatory responses by Activin A[369]. Additionally, GDF15 has been described as macrophage inhibitory cytokine-1[370]. It is involved in suppression of some immune cells via immunosenescence[306], enhances phagocytosis by dendritic cells and involved in tumour immune evasion[371]. It is also a good diagnostic and prognostic in patients with colorectal cancer[372,373]. Similarly, Wnt5a has an emerging role in immunosuppression[374]. It has also been implicated in increased bacterial phagocytosis, and ameliorated bacterial killing by macrophages[312].

The examined SASP components GDF15, Activin A and Wnt5a showed only a modest influence on *Salmonella* invasion, which is consistent with the effect seen with tox$^{\text{WT-SASP}}$ and findings reported in Ibler et al 2019[106]. Given that *Salmonella* invades host cells in the absence of SASP components, it is possible that SASP plays a more significant role in other aspects of *Salmonella* host-pathogen interactions. Indeed, it is interesting to speculate that *Salmonella* could hijack long-lived, death-resistant senescent host cells to facilitate persistent infections.

Part III

Discussion

Chapter 7

Discussion

Senescence could be considered a good servant, but a bad master. Whilst its benefits are evident in development, wound healing and tumour-suppression[182,186], chronic senescence can render the organisms more susceptible to age-related pathologies such as Alzheimer's and cardiovascular diseases, and counterintuitively even cancer[176]. Ageing organisms are more susceptible to infections[224,225], as observed in the recently emerged Coronavirus pandemic (COVID-19)[375]. Similarly, mortality of people >50 years old infected with *Salmonella* Typhi is significantly higher relative to their younger counterparts[376].

In the past decade, the interlink between senescence and infections has attracted the attention of cell biologists, giving rise to the emerging research avenue of senescence and bacterial host-pathogen interactions[213]. Whether pathogens accelerate senescence in local infection niches to establish infection is unclear. My thesis explored the effect of the typhoid toxin of *Salmonella* Typhi on host cell responses implicated in typhoid fever. My thesis highlights three main findings relevant to senescence and the host-pathogen interaction field: i) the typhoid toxin causes premature cellular senescence-like responses via replication stress and persistent γH2AX foci; ii) tox$^{\text{WT-SASP}}$ is divergent from SASP of other acute DNA damage inducers; iii) the typhoid toxin subverts the host's TGFβ signalling pathway to transmit senescence and potentially enhance invasion into naive cells.

7.1 Does the typhoid toxin induce true senescence?

Senescence is a dynamic, multi-step phenomenon that evolves over a long period of time and confers continuous molecular changes over weeks and months. It is generally recognised that cultured cells reach full senescence weeks post-exposure to the inducer, and remain viable for months thereafter[168,377]. As observations reported in this thesis were extended to 96h, it could be argued that key senescence hallmarks such as 'permanent' cell-cycle arrest are yet to be addressed. Durable cell-cycle arrest up to 7-days was observed with typhoid toxin[106] and this thesis revealed additional markers of senescence, e.g. p21 expression, lamin B downregulation, persistent DDRs. Nevertheless, an undefined

stress response that may, or may not later develop into senescence could also explain the phenotypes and so timepoints could be extended in the future to align with senescence studies. This will likely require cell culture experiments modelling chronic infection, which are under development. Even so, the acute senescence responses addressed in this thesis were chosen specifically to investigate their influence on initial decisive host-pathogen interactions, e.g. host cell invasion.

This thesis explored tox$^{\text{WT-SASP}}$ at two time-points (48h and 96h), with few matches to the SASP Atlas[174]. As SASP is dynamic, it develops over time and not all factors are secreted simultaneously[175,189]. Therefore, it would be expected if the typhoid toxin induces 'true' SASP that it would display plasticity as well, which should be examined at diverse timepoints. This would provide insight into the host secretome in chronic toxin-secreting *Salmonella* infections.

7.2   Host secretomes as a target of bacterial pathogens

This thesis reveals that bacterial pathogens employ sophisticated toxins to manipulate the host secretome and reprogram naive bystander cells. This opens up the possibility that pathogens are able to remodel multiple cells within the infection niche from a single infected cell. This virulence strategy may not be unique to SASP and pathogen-induced secretomes likely have broader significance in host-pathogen interactions. For instance, single-cell RNA sequencing revealed that dendritic cells infected with invasive S. Typhimurium (ST313) showed regulation of host secreted proteins that reprogram transcription profiles of bystander cells and result in immune evasion[378]. Whilst the cell fate of these infected cells was unaddressed, a notable gene reported was IL-1β which is a known SASP, but also implicated in inflammasome activation during pyroptosis[378,379,380]. Highlighting the importance of pathogen manipulation of the host secretome is the fact that the non-invasive S. Typhimurium (ST19) counterpart showed a differential secretome which was proposed to account for the distinct disease outcomes, e.g. bacteremia[378].

My thesis provides a new platform of research that can be used to investigate host secretory responses to diverse pathogen-induced cell fates and their influence on infection niches. In particular, this thesis contributed to dissecting a secretome induced by a bacterial toxin, using three different techniques, under a senescence-like stress response.

7.3   Is senescence an efficient hijack target for a bacterial virulence factor?

Taking into consideration that senescence can be host-protective, it is undoubtedly a risky hijack target for bacteria[188,189]. Senescent cells typically secrete inflammatory SASP molecules to recruit immune cells, eliminate pathological cells and protect the host. For instance, SASP-dependent recruitment of cytotoxic T-cells and macrophages eliminates neoplastic tumour formation, prevents tumour

progression and promotes host survival[381,382]. However, due to the heterogeneous nature of SASP which is context-dependent, some factors would be protective, whilst others could promote pathology. Previous literature implicate bacterial-induced pro-inflammatory senescence in tumour progression and establishment of pathology, such as with the case of *E. coli*'s colibactin and *H. ducryei*'s CDT[222,240,383]. Additionally, SASP can transmit senescence to immune cells resulting in an immuno-suppressive phenotype via a process known as immunosenescence[384], which could permit pathogen persistence and survival. We previously published that tox$^{\text{WT-SASP}}$ transmitted senescence, and promoted *Salmonella* infection in naive THP1 macrophages in a CdtB-dependent manner. Tox$^{\text{WT-SASP}}$, and not APH$^{\text{SASP}}$ was able to enhance invasion in bystander cells, which suggested pathogen hijacking of senescence[106]. Therefore, to further our understanding of pathogen subversion of senescence, the DDR was examined and the SASP proteome elucidated by LC-MS/MS.

7.4 The typhoid toxin induces premature ageing *in vitro* and *in vivo*.

In **Chapter 3**, I presented evidence of the typhoid toxin inducing senescence-like phenotypes *in vitro* similar to known chemical inducers of senescence. The toxin induced: i) replication stress marked by RPA exhaustion, ii) persistent DDR markers such as γH2AX and 53BP1 foci; iii) increased p21 expression in intoxicated cells; iv) lamin B1 down-regulation and v) SASP phenotype that transmits senescence and enhances invasion in naive cells[106]. Whilst the concentration of typhoid toxin during infection is unknown, I showed that picogram amounts of toxin were sufficient to induce γH2AX foci, cell cycle arrest and SA-β-gal up-regulation. Additionally, *Salmonella* infections resulted in transmissible senescence in a CdtB-dependent manner, implicating toxin-induced senescence during infections. Despite the ability of LPS to induce DNA damage and senescence[385,386], *Salmonella* lacking CdtB did not induce SASP, which indicates that PAMPs are insufficient for *Salmonella* induction of senescence and would require dedicated virulence factors, in this case - the typhoid toxin.

Intravenous injection of typhoid toxin indicated a role in acute typhoid fever symptoms and lethality[81,97] while mouse infection experiments revealed a role for the toxin in promoting host survival to facilitate chronic *Salmonella* carriage[78]. A common feature of both studies was toxin suppression of immune responses. Thus, it is reasonable to hypothesise that senescence might contribute to the *in vivo* role of the toxin. In concordance with my findings and at the time of writing this thesis, a recently published article presented evidence of typhoid toxin-induced senescence during infection *in vivo*[107] marked by NFκB activation, p16 activation and histological stain of lipofuschin. Despite this senescence phenotype, the typhoid toxin reduced recruitment of inflammatory T-cells and sustained levels of non-inflammatory macrophages, which is consistent with an anti-inflammatory SASP profile reported in **Chapter 5**.

In contrast to findings in animal models, a human infection challenge study conducted in 2019 using

wild-type *Salmonella* Typhi revealed that the typhoid toxin did not underlie acute typhoid fever in humans[100]. In fact, disease manifestation was less severe than the toxin-null mutant, which supports mouse infection studies by indicating a host-protective role played by the toxin. Furthermore, the duration of wild-type bacteraemia was reduced and immune responses of B cells were ameliorated compared to the toxin null mutant, suggesting an immune-repressive role of the toxin. It is important to note that due to ethical considerations and the small number of volunteers, the results are not representative of *S.* Typhi infections in endemic countries, and do not give insight into severe, chronic typhoid fever. All *in vivo* studies, together with my proteomic analysis *in vitro*, show that the typhoid toxin plays an immunosuppressive role which is consistent with the stealth strategy of typhoidal *Salmonella*[78,100,107].

7.5 Immuno-modulatory functions of TGFβ and Wnt5a pathways

In accordance with the human infection challenge results, LC-MS/MS bioinformatic analysis of intoxicated fibroblast HT1080 cells in serum-free media, presented in this thesis, showed the repression of some inflammatory interleukins such as IL-6, and the up-regulation of GDF15, Activin A and Wnt5a implicated in immunosuppression (**Fig.7.1**) . Interestingly, both TGFβ ligands and Wnt signaling pathways have implications in immuno-modulation. For instance, disruption of TGFβ signaling in immune cells such as T cells and dendritic cells resulted in spontaneous colitis in mouse models, and was dysregulated in patients of inflammatory bowel disease[387,388]. Activin A was previously recognised as an immunological cytokine that results in the differentiation of the inflammatory M1 macrophage into the immunosuppressive M2 phenotype[389]. Additionally, GDF15 has also been implicated in immunosenescence, whereby it inhibits macrophages and maturation of dendritic cells resulting in immune evasion[371]. Therefore, the increased invasion in fibroblast cells treated with purified GDF15 could provide a novel insight into a pathogen-subversion mechanism whereby the bacteria are up-taken, but not eliminated by immune cells.

Interestingly, upon inflammatory stimulation via LPS, Wnt5a is anti-inflammatory, blocks differentiation of M1 macrophages, and does not affect M2 macrophages also leading to immunosuppression[390]. Given that Wnt5a, GDF15 and Activin A are all up-regulated in a toxin-dependent manner, and confer immunomodulatory functions, proposes an intriguing question whether indeed these factors are essential for the typhoid toxin phenotypes *in vivo*.

This thesis presented evidence that the typhoid toxin induces transmissible senescence partially via Activin A and Wnt5a, which was ameliorated via their knockdown and chemical inhibition. The fact that Activin A enhanced transmissible senescence and GDF15 enhanced invasion uncouples transmissible senescence from *Salmonella* invasion and implicates a complex cooperative network of TGFβ ligands that mediate a pathogen-hijack mechanism via SASP. On the contrary, Wnt5a, which is a
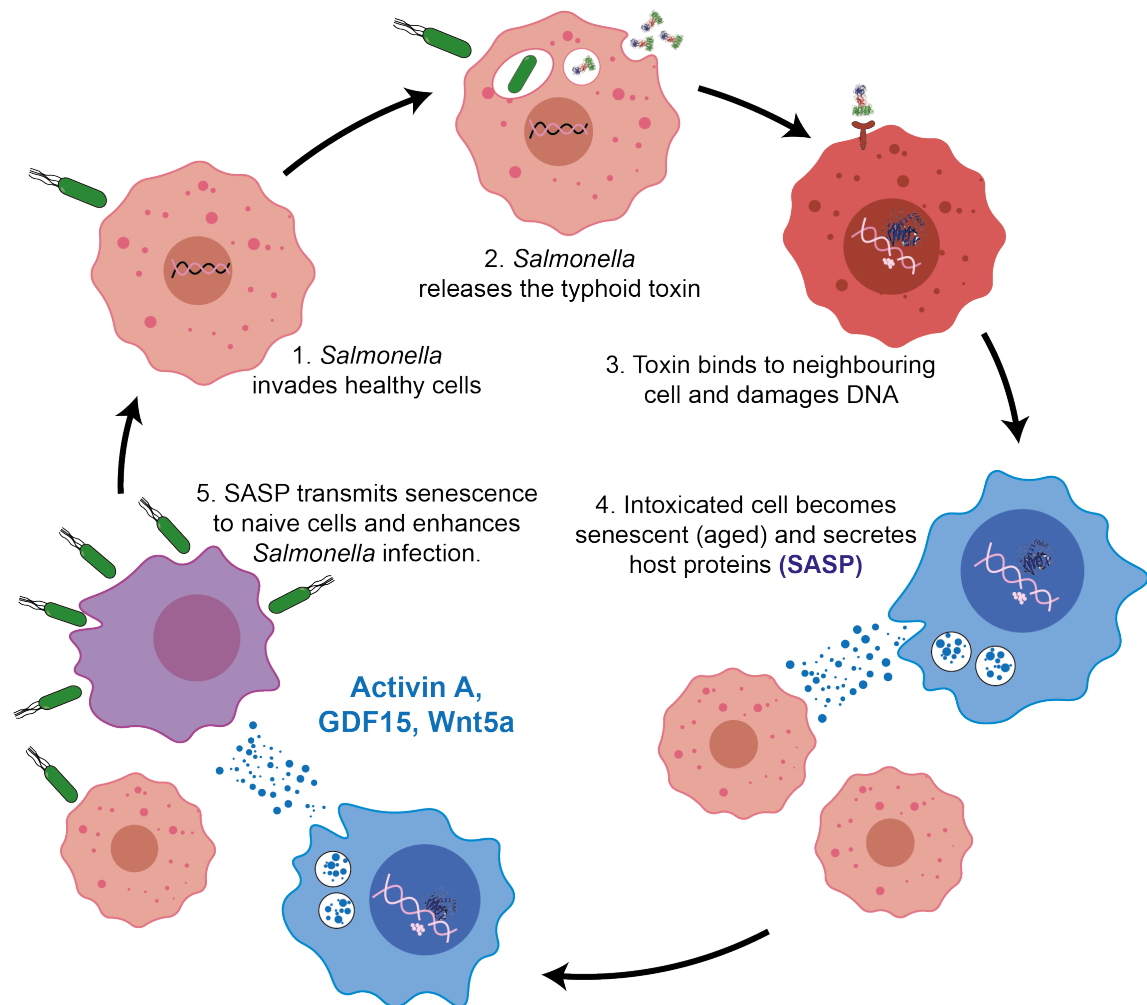
Figure 7.1|Proposed mechanism of disease that would aid in transmission of senescence, enhanced invasion and potential chronic carriage of *Salmonella*. The role of these secreted SASP have been implicated in immuno-modulation and therefore are important to examine in *Salmonella* infections

toxin-specific secreted protein, might confer host protection as well. The debilitated cellular state in intoxicated cells and enhanced invasion in naive cells in Wnt5a knockdown cells implicates it in a potential pro-host survival mechanism. However, the opposing effect on invasion observed when cells were treated with purified Wnt5a indicate that it might be controlled in a more complex mechanism whether temporally, by concentration, or downstream signalling, which were unexplored in this thesis. These results show that senescence as a pathogen hijack target is not black and white, and constitute an interplay between host-protection and pathogen-hijack mechanisms in one context.

7.6   Future directions

This thesis has opened many research questions that would need to be addressed to enhance our understanding of the typhoid toxin and the establishment of invasive *Salmonella* infections.

Examining SASPs *in vivo*. This thesis used HT1080s, a fibrosarcoma cell-line, to characterise the SASP constituents and their role during invasion. It would be important to establish core SASPs

induced by the typhoid toxin in other non-carcinogenic primary cell lines including bone marrow derived macrophages, and the colonic epithelial HIEC-6 cells. More complex systems, such as organoids of primary gut epithelial cells, could also be used to simulate a more physiologically relevant environment for examining SASP and *Salmonella* invasion. More importantly, the identified putative proteins of interest should be examined *in vivo* in animal models upon toxigenic *Salmonella* infection. Previous work showed that SASP of mice *in vivo* was different from SASP of mouse cultured cells[391]. Given that a human infection challenge model with *S.* Typhi was carried out[100], LC-MS/MS could be carried out on the volunteers plasma to examine biomarkers of senescence, and then comparatively analysed to the proteomics data in this thesis.

Alternative role of toxin^WT-SASP in persistence and chronic carriage. *Salmonella* was previously shown to target aged cells *in vivo* and *in vitro*[227]. Following these findings, Ibler et al 2019 showed that the typhoid toxin hijacks senescence to induce premature ageing in bystander cells via SASP to promote infection[106]. However, although my data shows an increase in invasion due to identified SASP factors via Wnt5a and GDF15, the change was modest. Therefore, it is possible to assume a different function to toxin-induced senescence and SASP. Whilst tox^WT-SASP could be modulating the actin cytoskeleton, SASP is better studied for its anti-apoptotic properties.

Persistence and chronic carriage of *S.* Typhi were attributed to the CdtB subunit of the typhoid toxin[78]. To allow for *Salmonella* persistence, host cells are required to survive. Hence, it could be hypothesised that tox^WT-SASP propagate anti-apoptotic signals to bystander cells, prolonging host cell survival and as a result allows for *Salmonella* persistence. Thus, it would be interesting to examine whether *Salmonella* persistence is facilitated by intracellular survival within cell death-resistant senescent host cells. .

Effect of toxin^WT-SASP on *Salmonella* replication. The emergence of a prevalent antibiotic resistant strain is what makes *Salmonella* an important issue to tackle[42]. Whilst antibiotics are usually the go-to treatments, sometimes they are unable to eliminate all *Salmonella* leading to persistence and chronic carriage observed in typhoid patients. Experiments *in vivo* showed that the rate of *Salmonella* replication determines survival or mortality of the bacteria upon antibiotic treatments. Antimicrobial therapy had the biggest impact on fast growing bacteria[392]. Slow growing bacteria with low metabolic activity can evade antibiotics and survived best, with limited impact on disease, but the moderate growing bacteria survived and dominated the antimicrobial resistance[392]. Whilst this project examined *Salmonella* invasion into host cells, a preliminary experiment showed tox^WT-SASP might ameliorate the rate of *Salmonella* replication. Therefore it is essential to explore whether increased invasion is also accompanied by slower growing bacteria, which might influence chronic carriage and antimicrobial resistant typhoid.

Senolytics as a therapeutic approach. Senolytics, which are chemical compounds that selectively kill senescent cells have become the focus of the senescence field[393], however its impact *in vivo* is still in its infancy. Many research groups established that senolytics alleviate and improve many

age-related pathologies in mice including osteoarthiritis, diabetes, cardiovascular health amongst others[393,394,395,396]. Given the increased susceptibility of senescent cells to *Salmonella* infections[227], it is intriguing to pose the question whether senolytics would reduce SASP and as a consequence reduce *S.* Typhi infection burden. Interestingly, a clinical trial in the late 1990s, using azithromycin, a currently renowned senolytic, has shown high efficacy in curing typhoid fever patients[397]. Although it is sensible to ablate senescent cells, senescence has important physiological roles and more clinical work is underway to determine the cost-benefit balance of senolytics as a therapeutic intervention for senescence-driven diseases.

Metabolomic SASP is a potentially vital niche to explore. Senescent cells are metabolically active and characterised by increased secretion profile. Whilst there is an abundance of research articles addressing SASP in a proteomic approach, very few papers explore metabolomic SASP. Multiple non-protein molecules such as DNA, RNA, lipids, ROS, amongst others are secreted from senescent cells via exosomes[398,399,400]. Metabolomic SASP is also highly dynamic and context-dependent, but significantly understudied. Understanding how the typhoid toxin modulates metabolomic SASP could prove insightful in *Salmonella* Typhi-specific biomarkers important for non-invasive diagnostics and therapeutic interventions.

Exploring senescence using a new variant of the toxin. A recent paper discovered a new variant of the typhoid toxin that uses an alternative "B" subunit, namely PltC in place of PltB[231]. Although it was less potent than the holotoxin with PltB, experiments on mouse models showed higher survival rate after infection with *Salmonella* encoding PltC, and lower recruitment of immune cells, specifically white blood cells such as lymphocytes and monocytes. It is intriguing to hypothesise that this new variant of the typhoid toxin might confer immunosenescence or facilitate chronic carriage of *Salmonella*.

7.7   Concluding remarks

This thesis provided, for the first time, an unbiased compendium of SASP proteins induced by a bacterial toxin using LC-MS/MS in combination with GeneChip microarray transcriptomics data to pinpoint putative players involved in toxin-induced phenotype (i.e. primary and transmissible senescence, and enhanced invasion). The project demonstrated that even though DDRs were similar to other senescence inducers, tox$^{\text{WT-SASP}}$ constituents are divergent from other SASPs. I conclude that *Salmonella* subverts the senescence phenotype in favour of infection via multiple, possibly redundant, ligands that activate the TGFβ signalling pathway. As the typhoid toxin is related to a large family of CDTs, this thesis acts as a stepping stone for further examination of senescence and host-pathogen responses, not only in typhoid fever, but also other diseases caused by CDT-secreting bacteria. At the centre of this thesis, is the idea that bacterial pathogens activate DDRs to reprogram multicellular infection niches remotely from a single infected cell by hijacking the host secretome.

Part IV

Materials and Methods

Chapter 8

Biochemical assays

8.1 Bacterial transformation

8.1.1 Creating Chemically Competent Cells

This process was carried out near a blue flame with no antibiotics. An overnight culture of 50 µl of DH5α *E. coli* in 5 ml sterile LB broth (Millipore, 28713) was created in a shaking incubator at 37°C, 200 rpm. Next, a day culture was carried out by adding 5 ml culture to 500 ml of sterile LB broth until it reached an OD of 0.4-0.6 in the same conditions. The culture was subsequently aliquoted in 10 × 50 ml falcon tubes and kept on ice for the subsequent steps. The cultures were centrifuged at 3000 rpm (i.e. ~2000 × g) for 10 mins in Beckman Coulter centrifuge. The supernatant was discarded in Virkon (SLS, L2897) and the pellets were resuspended in two 40 ml of sterile 0.1M CaCl$_2$ (Sigma, C5670). Centrifugation was repeated and both pellets were washed with 25 ml of sterile 0.1M CaCl$_2$. Subsequently, each pellet was resuspended in 2-3 ml of autoclaved CaCl$_2$ with glycerol (Sigma-Aldich, G5516) and stored in 50 µl aliquots in -80°C until ready to use. The importance of CaCl$_2$ as a washing and storage buffer is to attract DNA into the cells during transformation.

8.1.2 Transformation in chemically competent cells

DH5α aliquots were thawed on ice and 1 µl of plasmid DNA (equivalent of ~200 ng) was added to each aliquot (50 µl) and incubated on ice for 30 mins. Bacteria were heat shocked for 30 seconds at 42°C then immediately incubated on ice for 5 mins. They were then incubated in 900 µl of SOC media (BioBasic, SD7009) at 37°C for 1h. Next, cultures were pelleted at 13000 rpm for 1 min and resuspended in ~200 µl SOC media. Bacteria were then spread, using rotational movement of an L-shaped spreader, onto LB-agar (Sigma-Aldrich, L2897) plates with the relevant antibiotic(s) and incubated overnight at 37°C and observed for colonies.

8.1.3 Transformation in electrically-competent cells.

E. coli B21 Rosetta, resistant to chloramphenicol, in 50 µl aliquots were thawed on ice and 200 ng of DNA was added to them. Bacteria with DNA were transferred to ice-cold electroporation cuvette and electroporated at 1.25 V for ∼4 ms. Bacteria were allowed to cool down on ice for 5 mins then cultured in 900 ul SOC media and incubated in a shaking incubator at 37°C for 1 h at 200 rpm. Next, cultures were pelleted at 13000 rpm for 1 min and resuspended in ∼200 µl SOC media. Bacteria were then spread, using an L-shaped spreader, onto LB-agar plates with the relevant antibiotic(s) and incubated overnight at 37°C and observed for colonies.

8.2 Purifying recombinant typhoid toxin using Ni- NTA beads.

8.2.1 Expressing the typhoid toxin in *E. coli*

Plasmid encoding the typhoid toxin was transformed into chemically competent cells C41 strains using the same method previously described[81,106]. Electrical or chemical transformation was carried out using the T7 expression vector pETDuet1-pltB-HIS/pltA-MYC/cdtB-FLAG. Three bacterial colonies were inoculated in 30 ml of LB broth (i.e. a colony per 10 ml broth) containing ampicillin antibiotic (Melford Lab, A0104) at 100 µg/ml overnight at 37°C in a shaking incubator at 200 rpm. The overnight culture was diluted 1:100 in an ampicillin-containing LB broth and incubated at 37°C in a shaking incubator at 200 rpm until OD_{600} of 0.8-0.9 was reached. This is to ensure that the bacteria are at the late-end of the exponential phase to synthesize masses of protein. A 1 ml sample was taken and OD_{600} measured. Hereafter, every sample collected was measured for OD_{600}, the bacteria were centrifuged at 13000 rpm for 1 min and the pellet was resuspended in a calculated volume of SDS urea (50 mM Tris pH 6.8, 8 M Urea, 2% SDS, 0.3% Bromo blue) using the following equation

$$Volume\ of\ SDS\ Urea\ for\ resuspension\ (\mu l) = OD_{600} \times 200$$

Protein production was then induced using 0.1 mM Isopropyl β-D-1-thiogalactopyranoside (IPTG) insert product code at 18°C overnight. The next day, a sample of the bacteria was collected. Cultures were then pelleted at 6000 × g and supernatant discarded. The pellet was resuspended and homogenised in 50 ml Tris Buffer Saline pH 7.4 (TBS) containing 20 mM Tris, 150 mM NaCl). Subsequently, glycerol (Sigma-Aldrich, G5516) was added to the suspension at a final concentration of 10%, and two tablets of cOmpleteTM, Mini, EDTA-free Protease Inhibitor Cocktail per 50 ml solution (Roche, 11836170001) were added to stabilize proteins and generate a high yield of purified toxin. The resuspended bacteria were then lysed using a french press machine at 25 KPSI and the lysate was centrifuged at 60,000 × g for 60 mins at 4 C. Considering volumes of culture at the point of collection the equivalent of 1 ml culture was collected. For example, if the starter culture is 3L (i.e. 3000 ml) and the volume of the lysate after resuspension with glycerol is 75 ml then, (75/3000 = 25 µl) should

be collected and made up to 200 µl using SDS-Urea.

A sample of the supernatant was collected as the "soluble proteins" sample. The insoluble pellet was homogenised in 20 ml TBS and an "insoluble proteins" sample was collected.

8.2.2 Binding the toxin to Ni-NTA agarose by affinity chromatography.

The toxin contains a 6×-His tag on its PltB subunits therefore allowing Ni-NTA beads to specifically bind the typhoid toxin. 1 ml bed volume of Ni-NTA agarose beads (Jena Bioscience, AC-501-25) was washed with MQ water and then incubated with lysate on a rotating wheel for 1 hour to allow for affinity chromatography. The mix was subsequently immobilised in a column, and a sample of the flow through was collected. The beads were then washed with 50 ml of washing buffer (20 mM Tris-HCl pH 7.4, 500 mM NaCl) and a sample of the wash was collected. The toxin was then eluted off in 1 ml batched using the elution buffer (20 mM Tris-HCl pH 7.4, 50 mM NaCl, 250 mM imidazole). Imidazole is a competitive binder of the Ni-NTA that would elute the bound typhoid toxin. Each elution collected was tested for the presence of protein using Bradford assay in a 96-well format as previously described, and elution was halted when the blue colour no longer appeared. All elution fractions were combined together. 5 µl of the elution was mixed with 15 µl SDS-Urea to run on a gel.

All samples collected were assessed on protein gels and stained with Colloidal Blue stain, Coomassie stain or western blotting.

8.2.3 Dialysis of imidazole out of the toxin elutions

The combined fractions were poured into a sealed dialysis tubing (Fisher Scientific, 11465879), placed in a dialysis buffer (TBS) and stirred at 4°C overnight. The solution was then centrifuged at 13,000 rpm for 1 minute to pellet and remove any proteins that crashed out of solution. Finally, 20% glycerol was added to the solution for preservation and stored in -80°C freezer until intoxication (described in **Section 9.2**).

8.3 Protein concentration measurement using Bradford assay

Bradford Reagent (Sigma-Aldrich, B6916) was diluted 1:1 with milliQ water before any quantification. It was either used for qualitative (e.g. during toxin purification) or quantitative measure (e.g. for mass spectrometry).

Qualitatively: 200-400 µl of the diluted solution was pipetted in a 96-well plate and 1 µl sample was mixed in each well. The appearance of a blue precipitate indicates presence of proteins. The higher the protein concentration, the darker the colour.

Quantitatively: A BSA standard curve was created by mixing increasing masses of BSA 2 mg/ml standard solution (Thermo Scientific, #23210) with 1 ml of diluted Bradford reagent. OD_{600} was then measured using a spectrophotometer and a mass standard curve created using Graphpad Prism. Known volumes of the sample with an unknown concentration was then mixed with the Bradford solution and OD_{600} measured in the same way. Mass of protein was then interpolated from the standard curve and divided by volume pipetted into Bradford to calculate the concentration.

8.4 Protein gels

8.4.1 Preparation of whole cell lysate samples.

Cells were either seeded in 10 cm dishes (Corning) or 6-well plates (CellStar, 657160) at a density which would reach 70-80% confluency at the end of the experiment. Cells were washed three times with sterile PBS (Sigma Aldrich, D8537), and left in PBS the third time. Using a cell scraper, cells were gently scraped across the whole plate and transferred into Eppendorf tubes. Cells were centrifuged at 2000 rpm for 5 mins and resuspended in 1 ml of PBS. OD_{600} was measured using a spectrophotometer and recorded. To calculate the volume of sample buffer to use i.e. SDS-Urea (50 mM Tris pH 6.8, 8 M Urea, 2% SDS, 0.3% Bromo blue) with 1% β-mercaptoethanol (Merck, 805740), the following equation was used:

Volume of SDS Urea for resuspension (μl) = OD_{600} × 250 × volume of cells in suspension (i.e. 1)

Cells were pelleted at the same speed, PBS was removed, then the cells were resuspended in the calculated volume of the sample buffer. Cells were then boiled for 5 minutes at 95°C and run on SDS-PAGE gel or stored in -20°C.

8.4.2 Making in-house SDS-PAGE protein gels

Protein gels were cast in the lab using BioRad Mini PROTEAN Tetra Cell Casting Stand Clamps (1658050) or Mini-PROTEAN 3 Multi-Casting Chamber (165-4110). Protein gels consisted of two entities: A resolving gel **(Table 8.1)** that separates the different proteins and a stacking gel **(Table 8.2)** that contained the loaded wells .

Resolving gel (9% Bis-tris acrylamide gel) for 100 ml		
Solution	Volume for 100 ml stock (ml)	Final concentration
37.5:1 (40%) Acrylamide/Bis solution (1610148)	22.5	9%
2.5 M Bis-Tris pH 6.5	14.25	356 mM
20% SDS	0.5	0.1%
MQ water	62.75	62.75%

Table 8.1|Protocol for creating the resolving gel of a western blot gel

Stacking gel (5% Bis-Tris acrylamide gel) for 100 ml		
Solution	Volume for 100 ml stock (ml)	Final concentration
29:1 (30%) Acrylamide/Bis solution (1610156)	16.6	5%
2.5 M Bis-Tris pH 6.5	14.25	356 mM
20% SDS	0.5	0.1%
MQ water	68.65	68.65%

Table 8.2|Protocol for creating the stacking gel of a western blot gel

To polymerisation the gels, a few crystals (final concentration $\sim 0.1\%$) of Ammonium Persulfate (APS; Melford, A1512); used for cross- linking), and N,N,NN-Tetramethylethylenedi (TEMED; Sigma Aldrich, T9281) used as a catalyst at 1:1000 dilution) were dissolved in pre-prepared resolving gel solution and pipetted in a casting chamber (~ 9 ml). A small amount of isopropanol was used to remove bubbles, and the solution was left to polymerise. Once complete, the isopropanol was poured out and APS and TEMED were dissolved in the same concentration for the stacking gel. Approximately 2 ml of the stacking gel were pipetted on top of the resolving gel and either a 10-well or a 15-well comb was placed before its polymerisation. When polymerised, the gels were stored in a humidified box in the refrigerator until ready to be run. Gels were stored for a maximum of a week and discarded if not used.

8.4.3   Running a protein a gel

Samples were loaded in wells using Fisherbrand™ Gel-Loading Tips (11927734) and gels were run at 40 mA/gel in Mini-PROTEAN Tetra System (Bio-RAD) in either MES or MOPS buffers (Life Technologies, NP0001, NP0002 respectively) depending on the size of the protein of interest.

PageRuler Plus Prestained Protein Ladder (Thermo Scientific, #26619) was used as a protein size standard. After running the gel, it was either used for Commassie staining, Colloidal staining or western blotting.

8.5 Coomassie and Colloidal staining for global protein visualisation

Once gels were run, they were incubated in a small petri dish containing Coomassie (50% methanol, 10% acetic acid, 2.5 g/L Blue R250) or Colloidal Blue (10% ammonium sulphate, 0.1% Coomassie G250, 3% orthophosphoric acid, 20% ethanol) for 3-4 hours or until protein bands appear. The stain was then discarded appropriately and the gels were washed regularly with water to remove non-specific stain. Gels were then imaged using Gel Doc EZ Imaging System.

8.6 Western Blotting

Pre-run protein gels were rinsed in MQ water and transferred onto PVDF membranes (Thermo Scientific, 88518) using wet electroblotting, or semi-dry electroblotting. Prior to transfer, the PVDF membrane was cut into the appropriate size and activated via 100% methanol (Sigma-Aldrich, 900658) for 30 seconds.

Wet transfer. Activated PVDF membranes were submerged into a fresh transfer buffer (20mM Tris-base, 150 mM Glycine, and 20% methanol v/v). A transfer pad was prepared by assembling a sandwich in the following order: black frame (negative electrode), sponge, 3 layers of filter papers (BioRad, 1703931), pre-wet gel in the transfer buffer, 3 layers of filter papers, transfer sponge, and finally close the clear frame (positive electrode). The transfer tank was filled with a fresh transfer buffer and the sandwich inserted with the black frames of the holder and the sandwich aligned together. The transfer was then initiated at 400 mA for 80 min or 20-22 mV for 800-999 min.

Semi-dry transfer. Either Trans-Blot Turbo Transfer System (Bio- rad, 1704150), or iBlot 2 (Thermofisher Scientific, IB21001) were used per manufacturer's instructions. The transfer was carried out using a preset program of incremental voltage steps (total of 7 mins): 20 V for 1 min, 23 V for 4 min, then 25 V for 2 min.

Membranes were then carefully separated from the transfer system and blocked with Odyssey Blocking Buffer (927-40000, Li-Cor) for 1 hour or 5% non-fat dried milk (Tenak, A08300500) in tris-buffered saline (TBS; Millipore, 524750-1EA). If OBB was used, all subsequent incubations were in PBS (Biotech, PD8117) with 0.1% tween. If 5% milk was used, all subsequent washes were in 5% milk in TBS. After blocking, membranes were washed 3 times in PBS with 0.1% tween (PBST) or TBS for 5 mins each. The blots were then incubated with primary antibody diluted in the relevant buffer

(Table 8.3) for 1 hour at room temperature or overnight at 4°C on a rotator and washed 3 times for 5 mins each. Next, a fluorescent secondary antibody, specific to the species of the primary antibody was diluted in in the relevant buffer (1:10000) for 30 minutes - 1 hour before being washed with PBST or TBS twice (Table 8.4). The blots were imaged using Li-Cor scanner (OdysseySa 100 µm resolution, 300 µm depth). All antibodies were stored in their respective buffer at 4°C for short-term or -80°C for long-term storage and future reuse. Blots were then processed using Image Studio software and Photoshop.

Primary antibodies used for Western blotting			
Target protein	Species	Product code	Dilution
FLAG M2	mouse monoclonal	Sigma-Aldrich 5F3165	1:1000
c-myc	rabbit monoclonal	Abcam 32072	1:500
5X-His	mouse monoclonal	Qiagen 34660	1:500
γH2AX (ser-139)	rabbit monoclonal mouse monoclonal	Cell Signalling #9718 Merck/Sigma 05-636	1:1000
α-tubulin	mouse monoclonal	Abcam ab7291 Invitrogen 62204	1:1000-1:5000
p21 Waf1/Cip1	rabbit monoclonal	Cell Signalling technology 2947	1:1000
Wnt5a/b	rabbit monoclonal	Cell Signalling Technology 2530	1:1000

Table 8.3|Primary antibodies used for western blotting, their product codes and dilution factor.

Secondary antibodies used for Western blotting			
Secondary antibody	Source	Product code	Dilution
IRDye® 800CW anti-Mouse IgG	Donkey	Licor 926-32210	1:10000
IRDye® 680RD anti-Rabbit IgG	Donkey	Licor 926-68071	1:10000

Table 8.4|Secondary antibodies used for western blotting, their product codes and dilution factor.

Chapter 9

Cell Culture, staining and microscopy

9.1 Cell culture

9.1.1 Cells revival

Cells were kept frozen in 10% sterile DMSO (Sigma-Aldrich, D2438) and 90% complete media in -80°C until they were revived. Cells were thawed for 1 min at 37°C then diluted 1:10 with complete growth media to reduce DMSO concentration. The cells were then pelleted by centrifugation at 2000 rpm for 5 mins. Media was aspirated and cells were resuspended in 1 ml of complete growth media. Cells were then transferred to T25 flasks, then T75 or T175 (Greiner, 690175, 658175, or 660175 respectively) depending on the amount of cells.

9.1.2 Cell maintenance

Cells were maintained in a humidified incubator (Panasonic, MCO-170AICUV-PE) at 37°C and 5% CO_2. Cells were passaged every 2-3 days in their appropriate media according to instructions depicted on ATCC website. Depending on the cell type, either Dulbecco's Modified Eagle's Medium - high glucose (DMEM; Sigma Aldrich, D6546), Dulbecco's Modified Eagle's Medium/Nutrient Mixture F-12 Ham (DMEM F12 Ham; Sigma Aldrich, D6421), or Eagle's Minimum Essential Media (EMEM; Sigma Aldrich, M4655). **Table 9.1** summarises information about each cell line and their culturing method.

To prepare complete growth media, 10% fetal bovine serum (FBS) (Sigma Aldrich, F7524), 10 U/ml Penicillin/Streptomycin (Gibco, 11548876), 50 µg/ml Kanamycin sulphate (BioBasic, KB0286) and 2 mM L-glutamine (Thermofisher Scientific, #25030024), were added if not already in the media. Culture media was stored at 4°C for up to 3 months.

Cell line	Cell type	Organism	Culture media	Passage density
HT1080	fibrosarcoma epithelial cells	human	DMEM	1:6 - 1:10
HAP1	Near-haploid chronic myelogenous leukemia cells	human	DMEM	1:6 - 1:10
hTERT RPE-1	Retinal epithelial cells	human	DMEM/F12 Ham	1:6 - 1:10
IMR90	lung fibroblasts	human	EMEM	1:2-1:3
Caco-2	Colorectal adenocarcinoma epithelial cells	human	DMEM	1:6 - 1:10
NIH/3T3	fibroblast cells	mouse	DMEM	1:3-1:6 100% confluency avoided

Table 9.1|Cell lines used and their culturing method.

9.1.3   Passaging and cell seeding

Growth media was aspirated from the flask, and the cells were washed with an equivalent volume of sterile PBS (Sigma Aldrich, D8537). Cells were then trypsinized with 1 ml (in T25), 3 ml (in T75), or 5 ml (in T175) sterile trypsin (Sigma Aldrich, T4049) depending on the flask size for 3 to 5 minutes in the cell culture incubator. Once the majority of cells detached, the flask was tapped gently to dislodge any remaining attached cells. Trypsin was then neutralised using an equivalent amount of complete growth media. Cells were separated by pipetting them out against the bottom of the flask and placed in a falcon tube, then an appropriate volume was either taken back into a cell culture flask for maintenance or used for seeding an experiment.

9.1.4   Counting cells for seeding experiments.

After cell detachment as described in **Section 9.1.3**, 10 µl of suspended cells were pipetted under a coverglass in a glass haemocytometer (Hawksley, AC1000). Cells in the four corners of the haemocytometer were counted under a light microscope and averaged.

$$The\ number\ of\ cells/ml\ =\ average\ number\ \times\ 10^4$$

The volume of cell suspension to dilute in media was then calculated using the following equation:

$$Volume\ (ml) = \frac{number\ of\ cells\ to\ be\ seeded}{calculated\ number\ of\ cells/ml\ of\ suspension}$$

146

The volume calculated was diluted in complete growth media and divided across the required wells in culture plates.

9.2 Intoxication and drug application

9.2.1 Identifying the concentration of the toxin elution.

The stock concentration of the purified toxin was estimated by interpolation from a standard curve of a known concentration of purified recombinant GST-CdtB-FLAG, measured using a quantitative Bradford assay. To create the standard curve, a sample of the typhoid toxin and different dilutions of the purified CdtB were analysed using western blot. Antibodies against FLAG were used to blot for the recombinant CdtB and the CdtB subunit in the purified toxin. The intensity of FLAG was measured using ImageStudio Lite and plotted using Graphpad prism. The mass of the CdtB was extrapolated from the standard curve and divided by the loaded volume to estimate the concentration of the toxin stock.

Cultured cells were intoxicated using purified recombinant typhoid toxin (described in **Section 8.2**). Standard intoxication dose was 20 ng/ml unless otherwise indicated.

9.2.2 Standard intoxication procedure.

Culture media was aspirated off and replaced with media containing 20 ng/ml toxin for 2h on the chosen cell line. Next, cells were washed three times with sterile PBS to remove any extracellular toxin and chased with fresh complete growth media for the duration of the experiment until fixation or conditioned media harvest.

9.2.3 Drug and recombinant protein application.

Cells were treated with drugs listed in **Table 9.2** with the relevant incubation times. The cells were then washed 3 times with sterile PBS and chased with fresh complete growth media for the duration of the experiments. Alternatively, cells were treated with commercially available purified proteins at the indicated concentrations unless otherwise indicated in figure legends (**Table 9.3**).

Drug concentration in cell culture				
Drug	**Mode of action**	**Working concentration**	**Pulse time**	**Product code**
Aphidicolin	inhibitor of DNA polymerase α	20 µM	24 h	Sigma-Aldrich (A0781)
Etoposide	Topoisomerase inhibitor	10 µM	24 h	Cayman Chemicals (12092)
IWP-2	inhibitor of Wnt production	2 µM	Throughout experiment duration	Cambridge Bioscience (SM39-2)
TGF-β RI Kinase Inhibitor III	selective inhibitor of activin receptor-like kinase 4, 5, and 7	1 µM	1 h pre-treatment and in SASP	Sigma-Aldrich (616453)
CID11210	Wnt signaling agonist	0.1-100 nM	5 days	Merck (Sml0698)

Table 9.2|Concentrations of drugs used in cell culture (unless otherwise stated in the thesis). All drugs were resuspended in sterile DMSO.

Recombinant proteins used in cell culture			
Protein	**Working concentration**	**Product code**	**Solvent**
TGFB3	10 ng/ml	CST 8425LC	20 mM Citrate, pH 3.0
Activin A	500 ng/ml	R&D Systems 338-AC-010	sterile 4 mM HCl
GDF15	200 ng/ml	R&D Systems 957-GD-025	sterile 4 mM HCl with 0.1% BSA
Wnt5a	500 ng/ml	R&D Systems 645-WN	sterile PBS with 0.1% BSA

Table 9.3|Recombinant proteins and their concentration used in cell culture. All proteins are human.

9.3   Knockdown using siRNA transfections.

Cells were transfected using Lipofectamine RNAiMax (Invitrogen, 13778-150) with small adjustments to their user manual. Briefly, per well of a 24-well plate format, 0.25 µl or 0.5 µl of Lipofectamine RNAiMax in 25 µl of serum-free, antibiotic-free DMEM, was mixed with 0.5 µl of 20 µM short-interfering RNA (siRNA) in 25 µl of serum-free, antibiotic-free DMEM for 5 minutes at room temperature with gentle tube flicking. The final concentration of siRNA in culture was 20 nM. The 50 µl mix of siRNA and lipofectamine were added to 450 µl complete growth DMEM, and incubated for 48h before any further treatments. Each siRNA is ON-TARGETplus SMARTpool from Horizon Discovery (**Table 9.4**).

siRNA product codes		
Target protein (siRNA)	**Source**	**Catalogue number**
Non-targeting Control	ON-TARGETplus SMARTpool	D-001810-01-20
PLK1	siGENOME Individual siRNA	D-003290-05-0020
Wnt5a	ON-TARGETplus SMARTpool	L-003939-00-0005
ACVR1/ALK2	ON-TARGETplus SMARTpool	L-004924-00-0005
ACVR1B/ALK 4	ON-TARGETplus SMARTpool	L-004925-00-0005
TGFBR1/ALK5	ON-TARGETplus SMARTpool	L-003929-00-0005
ACVR1C/ALK7	ON-TARGETplus SMARTpool	L-004929-02-0005
INHBA	ON-TARGETplus SMARTpool	L-011701-00-0005
Smad2	ON-TARGETplus SMARTpool	L-003561-00-0005
ADAM17	ON-TARGETplus SMARTpool	L-003453-00-0005

Table 9.4|List and product codes of siRNA used throughout the thesis. All siRNAs are from Horizon Discovery

9.4   Infection assays

9.4.1   Preparation of cells and bacterial culture.

Cells were seeded in a 24-well plate at 4×10^4 onto glass coverslips to reach approximately 80% confluency the next day. *Salmonella* strains used are for infections experiments are listed in **Table 9.5** .

Salmonella strains		
Serovar	**Strain**	**Kind gift from**
S. Javiana WT	S5-0395	Prof. Martin Weidmann[98,99]
S. Javiana ΔcdtB	M8-0540	Prof. Martin Weidmann[98,99]
S. Typhi Ty2	BRD948 vaccine strain	Prof. Gordon Dougan[401]
S. Typhi Ty2 ΔcdtB	BRD948 vaccine strain	Prof. Gordon Dougan[106]

Table 9.5|*Salmonella* strains used for infection.

A bacterial colony was cultured in 5 ml LB broth with the relevant antibiotic overnight at 37°C in a shaking incubator. Next day, 1:100 dilution of the overnight culture was performed in 10 ml LB

broth with the relevant antibiotic and incubated at 37°C in a shaking incubator until OD_{600} is close to 2.0 (i.e. 1.4 - 1.8). The following formula was used to normalise the culture to OD_{600} 2.0:

$$Volume\ to\ spin\ down\ (ml) = \frac{2.0}{calculated\ OD_{600}}$$

9.4.2 Preparation of infection media and infection

The volume calculated was added to Eppendorf tubes and spun down at 13,000 rpm for 1 minute. Supernatant was discarded as much as possible and the pellet was then resuspended in 1 ml of sterile PBS. The relevant volume of bacteria was pipetted onto the cells seeded in 24-well plates. The plate was then spun for 1 min at 1000 × g and incubated for 30 min at 37°C 5% CO_2. Infection media was then washed with PBS, and incubated with gentamicin-containing media (Chem Cruz, sc203334) 50 µg/ml for 1.5 h. Next, media containing a lower concentration of gentamicin (i.e. 10 µg/ml) was replaced for the duration of the experiment.

9.4.3 Invasion assay

NIH/3T3 cells were seeded at $2{\times}10^4$ cells per well in a 24-well plate and serum-starved 24h to deprive the cells of factors in FBS that might stimulate membrane ruffling. Serum-free conditioned media was added for the relevant duration before infection as described in **Section 9.4.2** using an MOI of 160. After high concentration of gentamicin for 1.5h, cells were washed 3× with PBS, then lysed using 1% triton X (VWR, 28817.295) in water for 5-10 mins, and pipetted vigorously. Next, the supernatant was transferred to a 96-well plate, and using a multichannel pipette, consecutive 10-fold titrations were carried out, by serial dilution (20 µl of supernatant with 180 µl PBS, etc). *Salmonella* were then cultured on agar plates with relevant antibiotics by spotting 5 µl of each dilution overnight in a dry incubator at 37°C. Colonies were then counted manually, and the highest, countable *Salmonella* colonies (i.e. the lowest dilution with visible colonies) were counted and normalised to calculate *Salmonella* colony forming units (CFUs).

9.4.4 MOI calculation

The number of bacteria at OD_{600} 1.0 was estimated to be $8{\times}10^8$ bacteria/ml. Since OD_{600} was normalised to 2, the number of bacteria was $16{\times}10^8$ bacteria/ml. Subsequently the following formula was used:

$$\frac{volume\ of\ infection\ media\ (ml)\ \times\ 16{\times}10^8}{number\ of\ seeded\ cells}$$

9.5 Survival assay

Media was removed from cells seeded in a 24-well plate and washed three times with PBS and 150 µl trypsin was added. Trypsin was neutralised with a 150 µl media and placed in an Eppendorf tube. 10 µl of cells was mixed with 10 µl trypan blue (Sigma-Aldrich, T8154) for 3 minutes at room temperature, and 10 µl were applied in a haemocytometer. Blue cells were counted as dead cells and transparent cells were counted as viable. Then, the following calculations were carried out and represented in bar graphs:

No. of viable cell/ml = No. of live cells counted dilution (i.e. 2) × 10,000
No. of dead cell/ml= No. of dead cells counted dilution (i.e. 2) × 10,000

$$\% \ viability = \frac{No. \ of \ viable \ cells}{total \ cells} \times 100$$

9.6 Clonogenic Assay

Cells were seeded at 2000 cells in a 10 cm dish. Cells were treated as described previously and incubated in fresh media for 7 days. Media was aspirated and cells were air-dried. Next, 80% ethanol was applied to cells for 15 minutes, then removed and air-dried. Methylene blue (1%) was added for 1 hour, washed off with distilled water until the background colour disappears and then air-dried before images were taken.

9.7 Conditioned media harvest

Conditioned media was harvested using stripettes and pipetted into falcon tubes. Conditioned media were then centrifuged at 6000 × g for 5 mins to pellet the cells before filtering using a syringe and 0.2 µm filters to prevent cell contamination and release of other factors due to bursting due to the filtration pressure. The centrifugation step is to remove any cells that would otherwise burst releasing non-SASP proteins into the conditioned media, and the filtration is an extra step to filter out cells from the conditioned media. Conditioned media was then stored at -20°C for short term storage and -80°C for long term storage. Before incubation on cells, conditioned media was either supplemented 1:1 with complete growth media, or 10% FBS if conditioned media was serum-free.

9.8 Histological stain of SA-β-gal

Senescence-associated βgal (SA-β-gal) was stained as per the protocol denoted in Senescence β-Galactosidase Staining Kit (Cell Signalling Technology #9860S). Images were captured using DinoEye AM423X.

9.9   SPiDER β-gal fluorescence

Cellular Senescence Detection Kit - SPiDER β-Gal (Dojindo Molecular Technologies, SG-04) was used according to the manual. Briefly, McIlvaine buffer was made by mixing 0.1 mol/L citric acid solution and 0.2 mol/L sodium phosphate solution at 1:1.7 ratio respectively. The buffer was acidified to pH6 by adding more citric acid, then the buffer was diluted 5× in milliQ water. Resuspended SPiDER β-gal was diluted in McIlvaine buffer 1:1000 and applied on fixed cells in a 37℃ incubator without CO_2. Before staining for other proteins, cells were incubated with 0.1% triton X-100 in PBS (Biotech, PD8117) for 30 mins at room temperature and then immunofluorescence described below.

9.10   CellEvent Senescence Green Detection

Staining was carried out according to the detection kit manual (Invitrogen, C10851). Briefly, after the cells were fixed with 4% PFA (Sigma-Aldrich, P6148) in PBS , they were washed with 1% BSA (Sigma-Aldrich, 1073508600) in PBS to remove fixative. Next, staining solution constituting CellEventTM Senescence Green Probe diluted 1:1000 in the CellEventTM Senescence Buffer was applied on cells and incubated for 2h in a 37℃ incubator without CO_2. The cells were then washed in PBS before immunofluorescence staining of other proteins resumed as previously described. The probe was imaged using a FITC filter set. Where immunofluorescent, and EdU were to be co-stained with CellEvent Green, the order of assays were CellEvent Senescence Green, EdU staining Kit, and then immunofluorescence.

9.11   EdU staining

Click-iT™ EdU Cell Proliferation Kit for Imaging, Alexa Fluor™ 647 dye (Thermofisher, C10340) was used per the manufacturer's instruction. Depending on the duplication time of each cell line, EdU incubation in culture was adjusted. For example, HT1080 duplication time is 18h, therefore EdU was added to the culture 18-24h before fixation. Post-fixation, the reagent's volumes were economically reduced at a ratio of 1:16 to allow for more experiments using the kit.

9.12   Immunofluorescence staining for cell culture

Cells were seeded at the appropriate density for each experiment on glass coverslips 13 mm. At the end of the experiment, media was washed off three times with PBS, then fixed with 4% paraformaldehyde (PFA) in PBS for 10-15 mins at room temperature. The fixative solution was removed and disposed of appropriately. Cells were washed two more times with PBS (Biotech, PD8117) and stored in the fridge until the staining began.

Cells were blocked and permeabilised using a blocking buffer containing 3% BSA (Sigma-Aldrich, 1073508600), 0.2% Triton X-100 (VWR, 28817.295) in PBS, at room temperature for 1h then coverslips were dipped in a reservoir with. Next, primary antibodies were applied in the relevant PBS 0.2% Triton X-100 for either an hour at room temperature or overnight at 4°C then dipped in a reservoir with PBS (**Table 9.6**). Secondary antibody was next applied for 30 mins in 1:500 dilution in PBS 0.2% Triton X-100 (**Table 9.7**). Finally, the cells were counter-stained with DAPI (6 µg/ml) in PBS Triton X-100 for 3 mins at room temperature, washed with PBS then water and left to dry for 30 minutes. Coverslips were then mounted on 6 µl of VectaShield mounting agent (Vector Lab, H1200), and sealed before being imaged on the Nikon Widefield Microscope.

Primary antibodies used for immunofluorescence			
Target protein	**Species**	**Product code**	**Dilution**
γH2AX (ser-139)	rabbit monoclonal mouse monoclonal	Cell Signalling #9718 Merck/Sigma 05-636	1:1000
RPApT21	rabbit polyclonal	Abcam ab61065 ab109394	1:1000
53BP1	rabbit polyclonal	Novus Biotechnology NB100-304	1:1000
Lamin A/C	mouse monoclonal	Santa Cruz sc7292	1:1000
Lamin B1	rabbit polyclonal	Abcam ab16048	1:1000
c-myc	rabbit monoclonal	Abcam ab32072	1:500
α-tubulin	mouse monoclonal	Abcam ab7291 Invitrogen 62204	1:1000
phospho-smad 2 (Ser465/467)	rabbit monoclonal	Cell Signalling Technology 3108	1:500-1:1000
phospho-smad1/5 (Ser463/465)	rabbit monoclonal	Cell Signalling Technology 9516	1:500-1:1000
Activin A	rabbit polyclonal	Novus Biotechnology NBP1-30928	1:500
Wnt5a/b	rabbit monoclonal	Cell Signalling Technology 2530	1:500
Wnt5a	rabbit monoclonal	Abcam ab179824	1:500
Salmonella	rabbit polyclonal	Abcam ab35156	1:200

Table 9.6|Primary antibodies used for immunofluorescence, their product codes and dilution factor.

Secondary antibodies used for immunofluorescence			
Secondary antibody	**Source**	**Product code**	**Dilution**
anti-rb 568 IgG, Alexa Fluor	Donkey	Invtirogen A11036	1:500
anti mouse 488 IgG, Alexa Fluor	Donkey	Invitrogen A21202	1:500
anti rabbit 488 IgG, Alexa Fluor	Goat	Invitrogen A11008	1:500
anti-ms 594 IgG, Alexa Fluor	Donkey	Invitrogen A21203	1:500
anti-ms 647 IgG, Alexa Fluor	Goat	Invitrogen A-21240	1:500

Table 9.7|Secondary antibodies used for immunofluorescence, their product codes and dilution factor.

9.13   Microscopy

9.13.1   Nikon Wide-field Live-cell system

Fixed cells were imaged using Nikon's Inverted Ti eclipse equipped with an Andor Zyla sCMOS camera (2560 x 2160; 6.5µm pixels). The objectives used were Plan Apo 10x (NA 0.45); Plan Apo 20x (NA 0.75); Plan Fluor 40x oil (NA 1.3); Apo 60x oil (NA 1.4); Plan Apo 100x Ph oil (Na 1.45); Plan Apo VC 100x oil (NA 1.4). Quad emission filters for used with SpectraX LED excitation (395nm, 470nm, 561nm, 640nm). The imaging software used was NIS elements software.

9.13.2   Olympus CK30

Histology staining of SA-β-gal was imaged using an Olympus Wide-field microscope CK30 10x objective and captured with Dino-Lite adaptor and Dino-Lite software. Images were then processed using Adobe Lightroom to neutralise colours with good white-balance.

9.13.3   Nikon Eclipse Ts2

For phase-contrast images of histologically stained SA-β-gal, the inverted microscope Nikon Eclipse Ts2 equipped with sCMOS Ds-Fi-3 camera with built-in Diascopic, high-intensity LED illumination system at 10x and 40x objective lenses.

9.14   Illustrations, Image Processing and Quantification

Adobe Illustrator was used to manually hand-draw illustrations, and assemble all results figures.

9.14.1 Microscopy Image processing

Fiji 2.1.0/1.53c macro code was created to automate processed images. Briefly, brightness and contrast are normalised across all images of interest, a pre-set ROI is used to crop images to regions of interest, and a pre-set scale bar is added. DAPI nuclei are then outlined, overlaid with the other channels and saved as png files. Many variants of the code has been created to cater for 2-channel, 3-channel and 4-channel images, with either normal composite images or with DAPI outlines. The codes can be found via this link: https://drive.google.com/drive/folders/1SwUO-bgyW0rjY9MetAfKGtdd77FsCahF?usp= sharing

9.14.2 Manual quantification

For histological SA-β-gal, images were opened in FIJI and cell counter plugin was used. Raw numbers were then recorded in Microsoft Excel.

9.14.3 Automatic quantification - RING tracking

Analysis of the RING phenotype was carried out using MATLAB image processing code, which was published[106] and publicly available via https://github.com/nbul/Nuclei. To differentiate between γH2AX negative cells and pan staining cells, γH2AX upper-quartile of untreated cells were used as a cutoff.

9.14.4 CellProfiler: Semi-automatic quantification

γH2AX foci: CellProfiler 4.0.7 was used to automate quantifying foci and their sizes. A pipeline was created to identify nuclei with a manually determined threshold. RING positive cells were removed manually from the analysis and foci intensity was enhanced. Foci in each nucleus was then identified using a threshold obtained manually.

Lamins: To quantify the change in lamin intensity, each nucleus was first thresholded in FIJI and then input into CellProfiler. Next, the maximum intensity of the lamin channel at the edge of each nucleus was measured. To mitigate the intensity variations between images, the intensity of the centre of the nucleus was measured and a ratio between the edge and middle intensity was calculated and displayed in bar charts.

SA-β-gal: To quantify fluorescent SA-β-gal positive nuclei, the SA-β-gal channel was initially thresholded in FIJI and then input into CellProfiler. Each cell was identified by expanding an area around the nucleus (around 50 px). A positive nucleus was identified depending on the fraction of SA-β-gal overlapping with each cell, which was set manually depending on experiment.

Other nuclear components: Other nuclear components were quantified by either i) using a manual signal threshold and automatic classification within CellProfiler, or ii) by measuring intensity and setting a threshold using the negative control's upper quartile.

Other cytplasmic components: Global image intensity for the protein was quantified, and divided by the number of nuclei counted.

9.15   Statistical analysis

Graphs and statistical analysis were carried out using GraphPad Prism 9. Statistical analysis method is indicated in each legend as appropriate. Significance is denoted by asterisks (*) where *$p<0.05$, **$p<0.01$, ***$p<0.001$ and ****$p<0.0001$.

Chapter 10

Mass Spectrometry Proteomics

10.1 Bioorthogonal Noncanonical Amino Acid Tagging (BON-CAT)

10.1.1 Click-iT™ AHA metabolic tagging of cells in culture

L-azidohomoalanine (Thermofisher Scientific #C10102) is a methionine analogue used to tag newly synthesized proteins produced by cells in culture for mass spectrometry purposes. The tag is useful when proteins need to be purified from FBS containing media for better mass spectrometry sensitivity. It is light-sensitive, therefore wherever used, it was hidden from light.

HT1080 were seeded in 6 well-plates in complete media and treated as previously described. Cells were washed with PBS three times, then starved with methionine-free DMEM (Thermofisher Scientific, #21013-024) for 30 minutes to 1h. Methionine-free media was created by adding 50 ml dialysed heat inactivated FBS (Hyclone, 12349822), 10 ml L-glutamine (Thermofisher Scientific #25030032), 10 ml L-cystine HCl (Sigma- Aldrich, 57579), 5 ml sodium pyruvate (Sigma-Aldrich, S8636), 1% Kanamycin, and 1% Pen/Strep (Gibco, #11548876) to 450 ml of DMEM methionine-free media. Next, 100 µM AHA in methionine-free media was applied in 1.5 ml in each 6-well plate for the duration indicated in the results section then harvested as previously described in **Section 9.7**. The samples were stored away from light at -80°C until enrichment for mass spectrometry.

10.1.2 Enrichment of newly synthesized proteins tagged with AHA

Samples were hidden from light throughout the experiment to prevent degradation of the tag. Water used for washes and preparing reagents was HPLC-grade (Fisher Chemical, W6-1).

Samples were thawed in a 37°C water bath. One tablet of Roche protease inhibitor cocktail (Merck, 11836170001) was crushed per 40 ml of conditioned media tagged with AHA (CM^{AHA}) to preserve harvested proteins. CM^{AHA} was centrifuged through amicon filters with 3 KDa cutoff to concentrate

the proteins down to 500 µl at 4000 ×g swing bucket centrifuge at 4°C. The concentrated proteins were collected for enrichment and the flow-through was stored at -20°C for future use. Click-iT™ Protein Enrichment Kit (Thermofisher Scientific, C10416) was used to select for AHA labelled proteins in concentrated media as per their instructions with slight modifications. Per 500 µl concentrated CM^AHA, 500 µl of urea lysis buffer containing 8 M urea (Melford, U1363), 200 mM Tris pH 8 (Sigma-Aldrich, T1503), 4% CHAPS, 1 M NaCl was added. The mixture was then centrifuged at 10,000 ×g for 5 mins and placed on ice. The sample was then incubated with 100 µl bed volume of alkyne beads and half the catalyst solution described in the kit's manual was used overnight in a roller away from light. This allows alkyne beads to bind the azide motif of the AHA in labelled proteins via click chemistry reaction.

10.1.3   Reduction and alkylation of the Resin-Bound proteins

The reaction mix was centrifuged at 1000 ×g for 1 minute, and the supernatant was collected and stored in -20°C in case of repetition needed. Resin was washed with water and centrifuged at 1000 ×g for 1 minute. The supernatant was discarded. Subsequently, 0.5 ml of SDS wash buffer and 10 µl of 0.5 M TCEP were added to the resin. TCEP was used instead of DTT, which was suggested by the protocol, as it would interact with iodoacetamide, an alkylating agent used in later stages. The mixture was heated at 70°C in a Thermomixer at 600 rpm for 15 mins then cooled down at room temperature for a further 15 mins. The mixture was centrifuged at 1000 ×g for 5 minutes and the supernatant was discarded. Next 500 µl of 20 mM iodoacetamide in the SDS wash buffer was added to each reaction and incubated for 30 mins in a Thermomixer at 6000 rpm in the dark.

10.1.4   Stringent washing of the resin to remove non-specifically bound proteins

The resin was transferred to a spin column (Wizard, Promega) and centrifuged quickly in an Eppendorf using a picofuge for a few seconds. Resin tube was washed with 500 µl HPLC-grade water and centrifuged again. Subsequently, using vacuum flow, the columns were washed with 20 ml of SDS wash buffer, 8M Urea/100 mM Tris-HCl pH 8, 20% isopropanol and 20% acetonitrile in that order. All flow-through solutions were discarded.

10.1.5   Digestion of resin-bound beads to peptides.

The column was rinsed with 500 µl of 50 mM ammonium bicarbonate and centrifuged briefly in an Eppendorf in a picofuge for a few seconds to remove excess liquid. Next, 150 µl of 50 mM ammonium bicarbonate was added to the spin column, resuspended using a cut pipette tip and transferred to a clean tube. Then, 1 mg of Pierce MS grade trypsin (Fisher Scientific, 13464189) i.e. 10 µl of 0.1 mg/ml and resuspended in 0.1% TFA (Merck, 108262), was added to the resin slurry, and incubated

at 37°C overnight in a Thermomixer at 800 rpm.

10.1.6   Desalting the digested peptides

Peptides must be desalted to remove salts and urea from the digestion buffer that would affect the Orbitrap. Stagetips C18, 200 µl tip (Thermofisher Scientific) were washed with 100 µl of 0.1% TFA/50% ACN (Sigma-Aldrich, 900667) to acidify the pH as peptides bind better in acidic conditions. The stage tip was washed again with 100 µl of 0.1% TFA.

Samples were acidified by adding TFA to a final concentration of 0.4%. TFA was added as needed until pH 2 was reached. The peptide samples were added to the stage tip. The samples were slowly passed through the stage tip 3 times then washed with 100 µl of 0.1% TFA. Slowly, the peptides were eluted with 100 µl of 0.1% TFA/50% ACN.

10.2   Sample preparation of serum-free (SF) and Essential 8 (E8) conditioned media

10.2.1   Harvesting SASP proteins

Post-intoxication in complete media as described in **Section 9.2**, cells were incubated with either serum-free DMEM or stem cell media Essential 8 (Thermofisher, A1517001). Serum-free media was created as described in Section 9.1.2 without the addition of FBS. As cells were mostly viable with only 24h incubation, cells were split into 2 sets, and each day a single set was incubated for 24h (ie. plate 1 for 0-24h, plate 2 for 24-48h) and fractions were then combined.

However, as cells were viable in E8 media for 48h, cells were cultured in E8 for 48h without any media change (0-48h plate). For both serum-free and E8 conditioned media, a home-made protease mixture of leupeptin, pepstatin, and chymostatin (Sigma Aldrich, 62070, 77170, C7268, respectively) each at a final concentration of 10 µg/ml), as soon as they were harvested. Samples were then stored in -80°C until S-trap digestion.

Samples were concentrated by centrifuging through amicon filters with 3 KDa cutoff (Merck, ufc900324) down to 250 µl at 4000×g using swing bucket centrifuge at 4°C. The concentrated proteins were used for enrichment and the flow through was stored at -20°C for future use.

10.2.2   S-Trap digestion of proteins

Next, the samples were normalised by volume where 50 µl of the concentrated media was used for S-trap digestion.

Equal volume of 2x S-trap lysis buffer containing 10% SDS (Sigma-Adrich, 05030), 100mM TEAB,

pH 7.55 (Thermofisher, 90114) was added to the samples (i.e. 50 µl). Next, the samples were reduced by adding TCEP (Merck, 646547) at a final concentration of 10 mM. The samples were then heated at 70°C for 15 mins at 750 rpm in a shaking incubator. SDS from the lysis buffer with a reducing agent leads to denaturation and reduction of disulphide bonds important in secretory proteins. The samples were then cooled down for 5 mins at room temperature.

Next, the samples were alkylated by adding twice the concentration of TCEP for iodoacetamide (Merck, I6125), i.e. 20 mM, and pipetted really well, to prevent the reformation of the disulphide bonds. The solution was kept in the dark for 30 mins at room temperature.

The samples were then acidified by adding aqueous phosphoric acid to a final concentration of 1.2%. The acidification step is essential for the S-trap to bind proteins.

S-trap binding buffer (90% aqueous methanol, 0.1M TEAB, pH 7.1) was added to the solution in a ratio of 1:7. Samples were then loaded into the S-trap columns (Protifi, C02), 150 µl at a time gently without poking the bottom and centrifuged at 4000 x g for 10 seconds to pass through the S-trap. The S-trap was then washed 3X with 150 µl binding buffer before transferring it to a clean 2 ml Eppendorf tube. MS grade trypsin (Fisher Scientific, 13464189) resuspended in 0.1% TFA was then added to a ratio of 1:10 trypsin:protein w/w in 50 mM TEAB buffer. At least 30 µl of trypsin in TEAB buffer was added to the samples and air bubbles were avoided. The S-trap was sealed with parafilm, and incubated at 47°C for 1 hr without shaking. The peptides were then eluted by adding 40 µl of 50 mM TEAB, 40 µl of 0.2% aqueous formic acid (Fisher Chemical, A117-50)and 40 µl of 50% ACN containing 0.2% aqueous formic acid in that order and passing the buffers through the trap at 4000 ×g for 10 seconds before adding the next. Store till ready for drying and LC-MS/MS analysis.

10.3   Drying and preparing samples for Orbitrap injections.

Samples were centrifuged in a SpeedVac (Eppendorf) at 45°C for 60-90 minutes with Eppendorf tube lids open to allow for evaporation, with vacuum setting V-AQ. Once samples were dried, peptides were resuspended in 0.5% formic acid and mixed by vortex at the lowest speed for 10 minutes. Samples were then transferred to labelled polypropylene vials (Thermo Scientific #160134) and injected in the orbitrap.

10.4   Mass Spectrometry Data Analysis

10.4.1   LC-MS/MS analysis

18 µl of each sample was analysed by nanoflow LC-MS/MS using an Orbitrap Elite (Thermo Fisher) hybrid mass spectrometer equipped with an easyspray source, coupled to an Ultimate RSLCnano LC System (Dionex). The system was controlled by Xcalibur 3.0.63 (Thermo Fisher) and DCMSLink

(Dionex). Peptides were desalted on-line using an Acclaim PepMap 100 C18 nano/capillary BioLC, 100A nanoViper 20 mm x 75 μm I.D. particle size 3 μm (Fisher Scientific) and then separated using a 125-min gradient from 5 to 35% buffer B (0.5% formic acid in 80% acetonitrile) on an EASY-Spray column, 50 cm × 50 μm ID, PepMap C18, 2 μm particles, 100 Å pore size (Fisher Scientific). The Orbitrap Elite was operated with a cycle of one MS (in the Orbitrap) acquired at a resolution of 60,000 at m/z 400, with the top 20 most abundant multiply charged (2+ and higher) ions in a given chromatographic window subjected to MS/MS fragmentation in the linear ion trap. An FTMS target value of 1e6 and an ion trap MSn target value of 1e4 were used with the lock mass (445.120025) enabled. Maximum FTMS scan accumulation time of 500 ms and maximum ion trap MSn scan accumulation time of 100 ms were used. Dynamic exclusion was enabled with a repeat duration of 45 s with an exclusion list of 500 and an exclusion duration of 30 s.

10.4.2   MaxQuant Analysis

All raw mass spectrometry data were analysed with MaxQuant version 1.6.10.43. Data were cross-referenced against a human UniProt sequence database (June 2015) using the following search parameters: digestion set to Trypsin/P with a maximum of 2 missed cleavages, methionine oxidation and N-terminal protein acetylation as variable modifications, cysteine carbamidomethylation as a fixed modification, match between runs enabled with a match time window of 0.7 min and a 20-min alignment time window, label-free quantification enabled with a minimum ratio count of 2, minimum number of neighbours of 3 and an average number of neighbours of 6. A first search precursor tolerance of 20ppm and a main search precursor tolerance of 4.5 ppm was used for FTMS scans and a 0.5 Da tolerance for ITMS scans. A protein FDR of 0.01 and a peptide FDR of 0.01 were used for identification level cut-offs.

10.4.3   Perseus Bioinformatic Analysis

MaxQuant output was loaded into Perseus version 1.5.6.0 and all LFQ intensities were set as main columns. The matrix was filtered to remove all proteins that were potential contaminants, only identified by site and reverse sequences. LFQ intensities were then transformed using log2(x) default function. To group experimental conditions, rows were categorically annotated with their condition names. Rows with no LFQ intensities in all categorized groups were eliminated by filtering rows based on valid value in at least one group with a minimum number of 3 out of 4 repeats for statistical analysis.

Subsequently, data were visualized using multi-scatter plots and Pearson's correlation analysis and outliers removed. Data were then normalised by subtracting column medians and missing values were randomly imputed with a width of 0.3 and downshift of 1.8 from the standard deviation.

In order to identify quantitatively enriched proteins between groups, two-sided Student's t-tests

were performed with a permutation-based FDR calculation (FDR = 0.05) with an (S0) =0.1. Data was then exported into an excel file and input into GraphPad Prism to create the figures and plots presented.

Bibliography

1. World Health Organization. Typhoid vaccines: WHO position paper, March 2018 – Recommendations. *Vaccine*, 37(2):214–216, 1 2018.

2. Li Liu, Hope L. Johnson, Simon Cousens, Jamie Perin, Susana Scott, Joy E. Lawn, Igor Rudan, Harry Campbell, Richard Cibulskis, Mengying Li, Colin Mathers, and Robert E. Black. Global, regional, and national causes of child mortality: An updated systematic analysis for 2010 with time trends since 2000. *The Lancet*, 379(9832):2151–2161, 6 2012.

3. Robert Bain, Ryan Cronk, Rifat Hossain, Sophie Bonjour, Kyle Onda, Jim Wright, Hong Yang, Tom Slaymaker, Paul Hunter, Annette Prüss-Ustün, and Jamie Bartram. Global assessment of exposure to faecal contamination through drinking water based on a systematic review. *Tropical Medicine and International Health*, 19(8):917–927, 2014.

4. Ohad Gal-Mor, Erin C Boyle, Guntram A Grassl, Constantino López-Macías, Laurel L Lenz, and Ranjit Kumar. Same species, different diseases: how and why typhoidal and non-typhoidal Salmonella enterica serovars differ. *Front Microbiol.*, 5(391), 2014.

5. John E. (John Eugene) Bennett, Raphael Dolin, Martin J. Blaser, and R. Gordon (Robert Gordon) Douglas. *Mandell, Douglas, and Bennett's principles and practice of infectious diseases*. Elsevier Saunders, 8 edition, 2015.

6. Jeffrey D. Stanaway, Andrea Parisi, Kaushik Sarkar, Brigette F. Blacker, Robert C. Reiner, Simon I. Hay, Molly R. Nixon, Christiane Dolecek, Spencer L. James, Ali H. Mokdad, Getaneh Abebe, Elham Ahmadian, Fares Alahdab, Birhan Tamene T. Alemnew, Vahid Alipour, Fatemeh Allah Bakeshei, Megbaru Debalkie Animut, Fereshteh Ansari, Jalal Arabloo, Ephrem Tsegay Asfaw, Mojtaba Bagherzadeh, Quique Bassat, Yaschilal Muche Muche Belayneh, Félix Carvalho, Ahmad Daryani, Feleke Mekonnen Demeke, Asmamaw Bizuneh Bizuneh Demis, Manisha Dubey, Eyasu Ejeta Duken, Susanna J. Dunachie, Aziz Eftekhari, Eduarda Fernandes, Reza Fouladi Fard, Getnet Azeze Gedefaw, Birhanu Geta, Katherine B. Gibney, Amir Hasanzadeh, Chi Linh Hoang, Amir Kasaeian, Amir Khater, Zelalem Teklemariam Kidanemariam, Ayenew Molla Lakew, Reza Malekzadeh, Addisu Melese, Desalegn Tadese Mengistu, Tomislav Mestrovic, Bartosz Miazgowski, Karzan Abdulmuhsin Mohammad, Mahdi Mohammadian, Abdollah Mohammadian-Hafshejani, Cuong Tat Nguyen, Long Hoang Nguyen, Son Hoang

Nguyen, Yirga Legesse Nirayo, Andrew T. Olagunju, Tinuke O. Olagunju, Hadi Pourjafar, Mostafa Qorbani, Mohammad Rabiee, Navid Rabiee, Anwar Rafay, Aziz Rezapour, Abdallah M. Samy, Sadaf G. Sepanlou, Masood Ali Shaikh, Mehdi Sharif, Mika Shigematsu, Belay Tessema, Bach Xuan Tran, Irfan Ullah, Ebrahim M. Yimer, Zoubida Zaidi, Christopher J.L. Murray, and John A. Crump. The global burden of non-typhoidal salmonella invasive disease: a systematic analysis for the Global Burden of Disease Study 2017. *The Lancet Infectious Diseases*, 19(12):1312–1324, 12 2019.

7. Abdoulie Kanteh, Abdul Karim Sesay, Nabil-Fareed Alikhan, Usman Nurudeen, Rasheed Salaudeen, Jarra Manneh, Yekini Olatunji, and Grant Mackenzie. Invasive atypical non-typhoidal Salmonella serovars in The Gambia 1 2. *bioRxiv*, page 2021.02.18.431831, 2 2021.

8. John A. Crump, Maria Sjölund-Karlsson, Melita A. Gordon, and Christopher M. Parry. Epidemiology, clinical presentation, laboratory diagnosis, antimicrobial resistance, and antimicrobial management of invasive Salmonella infections, 7 2015.

9. Girish Ramachandran, Darren J. Perkins, Patrick J. Schmidlein, Mohan E. Tulapurkar, and Sharon M. Tennant. Invasive Salmonella Typhimurium ST313 with Naturally Attenuated Flagellin Elicits Reduced Inflammation and Replicates within Macrophages. *PLoS Neglected Tropical Diseases*, 9(1), 2015.

10. Byron M. Stuart and Roscoe L. Pullen. Typhoid: Clinical Analysis of 360 Cases. *Archives of internal medicine (Chicago, Ill. : 1908)*, 78(6):629–661, 12 1946.

11. Gordon Dougan and Stephen Baker. ¡i¿Salmonella enterica¡/i¿ Serovar Typhi and the Pathogenesis of Typhoid Fever. *Annual Review of Microbiology*, 68(1):317–336, 9 2014.

12. John A Crump, Stephen P Luby, and Eric D Mintz. The global burden of typhoid fever. *Bulletin of the World Health Organization*, 82(5):346–53, 5 2004.

13. Geoffrey C Buckle, Christa L Fischer Walker, and Robert E Black. Typhoid fever and paratyphoid fever: Systematic review to estimate global morbidity and mortality for 2010. *Journal of global health*, 2(1):010401, 6 2012.

14. Jacqueline Deen, Lorenz von Seidlein, Finn Andersen, Nelson Elle, Nicholas J. White, and Yoel Lubell. Community-acquired bacterial bloodstream infections in developing countries in south and southeast Asia: A systematic review, 6 2012.

15. Elizabeth A. Reddy, Andrea V. Shaw, and John A. Crump. Community-acquired bloodstream infections in Africa: a systematic review and meta-analysis, 6 2010.

16. Ohad Gal-Mor. Persistent infection and long-term carriage of typhoidal and nontyphoidal salmonellae, 1 2019.

17. Alex Marzel, Prerak T. Desai, Alina Goren, Yosef Ilan Schorr, Israel Nissan, Steffen Porwollik, Lea Valinsky, Michael Mcclelland, Galia Rahav, and Ohad Gal-Mor. Persistent infections by

nontyphoidal salmonella in humans: Epidemiology and genetics. *Clinical Infectious Diseases*, 62(7):879–886, 4 2016.

18. Philip P Mortimer. Mr N the milker, and Dr Koch's concept of the healthy carrier. *The Lancet*, 353(9161):1354–1356, 4 1999.

19. M M Levine, R E Black, and C Lanata. Precise estimation of the numbers of chronic carriers of Salmonella typhi in Santiago, Chile, an endemic area. *The Journal of infectious diseases*, 146(6):724–6, 12 1982.

20. Geoffrey Gonzalez-Escobedo and John S. Gunn. Gallbladder epithelium as a niche for chronic salmonella carriage. *Infection and Immunity*, 81(8):2920–2930, 8 2013.

21. Verónica Urdaneta, Sara B. Hernández, and Josep Casadesús. Mutational and non mutational adaptation of Salmonella enterica to the gall bladder. *Scientific Reports*, 9(1):1–11, 12 2019.

22. John S. Gunn, Joanna M. Marshall, Stephen Baker, Sabina Dongol, Richelle C. Charles, and Edward T. Ryan. Salmonella chronic carriage: Epidemiology, diagnosis, and gallbladder persistence, 11 2014.

23. A. M. Prouty, W. H. Schwesinger, and J. S. Gunn. Biofilm formation and interaction with the surfaces of gallstones by Salmonella spp. *Infection and Immunity*, 70(5):2640–2649, 2002.

24. Robert W. Crawford, Deanna L. Gibson, William W. Kay, and John S. Gunn. Identification of a bile-induced exopolysaccharide required for salmonella biofilm formation on gallstone surfaces. *Infection and Immunity*, 76(11):5341–5349, 11 2008.

25. C. A. Fux, J. W. Costerton, P. S. Stewart, and P. Stoodley. Survival strategies of infectious biofilms, 1 2005.

26. Enea Gino Di Domenico, Ilaria Cavallo, Martina Pontone, Luigi Toma, and Fabrizio Ensoli. Biofilm Producing Salmonella Typhi: Chronic Colonization and Development of Gallbladder Cancer. *International journal of molecular sciences*, 18(9), 8 2017.

27. Jill Koshiol, Aniela Wozniak, Paz Cook, Christina Adaniel, Johanna Acevedo, Lorena Azócar, Ann W Hsing, Juan C Roa, Marcela F Pasetti, Juan F Miquel, Myron M Levine, Catterina Ferreccio, the Gallbladder Cancer Chile Working Gallbladder Cancer Chile Working Group, Carmen Gloria Aguayo, Sergio Baez, Alfonso Díaz, Héctor Molina, Carolina Miranda, Claudia Castillo, Andrea Tello, Gonzalo Durán, Carolina Paz Delgado, Rodrigo Quevedo, Susana Pineda, Tiare la Barra, Cristian Reyes, Cristina Alegría, Claudia Aguayo, Héctor Losada, Juan Carlos Arraya, Enrique Bellolio, Oscar Tapia, Jaime López, Karie Medina, Paulina Barraza, Sandra Catalán, Pía Riquelme, Lorena Órdenes, Raúl Garcés, Claudia Duarte, and Allan Hildesheim. Salmonella enterica serovar Typhi and gallbladder cancer: a case-control study and meta-analysis. *Cancer medicine*, 5(11):3310–3235, 11 2016.

28. Geoffrey Gonzalez-Escobedo, Joanna M. Marshall, and John S. Gunn. Chronic and acute infection of the gall bladder by Salmonella Typhi: Understanding the carrier state. *Nature Reviews Microbiology*, 9(1):9–14, 1 2011.

29. MK Bhan, Rajiv Bahl, and Shinjini Bhatnagar. Typhoid and paratyphoid fever. *The Lancet*, 366(9487):749–762, 8 2005.

30. Tiziana Scanu, Robbert M. Spaapen, Jeroen M. Bakker, Chandra Bhan Pratap, Lin-en Wu, Ingrid Hofland, Annegien Broeks, Vijay Kumar Shukla, Mohan Kumar, Hans Janssen, Ji-Ying Song, E. Andra Neefjes-Borst, Hein te Riele, David W. Holden, Gopal Nath, and Jacques Neefjes. Salmonella Manipulation of Host Signaling Pathways Provokes Cellular Transformation Associated with Gallbladder Carcinoma. *Cell Host & Microbe*, 17(6):763–774, 6 2015.

31. Robert H. Gilman, Miguel Terminel, Myron M. Levine, Pablo Hernandez-Mendoza, and Richard B. Hornick. RELATIVE EFFICACY OF BLOOD, URINE, RECTAL SWAB, BONE-MARROW, AND ROSE-SPOT CULTURES FOR RECOVERY OF SALMONELLA TYPHI IN TYPHOID FEVER. *The Lancet*, 305(7918):1211–1213, 5 1975.

32. Jason R. Andrews and Edward T. Ryan. Diagnostics for invasive Salmonella infections: Current challenges and future directions, 6 2015.

33. M. Hussein Gasem, M. W.V. Dolmans, B. Bambang Isbandrio, H. Wahyono, M. Keuter, and R. Djokomoeljanto. Culture of Salmonella typhi and Salmonella paratyphi from blood and bone marrow in suspected typhoid fever. *Tropical and Geographical Medicine*, 47(4):164–167, 1995.

34. J. Wain, P. V.B. Bay, H. Vinh, N. M. Duong, T. S. Diep, A. L. Walsh, C. M. Parry, R. P. Hasserjian, V. A. Ho, T. T. Hien, J. Farrar, N. J. White, and N. P.J. Day. Quantitation of bacteria in bone marrow from patients with typhoid fever: Relationship between counts and clinical features. *Journal of Clinical Microbiology*, 39(4):1571–1576, 2001.

35. Christopher M. Parry, Lalith Wijedoru, Amit Arjyal, and Stephen Baker. The utility of diagnostic tests for enteric fever in endemic locations, 2011.

36. T. E. WOODWARD and J. E. SMADEL. Preliminary report on the beneficial effect of chloromycetin in the. *Annals of internal medicine*, 29(1):131–134, 1948.

37. Christopher M. Parry, Tran Tinh Hien, Gordon Dougan, Nicholas J. White, and Jeremy J. Farrar. Typhoid Fever. *New England Journal of Medicine*, 347(22):1770–1782, 11 2002.

38. Farah N Qamar, Mohammad T Yousafzai, Irum F Dehraj, Sadia Shakoor, Seema Irfan, Aneeta Hotwani, Muhammad J Hunzai, Rozina S Thobani, Najeeb Rahman, Junaid Mehmood, Caitlin Hemlock, Ashraf M Memon, Jason R Andrews, Stephen P Luby, Denise O Garrett, Ashley T Longley, Kashmira Date, and Samir K Saha. Antimicrobial Resistance in Typhoidal Salmonella: Surveillance for Enteric Fever in Asia Project, 2016–2019. *Clinical Infectious Diseases*, 71(Supplement_3):S276–S284, 12 2020.

39. Adnan Mannan, Mohammad Shohel, Sultana Rajia, Niaz Uddin Mahmud, Sanjana Kabir, and Imtiaj Hasan. A cross sectional study on antibiotic resistance pattern of Salmonella typhi clinical isolates from Bangladesh. *Asian Pacific Journal of Tropical Biomedicine*, 4(4):306–311, 2014.

40. Zoe A. Dyson, Elizabeth J. Klemm, Sophie Palmer, and Gordon Dougan. Antibiotic resistance and typhoid. *Clinical Infectious Diseases*, 68(Supplement_2):S165–S170, 3 2019.

41. Nelly Mejia, Farah Qamar, Mohammad T. Yousafzai, Jamal Raza, Denise O. Garrett, Kashmira Date, Taiwo Abimbola, and Sarah W. Pallas. Typhoid and Paratyphoid Cost of Illness in Pakistan: Patient and Health Facility Costs from the Surveillance for Enteric Fever in Asia Project II. *Clinical Infectious Diseases*, 71(Supplement_3):S319–S335, 11 2020.

42. Vanessa K Wong, Stephen Baker, Derek J Pickard, Julian Parkhill, Andrew J Page, Nicholas A Feasey, Robert A Kingsley, Nicholas R Thomson, Jacqueline A Keane, François-Xavier Weill, David J Edwards, Jane Hawkey, Simon R Harris, Alison E Mather, Amy K Cain, James Hadfield, Peter J Hart, Nga Tran Vu Thieu, Elizabeth J Klemm, Dafni A Glinos, Robert F Breiman, Conall H Watson, Samuel Kariuki, Melita A Gordon, Robert S Heyderman, Chinyere Okoro, Jan Jacobs, Octavie Lunguya, W John Edmunds, Chisomo Msefula, Jose A Chabalgoity, Mike Kama, Kylie Jenkins, Shanta Dutta, Florian Marks, Josefina Campos, Corinne Thompson, Stephen Obaro, Calman A MacLennan, Christiane Dolecek, Karen H Keddy, Anthony M Smith, Christopher M Parry, Abhilasha Karkey, E Kim Mulholland, James I Campbell, Sabina Dongol, Buddha Basnyat, Muriel Dufour, Don Bandaranayake, Take Toleafoa Naseri, Shalini Pravin Singh, Mochammad Hatta, Paul Newton, Robert S Onsare, Lupeoletalalei Isaia, David Dance, Viengmon Davong, Guy Thwaites, Lalith Wijedoru, John A Crump, Elizabeth De Pinna, Satheesh Nair, Eric J Nilles, Duy Pham Thanh, Paul Turner, Sona Soeng, Mary Valcanis, Joan Powling, Karolina Dimovski, Geoff Hogg, Jeremy Farrar, Kathryn E Holt, and Gordon Dougan. Phylogeographical analysis of the dominant multidrug-resistant H58 clade of Salmonella Typhi identifies inter- and intracontinental transmission events. *Nature Genetics*, 47(6):632–639, 6 2015.

43. Elizabeth J Klemm, Sadia Shakoor, Andrew J Page, Farah Naz Qamar, Kim Judge, Dania K Saeed, Vanessa K Wong, Timothy J Dallman, Satheesh Nair, Stephen Baker, Ghazala Shaheen, Shahida Qureshi, Mohammad Tahir Yousafzai, Muhammad Khalid Saleem, Zahra Hasan, Gordon Dougan, and Rumina Hasan. Emergence of an Extensively Drug-Resistant Salmonella enterica Serovar Typhi Clone Harboring a Promiscuous Plasmid Encoding Resistance to Fluoroquinolones and Third-Generation Cephalosporins. *mBio*, 9(1), 3 2018.

44. Kathryn E. Holt, Minh Duy Phan, Stephen Baker, Pham Thanh Duy, Tran Vu Thieu Nga, Satheesh Nair, A. Keith Turner, Ciara Walsh, Séamus Fanning, Sinéad Farrell-Ward, Shanta Dutta, Sam Kariuki, François Xavier WeillFranç, Julian Parkhill, Gordon Dougan, and John Wain. Emergence of a globally dominant inchi1 plasmid type associated with multiple drug resistant typhoid. *PLoS Neglected Tropical Diseases*, 5(7):1245, 2011.

45. Nicholas A. Feasey, Katherine Gaskell, Vanessa Wong, Chisomo Msefula, George Selemani, Save Kumwenda, Theresa J. Allain, Jane Mallewa, Neil Kennedy, Aisleen Bennett, Joram O. Nyirongo, Patience A. Nyondo, Madalitso D. Zulu, Julian Parkhill, Gordon Dougan, Melita A. Gordon, and Robert S. Heyderman. Rapid Emergence of Multidrug Resistant, H58-Lineage Salmonella Typhi in Blantyre, Malawi. *PLoS Neglected Tropical Diseases*, 9(4):e0003748, 4 2015.

46. Carl Llor and Lars Bjerrum. Antimicrobial resistance: Risk associated with antibiotic overuse and initiatives to reduce the problem, 2014.

47. Wim L Cuypers, Jan Jacobs, Vanessa Wong, Elizabeth J Klemm, Stijn Deborggraeve, and Sandra Van Puyvelde. Fluoroquinolone resistance in Salmonella: insights by whole-genome sequencing. *Microbial Genomics*, 4(7), 7 2018.

48. Calman A. MacLennan, Laura B. Martin, and Francesca Micoli. Vaccines against invasive Salmonella disease: Current status and future directions, 2014.

49. Michael E. Pichichero. Protein carriers of conjugate vaccines Characteristics, development, and clinical trials, 12 2013.

50. Monjori Mitra, Nitin Shah, Apurba Ghosh, Suparna Chatterjee, Iqbal Kaur, Nisha Bhattacharya, and Suparna Basu. Efficacy and safety of vi-tetanus toxoid conjugated typhoid vaccine (PedaTyph™) in Indian children: School based cluster randomized study. *Human Vaccines and Immunotherapeutics*, 12(4):939–945, 4 2016.

51. Mila Shakya, Rachel Colin-Jones, Katherine Theiss-Nyland, Merryn Voysey, Dikshya Pant, Nicola Smith, Xinxue Liu, Susan Tonks, Olga Mazur, Yama G. Farooq, Jenny Clarke, Jennifer Hill, Anup Adhikari, Sabina Dongol, Abhilasha Karkey, Binod Bajracharya, Sarah Kelly, Meeru Gurung, Stephen Baker, Kathleen M. Neuzil, Shrijana Shrestha, Buddha Basnyat, and Andrew J. Pollard. Phase 3 Efficacy Analysis of a Typhoid Conjugate Vaccine Trial in Nepal. *New England Journal of Medicine*, 381(23):2209–2218, 12 2019.

52. Virginia E. Pitzer, Cayley C. Bowles, Stephen Baker, Gagandeep Kang, Veeraraghavan Balaji, Jeremy J. Farrar, and Bryan T. Grenfell. Predicting the Impact of Vaccination on the Transmission Dynamics of Typhoid in South Asia: A Mathematical Modeling Study. *PLoS Neglected Tropical Diseases*, 8(1):40, 2014.

53. Roman G. Gerlach, Daniela Jäckel, Bärbel Stecher, Carolin Wagner, Andrei Lupas, Wolf Dietrich Hardt, and Michael Hensel. Salmonella Pathogenicity Island 4 encodes a giant non-fimbrial adhesin and the cognate type 1 secretion system. *Cellular Microbiology*, 9(7):1834–1850, 7 2007.

54. Sandra L. Marcus, John H. Brumell, Cheryl G. Pfeifer, and B. Brett Finlay. Salmonella pathogenicity islands: Big virulence in small packages, 2000.

55. Martin Lorkowski, Alfonso Felipe-López, Claudia A Danzer, Nicole Hansmeier, and Michael Hensel. Salmonella enterica invasion of polarized epithelial cells is a highly cooperative effort. *Infection and immunity*, 82(6):2657–67, 6 2014.

56. Olivia Steele-Mortimer. The Salmonella-containing vacuole-Moving with the times, 2 2008.

57. Katelyn Knuff and B. Brett Finlay. What the SIF Is happening—The role of intracellular Salmonella-induced filaments. *Frontiers in Cellular and Infection Microbiology*, 7(JUL):335, 7 2017.

58. Viktoria Liss, A. Leoni Swart, Alexander Kehl, Natascha Hermanns, Yuying Zhang, Deepak Chikkaballi, Nathalie Böhles, Jörg Deiwick, and Michael Hensel. Salmonella enterica Remodels the Host Cell Endosomal System for Efficient Intravacuolar Nutrition. *Cell Host & Microbe*, 21(3):390–402, 3 2017.

59. Rita Figueira and David W. Holden. Functions of the Salmonella pathogenicity island 2 (SPI-2) type III secretion system effectors, 5 2012.

60. Carmen R. Beuzón, Suzana P. Salcedo, and David W. Holden. Growth and killing of a Salmonella enterica serovar Typhimurium sifA mutant strain in the cytosol of different host cell lines. *Microbiology*, 148(9):2705–2715, 9 2002.

61. S. G. Garvis, C. R. Beuzón, and D. W. Holden. A role for the PhoP/Q regulon in inhibition of fusion between lysosomes and Salmonella-containing vacuoles in macrophages. *Cellular Microbiology*, 3(11):731–744, 2001.

62. Shehla Hashim, Konark Mukherjee, Manoj Raje, Sandip K. Basu, and Amitabha Mukhopadhyay. Live Salmonella modulate expression of Rab proteins to persist in a specialized compartment and escape transport to lysosomes. *Journal of Biological Chemistry*, 275(21):16281–16288, 5 2000.

63. Kieran McGourty, Teresa L. Thurston, Sophie A. Matthews, Laurie Pinaud, Luís Jaime Mota, and David W. Holden. Salmonella inhibits retrograde trafficking of mannose-6-phosphate receptors and lysosome function. *Science*, 338(6109):963–967, 11 2012.

64. Sandeepa M. Eswarappa, Vidya Devi Negi, Sangeeta Chakraborty, B. K.Chandrasekhar Sagar, and Dipshikha Chakravortty. Division of the Salmonella-containing vacuole and depletion of acidic lysosomes in Salmonella-infected host cells are novel strategies of Salmonella enterica to avoid lysosomes. *Infection and Immunity*, 78(1):68–79, 1 2010.

65. Leigh A. Knodler, Shauna M. Crowley, Ho Pan Sham, Hyungjun Yang, Marie Wrande, Caixia Ma, Robert K. Ernst, Olivia Steele-Mortimer, Jean Celli, and Bruce A. Vallance. Noncanonical inflammasome activation of caspase-4/caspase-11 mediates epithelial defenses against enteric bacterial pathogens. *Cell Host and Microbe*, 16(2):249–256, 8 2014.

66. Sanjeev Mariathasan, Kim Hewton, Denise M. Monack, Domagoj Vucic, Dorothy M. French, Wyne P. Lee, Meron Roose-Girma, Sharon Erickson, and Vishva M. Dixit. Differential activation of the inflammasome by caspase-1 adaptors ASC and Ipaf. *Nature*, 430(6996):213–218, 7 2004.

67. Mikael E. Sellin, Anna A. Müller, Boas Felmy, Tamas Dolowschiak, Médéric Diard, Aubry Tardivel, Kendle M. Maslowski, and Wolf Dietrich Hardt. Epithelium-intrinsic NAIP/NLRC4 inflammasome drives infected enterocyte expulsion to restrict salmonella replication in the intestinal mucosa. *Cell Host and Microbe*, 16(2):237–248, 8 2014.

68. Yue Zhao and Feng Shao. Diverse mechanisms for inflammasome sensing of cytosolic bacteria and bacterial virulence, 2 2016.

69. Sebastian E. Winter, Maria G. Winter, Vidya Atluri, Victor Poon, Everton L. Romão, Renée M. Tsolis, and Andreas J. Bäumler. The flagellar regulator TviA reduces pyroptosis by Salmonella enterica serovar Typhi. *Infection and Immunity*, 83(4):1546–1555, 4 2015.

70. Sarah Carden, Chinyere Okoro, Gordon Dougan, and Denise Monack. Non-typhoidal Salmonella Typhimurium ST313 isolates that cause bacteremia in humans stimulate less inflammasome activation than ST19 isolates associated with gastroenteritis. *Pathogens and disease*, 73(4):23, 6 2015.

71. Hanna K. de Jong, Chris M. Parry, Tom van der Poll, and W. Joost Wiersinga. Host-Pathogen Interaction in Invasive Salmonellosis. *PLoS Pathogens*, 8(10):e1002933, 10 2012.

72. Parameth Thiennimitr, Sebastian E. Winter, Maria G. Winter, Mariana N. Xavier, Vladimir Tolstikov, Douglas L. Huseby, Torsten Sterzenbach, Renée M. Tsolis, John R. Roth, and Andreas J. Bäumler. Intestinal inflammation allows Salmonella to use ethanolamine to compete with the microbiota. *Proceedings of the National Academy of Sciences of the United States of America*, 108(42):17480–17485, 10 2011.

73. Bärbel Stecher, Riccardo Robbiani, Alan W Walker, Astrid M Westendorf, Manja Barthel, Marcus Kremer, Samuel Chaffron, Andrew J Macpherson, Jan Buer, Julian Parkhill, Gordon Dougan, Christian von Mering, and Wolf-Dietrich Hardt. Salmonella enterica Serovar Typhimurium Exploits Inflammation to Compete with the Intestinal Microbiota. *PLoS Biology*, 5(10):e244, 8 2007.

74. B A McCormick, S I Miller, D Carnes, and J L Madara. Transepithelial signaling to neutrophils by salmonellae: a novel virulence mechanism for gastroenteritis. *Infection and immunity*, 63(6):2302–9, 6 1995.

75. Kathryn G. Watson and David W. Holden. Dynamics of growth and dissemination of Salmonella in vivo. *Cellular Microbiology*, 12(10):1389–1397, 10 2010.

76. Ion Rusan Vladoianu, Hernán R. Chang, and Jean Claude Pechère. Expression of host resistance to Salmonella typhi and Salmonella typhimurium: bacterial survival within macrophages of murine and human origin. *Microbial Pathogenesis*, 8(2):83–90, 1990.

77. Jeongmin Song, Tim Willinger, Anthony Rongvaux, Elizabeth E Eynon, Sean Stevens, Markus G Manz, Richard A Flavell, and Jorge E Galán. A mouse model for the human pathogen Salmonella typhi. *Cell host & microbe*, 8(4):369–76, 10 2010.

78. Lisa Del Bel Belluz, Riccardo Guidi, Ioannis S. Pateras, Laura Levi, Boris Mihaljevic, Syed Fazle Rouf, Marie Wrande, Marco Candela, Silvia Turroni, Claudia Nastasi, Clarissa Consolandi, Clelia Peano, Toma Tebaldi, Gabriella Viero, Vassilis G. Gorgoulis, Thorbjørn Krejsgaard, Mikael Rhen, and Teresa Frisan. The Typhoid Toxin Promotes Host Survival and the Establishment of a Persistent Asymptomatic Infection. *PLOS Pathogens*, 12(4):e1005528, 4 2016.

79. Océane C.B. Martin, Anna Bergonzini, Federica D'Amico, Puran Chen, Jerry W. Shay, Jacques Dupuy, Mattias Svensson, Maria G. Masucci, and Teresa Frisan. Infection with genotoxin-producing Salmonella enterica synergises with loss of the tumour suppressor APC in promoting genomic instability via the PI3K pathway in colonic epithelial cells. *Cellular Microbiology*, 21(12), 12 2019.

80. Chantal G. Forest, Elyse Ferraro, Sébastien C. Sabbagh, and France Daigle. Intracellular survival of Salmonella enterica serovar Typhi in human macrophages is independent of Salmonella pathogenicity island (SPI)-2. *Microbiology*, 156(12):3689–3698, 12 2010.

81. Jeongmin Song, Xiang Gao, and Jorge E. Galán. Structure and function of the Salmonella Typhi chimaeric A 2 B 5 typhoid toxin. *Nature*, 499(7458):350–354, 2013.

82. Ramkumar Mathur, Hyunju Oh, Dekai Zhang, Sung-Gyoo Park, Jin Seo, Alicia Koblansky, Matthew S. Hayden, and Sankar Ghosh. A Mouse Model of Salmonella Typhi Infection. *Cell*, 151(3):590–602, 10 2012.

83. M Firoz Mian, Elisabeth A Pek, Meghan J Chenoweth, and Ali A Ashkar. Humanized mice are susceptible to Salmonella typhi infection. *Cellular & molecular immunology*, 8(1):83–7, 1 2011.

84. Michael McClelland, Kenneth E. Sanderson, John Spieth, Sandra W. Clifton, Phil Latreille, Laura Courtney, Steffen Porwollik, Johar Ali, Mike Dante, Feiyu Du, Shunfang Hou, Dan Layman, Shawn Leonard, Christine Nguyen, Kelsi Scott, Andrea Holmes, Neenu Grewal, Elizabeth Mulvaney, Ellen Ryan, Hui Sun, Liliana Florea, Webb Miller, Tamberlyn Stoneking, Michael Nhan, Robert Waterston, and Richard K. Wilson. Complete genome sequence of Salmonella enterica serovar Typhimurium LT2. *Nature*, 413(6858):852–856, 10 2001.

85. Robert A. Kingsley, Chisomo L. Msefula, Nicholas R. Thomson, Samuel Kariuki, Kathryn E. Holt, Melita A. Gordon, David Harris, Louise Clarke, Sally Whitehead, Vartul Sangal, Kevin Marsh, Mark Achtman, Malcolm E. Molyneux, Martin Cormican, Julian Parkhill, Calman A. MacLennan, Robert S. Heyderman, and Gordon Dougan. Epidemic multiple drug resistant Salmonella Typhimurium causing invasive disease in sub-Saharan Africa have a distinct genotype. *Genome Research*, 19(12):2279–2287, 12 2009.

86. Michael McClelland, Kenneth E Sanderson, Sandra W Clifton, Phil Latreille, Steffen Porwollik, Aniko Sabo, Rekha Meyer, Tamberlyn Bieri, Phil Ozersky, Michael McLellan, C Richard Harkins, Chunyan Wang, Christine Nguyen, Amy Berghoff, Glendoria Elliott, Sara Kohlberg, Cindy Strong, Feiyu Du, Jason Carter, Colin Kremizki, Dan Layman, Shawn Leonard, Hui Sun,

Lucinda Fulton, William Nash, Tracie Miner, Patrick Minx, Kim Delehaunty, Catrina Fronick, Vincent Magrini, Michael Nhan, Wesley Warren, Liliana Florea, John Spieth, and Richard K Wilson. Comparison of genome degradation in Paratyphi A and Typhi, human-restricted serovars of Salmonella enterica that cause typhoid. *Nature Genetics*, 36(12):1268–1274, 12 2004.

87. Stefania Spanò and Jorge E Galán. A Rab32-dependent pathway contributes to Salmonella Typhi host restriction. *NIH Public Access*, 338(6109):960–963, 2012.

88. Tamding Wangdi, Sebastian E Winter, and Andreas J Bäumler. Typhoid fever: "you can't hit what you can't see". *Gut microbes*, 3(2):88–92, 2012.

89. R. Paul Wilson, Sebastian E. Winter, Alanna M. Spees, Maria G. Winter, Jessalyn H. Nishimori, Jesus F. Sanchez, Sean Paul Nuccio, Robert W. Crawford, Çagla Tükel, and Andreas J. Bäumler. The Vi capsular polysaccharide prevents complement receptor 3-mediated clearance of Salmonella enterica serotype Typhi. *Infection and Immunity*, 79(2):830–837, 2 2011.

90. D M Hone, S R Attridge, B Forrest, R Morona, D Daniels, J T LaBrooy, R C Bartholomeusz, D J Shearman, and J Hackett. A galE via (Vi antigen-negative) mutant of Salmonella typhi Ty2 retains virulence in humans. *Infection and immunity*, 56(5):1326–33, 5 1988.

91. Erik Haghjoo and Jorge E Galán. Salmonella typhi encodes a functional cytolethal distending toxin that is delivered into host cells by a bacterial-internalization pathway. *Proceedings of the National Academy of Sciences of the United States of America*, 101(13):4614–9, 3 2004.

92. Jorge E Galán. Typhoid toxin provides a window into typhoid fever and the biology of Salmonella Typhi. *Proceedings of the National Academy of Sciences of the United States of America*, 113(23):6338–44, 6 2016.

93. Henk C den Bakker, Andrea I Moreno Switt, Gregory Govoni, Craig A Cummings, Matthew L Ranieri, Lovorka Degoricija, Karin Hoelzer, Lorraine D Rodriguez-Rivera, Stephanie Brown, Elena Bolchacova, Manohar R Furtado, and Martin Wiedmann. Genome sequencing reveals diversification of virulence factor content and possible host adaptation in distinct subpopulations of Salmonella enterica. *BMC Genomics*, 12(1), 12 2011.

94. Sohyoung Lee, Yi An Yang, Shawn K. Milano, Tri Nguyen, Changhwan Ahn, Ji Hyun Sim, Andrew J. Thompson, Eric C. Hillpot, Gyeongshik Yoo, James C. Paulson, and Jeongmin Song. Salmonella Typhoid Toxin PltB Subunit and Its Non-typhoidal Salmonella Ortholog Confer Differential Host Adaptation and Virulence. *Cell Host and Microbe*, 27(6):937–949, 6 2020.

95. Hélène Hodak and Jorge E. Galán. A Salmonella Typhi homologue of bacteriophage muramidases controls typhoid toxin secretion. *EMBO Reports*, 14(1):95–102, 1 2013.

96. Stefania Spanò, Juan E. Ugalde, and Jorge E. Galán. Delivery of a Salmonella Typhi Exotoxin from a Host Intracellular Compartment. *Cell Host & Microbe*, 3(1):30–38, 1 2008.

97. Dragana Nešić, Yun Hsu, and C. Erec Stebbins. Assembly and function of a bacterial genotoxin. *Nature*, 429(6990):429–433, 5 2004.

98. Rachel A. Miller and Martin Wiedmann. The cytolethal distending toxin produced by nontyphoidal Salmonella serotypes javiana, montevideo, oranienburg, and mississippi induces DNA damage in a manner similar to that of serotype Typhi. *mBio*, 7(6), 1 2016.

99. Rachel A. Miller, Michael I. Betteken, Xiaodong Guo, Craig Altier, Gerald E. Duhamel, and Martin Wiedmann. The typhoid toxin produced by the Nontyphoidal Salmonella enterica Serotype javiana is required for induction of a DNA damage response in Vitro and systemic spread in Vivo. *mBio*, 9(2), 3 2018.

100. Malick M. Gibani, Elizabeth Jones, Amber Barton, Celina Jin, Juliette Meek, Susana Camara, Ushma Galal, Eva Heinz, Yael Rosenberg-Hasson, Gerlinde Obermoser, Claire Jones, Danielle Campbell, Charlotte Black, Helena Thomaides-Brears, Christopher Darlow, Christina Dold, Laura Silva-Reyes, Luke Blackwell, Maria Lara-Tejero, Xuyao Jiao, Gabrielle Stack, Christoph J. Blohmke, Jennifer Hill, Brian Angus, Gordon Dougan, Jorge Galán, and Andrew J. Pollard. Investigation of the role of typhoid toxin in acute typhoid fever in a human challenge model. *Nature Medicine*, 25(7):1082–1088, 7 2019.

101. Alexander Chong, Sohyoung Lee, Yi-An Yang, and Jeongmin Song. The Role of Typhoid Toxin in Salmonella Typhi Virulence. *The Yale journal of biology and medicine*, 90(2):283–290, 6 2017.

102. Joseph M. DiRienzo. Cytolethal Distending Toxin: A Unique Variation on the AB Toxin Paradigm. *New Journal of Science*, 2014:1–26, 9 2014.

103. M. Lara-Tejero and J. E. Galán. CdtA, CdtB, and CdtC form a tripartite complex that is required for cytolethal distending toxin activity. *Infection and Immunity*, 69(7):4358–4365, 7 2001.

104. Margaret Pittman. Pertussis toxin: The cause of the harmful effects and prolonged immunity of whooping cough. a hypothesis. *Reviews of Infectious Diseases*, 1(3):401–412, 1979.

105. Xiang Gao, Lingquan Deng, Gabrielle Stack, Hai Yu, Xi Chen, Yuko Naito-Matsui, Ajit Varki, and Jorge E. Galán. Evolution of host adaptation in the Salmonella typhoid toxin. *Nature Microbiology*, 2(12):1592–1599, 12 2017.

106. Angela E M Ibler, Mohamed ElGhazaly, Kathryn L Naylor, Natalia A Bulgakova, Sherif F. El-Khamisy, and Daniel Humphreys. Typhoid toxin exhausts the RPA response to DNA replication stress driving senescence and Salmonella infection. *Nature Communications*, 10(1):4040, 2019.

107. Océane C.B. Martin, Anna Bergonzini, Maria Lopez Chiloeches, Eleni Paparouna, Deborah Butter, Sofia D.P. Theodorou, Maria M. Haykal, Elisa Boutet-Robinet, Toma Tebaldi, Andrew Wakeham, Mikael Rhen, Vassilis G. Gorgoulis, Tak Mak, Ioannis S. Pateras, and Teresa Frisan.

Influence of the microenvironment on modulation of the host response by typhoid toxin. *Cell Reports*, 35(1), 4 2021.

108. Shu-Jung Chang, Jeongmin Song, and Jorge E Galán. Receptor-Mediated Sorting of Typhoid Toxin during Its Export from Salmonella Typhi-Infected Cells. *Cell host & microbe*, 20(5):682–689, 11 2016.

109. Lingquan Deng, Jeongmin Song, Xiang Gao, Jiawei Wang, Hai Yu, Xi Chen, Nissi Varki, Yuko Naito-Matsui, Jorge E Galán, and Ajit Varki. Host adaptation of a bacterial toxin from the human pathogen Salmonella Typhi. *Cell*, 159(6):1290–9, 12 2014.

110. G Edsall, S Gaines, M Landy, W D Tigertt, H Sprinz, R J Trapani, A D Mandel, and A S Benenson. Studies on infection and immunity in experimental typhoid fever. I. Typhoid fever in chimpanzees orally infected with Salmonella typhosa. *The Journal of experimental medicine*, 112(1):143–66, 7 1960.

111. Shu-Jung Chang, Sheng Chih Jin, Xuyao Jiao, and Jorge E. Galán. Unique features in the intracellular transport of typhoid toxin revealed by a genome-wide screen. *PLOS Pathogens*, 15(4):e1007704, 4 2019.

112. Somshuvra Mukhopadhyay and Adam D. Linstedt. Retrograde trafficking of AB5 toxins: Mechanisms to therapeutics, 10 2013.

113. Jeffrey M. Williams and Billy Tsai. Intracellular trafficking of bacterial toxins, 8 2016.

114. Kirsten Sandvig and Bo van Deurs. Membrane Traffic Exploited by Protein Toxins. *Annual Review of Cell and Developmental Biology*, 18(1):1–24, 11 2002.

115. Kirsten Sandvig, Tore Skotland, Bo Van Deurs, and Tove Irene Klokk. Retrograde transport of protein toxins through the Golgi apparatus, 9 2013.

116. Jin A. Cho, Daniel J.-F. Chinnapen, Emil Aamar, Yvonne M. te Welscher, Wayne I. Lencer, and Ramiro Massol. Insights on the trafficking and retro-translocation of glycosphingolipid-binding bacterial toxins. *Frontiers in Cellular and Infection Microbiology*, 2:51, 4 2012.

117. Roger D. Kornberg. Chromatin structure: A repeating unit of histones and DNA. *Science*, 184(4139):868–871, 5 1974.

118. Karolin Luger, Armin W. Mäder, Robin K. Richmond, David F. Sargent, and Timothy J. Richmond. Crystal structure of the nucleosome core particle at 2.8 Å resolution. *Nature*, 389(6648):251–260, 1997.

119. Gina Arents and Evangelos N Moudrianakis. Topography of the histone octamer surface: repeating structural motifs utilized in the docking of nucleosomal DNA. *Proceedings of the National Academy of Sciences*, 90(22):10489–10493, 11 1993.

120. Steven W. Criscione, Yee Voan Teo, and Nicola Neretti. The Chromatin Landscape of Cellular Senescence, 11 2016.

121. Andrew J. Bannister and Tony Kouzarides. Regulation of chromatin by histone modifications, 3 2011.

122. Katrien Vermeulen, Dirk R. Van Bockstaele, and Zwi N. Berneman. The cell cycle: a review of regulation, deregulation and therapeutic targets in cancer. *Cell Proliferation*, 36(3):131–149, 6 2003.

123. Amit Deshpande, Peter Sicinski, and Philip W. Hinds. Cyclins and cdks in development and cancer: A perspective, 4 2005.

124. Naoko Ohtani, Kimi Yamakoshi, Akiko Takahashi, and Eiji Hara. The p16INK4a-RB pathway: Molecular link between cellular senescence and tumor suppression, 8 2004.

125. Nimrat Chatterjee and Graham C. Walker. Mechanisms of DNA damage, repair, and mutagenesis, 6 2017.

126. Monika Podhorecka, Andrzej Skladanowski, and Przemyslaw Bozko. H2AX phosphorylation: Its role in DNA damage response and cancer therapy, 2010.

127. Arkady Celeste, Oscar Fernandez-Capetillo, Michael J. Kruhlak, Duane R. Pilch, David W. Staudt, Alicia Lee, Robert F. Bonner, William M. Bonner, and André Nussenzweig. Histone H2AX phosphorylation is dispensable for the initial recognition of DNA breaks. *Nature Cell Biology*, 5(7):675–679, 7 2003.

128. Sandeep Burma, Benjamin P. Chen, Michael Murphy, Akihiro Kurimasa, and David J. Chen. ATM Phosphorylates Histone H2AX in Response to DNA Double-strand Breaks. *Journal of Biological Chemistry*, 276(45):42462–42467, 11 2001.

129. Abdelghani Mazouzi, Alexey Stukalov, André C. Müller, Doris Chen, Marc Wiedner, Jana Prochazkova, Shih-Chieh Chiang, Michael Schuster, Florian P. Breitwieser, Andreas Pichlmair, Sherif F. El-Khamisy, Christoph Bock, Robert Kralovics, Jacques Colinge, Keiryn L. Bennett, and Joanna I. Loizou. A Comprehensive Analysis of the Dynamic Response to Aphidicolin-Mediated Replication Stress Uncovers Targets for ATM and ATMIN. *Cell Reports*, 15(4):893–908, 4 2016.

130. Irene M. Ward and Junjie Chen. Histone H2AX Is Phosphorylated in an ATR-dependent Manner in Response to Replicational Stress. *Journal of Biological Chemistry*, 276(51):47759–47762, 12 2001.

131. Bipasha Mukherjee, Chase Kessinger, Junya Kobayashi, Benjamin P.C. Chen, David J. Chen, Aloke Chatterjee, and Sandeep Burma. DNA-PK phosphorylates histone H2AX during apoptotic DNA fragmentation in mammalian cells. *DNA Repair*, 5(5):575–590, 5 2006.

132. Qi Ding, Yeturu V. R. Reddy, Wei Wang, Timothy Woods, Pauline Douglas, Dale A. Ramsden, Susan P. Lees-Miller, and Katheryn Meek. Autophosphorylation of the Catalytic Subunit of the DNA-Dependent Protein Kinase Is Required for Efficient End Processing during DNA Double-Strand Break Repair. *Molecular and Cellular Biology*, 23(16):5836–5848, 8 2003.

133. Hongyan Wang, Minli Wang, Huichen Wang, Wilfried Böcker, and George Iliakis. Complex H2AX phosphorylation patterns by multiple kinases including ATM and DNA-PK in human cells exposed to ionizing radiation and treated with kinase inhibitors. *Journal of Cellular Physiology*, 202(2):492–502, 2 2005.

134. Nnennaya Kanu and Axel Behrens. ATMINistrating ATM signaling. *Cell Cycle*, 7(22):3483–3486, 11 2008.

135. S. Matsuoka, B. A. Ballif, A. Smogorzewska, E. R. McDonald, K. E. Hurov, J. Luo, C. E. Bakalarski, Z. Zhao, N. Solimini, Y. Lerenthal, Y. Shiloh, S. P. Gygi, and S. J. Elledge. ATM and ATR Substrate Analysis Reveals Extensive Protein Networks Responsive to DNA Damage. *Science*, 316(5828):1160–1166, 5 2007.

136. Keith W. Caldecott. Single-strand break repair and genetic disease, 8 2008.

137. Michelle K. Zeman and Karlene A. Cimprich. Causes and consequences of replication stress, 1 2014.

138. Marc S Wold. REPLICATION PROTEIN A:A Heterotrimeric, Single-Stranded DNA-Binding Protein Required for Eukaryotic DNA Metabolism. *Annual Review of Biochemistry*, 66(1):61–92, 6 1997.

139. Vitaly M. Vassin, Rachel William Anantha, Elena Sokolova, Shlomo Kanner, and James A. Borowiec. Human RPA phosphorylation by ATR stimulates DNA synthesis and prevents ssDNA accumulation during DNA-replication stress. *Journal of Cell Science*, 122(22):4070–4080, 11 2009.

140. Felix E. Kemmerich, Peter Daldrop, Cosimo Pinto, Maryna Levikova, Petr Cejka, and Ralf Seidel. Force regulated dynamics of RPA on a DNA fork. *Nucleic Acids Research*, 44(12):5837–5848, 7 2016.

141. Lee Zou and Stephen J. Elledge. Sensing DNA damage through ATRIP recognition of RPA-ssDNA complexes. *Science*, 300(5625):1542–1548, 6 2003.

142. Qinghua Liu, Saritha Guntuku, Xian Shu Cui, Shuhei Matsuoka, David Cortez, Katsuyuki Tamai, Guangbin Luo, Sandra Carattini-Rivera, Francisco DeMayo, Allan Bradley, Larry A. Donehower, and Stephen J. Elledge. Chk1 is an essential kinase that is regulated by Atr and required for the G2/M DNA damage checkpoint. *Genes and Development*, 14(12):1448–1459, 6 2000.

143. Fabrizio D'Adda Di Fagagna. Living on a break: Cellular senescence as a DNA-damage response, 7 2008.

144. Robert S. Weiss, Shuhei Matsuoka, Stephen J. Elledge, and Philip Leder. Hus1 acts upstream of Chk1 in a mammalian DNA damage response pathway. *Current Biology*, 12(1):73–77, 1 2002.

145. Randal S. Tibbetts, Kathryn M. Brumbaugh, Josie M. Williams, Jann N. Sarkaria, William A. Cliby, Sheau Yann Shieh, Yoichi Taya, Carol Prives, and Robert T. Abraham. A role for ATR in the DNA damage-induced phosphorylation of p53. *Genes and Development*, 13(2):152–157, 1 1999.

146. Karlene A. Cimprich and David Cortez. ATR: An essential regulator of genome integrity, 8 2008.

147. Alexandros G. Georgakilas, Olga A. Martin, and William M. Bonner. p21: A Two-Faced Genome Guardian, 4 2017.

148. Luis Ignacio Toledo, Matthias Altmeyer, Maj-Britt Rask, Claudia Lukas, Dorthe Helena Larsen, Lou Klitgaard Povlsen, Simon Bekker-Jensen, Niels Mailand, Jiri Bartek, and Jiri Lukas. ATR Prohibits Replication Catastrophe by Preventing Global Exhaustion of RPA. *Cell*, 155(5):1088–1103, 11 2013.

149. Wendy J. Cannan and David S. Pederson. Mechanisms and Consequences of Double-Strand DNA Break Formation in Chromatin, 1 2016.

150. Brandon J. Lamarche, Nicole I. Orazio, and Matthew D. Weitzman. The MRN complex in double-strand break repair and telomere maintenance, 9 2010.

151. Raquel Cuella-Martin, Catarina Oliveira, Helen E. Lockstone, Suzanne Snellenberg, Natalia Grolmusova, and J. Ross Chapman. 53BP1 Integrates DNA Repair and p53-Dependent Cell Fate Decisions via Distinct Mechanisms. *Molecular Cell*, 64(1):51–64, 10 2016.

152. Myriam Cuadrado, Barbara Martinez-Pastor, Matilde Murga, Luis I Toledo, Paula Gutierrez-Martinez, Eva Lopez, and Oscar Fernandez-Capetillo. ATM regulates ATR chromatin loading in response to DNA double-strand breaks. *The Journal of experimental medicine*, 203(2):297–303, 2 2006.

153. Zsuzsa Szondy, Zsolt Sarang, Beáta Kiss, Éva Garabuczi, and Krisztina Köröskényi. Anti-inflammatory mechanisms triggered by apoptotic cells during their clearance, 8 2017.

154. Stéphanie Solier and Yves Pommier. The nuclear γ-H2AX apoptotic ring: implications for cancers and autoimmune diseases. *Cellular and molecular life sciences : CMLS*, 71(12):2289–97, 6 2014.

155. Alejandra Hernandez-Segura, Jamil Nehme, and Marco Demaria. Hallmarks of Cellular Senescence. *Trends in Cell Biology*, 28(6):436–453, 6 2018.

156. Je-Jung Lee, In Ho Park, Woo Joong Rhee, Hee Sue Kim, and Jeon-Soo Shin. HMGB1 modulates the balance between senescence and apoptosis in response to genotoxic stress. *J*, 33:10942–10953, 2019.

157. Menderes Yusuf Terzi, Muzeyyen Izmirli, and Bulent Gogebakan. The cell fate: senescence or quiescence, 11 2016.

158. Mohammad Sabbir Siddiqui, Maxime François, Michael F. Fenech, and Wayne R. Leifert. Persistent γH2AX: A promising molecular marker of DNA damage and aging, 10 2015.

159. Jeremy E. Purvis, Kyle W. Karhohs, Caroline Mock, Eric Batchelor, Alexander Loewer, and Galit Lahav. p53 dynamics control cell fate. *Science*, 336(6087):1440–1444, 6 2012.

160. Christopher D. Wiley, James M. Flynn, Christapher Morrissey, Ronald Lebofsky, Joe Shuga, Xiao Dong, Marc A. Unger, Jan Vijg, Simon Melov, and Judith Campisi. Analysis of individual cells identifies cell-to-cell variability following induction of cellular senescence. *Aging Cell*, 16(5):1043–1050, 10 2017.

161. Bo Yun Lee, Jung A. Han, Jun Sub Im, Amelia Morrone, Kimberly Johung, Edward C. Goodwin, Wim J. Kleijer, Daniel DiMaio, and Eun Seong Hwang. Senescence-associated β-galactosidase is lysosomal β-galactosidase. *Aging Cell*, 5(2):187–195, 4 2006.

162. Brandon M. Hall, Vitaly Balan, Anatoli S. Gleiberman, Evguenia Strom, Peter Krasnov, Lauren P. Virtuoso, Elena Rydkina, Slavoljub Vujcic, Karina Balan, Ilya I. Gitlin, Katerina I. Leonova, Camila R. Consiglio, Sandra O. Gollnick, Olga B. Chernova, and Andrei V. Gudkov. p16(Ink4a) and senescence-associated β-galactosidase can be induced in macrophages as part of a reversible response to physiological stimuli. *Aging*, 9(8):1867–1884, 2017.

163. Norman E. Sharpless and Charles J. Sherr. Forging a signature of in vivo senescence, 7 2015.

164. Dina Dikovskaya, John J. Cole, Susan M. Mason, Colin Nixon, Saadia A. Karim, Lynn McGarry, William Clark, Rachael N. Hewitt, Morgan A. Sammons, Jiajun Zhu, Dimitris Athineos, Joshua D.G. Leach, Francesco Marchesi, John van Tuyn, Stephen W. Tait, Claire Brock, Jennifer P. Morton, Hong Wu, Shelley L. Berger, Karen Blyth, and Peter D. Adams. Mitotic Stress Is an Integral Part of the Oncogene-Induced Senescence Program that Promotes Multinucleation and Cell Cycle Arrest. *Cell Reports*, 12(9):1483–1496, 9 2015.

165. Zhiyong Mao, Zhonghe Ke, Vera Gorbunova, and Andrei Seluanov. Replicatively senescent cells are arrested in G1 and G2 phases. *Aging*, 4(6):431–435, 2012.

166. Adam Freund, Remi Martin Laberge, Marco Demaria, and Judith Campisi. Lamin B1 loss is a senescence-associated biomarker. *Molecular Biology of the Cell*, 23(11):2066–2075, 6 2012.

167. Takeshi Shimi, Veronika Butin-Israeli, Stephen A. Adam, Robert B. Hamanaka, Anne E. Goldman, Catherine A. Lucas, Dale K. Shumaker, Steven T. Kosak, Navdeep S. Chandel, and

Robert D. Goldman. The role of nuclear lamin B1 in cell proliferation and senescence. *Genes and Development*, 25(24):2579–2593, 12 2011.

168. Jan M van Deursen. The role of senescent cells in ageing. *Nature*, 509(7501):439–46, 5 2014.

169. Parisha P. Shah, Greg Donahue, Gabriel L. Otte, Brian C. Capell, David M. Nelson, Kajia Cao, Varun Aggarwala, Hazel A. Cruickshanks, Taranjit Singh Rai, Tony McBryan, Brian D. Gregory, Peter D. Adams, and Shelley L. Berger. Lamin B1 depletion in senescent cells triggers large-scale changes in gene expression and the chromatin landscape. *Genes and Development*, 27(16):1787–1799, 8 2013.

170. Aled J. Parry, Matthew Hoare, Dóra Bihary, Robert Hänsel-Hertsch, Stephen Smith, Kosuke Tomimatsu, Elizabeth Mannion, Amy Smith, Paula D'Santos, I. Alasdair Russell, Shankar Balasubramanian, Hiroshi Kimura, Shamith A. Samarajiwa, and Masashi Narita. NOTCH-mediated non-cell autonomous regulation of chromatin structure during senescence. *Nature Communications*, 9(1):1–15, 12 2018.

171. Katherine M. Aird and Rugang Zhang. Detection of senescence-associated heterochromatin foci (SAHF). *Methods in Molecular Biology*, 965:185–196, 2013.

172. Masashi Narita, Sabrina Nũnez, Edith Heard, Masako Narita, Athena W. Lin, Stephen A. Hearn, David L. Spector, Gregory J. Hannon, and Scott W. Lowe. Rb-mediated heterochromatin formation and silencing of E2F target genes during cellular senescence. *Cell*, 113(6):703–716, 6 2003.

173. Kevin W. McCool and Shigeki Miyamoto. DNA damage-dependent NF-κB activation: NEMO turns nuclear signaling inside out. *Immunological Reviews*, 246(1):311–326, 3 2012.

174. Nathan Basisty, Abhijit Kale, Okhee Jeon, Chisaka Kuehnemann, Therese Payne, Chirag Rao, Anja Holtz, Samah Shah, Luigi Ferrucci, Judith Campisi, and Birgit Schilling. A Proteomic Atlas of Senescence-Associated Secretomes for Aging Biomarker Development. *bioRxiv*, page 604306, 4 2019.

175. Jean Philippe Coppé, Christopher K. Patil, Francis Rodier, Y. Sun, Denise P. Muñoz, Joshua Goldstein, Peter S. Nelson, Pierre Yves Desprez, and Judith Campisi. Senescence-associated secretory phenotypes reveal cell-nonautonomous functions of oncogenic RAS and the p53 tumor suppressor. *PLoS biology*, 6(12), 2008.

176. Darren J Baker, Bennett G Childs, Matej Durik, Melinde E Wijers, Cynthia J Sieben, Jian Zhong, Rachel A. Saltness, Karthik B Jeganathan, Grace Casaclang Verzosa, Abdulmohammad Pezeshki, Khashayarsha Khazaie, Jordan D Miller, and Jan M. van Deursen. Naturally occurring p16Ink4a-positive cells shorten healthy lifespan. *Nature*, 530(7589):184–189, 2 2016.

177. Ming Xu, Tamar Pirtskhalava, Joshua N. Farr, Bettina M. Weigand, Allyson K. Palmer, Megan M. Weivoda, Christina L. Inman, Mikolaj B. Ogrodnik, Christine M. Hachfeld, Daniel G.

Fraser, Jennifer L. Onken, Kurt O. Johnson, Grace C. Verzosa, Larissa G.P. Langhi, Moritz Weigl, Nino Giorgadze, Nathan K. LeBrasseur, Jordan D. Miller, Diana Jurk, Ravinder J. Singh, David B. Allison, Keisuke Ejima, Gene B. Hubbard, Yuji Ikeno, Hajrunisa Cubro, Vesna D. Garovic, Xiaonan Hou, S. John Weroha, Paul D. Robbins, Laura J. Niedernhofer, Sundeep Khosla, Tamara Tchkonia, and James L. Kirkland. Senolytics improve physical function and increase lifespan in old age. *Nature Medicine*, 24(8):1246–1256, 8 2018.

178. L. Hayflick. The limited in vitro lifetime of human diploid cell strains. *Experimental Cell Research*, 37(3):614–636, 3 1965.

179. Fabrizio d'Adda di Fagagna, Philip M. Reaper, Lorena Clay-Farrace, Heike Fiegler, Philippa Carr, Thomas von Zglinicki, Gabriele Saretzki, Nigel P. Carter, and Stephen P. Jackson. A DNA damage checkpoint response in telomere-initiated senescence. *Nature*, 426(6963):194–198, 11 2003.

180. Manuel Serrano, Athena W. Lin, Mila E. McCurrach, David Beach, and Scott W. Lowe. Oncogenic ras provokes premature cell senescence associated with accumulation of p53 and p16(INK4a). *Cell*, 88(5):593–602, 3 1997.

181. Jirina Bartkova, Nousin Rezaei, Michalis Liontos, Panagiotis Karakaidos, Dimitris Kletsas, Natalia Issaeva, Leandros Vassilios F. Vassiliou, Evangelos Kolettas, Katerina Niforou, Vassilis C. Zoumpourlis, Munenori Takaoka, Hiroshi Nakagawa, Frederic Tort, Kasper Fugger, Fredrik Johansson, Maxwell Sehested, Claus L. Andersen, Lars Dyrskjot, Torben Ørntoft, Jiri Lukas, Christos Kittas, Thomas Helleday, Thanos D. Halazonetis, Jiri Bartek, and Vassilis G. Gorgoulis. Oncogene-induced senescence is part of the tumorigenesis barrier imposed by DNA damage checkpoints. *Nature*, 444(7119):633–637, 11 2006.

182. Raffaella Di Micco, Marzia Fumagalli, Angelo Cicalese, Sara Piccinin, Patrizia Gasparini, Chiara Luise, Catherine Schurra, Massimiliano Garré, Paolo Giovanni Nuciforo, Aaron Bensimon, Roberta Maestro, Pier Giuseppe Pelicci, and Fabrizio D'Adda Di Fagagna. Oncogene-induced senescence is a DNA damage response triggered by DNA hyper-replication. *Nature*, 444(7119):638–642, 2006.

183. Reut Yosef, Noam Pilpel, Nurit Papismadov, Hilah Gal, Yossi Ovadya, Ezra Vadai, Stav Miller, Ziv Porat, Shifra Ben-Dor, and Valery Krizhanovsky. p21 maintains senescent cell viability under persistent ¡scp¿DNA¡/scp¿ damage response by restraining ¡scp¿JNK¡/scp¿ and caspase signaling. *The EMBO Journal*, 36(15):2280–2295, 8 2017.

184. Boshi Wang, Jaskaren Kohli, and Marco Demaria. Senescent Cells in Cancer Therapy: Friends or Foes?, 10 2020.

185. Dorothy N.Y. Fan and Clemens A. Schmitt. Genotoxic stress-induced senescence. In *Methods in Molecular Biology*, volume 1896, pages 93–105. Humana Press Inc., 2019.

186. Muriel Rhinn, Birgit Ritschka, and William M Keyes. Cellular senescence in development, regeneration and disease. *Development*, 146(20), 10 2019.

187. Juan Carlos Acosta, Ana Banito, Torsten Wuestefeld, Athena Georgilis, Peggy Janich, Jennifer P Morton, Dimitris Athineos, Tae-Won Kang, Felix Lasitschka, Mindaugas Andrulis, Gloria Pascual, Kelly J Morris, Sadaf Khan, Hong Jin, Gopuraja Dharmalingam, Ambrosius P Snijders, Thomas Carroll, David Capper, Catrin Pritchard, Gareth J Inman, Thomas Longerich, Owen J Sansom, Salvador Aznar Benitah, Lars Zender, and Jesús Gil. A complex secretory program orchestrated by the inflammasome controls paracrine senescence. *Nature cell biology*, 15(8):978–90, 8 2013.

188. Audrey Lasry and Yinon Ben-Neriah. Senescence-associated inflammatory responses: aging and cancer perspectives. *Trends in Immunology*, 36(4):217–228, 4 2015.

189. Jean-Philippe Coppé, Pierre-Yves Desprez, Ana Krtolica, and Judith Campisi. The senescence-associated secretory phenotype: the dark side of tumor suppression. *Annual review of pathology*, 5:99–118, 2010.

190. Raffaella Di Micco, Valery Krizhanovsky, Darren Baker, and Fabrizio d'Adda di Fagagna. Cellular senescence in ageing: from mechanisms to therapeutic opportunities, 2 2021.

191. Marco Demaria, Naoko Ohtani, Sameh A. Youssef, Francis Rodier, Wendy Toussaint, James R. Mitchell, Remi-Martin Laberge, Jan Vijg, Harry Van Steeg, Martijn E.T. Dollé, Jan H.J. Hoeijmakers, Alain de Bruin, Eiji Hara, and Judith Campisi. An Essential Role for Senescent Cells in Optimal Wound Healing through Secretion of PDGF-AA. *Developmental Cell*, 31(6):722–733, 12 2014.

192. Daniel Muñoz-Espín, Marta Cañamero, Antonio Maraver, Gonzalo Gómez-López, Julio Contreras, Silvia Murillo-Cuesta, Alfonso Rodríguez-Baeza, Isabel Varela-Nieto, Jesús Ruberte, Manuel Collado, and Manuel Serrano. XProgrammed cell senescence during mammalian embryonic development. *Cell*, 155(5):1104, 11 2013.

193. Ana Banito and Scott W. Lowe. XA new development in senescence, 11 2013.

194. Valery Krizhanovsky, Monica Yon, Ross A. Dickins, Stephen Hearn, Janelle Simon, Cornelius Miething, Herman Yee, Lars Zender, and Scott W. Lowe. Senescence of Activated Stellate Cells Limits Liver Fibrosis. *Cell*, 134(4):657–667, 8 2008.

195. Juan C. Acosta, Ana O'Loghlen, Ana Banito, Maria V. Guijarro, Arnaud Augert, Selina Raguz, Marzia Fumagalli, Marco Da Costa, Celia Brown, Nikolay Popov, Yoshihiro Takatsu, Jonathan Melamed, Fabrizio d'Adda di Fagagna, David Bernard, Eva Hernando, and Jesús Gil. Chemokine Signaling via the CXCR2 Receptor Reinforces Senescence. *Cell*, 133(6):1006–1018, 6 2008.

196. Alexandre Iannello, Thornton W. Thompson, Michele Ardolino, Scott W. Lowe, and David H. Raulet. p53-dependent chemokine production by senescent tumor cells supports NKG2D-

dependent tumor elimination by natural killer cells. *Journal of Experimental Medicine*, 210(10):2057–2069, 2013.

197. Adi Sagiv and Valery Krizhanovsky. Immunosurveillance of senescent cells: The bright side of the senescence program, 12 2013.

198. Claudio Franceschi, Massimiliano Bonafè, Silvana Valensin, Fabiola Olivieri, Maria De Luca, Enzo Ottaviani, and Giovanna De Benedictis. Inflamm-aging. An evolutionary perspective on immunosenescence. In *Annals of the New York Academy of Sciences*, volume 908, pages 244–254. New York Academy of Sciences, 2000.

199. William R. Jeck, Alex P. Siebold, and Norman E. Sharpless. Review: A meta-analysis of GWAS and age-associated diseases, 10 2012.

200. Francis Rodier and Judith Campisi. Four faces of cellular senescence. *The Journal of cell biology*, 192(4):547–56, 2 2011.

201. A Krtolica, S Parrinello, S Lockett, P Y Desprez, and J Campisi. Senescent fibroblasts promote epithelial cell growth and tumorigenesis: a link between cancer and aging. *Proceedings of the National Academy of Sciences of the United States of America*, 98(21):12072–7, 10 2001.

202. Douglas V. Faget, Qihao Ren, and Sheila A. Stewart. Unmasking senescence: context-dependent effects of SASP in cancer, 8 2019.

203. Daniela Gnani, Stefania Crippa, Lucrezia della Volpe, Valeria Rossella, Anastasia Conti, Emanuele Lettera, Silvia Rivis, Marco Ometti, Gianfranco Fraschini, Maria Ester Bernardo, and Raffaella Di Micco. An early-senescence state in aged mesenchymal stromal cells contributes to hematopoietic stem and progenitor cell clonogenic impairment through the activation of a pro-inflammatory program. *Aging Cell*, 18(3), 6 2019.

204. Stéphane Lopes-Paciencia, Emmanuelle Saint-Germain, Marie Camille Rowell, Ana Fernández Ruiz, Paloma Kalegari, and Gerardo Ferbeyre. The senescence-associated secretory phenotype and its regulation. *Cytokine*, 117:15–22, 5 2019.

205. Thomas Kuilman, Chrysiis Michaloglou, Liesbeth C.W. Vredeveld, Sirith Douma, Remco van Doorn, Christophe J. Desmet, Lucien A. Aarden, Wolter J. Mooi, and Daniel S. Peeper. Oncogene-Induced Senescence Relayed by an Interleukin-Dependent Inflammatory Network. *Cell*, 133(6):1019–1031, 6 2008.

206. Christopher J. Huggins, Radek Malik, Sook Lee, Jacqueline Salotti, Sara Thomas, Nancy Martin, Octavio A. Quiñones, W. Gregory Alvord, Mary E. Olanich, Jonathan R. Keller, and Peter F. Johnson. C/EBPγ Suppresses Senescence and Inflammatory Gene Expression by Heterodimerizing with C/EBPβ. *Molecular and Cellular Biology*, 33(16):3242–3258, 8 2013.

207. Chanhee Kang, Qikai Xu, Timothy D. Martin, Mamie Z. Li, Marco Demaria, Liviu Aron, Tao Lu, Bruce A. Yankner, Judith Campisi, and Stephen J. Elledge. The DNA damage response

induces inflammation and senescence by inhibiting autophagy of GATA4. *Science*, 349(6255), 9 2015.

208. Adam Freund, Christopher K. Patil, and Judith Campisi. P38MAPK is a novel DNA damage response-independent regulator of the senescence-associated secretory phenotype. *EMBO Journal*, 30(8):1536–1548, 4 2011.

209. Olga Moiseeva, Xavier Deschênes-Simard, Emmanuelle St-Germain, Sebastian Igelmann, Geneviève Huot, Alexandra E. Cadar, Véronique Bourdeau, Michael N. Pollak, and Gerardo Ferbeyre. Metformin inhibits the senescence-associated secretory phenotype by interfering with IKK/NF-κB activation. *Aging Cell*, 12(3):489–498, 6 2013.

210. Alberto Toso, Ajinkya Revandkar, Diletta DiMitri, Ilaria Guccini, Michele Proietti, Manuela Sarti, Sandra Pinton, Jiangwen Zhang, Madhuri Kalathur, Gianluca Civenni, David Jarrossay, Erica Montani, Camilla Marini, Ramon Garcia-Escudero, Eugenio Scanziani, Fabio Grassi, Pier Paolo Pandolfi, Carlo V. Catapano, and Andrea Alimonti. Enhancing chemotherapy efficacy in pten-deficient prostate tumors by activating the senescence-associated antitumor immunity. *Cell Reports*, 9(1):75–89, 10 2014.

211. Katherine M. Aird, Osamu Iwasaki, Andrew V. Kossenkov, Hideki Tanizawa, Nail Fatkhutdinov, Benjamin G. Bitler, Linh Le, Gretchen Alicea, Ting Lin Yang, F. Brad Johnson, Ken Ichi Noma, and Rugang Zhang. HMGB2 orchestrates the chromatin landscape of senescence-associated secretory phenotype gene loci, 2016.

212. Shenghui He and Norman E. Sharpless. Senescence in Health and Disease, 6 2017.

213. Daniel Humphreys, Mohamed ElGhazaly, and Teresa Frisan. Senescence and Host-Pathogen Interactions, 7 2020.

214. Marta Czesnikiewicz-Guzik, Won Woo Lee, Dapeng Cui, Yuko Hiruma, David L. Lamar, Zhi Zhang Yang, Joseph G. Ouslander, Cornelia M. Weyand, and Jörg J. Goronzy. T cell subset-specific susceptibility to aging. *Clinical Immunology*, 127(1):107–118, 4 2008.

215. Marcia Bellon and Christophe Nicot. Telomere dynamics in immune senescence and exhaustion triggered by chronic viral infection, 10 2017.

216. John J Heath and Michael D Grant. The Immune Response Against Human Cytomegalovirus Links Cellular to Systemic Senescence, 3 2020.

217. Jens Bukh. The history of hepatitis C virus (HCV): Basic research reveals unique features in phylogeny, evolution and the viral life cycle with new perspectives for epidemic control, 2016.

218. Matthew Hoare, William T.H. Gelson, Abhi Das, Jean M. Fletcher, Susan E. Davies, Martin D. Curran, Sarah L. Vowler, Mala K. Maini, Arne N. Akbar, and Graeme J.M. Alexander. CD4+ T-lymphocyte telomere length is related to fibrosis stage, clinical outcome and treatment response in chronic hepatitis C virus infection. *Journal of Hepatology*, 53(2):252–260, 8 2010.

219. Matthew Hoare, Arun Shankar, Meera Shah, Simon Rushbrook, William Gelson, Susan Davies, Arne Akbar, and Graeme J.M. Alexander. γ-H2AX + CD8+ T lymphocytes cannot respond to IFN-α, IL-2 or IL-6 in chronic hepatitis C virus infection. *Journal of Hepatology*, 58(5):868–874, 5 2013.

220. Guijuan Feng, Ke Zheng, Tong Cao, Jinlong Zhang, Min Lian, Dan Huang, Changbo Wei, Zhifeng Gu, and Xingmei Feng. Repeated stimulation by LPS promotes the senescence of DPSCs via TLR4/MyD88-NF-κB-p53/p21 signaling. *Cytotechnology*, 70(3):1023–1035, 6 2018.

221. Nadège Bossuet-Greif, Julien Vignard, Frédéric Taieb, Gladys Mirey, Damien Dubois, Claude Petit, Eric Oswald, and Jean Philippe Nougayrède. The colibactin genotoxin generates DNA interstrand cross-links in infected cells. *mBio*, 9(2), 3 2018.

222. Thomas Secher, Ascel Samba-Louaka, Eric Oswald, and Jean-Philippe Nougayrède. Escherichia coli Producing Colibactin Triggers Premature and Transmissible Senescence in Mammalian Cells. *PLoS ONE*, 8(10):e77157, 10 2013.

223. Christelle Péré-Védrenne, Martina Prochazkova-Carlotti, Benoit Rousseau, Wencan He, Lucie Chambonnier, Elodie Sifré, Alice Buissonnière, Pierre Dubus, Francis Mégraud, Christine Varon, and Armelle Ménard. The cytolethal distending toxin subunit CdtB of Helicobacter hepaticus promotes senescence and endoreplication in xenograft mouse models of hepatic and intestinal cell lines. *Frontiers in Cellular and Infection Microbiology*, 7(JUN), 6 2017.

224. I. D. Gardner. The effect of aging on susceptibility to infection., 1980.

225. Kimberly A. Kline and Dawn M.E. Bowdish. Infection in an aging population, 2 2016.

226. Ji Ae Kim, Rak Kyun Seong, and Ok Sarah Shin. Enhanced viral replication by cellular replicative senescence. *Immune Network*, 16(5):286–295, 2016.

227. Jae Sung Lim, Hyon E. Choy, Sang Chul Park, Jung Min Han, Ik Soon Jang, and Kyung A. Cho. Caveolae-mediated entry of Salmonella typhimurium into senescent nonphagocytotic host cells. *Aging Cell*, 9(2):243–251, 4 2010.

228. Pooja Shivshankar, Angela R. Boyd, Claude J. Le Saux, I. Tien Yeh, and Carlos J. Orihuela. Cellular senescence increases expression of bacterial ligands in the lungs and is positively correlated with increased susceptibility to pneumococcal pneumonia. *Aging Cell*, 10(5):798–806, 10 2011.

229. Asmita Pal and Rita Kundu. Human Papillomavirus E6 and E7: The Cervical Cancer Hallmarks and Targets for Therapy, 1 2020.

230. Maite Baz-Martínez, Sabela Da Silva-Álvarez, Estefaniá Rodríguez, Jorge Guerra, Ahmed El Motiam, Anxo Vidal, Tomás Garciá-Caballero, Miguel González-Barcia, Laura Sánchez, César Munõz-Fontela, Manuel Collado, and Carmen Rivas. Cell senescence is an antiviral defense mechanism. *Scientific Reports*, 6, 11 2016.

231. Casey C. Fowler, Gabrielle Stack, Xuyao Jiao, Maria Lara-Tejero, and Jorge E. Galán. Alternate subunit assembly diversifies the function of a bacterial toxin. *Nature Communications*, 10(1):1–10, 12 2019.

232. Riccardo Guidi, Laura Levi, Syed Fazle Rouf, Speranta Puiac, Mikael Rhen, and Teresa Frisan. ¡i¿Salmonella enterica¡/i¿ delivers its genotoxin through outer membrane vesicles secreted from infected cells. *Cellular Microbiology*, 15(12):2034–2050, 12 2013.

233. K. Saiki, K. Konishi, T. Gomi, T. Nishihara, and M. Yoshikawa. Reconstitution and purification of cytolethal distending toxin of Actinobacillus actinomycetemcomitans, 6 2001.

234. Natalia S. Pellegata, Ronald J. Antoniono, J. Leslie Redpath, and Eric J. Stanbridge. DNA damage and p53-mediated cell cycle arrest: A reevaluation. *Proceedings of the National Academy of Sciences of the United States of America*, 93(26):15209–15214, 12 1996.

235. Jean Mc Arthur Lewis, Tony Nguyen Truong, and Martin Alexander Schwartz. Integrins regulate the apoptotic response to DNA damage through modulation of p53. *Proceedings of the National Academy of Sciences of the United States of America*, 99(6):3627–3632, 3 2002.

236. Y. Fedor, J. Vignard, M.-L. Nicolau-Travers, E. Boutet-Robinet, C. Watrin, B. Salles, and G. Mirey. From single-strand breaks to double-strand breaks during S-phase: a new mode of action of the ¡i¿Escherichia coli¡/i¿ Cytolethal Distending Toxin. *Cellular Microbiology*, 15(1):1–15, 1 2013.

237. Elisabeth Bezine, Julien Vignard, and Gladys Mirey. The Cytolethal Distending Toxin Effects on Mammalian Cells: A DNA Damage Perspective. *Cells*, 3(2):592–615, 6 2014.

238. C. Elwell, K. Chao, K. Patel, and L. Dreyfus. Escherichia coli CdtB mediates cytolethal distending toxin cell cycle arrest. *Infection and Immunity*, 69(5):3418–3422, 5 2001.

239. Rasika N. Jinadasa, Stephen E. Bloom, Robert S. Weiss, and Gerald E. Duhamel. Cytolethal distending toxin: A conserved bacterial genotoxin that blocks cell cycle progression, leading to apoptosis of a broad range of mammalian cell lineages, 7 2011.

240. Hana Blazkova, Katerina Krejcikova, Pavel Moudry, Teresa Frisan, Zdenek Hodny, and Jiri Bartek. Bacterial intoxication evokes cellular senescence with persistent DNA damage and cytokine signalling. *Journal of cellular and molecular medicine*, 14(1-2):357–67, 1 2010.

241. Ximena Cortes-Bratti, Christina Karlsson, Teresa Lagergård, Monica Thelestam, and Teresa Frisan. The Haemophilus ducreyi Cytolethal Distending Toxin Induces Cell Cycle Arrest and Apoptosis via the DNA Damage Checkpoint Pathways. *Journal of Biological Chemistry*, 276(7):5296–5302, 2 2001.

242. Malgorzata Piechota, Piotr Sunderland, Adrianna Wysocka, Maria Nalberczak, Malgorzata A. Sliwinska, Kasia Radwanska, and Ewa Sikora. Is senescence-associated β-galactosidase a marker of neuronal senescence? *Oncotarget*, 7(49):81099, 2016.

243. Hong Zhao and Zbigniew Darzynkiewicz. Biomarkers of cell senescence assessed by imaging cytometry. *Methods in Molecular Biology*, 965:83–92, 2013.

244. Stéphanie Solier and Yves Pommier. The apoptotic ring: A novel entity with phosphorylated histones H2AX and H2B, and activated DNA damage response kinases. *Cell Cycle*, 8(12):1853–1859, 6 2009.

245. Ping Yang, James J. Peairs, Ryotaro Tano, Nanfei Zhang, Jillian Tyrell, and Glenn J. Jaffe. Caspase-8-mediated apoptosis in human RPE cells. *Investigative Ophthalmology and Visual Science*, 48(7):3341–3349, 7 2007.

246. Andre Ivanov, Jeff Pawlikowski, Indrani Manoharan, John Van Tuyn, David M. Nelson, Taranjit Singh Rai, Parisha P. Shah, Graeme Hewitt, Viktor I. Korolchuk, Joao F. Passos, Hong Wu, Shelley L. Berger, and Peter D. Adams. Lysosome-mediated processing of chromatin in senescence. *Journal of Cell Biology*, 202(1):129–143, 7 2013.

247. Duane C. Hassane, Robert B. Lee, and Carol L. Pickett. Campylobacter jejuni cytolethal distending toxin promotes DNA repair responses in normal human cells. *Infection and Immunity*, 71(1):541–545, 1 2003.

248. Frédéric Alby, Raoul Mazars, Jean De Rycke, Emmanuelle Guillou, Véronique Baldin, Jean Marie Darbon, and Bernard Ducommun. Study of the cytolethal distending toxin (CDT)-activated cell cycle checkpoint: Involvement of the CHK2 kinase. *FEBS Letters*, 491(3):261–265, 3 2001.

249. Terence A. Agbor and Beth A. McCormick. Salmonella effectors: important players modulating host cell function during infection. *Cellular Microbiology*, 13(12):1858–1869, 12 2011.

250. Olga A Sedelnikova, Izumi Horikawa, Drazen B Zimonjic, Nicholas C Popescu, William M Bonner, and J Carl Barrett. Senescing human cells and ageing mice accumulate DNA lesions with unrepairable double-strand breaks. *Nature cell biology*, 6(2):168–70, 2 2004.

251. Valentina Minieri, Silvia Saviozzi, Giovanna Gambarotta, Marco Lo Iacono, Lisa Accomasso, Elisa Cibrario Rocchietti, Clara Gallina, Valentina Turinetto, and Claudia Giachino. Persistent DNA damage-induced premature senescence alters the functional features of human bone marrow mesenchymal stem cells. *Journal of Cellular and Molecular Medicine*, 19(4):734–743, 4 2015.

252. Ricardo Iván Martínez-Zamudio, Lucas Robinson, Pierre-François Roux, and Oliver Bischof. SnapShot: Cellular Senescence in Pathophysiology. *Cell*, 170(5):1044–1044, 8 2017.

253. Jan M. van Deursen. The role of senescent cells in ageing. *Nature*, 509(7501):439–446, 5 2014.

254. Sona Hubackova, Katerina Krejcikova, Jiri Bartek, and Zdenek Hodny. IL1-and TGFβ-Nox4 signaling, oxidative stress and DNA damage response are shared features of replicative, oncogene-induced, and drug-induced paracrine 'Bystander senescence'. *Aging*, 4(12):932–951, 2012.

255. Stéphanie Solier and Yves Pommier. MDC1 cleavage by caspase-3: a novel mechanism for inactivating the DNA damage response during apoptosis. *Cancer research*, 71(3):906–13, 2 2011.

256. Gabriel Ichim, Jonathan Lopez, Shafiq U. Ahmed, Nathiya Muthalagu, Evangelos Giampazolias, M. Eugenia Delgado, Martina Haller, Joel S. Riley, Susan M. Mason, Dimitris Athineos, Melissa J. Parsons, Bert vandeKooij, Lisa Bouchier-Hayes, Anthony J. Chalmers, Rogier W. Rooswinkel, Andrew Oberst, Karen Blyth, Markus Rehm, Daniel J. Murphy, and Stephen W.G. Tait. Limited Mitochondrial Permeabilization Causes DNA Damage and Genomic Instability in the Absence of Cell Death. *Molecular Cell*, 57(5):860–872, 3 2015.

257. Dominik Brokatzky, Benedikt Dörflinger, Aladin Haimovici, Arnim Weber, Susanne Kirschnek, Juliane Vier, Arlena Metz, Julia Henschel, Tobias Steinfeldt, Ian E Gentle, and Georg Häcker. A non-death function of the mitochondrial apoptosis apparatus in immunity. *The EMBO Journal*, 38(11):e100907, 6 2019.

258. Suzzanne F. Bradley and Carol A. Kauffman. Aging and the response to salmonella infection. *Experimental Gerontology*, 25(1):75–80, 1 1990.

259. Ching Wen Tseng, Pierre A. Kyme, Andrea Arruda, V. Krishnan Ramanujan, Wafa Tawackoli, and George Y. Liu. Innate immune dysfunctions in aged mice facilitate the systemic dissemination of methicillin-resistant S. aureus. *PLoS ONE*, 7(7), 7 2012.

260. Francis Rodier, Jean Philippe Coppé, Christopher K. Patil, Wieteke A.M. Hoeijmakers, Denise P. Muñoz, Saba R. Raza, Adam Freund, Eric Campeau, Albert R. Davalos, and Judith Campisi. Persistent DNA damage signalling triggers senescence-associated inflammatory cytokine secretion. *Nature Cell Biology*, 11(8):973–979, 2009.

261. Alejandra Hernandez-Segura, Tristan V. de Jong, Simon Melov, Victor Guryev, Judith Campisi, and Marco Demaria. Unmasking Transcriptional Heterogeneity in Senescent Cells. *Current Biology*, 27(17):2652–2660, 9 2017.

262. Katrin Eichelbaum, Markus Winter, Mauricio Berriel Diaz, Stephan Herzig, and Jeroen Krijgsveld. Selective enrichment of newly synthesized proteins for quantitative secretome analysis. *Nature Biotechnology*, 30(10):984–990, 10 2012.

263. Jigang Wang, Jianbin Zhang, Yew Mun Lee, Shukie Ng, Yin Shi, Zi-Chun Hua, Qingsong Lin, and Han-Ming Shen. Nonradioactive quantification of autophagic protein degradation with L-azidohomoalanine labeling. *Nature Protocols*, 12(2):279–288, 1 2017.

264. Talia D. Valentini, Sarah K. Lucas, Kelsey A. Binder, Lydia C. Cameron, Jason A. Motl, Jordan M. Dunitz, and Ryan C. Hunter. Bioorthogonal non-canonical amino acid tagging reveals translationally active subpopulations of the cystic fibrosis lung microbiota. *Nature Communications*, 11(1):1–11, 12 2020.

265. John D Bagert, Yushu J Xie, Michael J Sweredoski, Yutao Qi, Sonja Hess, Erin M Schuman, and David A Tirrell. Quantitative, time-resolved proteomic analysis by combining bioorthogonal noncanonical amino acid tagging and pulsed stable isotope labeling by amino acids in cell culture. *Molecular & cellular proteomics : MCP*, 13(5):1352–8, 5 2014.

266. Mathias Uhlén, Max J Karlsson, Andreas Hober, Anne-Sophie Svensson, Julia Scheffel, David Kotol, Wen Zhong, Abdellah Tebani, Linnéa Strandberg, Fredrik Edfors, Evelina Sjöstedt, Jan Mulder, Adil Mardinoglu, Anna Berling, Siri Ekblad, Melanie Dannemeyer, Sara Kanje, Johan Rockberg, Magnus Lundqvist, Magdalena Malm, Anna-Luisa Volk, Peter Nilsson, Anna Månberg, Tea Dodig-Crnkovic, Elisa Pin, Martin Zwahlen, Per Oksvold, Kalle von Feilitzen, Ragna S Häussler, Mun-Gwan Hong, Cecilia Lindskog, Fredrik Ponten, Borbala Katona, Jimmy Vuu, Emil Lindström, Jens Nielsen, Jonathan Robinson, Burcu Ayoglu, Diana Mahdessian, Devin Sullivan, Peter Thul, Frida Danielsson, Charlotte Stadler, Emma Lundberg, Göran Bergström, Anders Gummesson, Bjørn G Voldborg, Hanna Tegel, Sophia Hober, Björn Forsström, Jochen M Schwenk, Linn Fagerberg, and Åsa Sivertsson. The human secretome. *Science signaling*, 12(609), 11 2019.

267. Eileen Workman, Alex Veith, and Daniel J. Battle. U1A Regulates 3' Processing of the Survival Motor Neuron mRNA. *Journal of Biological Chemistry*, 289(6):3703–3712, 2 2014.

268. Han Seok Ko, Takashi Uehara, Kazuhiro Tsuruma, and Yasuyuki Nomura. Ubiquilin interacts with ubiquitylated proteins and proteasome through its ubiquitin-associated and ubiquitin-like domains. *FEBS Letters*, 566(1-3):110–114, 5 2004.

269. Birgitta Beatrix, Hideaki Sakai, and Martin Wiedmann. The α and β subunit of the nascent polypeptide-associated complex have distinct functions. *Journal of Biological Chemistry*, 275(48):37838–37845, 12 2000.

270. Pascale Gaudet, Michael S. Livstone, Suzanna E. Lewis, and Paul D. Thomas. Phylogenetic-based propagation of functional annotations within the Gene Ontology consortium. *Briefings in Bioinformatics*, 12(5):449–462, 9 2011.

271. Yi-An Yang, Alexander Chong, and Jeongmin Song. Why Is Eradicating Typhoid Fever So Challenging: Implications for Vaccine and Therapeutic Design. *Vaccines*, 6(3), 7 2018.

272. Olga Mendez, Vicente Peg, Candida Salvans, Mireia Pujals, Yolanda Fernandez, Ibane Abasolo, Jose Perez, Ana Matres, Marta Valeri, Josep Gregori, Laura Villarreal, Simo Schwartz, Santiago Ramon Y. Cajal, Josep Tabernero, Javier Cortes, Joaquín Arribas, and Josep Villanueva. Extracellular HMGA1 promotes tumor invasion and metastasis in triple-negative breast cancer. *Clinical Cancer Research*, 24(24):6367–6382, 12 2018.

273. Noa Feldman, Aviva Rotter-Maskowitz, and Eitan Okun. DAMPs as mediators of sterile inflammation in aging-related pathologies. *Ageing Research Reviews*, 24(Pt A):29–39, 11 2015.

274. B. D. Jones, H. F. Paterson, A. Hall, and S. Falkow. Salmonella typhimurium induces membrane ruffling by a growth factor-receptor-independent mechanism. *Proceedings of the National Academy of Sciences*, 90(21):10390–10394, 11 1993.

275. Mathias Uhlén, Linn Fagerberg, Bjö M. Hallström, Cecilia Lindskog, Per Oksvold, Adil Mardinoglu, Åsa Sivertsson, Caroline Kampf, Evelina Sjöstedt, Anna Asplund, Ing Marie Olsson, Karolina Edlund, Emma Lundberg, Sanjay Navani, Cristina Al Khalili Szigyarto, Jacob Odeberg, Dijana Djureinovic, Jenny Ottosson Takanen, Sophia Hober, Tove Alm, Per Henrik Edqvist, Holger Berling, Hanna Tegel, Jan Mulder, Johan Rockberg, Peter Nilsson, Jochen M. Schwenk, Marica Hamsten, Kalle Von Feilitzen, Mattias Forsberg, Lukas Persson, Fredric Johansson, Martin Zwahlen, Gunnar Von Heijne, Jens Nielsen, and Fredrik Pontén. Tissue-based map of the human proteome. *Science*, 347(6220), 1 2015.

276. Mathias Uhlen, Erik Björling, Per Oksvold, Linn Fagerberg, Anna Asplund, Cristina Al-Khalili Szigyarto, Anja Persson, Jenny Ottosson, Henrik Wernérus, Peter Nilsson, Emma Lundberg, Åsa Sivertsson, Sanjay Navani, Kenneth Wester, Caroline Kampf, Sophia Hober, Fredrik Pontén, and Mathias Uhlén. Mapping the human proteome using antibodies. *Molecular & cellular proteomics : MCP*, 6(8):1455–6, 8 2007.

277. Hirayuki Enomoto, Hideji Nakamura, Weidong Liu, and Shuhei Nishiguchi. Hepatoma-Derived Growth Factor: Its Possible Involvement in the Progression of Hepatocellular Carcinoma. *International Journal of Molecular Sciences*, 16(6):14086, 2015.

278. Maria Harmati, Edina Gyukity-Sebestyen, Gabriella Dobra, Laszlo Janovak, Imre Dekany, Okay Saydam, Eva Hunyadi-Gulyas, Istvan Nagy, Attila Farkas, Tibor Pankotai, Zsuzsanna Ujfaludi, Peter Horvath, Filippo Piccinini, Maria Kovacs, Tamas Biro, and Krisztina Buzas. Small extracellular vesicles convey the stress-induced adaptive responses of melanoma cells. *Scientific Reports*, 9(1):1–19, 12 2019.

279. Fangfang Li, Peixi Qin, Lisha Ye, Nishith Gupta, and Min Hu. A novel BR-SMAD is required for larval development in barber's pole worm Haemonchus contortus. *Microbial cell (Graz, Austria)*, 8(2):57–64, 12 2020.

280. Jiyoon Kim, Heon Yung Gee, and Min Goo Lee. Unconventional protein secretion – new insights into the pathogenesis and therapeutic targets of human diseases. *Journal of Cell Science*, 131(12), 6 2018.

281. Jihye Shin, Hye Jung Kim, Gamin Kim, Meiying Song, Se Joon Woo, Seung Taek Lee, Hoguen Kim, and Cheolju Lee. Discovery of melanotransferrin as a serological marker of colorectal cancer by secretome analysis and quantitative proteomics. *Journal of Proteome Research*, 13(11):4919–4931, 11 2014.

282. Jihye Shin, Sang Yun Song, Hee Sung Ahn, Byung Chull An, Yoo Duk Choi, Eun Gyeong Yang, Kook Joo Na, Seung Taek Lee, Jae Il Park, Seon Young Kim, Cheolju Lee, and Seung won Lee. Integrative analysis for the discovery of lung cancer serological markers and validation by MRM-MS. *PLoS ONE*, 12(8):e0183896, 8 2017.

283. Jihye Shin, Gamin Kim, Jong Won Lee, Ji Eun Lee, Yoo Seok Kim, Jong Han Yu, Seung Taek Lee, Sei Hyun Ahn, Hoguen Kim, and Cheolju Lee. Identification of ganglioside GM2 activator playing a role in cancer cell migration through proteomic analysis of breast cancer secretomes. *Cancer Science*, 107(6):828–835, 6 2016.

284. Chih Ching Wu, Chia Wei Hsu, Chi De Chen, Chia Jung Yu, Kai Ping Chang, Dar In Tai, Hao Ping Liu, Wen Hui Su, Yu Sun Chang, and Jau Song Yu. Candidate serological biomarkers for cancer identified from the secretomes of 23 cancer cell lines and the human protein atlas. *Molecular and Cellular Proteomics*, 9(6):1100–1117, 6 2010.

285. Paul Dowling and Martin Clynes. Conditioned media from cell lines: A complementary model to clinical specimens for the discovery of disease-specific biomarkers, 2 2011.

286. Mimi Tamamori-Adachi, Akane Koga, Takao Susa, Hiroko Fujii, Masao Tsuchiya, Hiroko Okinaga, Harumi Hisaki, Masayoshi Iizuka, Shigetaka Kitajima, and Tomoki Okazaki. DNA damage response induced by Etoposide promotes steroidogenesis via GADD45A in cultured adrenal cells. *Scientific Reports*, 8(1):9636, 12 2018.

287. Bow J. Tauro, David W. Greening, Rommel A. Mathias, Suresh Mathivanan, Hong Ji, and Richard J. Simpson. Two distinct populations of exosomes are released from LIM1863 colon carcinoma cell-derived organoids. *Molecular and Cellular Proteomics*, 12(3):587–598, 3 2013.

288. Michael Liem, Ching Seng Ang, and Suresh Mathivanan. Insulin Mediated Activation of PI3K/Akt Signalling Pathway Modifies the Proteomic Cargo of Extracellular Vesicles. *Proteomics*, 17(23-24):1600371, 12 2017.

289. Andrew Pincetic, Zhizhou Kuang, Eun Joo Seo, and Jonathan Leis. The Interferon-Induced Gene ISG15 Blocks Retrovirus Release from Cells Late in the Budding Process. *Journal of Virology*, 84(9):4725–4736, 5 2010.

290. Lilliana Radoshevich, Francis Impens, David Ribet, Juan J. Quereda, To Nam Tham, Marie Anne Nahori, Helene Bierne, Olivier Dussurget, Javier Pizarro-Cerdá, Klaus Peter Knobeloch, and Pascale Cossart. ISG15 counteracts Listeria monocytogenes infection. *eLife*, 4(AUGUST2015), 8 2015.

291. Ana Gutiérrez-Fernández, Clara Soria-Valles, Fernando G Osorio, Jesús Gutiérrez-Abril, Cecilia Garabaya, Alina Aguirre, Antonio Fueyo, María Soledad Fernández-García, Xose S Puente, and Carlos López-Otín. Loss of MT 1- MMP causes cell senescence and nuclear defects which can be reversed by retinoic acid . *The EMBO Journal*, 34(14):1875–1888, 7 2015.

292. Chang Xia, Zachary Braunstein, Amelia C. Toomey, Jixin Zhong, and Xiaoquan Rao. S100 proteins as an important regulator of macrophage inflammation, 1 2018.

293. Hsiao Ling Hsieh, Beat W. Schäfer, Bernd Weigle, and Claus W. Heizmann. S100 protein translocation in response to extracellular S100 is mediated by receptor for advanced glycation

endproducts in human endothelial cells. *Biochemical and Biophysical Research Communications*, 316(3):949–959, 4 2004.

294. Antero Salminen, Anu Kauppinen, and Kai Kaarniranta. Emerging role of NF-κB signaling in the induction of senescence-associated secretory phenotype (SASP), 4 2012.

295. Matthew Hoare, Yoko Ito, Tae Won Kang, Michael P. Weekes, Nicholas J. Matheson, Daniel A. Patten, Shishir Shetty, Aled J. Parry, Suraj Menon, Rafik Salama, Robin Antrobus, Kosuke Tomimatsu, William Howat, Paul J. Lehner, Lars Zender, and Masashi Narita. NOTCH1 mediates a switch between two distinct secretomes during senescence. *Nature Cell Biology*, 18(9):979–992, 9 2016.

296. Marius Raica and Anca Maria Cimpean. Platelet-derived growth factor (PDGF)/PDGF receptors (PDGFR) axis as target for antitumor and antiangiogenic therapy, 2010.

297. Thaned Kangsamaksin, Aino Murtomaki, Natalie M. Kofler, Henar Cuervo, Reyhaan A. Chaudhri, Ian W. Tattersall, Paul E. Rosenstiel, Carrie J. Shawber, and Jan Kitajewski. NOTCH decoys that selectively block DLL/NOTCH or JAG/NOTCH disrupt angiogenesis by unique mechanisms to inhibit tumor growth. *Cancer Discovery*, 5(2):182–197, 2015.

298. S. Talens, J. J.M.C. Malfliet, P. Th W. van Hal, F. W.G. Leebeek, and D. C. Rijken. Identification and characterization of α1-antitrypsin in fibrin clots. *Journal of Thrombosis and Haemostasis*, 11(7):1319–1328, 7 2013.

299. Chary López-Pedrera, Merce Jardí, Maria Del Mar Malagón, Julia Inglés-Esteve, Gabriel Dorado, Antonio Torres, Jordi Félez, and Francisco Velasco. Tissue factor (TF) and urokinase plasminogen activator receptor (uPAR) and bleeding complications in leukemic patients. *Thrombosis and Haemostasis*, 77(1):62–70, 1 1997.

300. Ortiz-Montero P, Londoño-Vallejo A, and Vernot JP. Senescence-associated IL-6 and IL-8 Cytokines Induce a Self- And Cross-Reinforced Senescence/Inflammatory Milieu Strengthening Tumorigenic Capabilities in the MCF-7 Breast Cancer Cell Line. *Cell communication and signaling : CCS*, 15(1), 2017.

301. J Malapeira, C Esselens, J J Bech-Serra, F Canals, and J Arribas. ADAM17 (TACE) regulates TGFβ signaling through the cleavage of vasorin. *Oncogene*, 30(16):1912–22, 4 2011.

302. Carl P. Blobel. ADAMs: key components in EGFR signalling and development. *Nature Reviews Molecular Cell Biology*, 6(1):32–43, 1 2005.

303. Karen Mendelson, Steven Swendeman, Paul Saftig, and Carl P Blobel. Stimulation of platelet-derived growth factor receptor beta (PDGFRbeta) activates ADAM17 and promotes metalloproteinase-dependent cross-talk between the PDGFRbeta and epidermal growth factor receptor (EGFR) signaling pathways. *The Journal of biological chemistry*, 285(32):25024–32, 8 2010.

304. Yue Shao, Qianqian Zheng, Wei Wang, Na Xin, Xiaowen Song, and Chenghai Zhao. Biological functions of macrophage-derived Wnt5a, and its roles in human diseases, 2016.

305. Hiroyuki Miyoshi, Rieko Ajima, Christine T. Luo, Terry P. Yamaguchi, and Thaddeus S. Stappenbeck. Wnt5a potentiates TGF-β signaling to promote colonic crypt regeneration after tissue injury. *Science*, 338(6103):108–113, 10 2012.

306. Brandt D. Pence, Johnathan R. Yarbro, and Russell S. Emmons. Growth differentiation factor-15 is associated with age-related monocyte immunosenescence. *bioRxiv*, page 2020.02.05.935643, 2 2020.

307. Guillaume Ha, Fanny De Torres, Nassim Arouche, Nassima Benzoubir, Ségolène Ferratge, Elie Hatem, Adrienne Anginot, and Georges Uzan. GDF15 secreted by senescent endothelial cells improves vascular progenitor cell functions. *PLOS ONE*, 14(5):e0216602, 5 2019.

308. Yuna Guo, Jessica L Ayers, Kelly T Carter, Ting Wang, Sean K Maden, Darwin Edmond, Polly Newcomb P, Christopher Li, Cornelia Ulrich, Ming Yu, and William M Grady. Senescence-associated tissue microenvironment promotes colon cancer formation through the secretory factor GDF15. *Aging cell*, 18(6):e13013, 2019.

309. Kenneth E Lipson, Carol Wong, Yuchin Teng, and Suzanne Spong. CTGF is a central mediator of tissue remodeling and fibrosis and its inhibition can reverse the process of fibrosis. *Fibrogenesis & Tissue Repair*, 5(S1), 12 2012.

310. Zac Sandy, Isabelle Cristine da Costa, and Christine K. Schmidt. More than meets the isg15: Emerging roles in the dna damage response and beyond, 11 2020.

311. Kaoru Tominaga. The emerging role of senescent cells in tissue homeostasis and pathophysiology. *Pathobiology of aging & age related diseases*, 5:27743, 2015.

312. George Maiti, Debdut Naskar, and Malini Sen. The Wingless homolog Wnt5a stimulates phagocytosis but not bacterial killing. *Proceedings of the National Academy of Sciences of the United States of America*, 109(41):16600–16605, 10 2012.

313. Nir Osherov and Ronen Ben-Ami. Modulation of Host Angiogenesis as a Microbial Survival Strategy and Therapeutic Target. *PLOS Pathogens*, 12(4):e1005479, 4 2016.

314. D. C. Spencer, N. L. Pienaar, and P. M. Atkinson. Disturbances of blood coagulation associated with Salmonella typhi infections. *Journal of Infection*, 16(2):153–161, 3 1988.

315. Jihye Shin, Jiheon Rhim, Yumi Kwon, Sun Young Choi, Sungho Shin, Chul Won Ha, and Cheolju Lee. Comparative analysis of differentially secreted proteins in serum-free and serum-containing media by using BONCAT and pulsed SILAC. *Scientific Reports*, 9(1):1–12, 12 2019.

316. Ronald F. Tucker, Gary D. Shipley, Harold L. Moses, and Robert W. Holley. Growth inhibitor from BSC-1 cells closely related to platelet type β transforming growth factor. *Science*, 226(4675):705–707, 1984.

317. A. B. Roberts, M. A. Anzano, L. M. Wakefield, N. S. Roche, D. F. Stern, and M. B. Sporn. Type β transforming growth factor: A bifunctional regulator of cellular growth. *Proceedings of the National Academy of Sciences of the United States of America*, 82(1):119–123, 1 1985.

318. Yun Zhang, Peter B. Alexander, and Xiao Fan Wang. TGF-β family signaling in the control of cell proliferation and survival. *Cold Spring Harbor Perspectives in Biology*, 9(4), 4 2017.

319. Joan Massagué and Qiaoran Xi. TGF-β control of stem cell differentiation genes The canonical model and its regulation. *FEBS Lett*, 586(14):1953–1958, 2012.

320. Byron J. Faler, Robyn A. Macsata, Dahlia Plummer, Lopa Mishra, and Anton N. Sidawy. Transforming Growth Factor-β and Wound Healing. *Perspectives in Vascular Surgery and Endovascular Therapy*, 18(1):55–62, 2006.

321. Laurens A. Van Meeteren and Peter Ten Dijke. Regulation of endothelial cell plasticity by TGF-β, 1 2012.

322. Kana Tominaga and Hiroshi I Suzuki. TGF-β Signaling in Cellular Senescence and Aging-Related Pathology. *International Journal of Molecular Sciences*, 20(20):5002, 10 2019.

323. Masato Morikawa, Rik Derynck, and Kohei Miyazono. TGF- β and the TGF-β family: Context-dependent roles in cell and tissue physiology, 5 2016.

324. Joan Massagué. TGFβ signalling in context, 10 2012.

325. Maria Namwanje and Chester W. Brown. Activins and inhibins: Roles in development, physiology, and disease. *Cold Spring Harbor Perspectives in Biology*, 8(7), 7 2016.

326. Yigong Shi and Joan Massagué. Mechanisms of TGF-β signaling from cell membrane to the nucleus, 6 2003.

327. Xin-Hua Feng and Rik Derynck. SPECIFICITY AND VERSATILITY IN TGF-β SIGNALING THROUGH SMADS. *Annual Review of Cell and Developmental Biology*, 21(1):659–693, 11 2005.

328. G. Manning, D. B. Whyte, R. Martinez, T. Hunter, and S. Sudarsanam. The protein kinase complement of the human genome, 2002.

329. Carl Henrik Heldin and Aristidis Moustakas. Signaling receptors for TGF-β family members. *Cold Spring Harbor Perspectives in Biology*, 8(8), 8 2016.

330. Charles J. David and Joan Massagué. Publisher Correction: Contextual determinants of TGFβ action in development, immunity and cancer (Nature Reviews Molecular Cell Biology (2018) DOI: 10.1038/s41580-018-0007-0), 2018.

331. Keiji Miyazawa and Kohei Miyazono. Regulation of TGF-β family signaling by inhibitory smads. *Cold Spring Harbor Perspectives in Biology*, 9(3):a022095, 3 2017.

332. Craig D. Albright, Rudolf I. Salganik, Corneliu N. Craciunescu, Mei-Heng Mar, and Steven H. Zeisel. Mitochondrial and microsomal derived reactive oxygen species mediate apoptosis induced by transforming growth factor-?1 in immortalized rat hepatocytes. *Journal of Cellular Biochemistry*, 89(2):254–261, 5 2003.

333. Young Sil Yoon, Jae Ho Lee, Sung Chul Hwang, Kyeong Sook Choi, and Gyesoon Yoon. TGF β1 induces prolonged mitochondrial ROS generation through decreased complex IV activity with senescent arrest in Mv1Lu cells. *Oncogene*, 24(11):1895–1903, 3 2005.

334. Serif Senturk, Mine Mumcuoglu, Ozge Gursoy-Yuzugullu, Burcu Cingoz, Kamil Can Akcali, and Mehmet Ozturk. Transforming growth factor-beta induces senescence in hepatocellular carcinoma cells and inhibits tumor growth. *Hepatology*, 52(3):966–974, 9 2010.

335. B. Hu, D. C. Tack, T. Liu, Z. Wu, M. R. Ullenbruch, and S. H. Phan. Role of Smad3 in the regulation of rat telomerase reverse transcriptase by TGFβ. *Oncogene*, 25(7):1030–1041, 2 2006.

336. Xiao Yang, Lin Chen, Xiaoling Xu, Cuiling Li, Cuifen Huang, and Chu Xia Deng. TGF-β/Smad3 signals repress chondrocyte hypertrophic differentiation and are required for maintaining articular cartilage. *Journal of Cell Biology*, 153(1), 2001.

337. Yoshinori KATAKURA, Eriko NAKATA, Yukiko TABIRA, Takumi MIURA, Kiichiro TERUYA, Toshie TSUCHIYA, and Sanetaka SHIRAHATA. Decreased Tumorigenicity In Vivo When Transforming Growth Factor ˆ—ˆbeta; Treatment Causes Cancer Cell Senescence. *Bioscience, Biotechnology, and Biochemistry*, 77(12), 2013.

338. Lenka Kubiczkova, Lenka Sedlarikova, Roman Hajek, and Sabina Sevcikova. TGF-β - an excellent servant but a bad master, 9 2012.

339. Hiroshi Hanafusa, Jun Ninomiya-Tsuji, Norihisa Masuyama, Michiru Nishita, Jun Ichi Fujisawa, Hiroshi Shibuya, Kunihiro Matsumoto, and Eisuke Nishida. Involvement of the p38 mitogen-activated protein kinase pathway in transforming growth factor-β-induced gene expression. *Journal of Biological Chemistry*, 274(38):27161–27167, 9 1999.

340. Azeddine Atfi, Si Ham Djelloul, Eric Chastre, Roger Davis, and Christian Gespach. Evidence for a role of Rho-like GTPases and stress-activated protein kinase/c-Jun N-terminal kinase (SAPK/JNK) in transforming growth factor β- mediated signaling. *Journal of Biological Chemistry*, 272(3):1429–1432, 1 1997.

341. Melanie T. Hartsough and Kathleen M. Mulder. Transforming growth factor β activation of p44mapk in proliferating cultures of epithelial cells. *Journal of Biological Chemistry*, 270(13):7117–7124, 3 1995.

342. N. A. Bhowmick, M. Ghiassi, A. Bakin, M. Aakre, C. A. Lundquist, M. E. Engel, C. L. Arteaga, and H. L. Moses. Transforming growth factor-β1 mediates epithelial to mesenchymal transdifferentiation through a RhoA-dependent mechanism. *Molecular Biology of the Cell*, 12(1):27–36, 2001.

343. Hirokazu Kotani, Kenji Takaishi, Takuya Sasaki, and Yoshimi Takai. Rho regulates association of both the ERM family and vinculin with the plasma membrane in MDCK cells. *Oncogene*, 14(14):1705–1713, 4 1997.

344. Gerard C. Blobe, William P. Schiemann, and Harvey F. Lodish. Role of Transforming Growth Factor β in Human Disease. *New England Journal of Medicine*, 342(18):1350–1358, 5 2000.

345. Birgit Spänkuch-Schmitt, Georg Wolf, Christine Solbach, Sibylle Loibl, Rainald Knecht, Manfred Stegmüller, Gunter Von Minckwitz, Manfred Kaufmann, and Klaus Strebhardt. Downregulation of human polo-like kinase activity by antisense oligonucleotides induces growth inhibition in cancer cells. *Oncogene*, 21(20):3162–3171, 5 2002.

346. Kevin Roarty, Sarah E. Baxley, Michael R. Crowley, Andra R. Frost, and Rosa Serra. Loss of TGF-β or Wnt5a results in an increase in Wnt/β-catenin activity and redirects mammary tumour phenotype. *Breast Cancer Research*, 11(2):R19, 4 2009.

347. Leonie Beljaars, Sara Daliri, Christa Dijkhuizen, Klaas Poelstra, and Reinoud Gosens. WNT-5A regulates TGF-β-related activities in liver fibrosis. *American Journal of Physiology-Gastrointestinal and Liver Physiology*, 312(3):G219–G227, 3 2017.

348. Carina Mill, Bethan Alice Monk, Helen Williams, Steven John Simmonds, Jamie Yancey Jeremy, Jason Lee Johnson, and Sarah Jane George. Wnt5a-Induced Wnt1-Inducible secreted protein-1 suppresses vascular smooth muscle cell apoptosis induced by oxidative stress. *Arteriosclerosis, Thrombosis, and Vascular Biology*, 34(11):2449–2456, 11 2014.

349. Marwa S. Asem, Steven Buechler, Rebecca Burkhalter Wates, Daniel L. Miller, and M. Sharon Stack. Wnt5a signaling in cancer, 9 2016.

350. Elena Sancho, Eduard Batlle, and Hans Clevers. SIGNALING PATHWAYS IN INTESTINAL DEVELOPMENT AND CANCER. *Annual Review of Cell and Developmental Biology*, 20(1):695–723, 11 2004.

351. Naoki Oshimori and Elaine Fuchs. The harmonies played by TGF-β in stem cell biology, 12 2012.

352. Nicholas Borcherding, David Kusner, Ryan Kolb, Qing Xie, Wei Li, Fang Yuan, Gabriel Velez, Ryan Askeland, Ronald J. Weigel, and Weizhou Zhang. Paracrine WNT5A signaling inhibits expansion of tumor-initiating cells. *Cancer Research*, 75(10):1972–1982, 5 2015.

353. Zhifeng Gu, Wei Tan, Guijuan Feng, Yan Meng, Biyu Shen, Hong Liu, and Chun Cheng. Wnt/β-catenin signaling mediates the senescence of bone marrow-mesenchymal stem cells from systemic lupus erythematosus patients through the p53/p21 pathway. *Molecular and Cellular Biochemistry*, 387(1-2):27–37, 2 2014.

354. Benjamin G. Bitler, Jasmine P. Nicodemus, Hua Li, Qi Cai, Hong Wu, Xiang Hua, Tianyu Li, Michael J. Birrer, Andrew K. Godwin, Paul Cairns, and Rugang Zhang. Wnt5a suppresses

epithelial ovarian cancer by promoting cellular senescence. *Cancer Research*, 71(19):6184–6194, 10 2011.

355. Mareike Lehmann, Qianjiang Hu, Yan Hu, Kathrin Hafner, Rita Costa, Anastasia van den Berg, and Melanie Königshoff. Chronic WNT/β-catenin signaling induces cellular senescence in lung epithelial cells. *Cellular Signalling*, 70:109588, 6 2020.

356. Baozhi Chen, Michael E. Dodge, Wei Tang, Jianming Lu, Zhiqiang Ma, Chih Wei Fan, Shuguang Wei, Wayne Hao, Jessica Kilgore, Noelle S. Williams, Michael G. Roth, James F. Amatruda, Chuo Chen, and Lawrence Lum. Small molecule-mediated disruption of Wnt-dependent signaling in tissue regeneration and cancer. *Nature Chemical Biology*, 5(2):100–107, 2 2009.

357. Yue Zhao, Chunmei Zhang, Ying Huang, Yang Yu, Rong Li, Min Li, Nana Liu, Ping Liu, and Jie Qiao. Up-Regulated Expression of WNT5a Increases Inflammation and Oxidative Stress via PI3K/AKT/NF-κB Signaling in the Granulosa Cells of PCOS Patients. *The Journal of Clinical Endocrinology & Metabolism*, 100(1):201–211, 1 2015.

358. Benjamin J. Povinelli and Michael J. Nemeth. Wnt5a regulates hematopoietic stem cell proliferation and repopulation through the ryk receptor. *Stem Cells*, 32(1):105–115, 1 2014.

359. Hugh Paterson, Brian Reeves, Robin Brown, Alan Hall, Mark Furth, Johannes Bos, Philip Jones, and Christopher Marshall. Activated N-ras controls the transformed phenotype of HT1080 human fibrosarcoma cells. *Cell*, 51(5):803–812, 12 1987.

360. Kuldeep Kumawat and Reinoud Gosens. WNT-5A: Signaling and functions in health and disease, 2 2016.

361. Amanda J Mikels and Roel Nusse. Purified Wnt5a Protein Activates or Inhibits β-Catenin–TCF Signaling Depending on Receptor Context. *PLoS Biology*, 4(4):e115, 4 2006.

362. Akira Sato, Hideki Yamamoto, Hiroshi Sakane, Hirofumi Koyama, and Akira Kikuchi. Wnt5a regulates distinct signalling pathways by binding to Frizzled2. *The EMBO Journal*, 29(1):41–54, 1 2010.

363. R. M. Liu and K. A. Gaston Pravia. Oxidative stress and glutathione in TGF-β-mediated fibrogenesis, 1 2010.

364. Sergey I. Dikalov and David G. Harrison. Methods for detection of mitochondrial and cellular reactive oxygen species, 2014.

365. Christina Schreck, Rouzanna Istvánffy, Christoph Ziegenhain, Theresa Sippenauer, Franziska Ruf, Lynette Henkel, Florian Gärtner, Beate Vieth, M. Carolina Florian, Nicole Mende, Anna Taubenberger, Áine Prendergast, Alina Wagner, Charlotta Pagel, Sandra Grziwok, Katharina S. Götze, Jochen Guck, Douglas C. Dean, Steffen Massberg, Marieke Essers, Claudia Waskow,

Hartmut Geiger, Mathias Schiemann, Christian Peschel, Wolfgang Enard, and Robert A.J. Oostendorp. Niche WNT5A regulates the actin cytoskeleton during regeneration of hematopoietic stem cells. *Journal of Experimental Medicine*, 214(1):165–181, 2017.

366. Kate E. Unsworth, Michael Way, Mark McNiven, Laura Machesky, and David W. Holden. Analysis of the mechanisms of Salmonella-induced actin assembly during invasion of host cells and intracellular replication. *Cellular Microbiology*, 6(11), 2004.

367. Eduard Batlle and Joan Massagué. Transforming Growth Factor-β Signaling in Immunity and Cancer, 4 2019.

368. David M. de Kretser, Robyn E. O'Hehir, Charles L. Hardy, and Mark P. Hedger. The roles of activin A and its binding protein, follistatin, in inflammation and tissue repair, 8 2012.

369. Akito Maeshima, Keiichiro Mishima, Shin Yamashita, Masao Nakasatomi, Masaaki Miya, Noriyuki Sakurai, Toru Sakairi, Hidekazu Ikeuchi, Keiju Hiromura, Yoshihisa Hasegawa, Itaru Kojima, and Yoshihisa Nojima. Follistatin, an activin antagonist, ameliorates renal interstitial fibrosis in a rat model of unilateral ureteral obstruction. *BioMed Research International*, 2014, 2014.

370. Fredrik E. Wiklund, Anna M. Bennet, Patrik K. E. Magnusson, Ulrika K. Eriksson, Fredrik Lindmark, Liyun Wu, Nasreen Yaghoutyfam, Christopher P. Marquis, Pär Stattin, Nancy L. Pedersen, Hans-Olov Adami, Henrik Grönberg, Samuel N. Breit, and David A. Brown. Macrophage inhibitory cytokine-1 (MIC-1/GDF15): a new marker of all-cause mortality. *Aging Cell*, 9(6):1057–1064, 12 2010.

371. Zhizhong Zhou, Weina Li, Yang Song, Lili Wang, Kuo Zhang, Jing Yang, Wei Zhang, Haichuan Su, and Yingqi Zhang. Growth Differentiation Factor-15 Suppresses Maturation and Function of Dendritic Cells and Inhibits Tumor-Specific Immune Response. *PLoS ONE*, 8(11):e78618, 11 2013.

372. U. Wallin, B. Glimelius, K. Jirström, S. Darmanis, R. Y. Nong, F. Pontén, C. Johansson, L. Påhlman, and H. Birgisson. Growth differentiation factor 15: A prognostic marker for recurrence in colorectal cancer. *British Journal of Cancer*, 104(10):1619–1627, 5 2011.

373. Michal Vocka, Daniel Langer, Vladimir Fryba, Jaromir Petrtyl, Tomas Hanus, Marta Kalousova, Tomas Zima, and Lubos Petruzelka. Growth/differentiation factor 15 (GDF-15) as new potential serum marker in patients with metastatic colorectal cancer. *Cancer Biomarkers*, 21(4):869–874, 2018.

374. Pablo Lopez-Bergami and Gastón Barbero. The emerging role of Wnt5a in the promotion of a pro-inflammatory and immunosuppressive tumor microenvironment, 9 2020.

375. Fabio Perrotta, Graziamaria Corbi, Grazia Mazzeo, Matilde Boccia, Luigi Aronne, Vito D'Agnano, Klara Komici, Gennaro Mazzarella, Roberto Parrella, and Andrea Bianco. COVID-19 and the elderly: insights into pathogenesis and clinical decision-making, 8 2020.

376. D. N. Taylor, R. A. Pollard, and P. A. Blake. Typhoid in the United States and the risk to the international traveler. *Journal of Infectious Diseases*, 148(3):599–602, 9 1983.

377. Marco De Cecco, Steven W. Criscione, Edward J. Peckham, Sara Hillenmeyer, Eliza A. Hamm, Jayameenakshi Manivannan, Abigail L. Peterson, Jill A. Kreiling, Nicola Neretti, and John M. Sedivy. Genomes of replicatively senescent cells undergo global epigenetic changes leading to gene silencing and activation of transposable elements. *Aging Cell*, 12(2):247–256, 2013.

378. Anna Aulicino, Kevin C. Rue-Albrecht, Lorena Preciado-Llanes, Giorgio Napolitani, Neil Ashley, Adam Cribbs, Jana Koth, B. Christoffer Lagerholm, Tim Ambrose, Melita A. Gordon, David Sims, and Alison Simmons. Invasive Salmonella exploits divergent immune evasion strategies in infected and bystander dendritic cell subsets. *Nature Communications*, 9(1):1–17, 12 2018.

379. Dongsheng Shang, Yin Hong, Wangwang Xie, Zhigang Tu, and Jun Xu. Interleukin-1β Drives Cellular Senescence of Rat Astrocytes Induced by Oligomerized Amyloid β Peptide and Oxidative Stress. *Frontiers in Neurology*, 11:929, 8 2020.

380. Kshiti Phulphagar, Lars I. Kühn, Stefan Ebner, Annika Frauenstein, Jonathan J. Swietlik, Jan Rieckmann, and Felix Meissner. Proteomics reveals distinct mechanisms regulating the release of cytokines and alarmins during pyroptosis. *Cell Reports*, 34(10):108826, 3 2021.

381. Wen Xue, Lars Zender, Cornelius Miething, Ross A. Dickins, Eva Hernando, Valery Krizhanovsky, Carlos Cordon-Cardo, and Scott W. Lowe. Senescence and tumour clearance is triggered by p53 restoration in murine liver carcinomas. *Nature*, 445(7128):656–660, 2 2007.

382. Tae Won Kang, Tetyana Yevsa, Norman Woller, Lisa Hoenicke, Torsten Wuestefeld, Daniel Dauch, Anja Hohmeyer, Marcus Gereke, Ramona Rudalska, Anna Potapova, Marcus Iken, Mihael Vucur, Siegfried Weiss, Mathias Heikenwalder, Sadaf Khan, Jesus Gil, Dunja Bruder, Michael Manns, Peter Schirmacher, Frank Tacke, Michael Ott, Tom Luedde, Thomas Longerich, Stefan Kubicka, and Lars Zender. Senescence surveillance of pre-malignant hepatocytes limits liver cancer development. *Nature*, 479(7374):547–551, 11 2011.

383. Antony Cougnoux, Guillaume Dalmasso, Ruben Martinez, Emmanuel Buc, Julien Delmas, Lucie Gibold, Pierre Sauvanet, Claude Darcha, Pierre Déchelotte, Mathilde Bonnet, Denis Pezet, Harald Wodrich, Arlette Darfeuille-Michaud, and Richard Bonnet. Bacterial genotoxin colibactin promotes colon tumour growth by inducing a senescence-associated secretory phenotype. *Gut*, 63(12):1932–1942, 12 2014.

384. Anna Aiello, Farzin Farzaneh, Giuseppina Candore, Calogero Caruso, Sergio Davinelli, Caterina Maria Gambino, Mattia Emanuela Ligotti, Nahid Zareian, and Giulia Accardi. Immunosenescence and its hallmarks: How to oppose aging strategically? A review of potential options for therapeutic intervention, 9 2019.

385. Kyung Ah Kim, Jin Ju Jeong, Sul Young Yoo, and Dong Hyun Kim. Gut microbiota lipopolysaccharide accelerates inflamm-aging in mice. *BMC Microbiology*, 16(1), 1 2016.

386. Hui Wang, Haiping Fu, Ruigong Zhu, Xuan Wu, Xian Ji, Xuesong Li, Hong Jiang, Zhe Lin, Xin Tang, Shixiu Sun, Jiajing Chen, Xin Wang, Qingguo Li, Yong Ji, and Hongshan Chen. BRD4 contributes to LPS-induced macrophage senescence and promotes progression of atherosclerosis-associated lipid uptake. *Aging*, 12(10):9240–9259, 5 2020.

387. Rajalakshmy Ramalingam, Claire B. Larmonier, Robert D. Thurston, Monica T. Midura-Kiela, Song Guo Zheng, Fayez K. Ghishan, and Pawel R. Kiela. Dendritic Cell-Specific Disruption of TGF-β Receptor II Leads to Altered Regulatory T Cell Phenotype and Spontaneous Multiorgan Autoimmunity. *The Journal of Immunology*, 189(8):3878–3893, 10 2012.

388. Leonid Gorelik and Richard A. Flavell. Abrogation of TGFβ signaling in T cells leads to spontaneous T cell differentiation and autoimmune disease. *Immunity*, 12(2):171–181, 2 2000.

389. Kenji Ogawa, Masayuki Funaba, Yan Chen, and Masafumi Tsujimoto. Activin A Functions as a Th2 Cytokine in the Promotion of the Alternative Activation of Macrophages. *The Journal of Immunology*, 177(10):6787–6794, 11 2006.

390. Caroline Bergenfelz, Catharina Medrek, Elin Ekström, Karin Jirström, Helena Janols, Marlene Wullt, Anders Bredberg, and Karin Leandersson. Wnt5a Induces a Tolerogenic Phenotype of Macrophages in Sepsis and Breast Cancer Patients. *The Journal of Immunology*, 188(11):5448–5458, 6 2012.

391. Bennett G. Childs, Matej Durik, Darren J. Baker, and Jan M. Van Deursen. Cellular senescence in aging and age-related disease: From mechanisms to therapy, 12 2015.

392. Beatrice Claudi, Petra Sprö, Anna Chirkova, Nicolas Personnic, Janine Zankl, Nura Schü Rmann, Alexander Schmidt, and Dirk Bumann. Phenotypic Variation of Salmonella in Host Tissues Delays Eradication by Antimicrobial Chemotherapy. *Cell*, 158:722–733, 2014.

393. J. L. Kirkland and T. Tchkonia. Senolytic drugs: from discovery to translation, 11 2020.

394. Fiona C. Lewis-McDougall, Prashant J. Ruchaya, Eva Domenjo-Vila, Tze Shin Teoh, Larissa Prata, Beverley J. Cottle, James E. Clark, Prakash P. Punjabi, Wael Awad, Daniele Torella, Tamara Tchkonia, James L. Kirkland, and Georgina M. Ellison-Hughes. Aged-senescent cells contribute to impaired heart regeneration. *Aging Cell*, 18(3), 6 2019.

395. Carolyn M. Roos, Bin Zhang, Allyson K. Palmer, Mikolaj B. Ogrodnik, Tamar Pirtskhalava, Nassir M. Thalji, Michael Hagler, Diana Jurk, Leslie A. Smith, Grace Casaclang-Verzosa, Yi Zhu, Marissa J. Schafer, Tamara Tchkonia, James L. Kirkland, and Jordan D. Miller. Chronic senolytic treatment alleviates established vasomotor dysfunction in aged or atherosclerotic mice. *Aging Cell*, 15(5):973–977, 10 2016.

396. Allyson K. Palmer, Tamara Tchkonia, Nathan K. LeBrasseur, Eduardo N. Chini, Ming Xu, and James L. Kirkland. Cellular senescence in type 2 diabetes: A therapeutic opportunity. *Diabetes*, 64(7):2289–2298, 7 2015.

397. Thomas Butler, C. B. Sridhar, M. K. Daga, Kamal Pathak, R. B. Pandit, Rasik Khakhria, Chandrashekhar N. Potkar, Michael T. Zelasky, and Raymond B. Johnson. Treatment of typhoid fever with azithromycin versus chloramphenicol in a randomized multicentre trial in India. *Journal of Antimicrobial Chemotherapy*, 44(2):243–250, 1 1999.

398. Masaki Takasugi. Emerging roles of extracellular vesicles in cellular senescence and aging, 4 2018.

399. Nathan Basisty, Abhijit Kale, Sandip Patel, Judith Campisi, and Birgit Schilling. The power of proteomics to monitor senescence-associated secretory phenotypes and beyond: toward clinical applications, 4 2020.

400. Emma L. James, Ryan D. Michalek, Gayani N. Pitiyage, Alice M. De Castro, Katie S. Vignola, Janice Jones, Robert P. Mohney, Edward D. Karoly, Stephen S. Prime, and Eric Kenneth Parkinson. Senescent human fibroblasts show increased glycolysis and redox homeostasis with extracellular metabolomes that overlap with those of irreparable DNA damage, aging, and disease. *Journal of Proteome Research*, 14(4):1854–1871, 4 2015.

401. David C. Lowe, Tor C. Savidge, Derek Pickard, Lars Eckmann, Martin F. Kagnoff, Gordon Dougan, and Steven N. Chatfield. Characterization of candidate live oral Salmonella typhi vaccine strains harboring defined mutations in aroA, aroC, and htrA. *Infection and Immunity*, 67(2):700–707, 1999.